

THE UNIVERSITY OF HULL

**Near Infrared Fluorescence Probes:
Towards Applications in Fluorescence Guided Surgery**

Being a Thesis submitted for Degree of Doctor of Philosophy
in University of Hull

By

Miffy Hok Yan Cheng, BSc (Hons)

December 2017

Abstract

Surgery has been a popular method for the treatment of cancers, in particular solid tumours; but the surgical margins for cancerous tissues are often indistinct and in most cases, the poor identification of residual cancer tissues can result in re-excision. Therefore, near infrared (NIR) fluorescence-guided surgery (FGS) is being developed as a real time intra-operative imaging technique to assist surgeons by improving the accuracy and precision of the removal of tumours.

However, current FDA approved fluorophores suffer from poor chemical stability, limited water-solubility, and lack selectivity toward neoplastic tissue, limiting their clinical application. These current challenges have led to the development of new and improved fluorophores capable of absorbing and emitting light at NIR wavelengths, negating autofluorescence and improving deeper light transmission.

Throughout this project, a series of BODIPYs, aza-BODIPYs and bacteriochlorins were synthesised and developed for bioimaging applications. Despite many of them showing interesting fluorescence properties, the investigation suggested aza-BODIPYs were the most promising red / NIR fluorophores (λ_{em} 600-700 nm) due to their excellent photostability. Methods have been developed to incorporate functionalities suitable for bioconjugation.

Different bioconjugation strategies have been explored to covalently conjugate the NIR fluorophores to a clinically relevant protein, peptide and antibody under mild conditions. The viability of aza-BODIPY conjugates against biological targets were investigated and a range of other novel targeted NIR fluorophores were successfully developed. *In vitro* fluorescence imaging was subsequently carried out to demonstrate the enhanced selectivity of the targeting NIR fluorophores toward overexpressed receptors on various cancer cells lines.

This project has demonstrated the potential of aza-BODIPY in biological imaging and developed targeted NIR fluorophores. Further biological evaluation is progressing with the eventual aim of developing a pre-clinical model for NIR FGS in oncology.

Acknowledgements

Despite my interests in science, with the fact that I have always been an extremely ordinary person, doing a PhD was honestly out of my mind. Therefore, I would really like to thank my supervisor Prof. Ross Boyle for all the support, guidance, trust and opportunity he has given to me. It was indeed very lucky for me to have met Ross during the second year of my undergraduate degree and for him to allow me to intrude in his lab during that summer. Throughout my PhD, he has been a lovely advisor for both science and life, where he has always been so kind and wise.

In addition, many thanks to all my collaborators: Dr. Michael Reithofer for providing the peptide for tyrosine coupling reactions. Prof. Steve Archibald and Dr. Juozas Domarkas for assisting with the CXCR4 peptide work. Dr. Vijay Chudasama and Dr. Antoine Maruani from UCL, for helping me with all the antibody work and for teaching me many bioconjugation techniques.

Similarly, thanks go to previous postdocs Dr. Francesca Bryden who spotted me among the others and believed in my ability to achieve my goals. I would also like to thank all the other postdocs: Dr. Cinzia Spagnul and Dr. João Rodrigues for being such great friends and for all the help and encouragements they have given to me that has given me confidence. Lastly, I must thank them all for teaching me a lot in both aspects of practical and theoretical chemistry.

Many thanks also go to Huguette Savoie for performing some of the biological aspects of this project and for teaching me all the biological techniques and knowledge I needed to do my own biology. Finally, I would like to thank her for many stories and advice she has shared with me.

Thanks also to everyone from the C120 lab: Guy Entract, Lauren Turner, Steven Yap, Jordon Sandland for making the lab an interesting place with all the funny and weird conversations, but of course more importantly the constant discussions about science. Lastly, I must not forget to mention about all the wonderful 70s music we played in the lab. In addition, thanks go to EPSRC funded NMSF for mass spectrometry data analysis and Rob Lewis for helping with the technical support for the NMR. I would also like to give my gratitude to a lot of students and staff from the Department of Chemistry for

being very helpful and supportive during my time at the University of Hull.

There are many friends I would like to thank, especially Guy for being a great and talented friend, thanks for being there for my ups and downs. Things would have been a whole lot different without him around, these years have been a lot of memories for us. There are so many things I could mention here, but **the point is** (my favourite phrase) I will always remember the discussions we had about fun projects and all the singing we did in the corridors. Special thanks also go to two others lovely friends, Brittany Wingham and Rhiannon Lee. Brittany for being such a genuine friend and a biological expert that solves a lot of my queries. Also, for literally knowing everyone to then help me to get access to so many equipment and people in biology. Despite I can never find Rhiannon and always miss her by a second, I would like to thank her for being a good friend and great collaborator/ dancer (Ok, Guy is also a great dancer).

Many thanks to all of my friends and family from all over the world for the continuous support. Most importantly, special thanks go to Dad for helping me to slowly build up the passion for science. If it wasn't for him to sacrifice a lot in his life and giving me all these opportunities to walk my own path, I could have never been able to chase my dream. Although we were miles apart I knew he has always been there for me, taking care of me, supporting me and being secretly proud of me, even when he never said it out loud. Finally, many thanks go Owen for his patient and understanding, I really appreciate all that he has done for me and taking care of me through rough times. Thank you for riding with me through all my emotional roller-coasters and for being here with me on this memorable journey.

Abbreviations

^1H -NMR	– Proton nuclear magnetic resonance
^{13}C -NMR	– Carbon nuclear magnetic resonance
^{11}B -NMR	– Boron nuclear magnetic resonance
^{19}F -NMR	– Fluorine nuclear magnetic resonance
AIBN	– Azobisisobutyronitrile
ALA	– Aminolaevulinic acid
APC	– Alkylphosphocholine
APL	– Aplaviroc
ASAP	– Atmospheric Solid Assisted Probe
BARAC	– Biarylazacyclooctynone
Bchl <i>a.</i>	– Bacteriochlorophyll <i>a.</i>
BCN	– Bicyclo[6.1.0]nonyne
$\text{BF}_3 \cdot \text{Et}_2\text{O}$	– Boron trifluoride diethyl etherate
BODIPY	– Borondipyrromethene
Boc	– Tert-Butoxycarbonyl
BSA	– Bovine serum albumin
CEA	– Carcinoembryonic antigen
CF	– Correction Factor
Chl <i>a.</i>	– Chlorophyll <i>a.</i>
CLSM	– Confocal laser scanning microscopy
CuAAC	– Copper catalysed Alkyne-Azide Cycloaddition
CXCR4	– Chemokine receptor type 4
DBU	– 1,8-Diazabicyclo[5.4.0]undec-7-ene
DCM	– Dichloromethane
DCU	– <i>N,N'</i> -Dicyclohexylurea
DDQ	– 2,3-Dichloro-5,6-dicyanobenzoquinone
DEA	– Diethylamine
DIBAC	– Methyl 5-(11,12-didehydrodibenzo[b,f]azocin-5(6H)-yl)-5-oxopentanoate
DIBO	– Dibenzylcyclooctyne
DIFO	– Difluorooctyne
DIPEA	– Diisopropylethylamine

DMA	– Dimethylacetamide
DMF	– Dimethylformamide
DMSO	– Dimethylsulphoxide
DTT	– Dithiothreitol
EDC	– 1-Ethyl-3-(3-dimethylaminopropyl)carbodiimide
EDG	– Electron donating group
EDTA	– Ethylenediaminetetraacetic acid
EGFR	– Epidermal growth factor receptor
EtOAc	– Ethyl acetate
EtOH	– Ethanol
eq	– Equivalents
EWG	– Electron withdrawing group
FACs	– Fluorescent-antibody conjugates
FACS	– Fluorescence-activated cell sorting
FBDP	– 4-formylbenzene diazonium hexafluorophosphate
Fc	– fragment crystallisable
FDA	– Food and Drug Administration
FGS	– Fluorescence guided surgery
FITC	– Fluorescein isothiocyanate
FPPCs	– Fluorescent probe-peptide conjugates
GPI	– Glycophosphatidylinositol
h	– hour
HER2	– Human epidermal growth factor receptor 2
HOBt	– Hydroxybenzotriazole
HOMO	– Highest occupied molecular orbital
HP	– Hydroxyl group appended free base porphyrin derivative
HPLC	– High performance liquid chromatography
ICG	– Indocyanine green
IgG	– Immunoglobulin G
LDL	– Lipoproteins
LDS	– Lithium dodecyl sulfate
LUMO	– Lowest occupied molecular orbital
mAb	– Monoclonal antibody

min	– Minutes
MALDI	– Matrix Assisted Laser Desorption/Ionization
MO	– Molecular orbitals
MOFO	– Monofluorinated cyclooctyne
MWCO	– Molecular weight cut off limits
NBS	– <i>N</i> -Bromosuccinimide
NCS	– <i>N</i> -Chlorosuccinimide
NH ₄ OAc	– Ammonium acetate
NHS	– <i>N</i> -Hydroxysuccinimide
NIR	– Near infrared
NMR	– Nuclear magnetic resonance
PAGE	– Polyacrylamide gel electrophoresis
PBG	– Porphobilinogen
Pcs	– Phthalocyanines
Pchl id <i>a</i> .	– Protochlorophyllide <i>a</i>
PDs	– Dibromopyridazinediones
PDT	– Photodynamic therapy
PeT	– Photoelectron transfer
PE	– Phycoerythrin
PEG	– Polyethylene glycol
PF ₆ ⁻	– Hexafluorophosphate ion
PK	– Pharmacokinetic
ppm	– Parts per million
PPIX	– Protoporphyrin IX
PTAD	– 4-Phenyl-3H-1,2,4-triazoline-3,5(4H)dione
rt	– room temperature
SDS	– Sodium dodecyl sulfate
SLN	– Sentinel lymph node
SNARF-DE	– seminaphthorhodaflor decyl
TAA	– Tumour associated antigens
TCCT	– Total Corrected Cellular Fluorescence
TCEP	– Tris(2-carboxyethyl)phosphine
TBAC	– Tetrabutylammonium chloride

TBAF	–Tetrabutylammonium fluoride
TBTA	– Tris(benzyltriazolylmethyl)amine
TBE	– Tris-borate-EDTA
TEA	– Triethylamine
TFA	– Trifluoroacetic acid
THF	– Tetrahydrofuran
THPTA	– Tris(3-hydroxypropyltriazolylmethyl)amine
TLC	– Thin-layer chromatography
TosMIC	– <i>p</i> -Toluenesulfonyl methylisocyanide
TMS	– Trimethylsilyl
TPP	– Tetraphenylporphyrin
UV-vis	– Ultraviolet-visible
VEGF	– Vascular endothelial growth factor

COSHH statement

All experiments carried out were in accordance with the University of Hull’s Health and Safety regulations. A COSHH assessment of health and safety risk associated with each experiment and all the procedures and precautions were followed. The associated documents were permitted by the supervisor Prof. Ross Boyle and the Health and Safety Officer Dr. Tom McCreedy.

Abstract ii

Acknowledgements iii

Abbreviations v

COSHH statement viii

Contents ix

1. Fluorescence guided surgery	1
1.1 NIR vs UV-vis	3
1.2 Colorectal cancer, glioma, breast cancer and lymph node metastasis detection	4
1.3 Development of fluorophores for cancer imaging	6
1.3.1 <i>FDA approved non-specific probes</i>	7
1.3.1.1 <i>5-Aminolevulinic acid (ALA) induced protoporphyrin-IX</i>	8
1.3.1.2 <i>Methylene blue</i>	8
1.3.1.3 <i>Indocyanine Green</i>	9
1.3.2 <i>Developments of preclinical NIR fluorescence probes</i>	10
1.3.2.1 <i>Fluorescein</i>	12
1.3.2.2 <i>Rhodamine</i>	13
1.3.2.3 <i>Cyanine dyes</i>	13
1.3.2.4 <i>Squaraines</i>	14
1.3.2.5 <i>Rylene dyes</i>	15
1.3.2.6 <i>Boron-dipyrromethene (BODIPY)</i>	16
1.3.2.7 <i>Tetrapyrrolics - phthalocyanine and porphyrin derivatives</i>	16
1.4 Targeting strategies	17
1.4.1 <i>Small molecule targeting</i>	18
1.4.2 <i>Peptide targeting</i>	20
1.4.3 <i>Protein targeting</i>	21

1.4.4	<i>Antibodies and antibody fragments</i>	22
1.4.5	<i>Activatable Probes</i>	26
1.5	Bioconjugation strategies	27
1.5.1.1	<i>Lysine modification</i>	28
1.5.1.2	<i>Cysteine</i>	30
1.5.1.3	<i>Tyrosine</i>	33
1.5.2	<i>Bioorthogonal chemistry</i>	36
1.5.2.1	<i>Copper Catalysed Azide Alkyne Cycloaddition</i>	37
1.5.2.2	<i>Strain Promoted Azide Alkyne Cycloaddition</i>	40
1.5.3	<i>NIR fluorophores</i>	43
2.	BODIPYs	45
2.1	Synthesis of BODIPYs.....	47
2.2	Extending wavelength	49
2.3	Result and discussion	50
2.3.1	<i>Pyrrole, 2,4-dimethylpyrrole and kryptopyrrole BODIPYs</i>	50
2.3.2	<i>Regioselective bromination</i>	56
2.3.3	<i>Diaryl-Knoevenagel condensation</i>	60
3.	Aza-BODIPY	67
3.1	Synthesis of Aza-BODIPY.....	68
3.1.1	<i>Synthetic approach to asymmetrically substituted aza-BODIPY</i> .70	
3.2	Structure modification of aza-BODIPY.....	70
3.2.1	<i>Fluoride displacement</i>	71
3.2.2	<i>Water solubilisation</i>	72
3.2.3	<i>Functionalisation for bioconjugation</i>	74
3.5	Results and discussion	75
3.5.1	<i>Clickable hydrophobic azido aza-BODIPY</i>	75

3.5.2	<i>B-O aza-BODIPY complexes</i>	78
3.5.3	<i>Water soluble aza-BODIPY</i>	81
3.5.4	<i>Clickable water-soluble azido aza-BODIPY</i>	85
3.5.5	<i>Synthesis of aza-BODIPY conjugate by click chemistry</i>	87
3.5.6	<i>Peptide coupling carboxylic acid functionalised aza-BODIPY</i> ...	89
3.5.7	<i>Clickable water-soluble alkyne functionalised aza-BODIPY</i>	93
3.5.8	<i>Synthesis of enhanced water-soluble aza-BODIPY through methyl ether protection</i>	95
3.5.9	<i>Synthesis of enhanced water-soluble aza-BODIPY through benzyl ether protection</i>	97
3.5.10	<i>Synthesis of enhanced water-soluble aza-BODIPY through PEG conjugation</i>	100
4.	Bacteriochlorins	103
4.1	Synthesis of bacteriochlorin	106
4.1.1	<i>Modification of natural bacteriochlorophylls</i>	106
4.1.2	<i>Reductive hydrogenation of porphyrins</i>	107
4.1.3	<i>OsO₄ mediated oxidative dihydroxylation of porphyrin</i>	108
4.1.4	<i>1,3 Dipolar cycloadditions to porphyrins</i>	109
4.1.5	<i>De novo synthesis of bacteriochlorin</i>	110
4.2	Imaging with bacteriochlorin	111
4.3	Result and discussion	113
4.3.1	<i>Synthesis of bacteriochlorin through diimide reduction</i>	113
4.3.2	<i>Synthesis of bacteriochlorin via 1,3-Dipolar Cycloaddition Reactions</i>	117
4.3.3	<i>Synthesis of lipophilic bacteriochlorin via Lindsey's Method</i> ...	122
5.	Bioconjugation to targeted moieties	127

5.1	Bioconjugation to tyrosine residues on peptides and proteins	127
5.1.1	<i>Synthesis of alkyne functionalised diazonium linker</i>	128
5.1.2	<i>Tyrosine selective modification followed by CuAAC reaction with model peptide</i>	129
5.1.3	<i>Photophysical studies of multiwavelength BODIPYs and aza-BODIPY</i>	134
5.1.4	<i>Tyrosine selective modification followed by CuAAC reaction on BSA</i>	135
5.1.5	<i>Cell imaging to produce fluorescence image</i>	143
5.2	Lysine residue bioconjugation from CXCR4 receptor targeting peptide	145
5.2.1	<i>Synthesis of water soluble aza-BODIPY cyclic FC131. AMBA peptide conjugate</i>	146
5.2.2	<i>Photophysical studies of peptide conjugate</i>	147
5.2.3	<i>Molecular modelling</i>	149
5.2.4	<i>FACS for binding affinity</i>	151
5.2.5	<i>In vitro studies of fluorescence imaging</i>	152
5.2.5.1	<i>Co-localisation studies with hCXCR4 FITC-antibody</i>	154
5.2.5.2	<i>Non-specific binding experiment with starting material</i>	156
5.3	Cysteine residue bioconjugation with Herceptin antibody	158
5.3.1	<i>Bioconjugation with anionic azido aza-BODIPY</i>	158
5.3.1.1	<i>In vitro imaging of NIR fluorescent conjugate</i>	161
5.3.2	<i>Photophysical studies and bioconjugation of an enhanced water-soluble azido aza-BODIPY</i>	163
5.3.2.1	<i>Cell preparation and confocal Imaging</i>	166
6.	Concluding remarks and future work	169

7.	Experimental section.....	172
7.1	Materials.....	172
7.2	Methods.....	173
7.2.1	<i>SDS-PAGE procedure.....</i>	<i>173</i>
7.2.2	<i>Purification of protein via size exclusion chromatography and diafiltration</i>	<i>174</i>
7.2.3	<i>Photostability experiment</i>	<i>174</i>
7.2.4	<i>Fluorescence quantum yield measurement</i>	<i>174</i>
7.2.5	<i>Cell preparation and confocal imaging</i>	<i>175</i>
7.2.5.1	<i>HeLa cells seeding and incubation conditions</i>	<i>175</i>
7.2.5.2	<i>U87.CXC4 and U87 cells seeding and incubation conditions...175</i>	
7.2.5.3	<i>BT-474 and MDA-MB-468 cells seeding and incubation conditions.....</i>	<i>176</i>
7.3	Synthesis	177
7.3.1	<i>BODIPY</i>	<i>177</i>
7.3.2	<i>Aza-BODIPY</i>	<i>206</i>
7.3.3	<i>Bacteriochlorins.....</i>	<i>252</i>
7.3.4	<i>Bioconjugation linker and conjugates</i>	<i>267</i>
8.	References	277
9.	Appendix	296
9.1	HPLC traces	296

Table of Schemes xiv

Scheme 1. Synthesis of symmetrical BODIPY <i>via</i> acid-catalysed condensation from pyrrole and aldehydes.....	47
Scheme 2. Synthesis of asymmetrical BODIPY <i>via</i> acid-catalysed condensation from pyrrole and acyl chloride.....	48
Scheme 3. Condensation-decarbonylation of pyrrole-2-carbaldehyde with the use of a phosphorus oxychloride to yield intermediate dipyrrens and BODIPY compounds. ⁷⁷	49
Scheme 4. Synthesis of azide PEG chains.....	53
Scheme 5. Cleavage of benzoic acid from the <i>meso</i> position of BODIPY.	54
Scheme 6. Synthesis of NHS ester aldehyde 17	54
Scheme 7. Synthesis of diaryl-Knoevenagel condensation.	61
Scheme 8. Knoevenagel condensation reaction of BODIPYs 12 with EWG.	61
Scheme 9. Knoevenagel condensation reaction with EDG to produce BODIPYs 24	63
Scheme 10. Knoevenagel condensation reaction of BODIPYs and benzaldehyde to form distyryl adducts.	65
Scheme 11. Synthesis of aza-dipyrrin by Roger <i>et al.</i> ²³⁸	68
Scheme 12. Attempted syntheses 5,5'-diarylaaza-dipyrrin from nitrile derivatives. ²³⁹	69
Scheme 13. Synthetic approach to symmetrical aza-BODIPY.....	69
Scheme 14. Synthetic approach of asymmetrically substituted aza-BODIPY	70
Scheme 15. Synthesis of aza-BODIPY containing cysteic acid.....	73
Scheme 16. Synthesis of aza BODIPY 32 with azide PEG chain.	76
Scheme 17. Attempted B-O chelation reaction of aza BODIPY with azide PEG chain moiety and Lewis acid – AlCl ₃	79
Scheme 18. Attempted B-O chelation reaction of aza BODIPY with aminoethanol using reactive leaving group - TMSOTf.	81
Scheme 19. Synthesis of anionic water-soluble aza-BODIPY.	82
Scheme 20. Synthesis of azido anionic aza-BODIPY.	85
Scheme 21. CuAAC reaction of lipophilic aza-BODIPY 32 with phenylacetylene.....	88
Scheme 22. CuAAC reaction of hydrophilic aza-BODIPY 40 with phenylacetylene.....	89
Scheme 23. Synthesis of NHS ester aza-BODIPY.	90
Scheme 24. Synthesis of water soluble anionic aza-BODIPY with carboxylic	

acid functionality.	91
Scheme 25. Peptide coupling reaction of carboxylic acid functionalised aza-BODIPY and aminoethanol.	93
Scheme 26. Synthesis of propargyl tosylate 48	93
Scheme 27. Synthesis of alkyne functionalised aza-BODIPY 49 and corresponding anionic aza-BODIPY 50	94
Scheme 28. Attempted synthesis of hexahydroxy aza-BODIPY 55	96
Scheme 29. Synthesis of 4-benzyloxyacetophenone 56	97
Scheme 30. Attempted synthesis of the 3+1 aza-BODIPY.	98
Scheme 31. Synthesis of the enhanced water-soluble azido aza-BODIPYs.	101
Scheme 32. Kishi <i>et al.</i> 's de novo synthesis of tolyporphyrins from dipyrin precursors.	111
Scheme 33. Synthesis of ortho-substituted 5,10,15,20-tetrakis(2,6-dichlorophenyl)porphyrin.	114
Scheme 34. Attempted synthesis of ortho-substituted 5,10,15,20-tetrakis(2,6-dichlorophenyl) bacteriochlorin.	114
Scheme 35. Attempted synthesis of bacteriochlorin 71 through 1,3-cycloaddition reaction with azomethine ylides.	118
Scheme 36. Synthesis of corresponding zinc chlorin 72 through 1,3-cycloaddition reaction with azomethine ylides.	119
Scheme 37. Attempted synthesis of corresponding zinc bacteriochlorin 73 through 1,3-cycloaddition reaction with azomethine ylides.	120
Scheme 38. Synthesis of lipophilic bacteriochlorin 82	123
Scheme 39. Reaction of 2,2-dimethoxyacetonitrile with the Grignard reagent to form 1,1-dimethoxy-4-methylpent-3-en-2-one.	124
Scheme 40. Synthesis of diazonium alkyne linker.	129
Scheme 41. Peptide modification on the tyrosine residue.	130
Scheme 42. CuAAC of anionic azido aza-BODIPY and tyrosine modified peptide.	131
Scheme 43. Tyrosine modification of BSA with an alkyne diazonium linker.	136
Scheme 44. Tyrosine modification with alkyne diazonium linker followed by CuAAC with varying wavelength BODIPYs.	138
Scheme 45. Synthesis of conjugate 94 from CPCR4.2 AMBA peptide 94 and 46	146
Scheme 46. Preparation of “clickable” trastuzumab 97	159
Scheme 47. Attempted preparation of aza-BODIPY–trastuzumab conjugate	

98.....	160
Scheme 48. Preparation of aza-BODIPY–trastuzumab conjugate 99	164

Table of Figure xvi

Figure 1. NIR fluorescence system to visualised targeted tumours. ¹¹	2
Figure 2. NIR fluorescence vs lower wavelength fluorescence. ¹⁶	4
Figure 3. NIR Fluorescence guided surgery providing a contrasting imaging to detect surgical margins. ¹	5
Figure 4. Possible interconversions of methylene blue to leucomethylene blue, causing quenching of fluorescence. ⁴⁹	9
Figure 5. Ionisation equilibria of fluorescein.....	13
Figure 6. Proposed photobleaching adducts of cyanine dyes.....	14
Figure 7. Thiol induced formation of non-fluorescence adducts based on nucleophilic attack at electron deficient central cyclobutane ring.....	15
Figure 8. Changes in optical spectrum of rylene as a function of concentration.....	16
Figure 9. Targeting moieties for fluorophores applied in fluorescence imaging.....	18
Figure 10. Signal to noise contrasts for <i>in vivo</i> tumor imaging with inmurine model using EC17 (intense autofluorescence) and OTL38 (no autofluorescence). (a) Fluorescence imaging of KB tumor (b) Fluorescence imaging of HeLa tumor.....	19
Figure 11. Chemical structure of cyclic peptide GE-137 labelled with Cy5 dye.....	20
Figure 12. Microscopy imaging of c-Met expression in normal colon and adenomatous polyp targeted by GE-137 conjugate; (a,b) no staining, (c,d) c-Met labelled FITC, (i,j) NIR fluorescence of GE-137 with i – showed reduced fluorescence due to lower c-Met expression whereas j – showed higher fluorescence that corresponds to the c-Met. ¹⁰⁰	21
Figure 13. Receptor mediated endocytosis with LDL. ¹⁰⁸	22
Figure 14. Structure and domains of a typical IgG.....	23
Figure 15. Mechanism of ligands and cetuximab binding. a) EGFR ligands bind to the extracellular domain of receptors and activate cell survival and proliferation. b) Cetuximab competitively binds to receptor and blocks signalling.....	25
Figure 16. Microscopy images: a) white light b) fluorescence c) DAPI nuclear stain with cetuximab-IRDye800CW selectively targeting	

primary tumour of oral squamous cell carcinoma. ¹²³	25
Figure 17. Antibody binding site on a GPI anchor for CEA.	26
Figure 18. a) Schematic diagram of porphyrin-lipid self-assembly into porphosomes nanovesicles and their application in <i>in vivo</i> fluorescence imaging. ¹²⁷ b) Lysosomal responsive aza-BODIPY. ¹²⁸	27
Figure 19. Common methods for lysine bioconjugation.	28
Figure 20. Selective fluorescent labelling of lysine residue of G-actin.	29
Figure 21. The conversion of carboxylate to NHS ester and subsequent hydrolysis.	30
Figure 22. Common methods for cysteine bioconjugation.	31
Figure 23. Schematic of disulphide exchange reaction.	32
Figure 24. Schematic of disulfide rebridging with dibromomaleimide.	32
Figure 25. Common methods for tyrosine bioconjugation.	33
Figure 26. Two step tyrosine modification through <i>O</i> -acetylation.	34
Figure 27. Selective tyrosine modification of BSA by FBDP for further bioorthogonal ligation.	34
Figure 28. Mannich-type three component selective modification of tyrosine residue of α -chymotrypsinogen A with rhodamine.	35
Figure 29. Bioconjugation of aplaviroc (APL) with PTAD to IgG antibody.	36
Figure 30. Bioorthogonal chemistry between modified functionality X and reactive partner Y.	36
Figure 31. Schematic of Staudinger ligation.	37
Figure 32. Schematic of ketone/hydroxylamine.	37
Figure 33. Schematic of Copper Catalysed Azide Alkyne Cycloaddition .	38
Figure 34. Possible mechanism for CuAAC reaction. ¹⁷⁹	39
Figure 35. Structures of accelerating ligands TBTA and THPTA.	39
Figure 36. Examples of CuAAC of fluorophores with biological molecules. ^{182,184}	40
Figure 37. General schematic of strain promoted azide-alkyne cycloaddition.	41
Figure 38. Reaction kinetics between different cycloalkyne derivatives. ¹⁸⁹	41
Figure 39. Disulfide rebridging of IgG antibody with dibromopyridazinediones functionalised with a strained alkyne and terminal alkyne for click reactions.	42
Figure 40. Bioconjugation strategy for fluorophores and BCN through the use of tetrazine linker. ¹⁹²	42

Figure 41. Alternative synthetic organic fluorophores.....	43
Figure 42. Schematic structure of a BODIPY core and internal quenching in 8-phenyl derivatives.	45
Figure 43. Typical UV-visible and fluorescence spectra of BODIPY, λ_{abs} (blue) and λ_{em} (orange).	46
Figure 44. The proposed structure of H-dimer (A) and J-dimer (B).....	46
Figure 45. Methods for extending the wavelength of BODIPYs into the NIR region.....	50
Figure 46. Alkyl- substituted pyrrolic units of BODIPYs as a possible resolution to freely rotating aryl group inducing fluorescence quenching.	51
Figure 47. Library of BODIPYs with the different pyrrolic unit and conjugatable functional groups.	52
Figure 48. UV-visible spectrum showing the λ_{abs} of unsubstituted BODIPYs 1-4 (hollow lines), 1,3,5,7,8-substituted BODIPYs 5-11 (solid lines) and 1,3,5,7, 8-substituted 1,2,3,5,6,7,8-substituted BODIPYs (dash lines) in 4.8 μM solution of DCM.....	55
Figure 49. Schematic structure of brominated BODIPYs.....	56
Figure 50. X-ray crystallography structure of BODIPY 19	56
Figure 51. Normalised UV-visible and fluorescence spectra of BODIPY, 1 (blue), 4 (orange), 18 (grey) and 19 (yellow) in DCM, λ_{abs} (solid line) and λ_{em} (dash line).	57
Figure 52. $^1\text{H-NMR}$ of attempted synthesis of BODIPY 20 , a broad singlet peak at 10.28 ppm indicating carboxylic acid formation.	58
Figure 53. $^1\text{H-NMR}$ of attempted synthesis of BODIPY 21 , showing the absence of aryl protons previously at 6.78 ppm and 7.01 ppm for the three collected fractions from column chromatography.....	59
Figure 54. Normalised UV-visible and fluorescence spectrum of 6 and 22 in DCM, λ_{abs} (solid line) and λ_{em} (dash line).	60
Figure 55. Proposed mechanistic explanation to the unreactive nature of 4-pyridinecarboxaldehyde with methyl BODIPY.	62
Figure 56. UV-visible and fluorescence spectra of 24 in DCM, λ_{abs} (blue) and λ_{em} (red).	64
Figure 57. Normalised UV-visible and fluorescence spectra of 25-27 in DCM, λ_{abs} (solid line) and λ_{em} (dash line).	65
Figure 58. Normalised fluorescence spectrum of BODIPY 8 , 9 , 11 and corresponding red BODIPYs 25-27 in DCM after Knoevenagel condensation.....	66

Figure 59. Chemical structure of aza-BODIPY and typical UV-visible and fluorescence spectrum, λ_{abs} (blue) and λ_{em} (orange).....	67
Figure 60. Structural modification of aza-BODIPY core.....	71
Figure 61. B-O chelation of aza-BODIPY.....	72
Figure 62. Aryl and alkynyl C-nucleophilic substitution of aza-BODIPY .	72
Figure 63. Water-soluble aza-BODIPYs	73
Figure 64. Glycoconjugated aza-BODIPY (A). Amino acid and peptide conjugates from maleimide aza-BODIPY(B)	74
Figure 65. Normalised UV-visible and fluorescence spectra of 32 in DCM, λ_{abs} (blue) and λ_{em} (orange).....	77
Figure 66. Proposed mechanism for the formation of alkoxy-BODIPY with AlCl_3	78
Figure 67. Hydrolysis of B-dimethoxy BODIPY derivatives. ²⁵⁶	80
Figure 68. Formation of monoalkoxy BODIPY with TMSOTf.....	80
Figure 69. Novel counter ion exchange method for disulfonated aza-BODIPY.	82
Figure 70. Normalised UV-visible (blue) and fluorescence (orange) spectra of 36 in DCM.	83
Figure 71. Normalised UV-visible (blue) and fluorescence (orange) spectra of 37 in water.....	84
Figure 72. Fluorescence spectra of 37 in methanol.....	84
Figure 73. Counter ion exchange method for azido anionic aza-BODIPY isolation.	86
Figure 74. Normalised UV-visible (blue) and fluorescence (orange) spectra of 40 in methanol.	86
Figure 75. Normalised UV-visible (blue) and fluorescence (orange) spectra of 40 in water.....	87
Figure 76. Normalised UV-visible (blue) and fluorescence (orange) spectra of carboxylic acid functionalised anionic aza-BODIPY 46 in methanol.	92
Figure 77. Normalised UV-visible (blue) and fluorescence (orange) spectrum of alkyne functionalised anionic aza-BODIPY 50 in methanol.....	94
Figure 78. Normalised UV-visible (blue) and fluorescence (orange) spectrum of methyl ether protected aza-BODIPY 54 in DCM.....	96
Figure 79. Normalised UV-visible (blue) and fluorescence (orange).spectra of <i>t</i> -butyl dibenzyl aza-BODIPY 61 in DCM	99
Figure 80. Normalised UV-visible (blue) and fluorescence (orange) spectrum of azido PEG 5k aza-BODIPY 68 in water.	102

Figure 81. Structure of bacteriochlorophyll <i>a</i> and its derivatives.	103
Figure 82. Schematic structure of bacteriochlorin and its 18 π aromatic system.....	104
Figure 83. Schematic structures and absorption spectrums of Pchl <i>a</i> , Chl <i>a</i> , and Bchl <i>a</i>	105
Figure 84. Chemical modifications of bacteriochlorophyll <i>a</i>	107
Figure 85. Whitlock diimide reduction ²⁷⁴ of porphyrin through <i>syn</i> -hydrogenation.....	108
Figure 86. Bacteriochlorin diastereoisomers generated from OsO ₄ mediated oxidation of porphyrin.....	109
Figure 87. Generalised scheme of 1,3 dipolar cycloaddition of porphyrins and chlorins to bacteriochlorins.	110
Figure 88. Lindsey approach of <i>de novo</i> synthesis using germinal dimethyldipyrrin to generate oxidation stable bacteriochlorin.	111
Figure 89. Structure of chlorin-bacteriochlorin dyads and optical reconstructions of fluorescence for ZnC-FbB (A) and FbC-FbC (B) with excitation at 650 or 675 nm and detection at 760 nm.	112
Figure 90. UV-visible spectra of Whitlock diimide reduction of ortho-substituted 5,10,15,20-tetrakis(2,6-dichlorophenyl)porphyrin to its relative bacteriochlorin 70 in DCM over a duration of 18 hours.	115
Figure 91. UV-visible spectrum of octachlorobacteriochlorin 70 in DCM before and after column chromatography.	116
Figure 92. Examples of sulfonated and halogenated tetraaryl bacteriochlorins. ³⁰⁷	117
Figure 93. Mechanism of 1,3-cycloaddition reaction of ,10,15,20-tetrakis(perfluorophenyl) porphyrin with azomethine ylides.....	118
Figure 94. Normalised UV-visible (blue) and fluorescence (orange) spectra of chlorin 72 in DCM.....	120
Figure 95. Possible Zn coordination forming a strong octahedral complex with azomethine ylide.	121
Figure 96. All known bis-adducts of isobacteriochlorins and bacteriochlorins generated through 1,3-dipole cycloaddition.....	122
Figure 97. UV-visible (green) and fluorescence (orange) spectra of 82 ...	125
Figure 98. UV-visible spectrum showing the tyrosine modified peptide (orange) in DMSO, peptide aza-BODIPY conjugate before purification (blue) and after purification (grey) in methanol.....	132
Figure 99. Normalised absorbance changes of 10 μ M PBS p.H 7.4 solution of aza-BODIPY 40 , ICG and methylene blue under continuous	

irradiation with NIR light band pass filter 685-733 nm for 60 minutes.	134
Figure 100. Highlighted tyrosine residues in the amino acid sequence for BSA protein. ³¹⁴	136
Figure 101. Proposed electrophilic aromatic substitution of tyrosyl moiety with diazonium linker.....	137
Figure 102. UV-visible spectrum of conjugate 91 after purification in PBS pH 7.4 solution, showing BSA (280 nm) and the azo linkage (360 nm).	137
Figure 103. Optical colour difference for diazonium linker tyrosine modified BSA conjugate 91 and three BODIPY-BSA conjugates 92a/b/c	138
Figure 104. Normalised UV-visible and fluorescence spectra of 92a , 92b and 92c in PBS solution pH 7.4.....	140
Figure 105. SDS-PAGE of conjugates 92a-c	141
Figure 106. MALDI-TOF of conjugate 92a - molecular weight increase 909 and <i>ca.1.73:1</i> (<i>BODIPY/BSA</i>).	142
Figure 107. MALDI-TOF of conjugate 92b - molecular weight increase 1062 and <i>ca.1.51:1</i> (<i>RedBODIPY/BSA</i>).....	142
Figure 108. CLSM images of HeLa cells incubated with (A) control – BSA autofluorescence ($\lambda_{ex} = 405$ nm), (B) BODIPY-BSA 92a conjugate ($\lambda_{ex} = 488$ nm), (C) RedBODIPY – BSA 92b conjugate ($\lambda_{ex} = 513$ nm) and (D) Aza-BODIPY – BSA 92c conjugate ($\lambda_{ex} = 633$ nm).....	143
Figure 109. Normalised UV-visible (blue) and fluorescence (orange) spectra of 94 in MeCN.	147
Figure 110. Photostability evaluation with NIR light illumination for 1 hour.	148
Figure 111. MO diagrams to show the HOMOs and LUMO of conjugate 94 and aza-BODIPY 46	149
Figure 112. Projection of frontier orbitals for guanidinium and its mesomeric effect on the aza-BODIPY core.....	150
Figure 113. HOMO and LUMO gaps of conjugate 94 and aza-BODIPY 46	151
Figure 114. A) Antibody (IgG2A) displacement concentration curve obtained for 94 in Jurkat.CXCR4 cells, ($n = 3$). B) CXCR4 expression in U87-CXCR4 (pink curve) vs U87 (blue curve) cells as determined by flow cytometry.	152
Figure 115. Calculated total corrected cellular fluorescence (TCCF) from confocal images of three different concentrations incubated with	

U87.CXCR4.....	153
Figure 116. CLSM images of U87.CXCR4 (CXCR4+) cells incubated with three concentrations of conjugate 94 and U87 (CXCR4-) cells incubated with 5 μ M ($\lambda_{\text{ex}} = 633$ nm).....	154
Figure 117. CLSM images of the co-localisation of FITC antibody ($\lambda_{\text{ex}} = 488$ nm) and conjugate ($\lambda_{\text{ex}} = 633$ nm) in a duel channel system.	155
Figure 118. Z-stack of the co-localisation experiment of FITC antibody ($\lambda_{\text{ex}} = 488$ nm) and conjugate ($\lambda_{\text{ex}} = 633$ nm) in a duel channel system. .	155
Figure 119. Calculated total corrected cellular fluorescence (TCCF) from the confocal images of co-localisation of FITC antibody and conjugate.	156
Figure 120. Z-stack of CXCR4+ and CXCR4- cells incubated with aza-BODIPY	157
Figure 121. Structure of PD-based re-bridging reagent.	159
Figure 122. SDS-PAGE of the conjugate with denaturing at 90 °C for 3 minutes (A &C) and without denaturing (B &D).	161
Figure 123. Z-stack of BT-474 (HER2+) cells incubated with FAC 98 ...	161
Figure 124. Z-stack of MDA-MB-468 (HER2-) cells incubated with FAC 98	162
Figure 125. Proposed mechanism for observed aggregation of conjugate: a) Formation of <i>H</i> -dimer, b) Non-covalent interaction, redistribution and non-stoichiometric.....	162
Figure 126. Photostability study for aza-BODIPY 68 and ICG in PBS (pH 7.4).	163
Figure 127. UV-visible (blue) and fluorescence (orange) spectra of conjugate 99 in PBS solution pH 7.4.....	165
Figure 128. SDS-PAGE of (from left to right): ladder / functionalised trastuzumab 97 / conjugate 99	165
Figure 129. CLSM images of BT-474 (HER2+) and MDA-MB-468 (HER2-) incubated with 5 μ M conjugate 99 and control.....	166
Figure 130. Z-stack images following 30 minutes incubation at 4 °C of 99 with BT-474 (HER2+) cells. Excitation at 633 nm by HeNe laser. ..	167
Figure 131. Z-stack images following 30 minutes incubation at 4 °C of 99 with MDA-MB-468 (HER2-) cells. Excitation at 633 nm with HeNe laser.	167
Figure 132. Calculated total corrected cellular fluorescence (TCCF) from the confocal images of BT-474 (HER2+) and MDA-MB-468 (HER2-) cells incubated with 99	168

Table of Tables xxii

Table 1. List of most commonly used FDA approved fluorescence agents for fluorescence guided surgery and their most intense absorption and emission wavelengths.....	7
Table 2 . List of chemically modified fluorescence probes used for laboratory research and their most intense absorption and emission wavelengths.	10
Table 3. Characteristics of an optimised NIR fluorescence probe: NIR emission, photostable, conjugatable, water soluble, low toxicity and ease of synthesis.	44
Table 4. The absorption, excitation and emission wavelength (nm) of BODIPY 1-13.....	55
Table 5. Stages of successful synthesis of aza-BODIPYs and their relevant precursors.	77
Table 6. Overview of functionalities investigated for aza-BODIPY conjugation to biological molecules.....	127
Table 7. UV-visible spectroscopic stoichiometric calculation before and after purification of peptide aza-BODIPY conjugate 90	133
Table 8. Fluorescence quantum yields of BODIPYs in methanol. Quantum yields were determined using two standards: fluorescein ($\Phi_f = 0.96$ in 0.1 M NaOH) ³¹¹ and rhodamine B ($\Phi_f = 0.31$ in water). ³¹²	135
Table 9. Stoichiometric calculation of molecule to protein ratio.	139
Table 10. Photophysical properties of aza-BODIPY 46 and conjugate 94 in acetonitrile at 298 K. The two reference systems used were cross-calibrated to fluorescein ($\Phi_f = 0.98$ in 0.1 M NaOH) ³¹¹ and rhodamine B ($\Phi_f = 0.30$ in water). ³¹²	148
Table 11. Photophysical properties of aza-BODIPY 68 at 298 K.	164
Table 12. Summary of NIR fluorescence imaging conjugates.	301

Table of Equations xxiii

Equation 1. Beer-Lambert law, A = absorption, ϵ = molar absorption coefficient, c = concentration, l = length of pathway. $A = \epsilon cl$	132
Equation 2. Rearrangement of the Beer-Lambert law to calculate the concentration. $c = A/\epsilon l$	132

1. Introduction

1. Fluorescence guided surgery

Surgery is the most common treatment for solid tumours.¹ Traditional surgery mostly relies on direct visualization of the patients' tumour, however there are often blurred surgical margins, where it becomes increasingly difficult for surgeons to decide whether to resect or leave tissue. In most cases, local recurrence and poor prognoses observed in patients are largely due to positive surgical margins, whereby unnoticed tumour tissues are not excised, necessitating re-excision. This limitation in surgery leads to poor outcomes in patients for several different types of cancers, such as head and neck², colorectal³, breast^{4,5}, and bladder cancer.⁶

Conventionally, biomedical imaging such as X-ray fluoroscopic imaging, ultrasound, MRI, SPECT and PET is often used before the operation.^{7,8} However, MRI only provides gross morphological information rather than functional information, with other techniques suffering from poor resolution. Moreover, imaging techniques such as ultrasound lack selective targeting to show specific visualisation of certain tumour tissue, whereas, X-ray fluoroscopic imaging, PET and SPECT expose the patient to ionising radiation. In addition, due to the high cost of these intraoperative imaging systems, their use is often limited to specialised medical conditions.⁹ The actual resection of tumorous tissue utilising the aforementioned imaging techniques has been exclusive to the surgeon's perception. Additional factors such as colorimetric and textural information, that would otherwise give a clearer image, are often unavailable to the surgeon, thereby limiting imaging to pre-operative planning and verification steps.

NIR fluorescence guided surgery is of growing interest to surgeons, due to the prospect of real-time imaging that the technique offers. In 2011, the first *in vivo* folate-fluorescein conjugate was applied successfully for use in fluorescence guided imaging in visualising ovarian cancer intraoperatively.¹⁰

Fluorescence guided surgery (FGS) works *via* the administration of a fluorescent probe; upon excitation by light, the tumour tissue fluoresces. The signal is then collected through an optical system, generating fluorescence images in the surgeon's display, as

demonstrated in **Figure 1**.¹¹ The use of far red / near infrared (NIR) excitation and emission is preferred due to enhanced tissue penetration by light in this region.

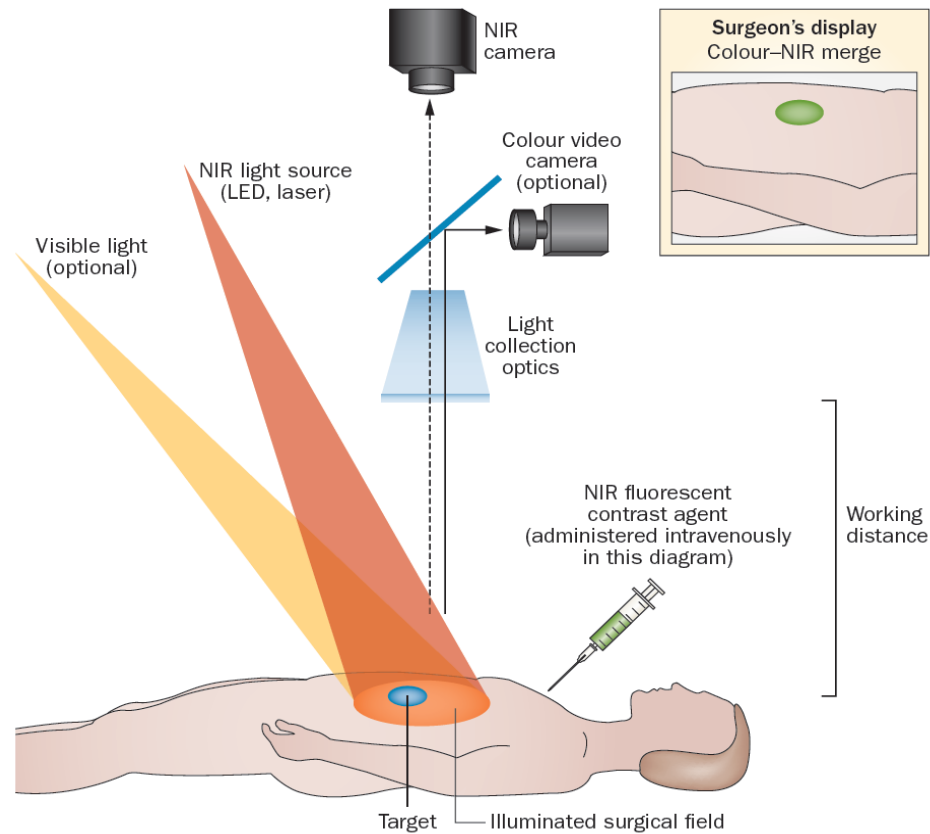


Figure 1. NIR fluorescence system to visualised targeted tumours.¹¹

In recent years, several intraoperative NIR fluorescence guided surgery systems have been developed for pre-clinical and clinical studies. Those studies confirmed the new systems have greatly improved the visualisation of tumours and have been clinically approved by the US Food and Drug Administration (FDA). Systems such as Novadaq SPY and the Photodynamic Eye imaging system have been applied to the detection of NIR fluorescence, and the latter was used in identifying cancerous sentinel lymph nodes (SLNs) in breast tumours. Due to recent advances in imaging systems technology, a small and simple unit now has the capability to detect both white light and fluorescence signals, with fast processing times and high sensitivity in real time. Images can be superimposed for a facile operative system that has become a more attractive proposition than traditional imaging methods for clinical applications.¹²

These systems allow the visualisation of tumours through the accumulation of the

fluorescence imaging agent in or around the tumour. This technique is of interest for applications in colorectal, glioma and breast cancer treatment.¹¹ In colorectal cancer, small neoplasia or early stage cancers are often missed by endoscopy¹³ because they are extremely difficult to identify under white light. Whereas, in glioma and breast cancer, brain¹⁴ and breast conserving surgeries are often performed, for the benefit of the patient, and accurate surgical margin identification is strongly dependent on visualisation of tumour and this factor is essential for the patients prognosis.¹⁵

1.1 NIR vs UV-vis

Overall, FGS can provide real time visualisation, which is superior in resolution and has high sensitivity, it can also significantly reduce the cost of imaging. These favourable properties are conducive to clinical translation, making this technique attractive for clinical use in tumour margin diagnosis. Despite the many benefits of this imaging technique, one of the major drawback is the penetration depth, this is due to the fact that many of the FDA approved, commercial fluorophores often only fluoresce in the visible light range. UV and visible light generally has much weaker penetration through tissues, hence reducing the overall fluorescence signal, resolution and sensitivity of the targeted fluorophore. However, these limitations can be addressed with the use of NIR FGS.

NIR fluorescence has many advantages over conventional lower wavelength fluorescence for *in vivo* fluorescence imaging applications. This is because NIR fluorophores can provide both deeper tissue penetration and enhanced signal to noise ratios. The depth of NIR detection can range from a few millimetres to centimetres, whereas for visible-range fluorescence this parameter is only a few micrometres. Background fluorescence caused by autofluorescence and scattering of light from water can also be greatly reduced to provides a stronger contrast between healthy and neoplastic tissue; allowing improvement in diagnostic accuracy and preoperative planning, preventing incomplete resection and preserving healthy tissue (**Figure 2**). These overall benefits of NIR fluorescence suggest the possibility of revolutionising the application of FGS in surgical treatments in oncology.

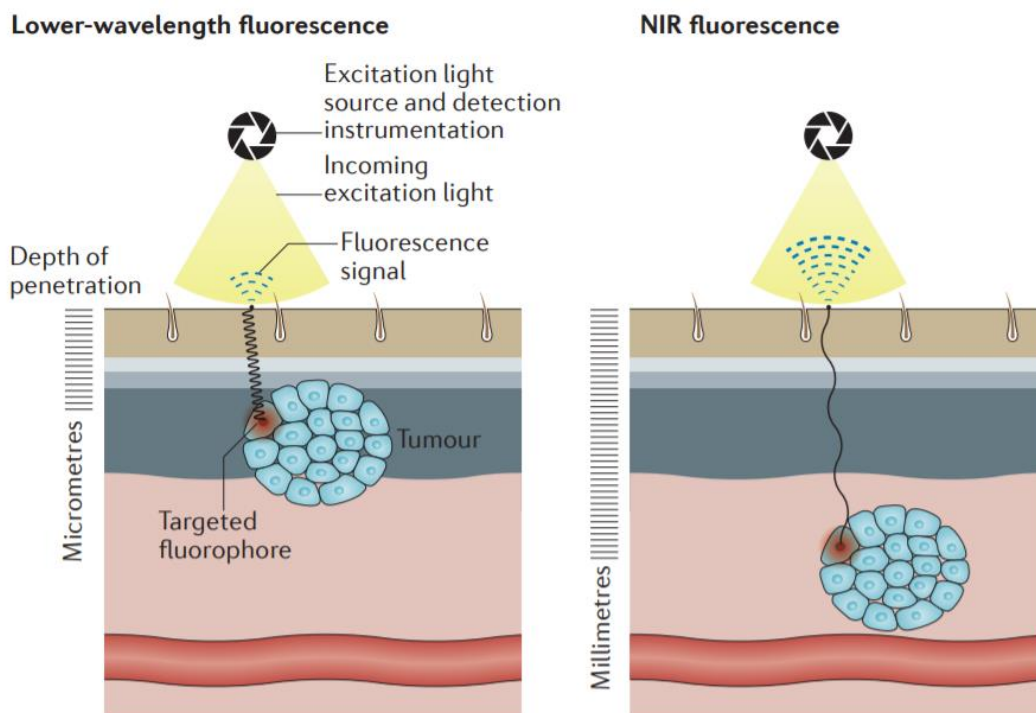


Figure 2. NIR fluorescence vs lower wavelength fluorescence.¹⁶

1.2 Colorectal cancer, glioma, breast cancer and lymph node metastasis detection

Colorectal cancer is a chronic disease and the third most abundant cancer worldwide, with an estimated 1 million new cases diagnosed and treated annually.¹⁷ It has drawn much attention in western countries due to its high incidence and rapidly increasing occurrences among the younger generation.¹⁸ Surgery is currently the most commonly used therapy for cancer, with an overall success rate of 45 %.¹⁹ In particular, it is the most common treatment prescribed for solid colorectal tumours.

Local excision of tumours can be performed either using an anastomosis or colostomy,²⁰ with both of these processes causing great discomfort and inconvenience. Despite advances in surgical interventions including techniques such as laparoscopy and other robot assisted surgeries,²¹ the overall rate of curing the cancer through surgery has remained stagnant, as a result of underdeveloped intraoperative visualisation.²²

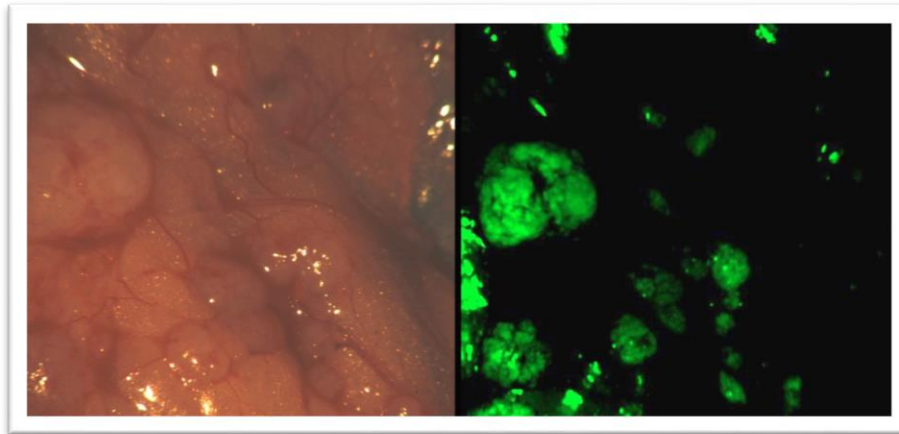


Figure 3. NIR Fluorescence guided surgery providing a contrasting imaging to detect surgical margins.¹

NIR FGS has also become a rapidly expanding field of interest in neurosurgery. Due to the complexity and delicate nature of the nervous system, surgical operations require extreme precision and dexterity, and have been recognised as a very demanding surgery to perform. With brain surgery careful preoperative planning is required, highlighting the importance of diagnostic tools used to image tumours prior to surgical treatment. In brain tumours, safe maximal resection is crucial to avoid debilitating morbidity caused by damage of brain tissues.²³ Conventionally, brain tumours are detected with CT and MRI scans followed by surgical resection of the tumour. However, the conventional imaging techniques used lack any intraoperative information, making the discrimination of tumour tissue challenging, consequently the average survival rate remains relatively low.²⁴ In recent years, NIR FGS of malignant gliomas has been applied and has shown promising results in determining the margin of tumours, thereby allowing radical resection to become much easier and, as a result, the use of FGS has now become accepted as a potential treatment for brain tumours with many ongoing clinical trials underway.^{25,26}

Similarly, many breast tumours are nonpalpable, making the diagnosis and surgery more difficult, resulting in a generally wide range in the positive margin that the surgeon can perform the resection on.^{27,28} SLN mapping is also a standard diagnostic technique requested for breast cancer to monitor for potential metastasis and as an alternative to conventional methods, NIR FGS along with fluorescence imaging can be used for SLN mapping to improve this diagnostic technique.²⁹ For breast cancer, flap reconstructive surgery can be followed upon the removal of the tumour. The success of

the surgery is often dependent on vessel identification and selection, which can be improved with the use of NIR fluorescence imaging.³⁰ Under NIR fluorescence angiography monitoring of the venous outflow and vessel identification have been carried out in clinical trials and the results of those reconstruction surgery suggested an improvement in flap survival and patient outcome.³¹

Lymph node metastasis is closely related to advanced colorectal cancer.³² Although histopathological analysis is regarded as the gold standard for detecting lymph node metastases, limitations associated with it include unnecessary resection of all anatomically susceptible lymph nodes.^{33,34}

In some clinical situations, SLN surgery would be carried out, as it provides better prognosis for patients.³⁵ Although SLN surgery has shown success in reducing unnecessary removal of lymph nodes, it is limited to breast cancer³⁵ and malignant melanoma³⁶ due to the complexity of lymphatic anatomy in other locations. In addition, around 20 to 30% of colorectal cancer patients who received a pathological negative result go on to develop lymph node metastases, and with localised cancer the acute metastases remain undetected by current pathological evaluation.³⁷ Currently, SLN mapping dye and tracers³⁸ are limited due to poor visualization below surface tissue and exposure to ionizing radiation respectively. In contrast, NIR imaging can provide sentinel lymph node mapping to evaluate the level of metastasis and provide corresponding treatments.

For colorectal cancer, NIR fluorescence guided SLN mapping has been extensively studied³⁹⁻⁴¹, showing significant reductions in the use of anaesthesia, cost and time of surgery.¹ Most importantly it has resulted in the improvement of intraoperative SLN detection.

Despite the major advance in alternative methods such as spectroscopic imaging, optical coherence tomography and photoacoustic imaging, these techniques have not fully materialised for clinical applications.

1.3 Development of fluorophores for cancer imaging

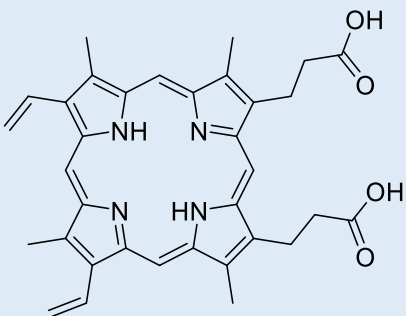
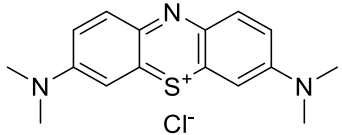
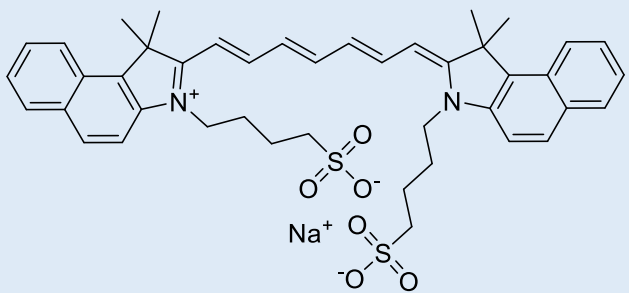
Although NIR FGS has many potential surgical applications for the treatment of many cancers, there are several remaining limitations that hinder the advancement of the

technique. These include photobleaching and photoinstability, autofluorescence, lack of targeting, poor tissue penetration of light, and toxicity issues with inorganic compounds. This is especially true of the current FDA approved fluorescence probes, which have no specificity for carcinomas. The working mechanism of fluorescence probes can be classified into the following two categories of non-specific, and targeted probes.

1.3.1 FDA approved non-specific probes

Currently, of the three most commonly used FDA approved fluorescence probes, none are specific to any cancer include, these are 5-ALA induced PPIX, methylene blue and indocyanine green (ICG) as shown in **Table 1**.

Table 1. List of most commonly used FDA approved fluorescence agents for fluorescence guided surgery and their most intense absorption and emission wavelengths.

Fluorescence Probes	Chemical Structure	λ_{abs} (nm)	λ_{em} (nm)
5-ALA induced PPIX		406	635
Methylene blue		668	688
ICG		800	810

1.3.1.1 5-Aminolevulinic acid (ALA) induced protoporphyrin-IX

5-ALA induced PPIX has been extensively studied for intraoperative identification of malignant gliomas. Stummer *et al.* reported a significant increase in complete resection rate, fewer recurrences and improved progression-free survival rate up to six months upon the use of orally administered 5-ALA to induce a PPIX fluorescence for intraoperative visualisation of brain tumours.¹⁴ Although PPIX is widely applied in gliomas and bladder cancers⁴², it is less suitable for colorectal cancers due to the high endogenous levels of PPIX in primary tumours and metastases of colorectal cancer, leading to autofluorescence.⁴³

Additionally, as the concentration of PPIX production depends on the sequential enzymatic pathway, factors such as temperature, pH, levels of oxygenation and glucose, and the inhibition of rate limiting enzymes can affect production of PPIX.⁴⁴ As these factors can vary between individuals, this could subsequently lead to the misidentification of tumour tissue. Fluorescence decay of the PPIX can also lead to reducing efficiency of the fluorescence properties with processes such as photobleaching causing the tumour fluorescence to quench over the course of an operation.⁴⁵ In addition, the fluorescence signal produced by PPIX is around 635 nm, limiting the tissue penetration of the exciting and emitted light. With this combination of limiting factors, PPIX has become less popular among the different classes of fluorescence probes.

1.3.1.2 Methylene blue

Methylene blue has been used previously as a visible blue dye for staining insulinomas and parathyroid glands⁴⁶, and has since been used as a visible clinical blue dye in surgery. Methylene blue was first introduced as a NIR fluorescence probe for imaging studies with a fluorescence of around 700 nm⁴⁷⁻⁴⁹ and it has since been used to provide contrast in the gastrointestinal tract by Ashitate *et al.*⁵⁰ Despite this, methylene blue has several limitations including fluorescence quenching upon increased concentration, high NIR autofluorescence, and observed toxicity.⁴⁹ Methylene blue can also undergo a reduction reaction to leucomethylene blue, leading to a quenching of fluorescence, as demonstrated in **Figure 4**. There is also significant light scattering from the excitation

light (656 to 678 nm), which interferes with the observed fluorescence, and thus inhibits surgical diagnosis.

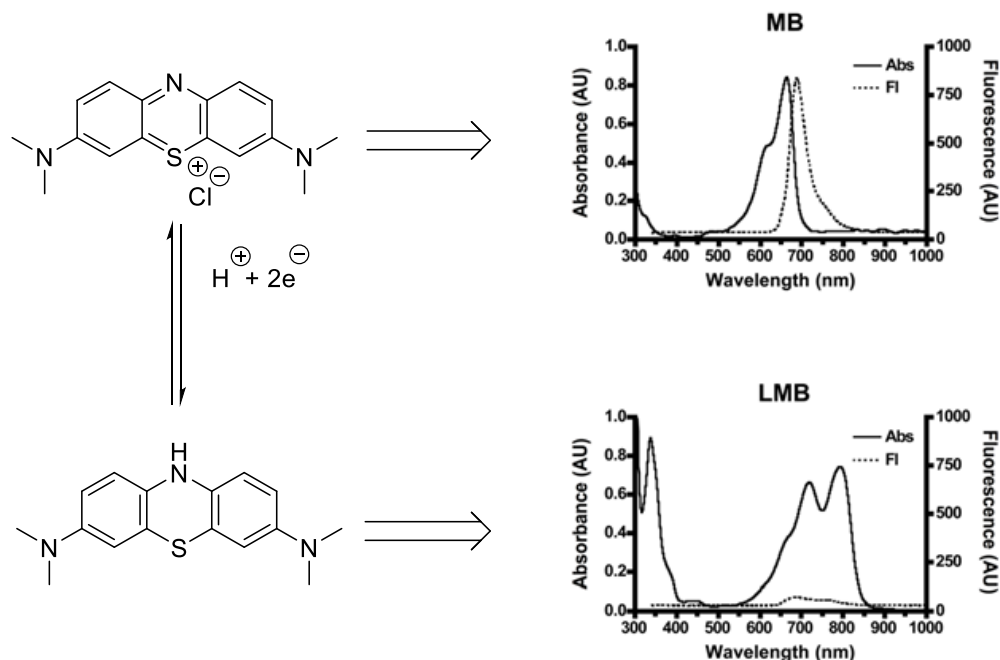


Figure 4. Possible interconversions of methylene blue to leucomethylene blue, causing quenching of fluorescence.⁴⁹

1.3.1.3 Indocyanine Green

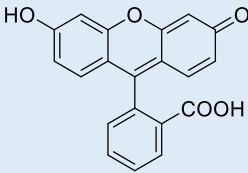
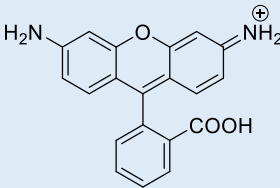
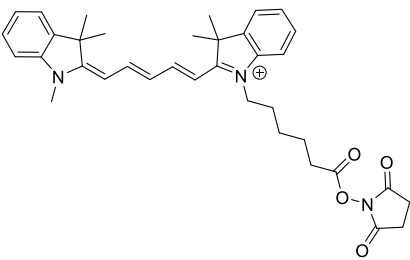
ICG has become the most popular NIR fluorescence probe due to its availability, low toxicity and FDA approval. The use of ICG in NIR fluorescence for the visualisation of colorectal hepatic metastases was demonstrated by Ishiazawa *et al.* Their results clearly showed a rim of fluorescence around the hepatic metastases intraoperatively. Crucially, some background signal in the surrounding tissue was observed several hours to days after administering.^{51,52} Due to the hydrophobicity of ICG, it has the tendency to bind to proteins in plasma, confining it to intravascular area making it especially suited for angiography and lymphography applications. Despite its popularity, this probe still suffers limitations including an inability to image deep tumours (>8 mm below the surface), an unstable photochemical nature with changes in pH environment,⁵³ and lack of selectivity for colorectal carcinomas. Furthermore, due to the chemical structure of ICG, it is synthetically challenging to modify in order to

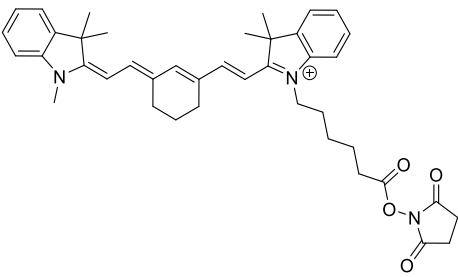
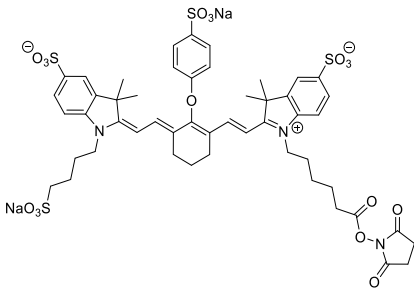
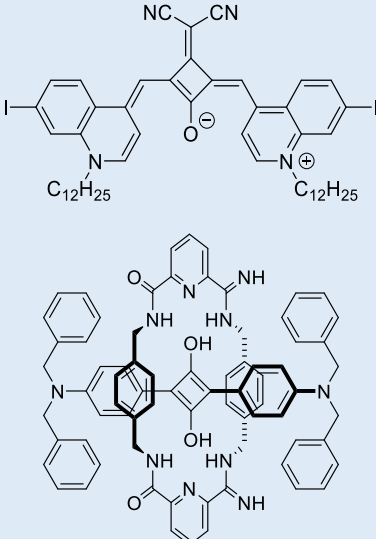
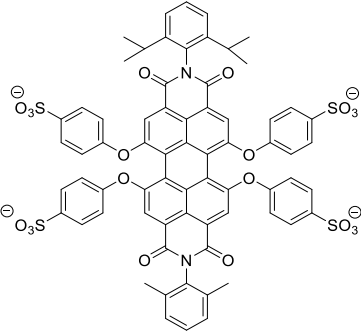
provide functionalised moieties without interfering with the optical performance⁵⁴, limiting its potential as a selectively targeted fluorescence probe.

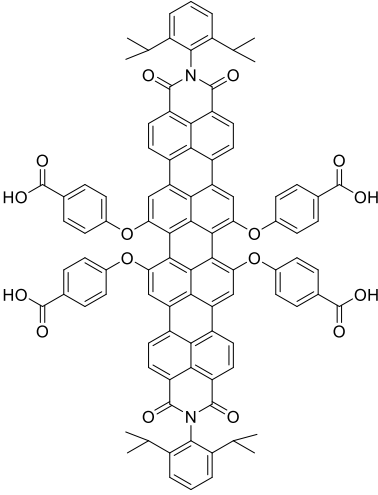
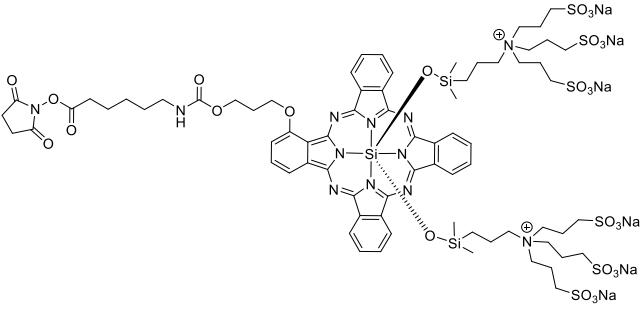
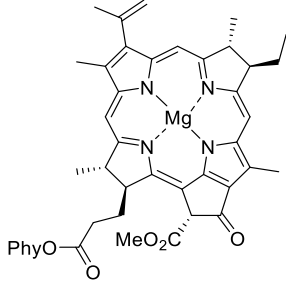
1.3.2 Developments of preclinical NIR fluorescence probes

Improved photostability and photophysical properties has also been another important preclinical development for NIR fluorophores. The most common strategies rely on extending the aromatic system, as well as increasing the structure rigidity of the fluorophores. These led to the developments of NIR fluorophores such as fluorone dyes, cyanine dyes, squaraines, rylene dyes, BODIPY, phthalocyanine and porphyrin derivatives as shown in **Table 2**.

Table 2 . List of chemically modified fluorescence probes used for laboratory research and their most intense absorption and emission wavelengths.

Fluorophore class	Chemical Structure	λ_{abs} (nm)	λ_{em} (nm)
Fluorone dyes Fluorescein		494	521
Rhodamine		543	627
Cyanine Cy5		650	670

<p>Cy7</p>	 <p>The structure shows a cyanine dye core consisting of two indole rings connected by a trimethine chain. The right-hand indole ring is substituted with a long alkyl chain (hexyl) and a succinimidyl ester group.</p>	<p>743</p>	<p>767</p>
<p>IRDye®800CW</p>	 <p>The structure shows a cyanine dye core with two indole rings. The left ring has a sodium sulfonate group (SO₃⁻Na) and a long alkyl chain (hexyl) with a sodium sulfonate group (NaO₃S). The right ring has a sodium sulfonate group (SO₃⁻) and a succinimidyl ester group.</p>	<p>778</p>	<p>794</p>
<p>Squaraine</p>	 <p>The top structure is a squaraine dye with a central squaraine ring substituted with two diethylamino groups (C₁₂H₂₅) and two cyano groups (NC=CN). The bottom structure is a more complex squaraine dye with a central squaraine ring substituted with two diethylamino groups (C₁₂H₂₅) and two hydroxyl groups (OH).</p>	<p>900</p>	<p>922</p>
<p>Rylene dyes</p>	 <p>The structure shows a rylene dye core consisting of a central naphthalene ring substituted with two diethylamino groups (N(CH₂CH₃)₂) and two sodium sulfonate groups (SO₃⁻Na).</p>	<p>567</p>	<p>670</p>

			
BODIPY		662	671
Porphyrins and phthalocyanine derivatives IRDye®700DX		680	687
Bchl a		748	764

1.3.2.1 Fluorescein

Fluorescein has been used as a fluorescent dye to highlight tumours since 1947 and it was first applied to localised gliomas in neurosurgery. Fluorescein antibody conjugates have also been reported for specific visualisation of colorectal carcinomas by Folli *et al.* through selective targeting, however, slow clearance has led to high background fluorescence in the blood and low tumour contrast.⁵⁵ Another disadvantage of fluorescein and many of its derivatives is that they are pH sensitive. This class of compound can exhibit multiple ionic equilibria, and under acidic conditions the

fluorescence would be significantly lowered or even entirely quenched due to the formation of cationic species or the corresponding spiralactam as shown in **Figure 5**.⁵⁶ Once again despite some demonstrations of the feasibility of fluorescein as a fluorescent probe, it suffers from high autofluorescence and has poor light penetration due its low wavelength of emission, making the class of dye less suitable as a fluorescence probe in NIR FGS.

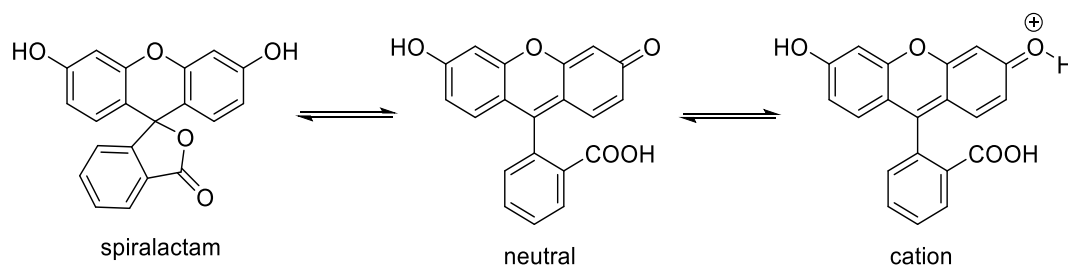


Figure 5. Ionisation equilibria of fluorescein

1.3.2.2 Rhodamine

Rhodamine has potential as an effective probe due to its high fluorescence quantum yield, yielding good contrast in FGS. Derivatives of the dye have been of particular interest for bioimaging with novel rhodamine derivatives reported as bioconjugates with dipeptide ligands⁵⁷ and inhibitors^{58,59} to selectively target ovarian, fibrosarcoma and breast cancer cell lines. However, the toxicity of rhodamine has been extensively studied over the last two decades, evidence has suggested that the toxicity level observed was unsuitable for use as a bio-imaging agent.⁶⁰⁻⁶² This class of compounds are similar to fluorescein as they also suffer the formation of lactone under acidic conditions resulting in loss of fluorescence.⁶³ Many structural modifications has been investigated to improve absorption and emission in the NIR regions, however, instability remain a challenge.

1.3.2.3 Cyanine dyes

Cyanine dyes have become a popular choice for use in fluorescence imaging due to their availability of conjugatable moieties and relatively low cost. Cyanine fluorophores consist of two heterocyclic aromatic ring systems with a polymethine bridge in between. One major advantage of cyanine dyes is the tuneable wavelength, achieved by extending conjugation with the polymethine bridge. The most common

cyanine dyes with extension of polymethine are pentamethine (Cy5) and heptamethine (Cy7) allowing the extension of the fluorescence into the far red and NIR regions. Many Cy5 conjugates have been synthesised with a focus on increased targeting specificity for various cancerous tissue.⁶⁴ Cy7 conjugates have been reported by Cheng *et al.* using AGFSLPAGC peptide ligands to target pancreatic tumours.⁶⁵ Other bioconjugations have also been performed by Yang *et al.* using the CD20 antigen to target Non-Hodgkin's lymphoma.⁶⁶ Among the cyanine dyes, IRDye[®]800CW is one of its most popular derivatives, due to its commercial availability, it has previously been used for many preclinical studies of fluorescence imaging of tumour cells; unfortunately most cyanine dyes suffer from rapid photobleaching and low fluorescence quantum yields⁶⁷ (**Figure 6**). Despite the volumes of research on these dyes, poor photostability and high levels of photobleaching, raise questions about how effective cyanine dyes are as fluorescent probes in a surgical operative environment, IRDye[®]800CW conjugates have, however, been among the few probes that have been used in clinical trials for NIR fluorescence imaging.

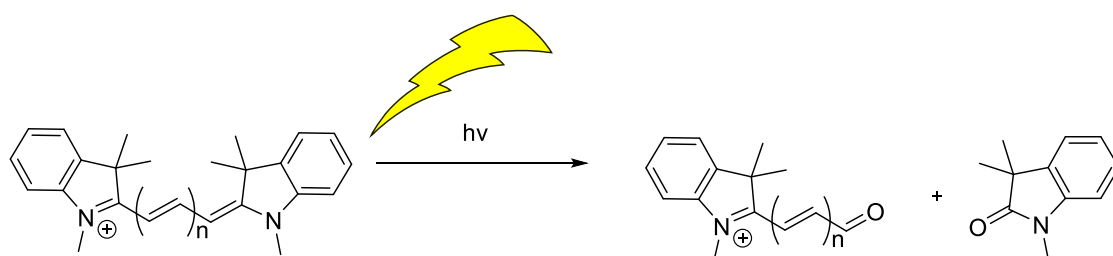


Figure 6. Proposed photobleaching adducts of cyanine dyes.

1.3.2.4 Squaraines

In search of NIR fluorophores, squaraines were discovered as one of the many classes of dyes with a NIR range emission that have been applied as bioimaging agents.⁶⁸ Due to the rigidity of the structure, squaraines possess good photostability as well as sharp and intense absorption bands. Conventionally, this series of dyes have an emission range below 700 nm, however Mayerhöffer *et al.* in 2012 discovered that halogenation of squaraines causes a bathochromic shift into the NIR region leading to more interest in this series of dyes.⁶⁹ However, major drawbacks remain, as the series of dyes still suffer from two attributes that most NIR dyes experience limiting their use in NIR FGS. Firstly, squaraines have poor water solubility giving them a propensity to aggregate, which could result in poor absorption and limited biological applications.⁷⁰ Secondly,

their susceptibility to attack by strong nucleophiles on the central squaraine ring, deactivating their optical properties, an effect that has been utilised as a detection method for thiols⁷¹ (**Figure 7**).

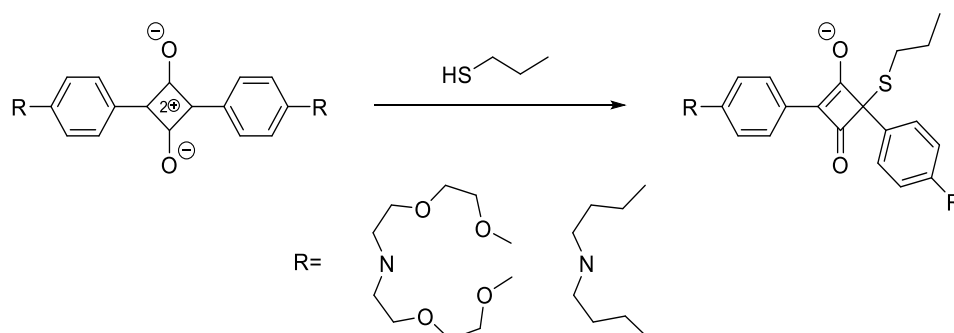


Figure 7. Thiol induced formation of non-fluorescence adducts based on nucleophilic attack at electron deficient central cyclobutane ring.

1.3.2.5 Rylene dyes

Rylene dyes are based on the rylene framework, consisting of repeating naphthalene units to form perylene and other derivatives. This series of dyes has been widely used in organic materials such as optoelectronic and photovoltaic devices, and light emitting diodes.⁷² This is due to their properties of tuneable wavelength allowing for a range of intense visible light absorptions, redox potentials, high photostability and high fluorescence quantum yields.⁷³ However, their biological applications have been limited due to poor solubility in aqueous solutions and the hydrophobic core having a tendency to form aggregates that could result in significant changes in optical properties as demonstrated in **Figure 8**.⁷⁴ This major limitation has been investigated by Margineanu *et al.*⁷⁴ and Müllen *et al.*^{75,76} in their studies into water solubilising rylene through modification of the diimide and bay region. Since water soluble rylene has only been developed recently, their *in vivo* behaviour has still to be investigated.

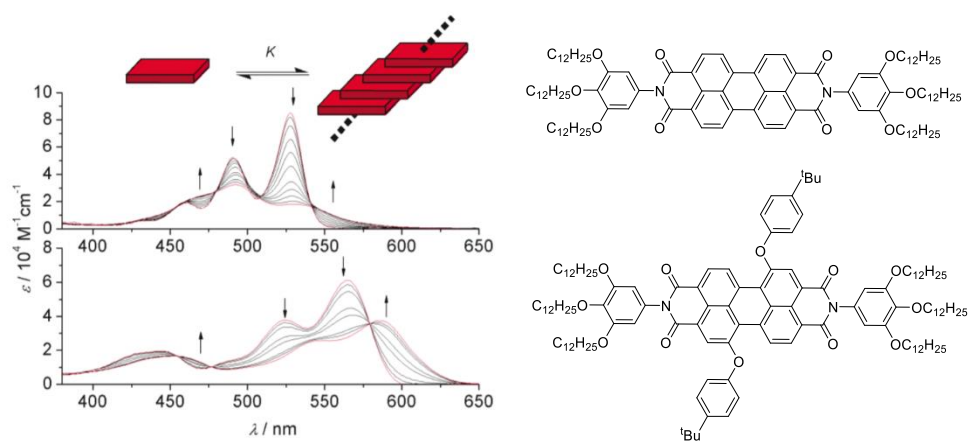


Figure 8. Changes in optical spectrum of rylene as a function of concentration.

1.3.2.6 Boron-dipyrromethene (BODIPY)

BODIPY is a class of fluorophore, which has received much interest in connection with their fluorescence properties and imaging applications. BODIPYs have a small Stokes shift, but with a high fluorescence quantum yield and high photostability. BODIPYs are widely deployed for many biological applications such as sensors and protein labelling.⁷⁷ Many commercial BODIPY dyes are available with bioconjugation functional groups, such as BODIPY FL, allowing conjugation to many biological molecules. However, despite the versatility of BODIPY for biological applications, most commercial BODIPYs generally absorb and fluoresce in the visible region, undermining its potentials for NIR FGS.

On-going research is being carried out to induce bathochromic shifts by heavy atom effects or extending the conjugation, but like most of the NIR fluorophores, extending conjugate can lead to aggregation and insolubility, therefore, progress for *in vivo* imaging application are yet to be reported.⁷⁸

1.3.2.7 Tetrapyrrolics - phthalocyanine and porphyrin derivatives

Tetrapyrrolic molecules such as porphyrins and phthalocyanines (Pcs) have also been extensively investigated for NIR fluorescence imaging due to their favourable optical properties. Porphyrins and Pcs are red and NIR emitting fluorophores with rigid aromatic structures. They have many advantageous photophysical properties making them suitable as NIR imaging agents, these include large virtual shifts, low levels of

photobleaching, high fluorescence quantum yields and tuneable wavelengths. Both classes of compound have been widely used as fluorescence imaging agents to study photodynamic therapy (PDT) mechanisms and, since many tetrapyrrolic molecules have now become commercially available, increased numbers of tetrapyrrolic compounds are used in clinical fluorescence imaging.⁷⁹ Among many of the commercial fluorescence dyes, IR Dye 700 DX is one of the more popular choices, with its structural origin being phthalocyanine based. Many cancer targeting bioconjugates have been synthesised for SLN mapping⁸⁰ and several types of cancer detection, such as breast⁸¹⁻⁸³, glioblastoma⁸⁴, lung⁸² and ovarian⁸⁵. In spite of the better photostability and decreased photobleaching rates in comparison to cyanine dyes, the functionalised moieties available for commercial purchase is restricted to an NHS ester only, meaning the chemodiversity for these dyes remain limited.

Despite ongoing efforts to introduce new NIR fluorophores, most suffer from a common problem, that is the modification strategies usually are accompanied by increased hydrophobicity leading to poor solubility in aqueous media. This can result in nonspecific binding and slow biological clearance. Hence, significantly restricting their overall application in biological environments.

1.4 Targeting strategies

Specificity and sensitivity of detection are important for imaging cancerous tissues. Targeting fluorophores usually requires conjugation of the fluorophore to tumour specific targeting units. Specificity can affect the imaging parameters as well as the amount of fluorescent dye that needs to be administered, it also provides more reproducibility and reliable discrimination of target tissues. Currently, the three commonly used, and FDA approved, fluorescent probes suffer from a lack of selectivity toward specific tumour tissues, limited by their chemodiversity for bioconjugation.

Currently, no targeted fluorophores under development have been FDA approved for clinical use in FGS, nevertheless, there are an increasing number of clinical trials employing targeted fluorophores. A variety of targeting strategies are under investigation at the present time. Targeted NIR fluorophores generally have a higher binding affinity toward a specific biomarker, such as overexpressed receptors, that are upregulated for cancerous cells.

Growth factor receptors are an example of a specific biomarker associated with cancer cells, which can be targeted by a variety of different targeting moieties such as small molecules, peptides, antibodies, small antibody fragments and proteins.⁸⁶ These moieties have been applied in the many diagnostic and therapeutic applications. Many new concepts such as activatable probes and multimodality fluorophores have also been developed as alternative targeting strategies (**Figure 9**).

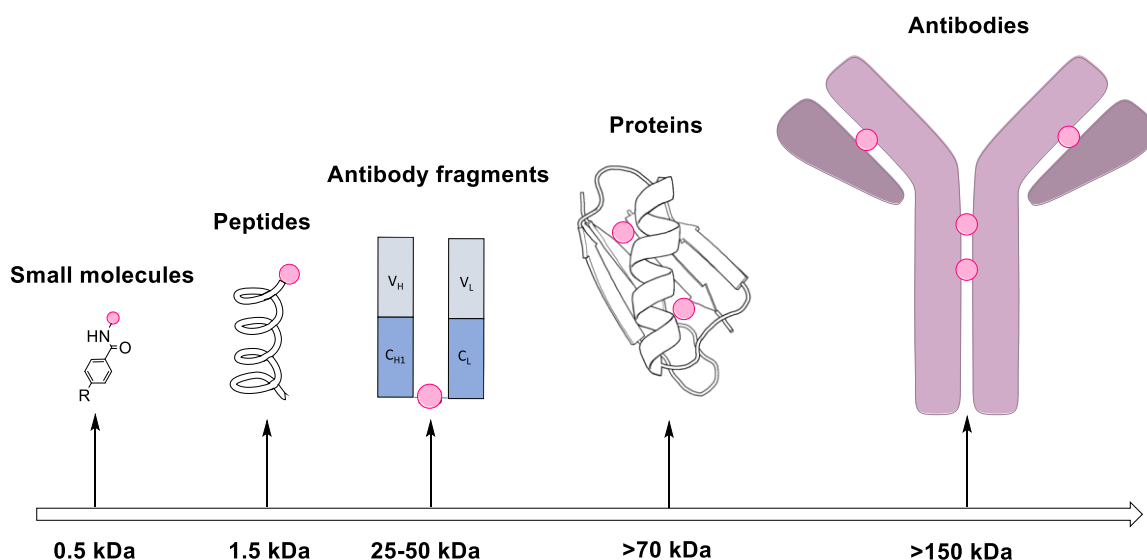


Figure 9. Targeting moieties for fluorophores applied in fluorescence imaging.

Introducing new fluorescent biomarker conjugates for clinical use is deemed challenging due to the many regulations and safety measurements required. In spite of these challenges, there have been attempts, including labelling of proteins with commercial dyes⁸⁷ and PET radionuclides⁸⁸ for preoperative visualisation. Most commercial fluorophores employed as targeting probes have been functionalised with coupling moieties reactive towards lysine residues.

1.4.1 Small molecule targeting

Small targeting molecules are low molecular weight (<900 Da) compounds that help to regulate biological processes. Small targeting molecules are advantageous, compared to large molecules such as antibodies, due to their favourable pharmacokinetic (PK) properties, providing fluorescence contrast at a much faster rate, thereby enabling rapid imaging after administration.⁸⁹ Conversely, small molecules are less amenable to chemical modification and conjugation, with even small structural manipulations

causing a negative effect in their targeting and PK properties. Many small molecules have been reported for selectively fluorescence imaging. Van Dam *et al.*¹⁰ performed sensitive and specific intraoperative detection of carcinomas of breast, lung and ovary, which expressed high level of folate receptor, with a fluorescein isothiocyanate (FITC) - folate conjugate – EC17, the group went on to carry out further detection of FR-a-positive ovarian cancer with a Cy7-folate conjugate – OTL38, reporting increases in signal to background ratio and other advantages of NIR over visible light fluorescence in imaging⁹⁰ (**Figure 10**).

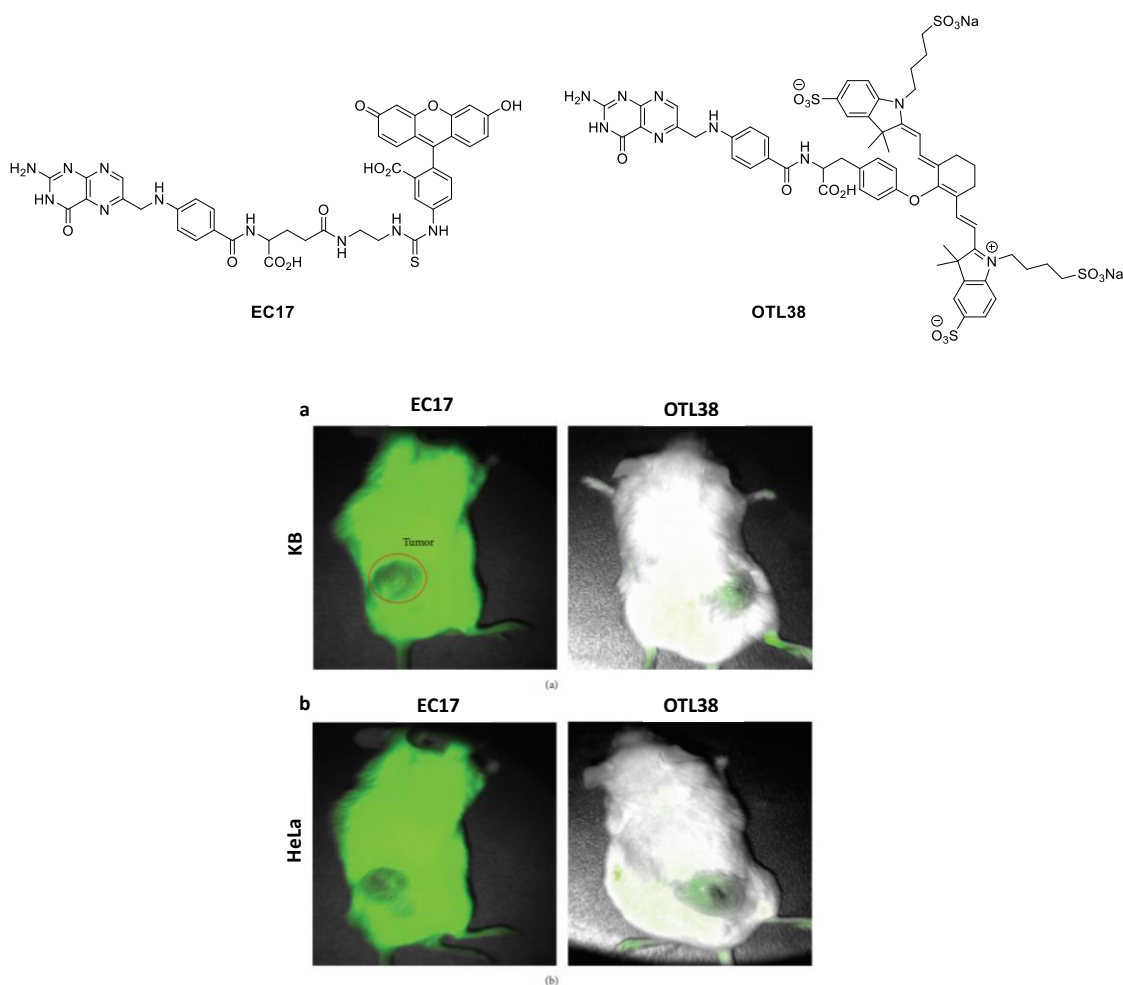


Figure 10. Signal to noise contrasts for *in vivo* tumor imaging with immurine model using EC17 (intense autofluorescence) and OTL38 (no autofluorescence). (a) Fluorescence imaging of KB tumor (b) Fluorescence imaging of HeLa tumor.

Other small molecules such as alkylphosphocholine (APC) analogues target cancerous specific uptake in lipid raft⁹¹ and CXCR4 receptor binding antagonist macrocycles series have also been utilised in glioblastoma⁹², breast⁹³ and colorectal⁹⁴ cancers.

1.4.2 Peptide targeting

Peptides are natural or synthetic chains of amino acids formed by peptide bond formation between carboxylic acid and amino groups of amino acids. The boundary between a peptide and a protein is the size of the molecule, typically being 50 amino acids or below to be classified as a peptide. The advantage of many small peptides over larger biomolecules for targeting receptors is the favourable biodistribution resulting in higher uptake, as well as rapid clearance, in the bloodstream. Moreover, peptides are known to be superior in penetrating cells due to their increased capillary permeability.⁸⁹ Peptides can also be readily synthesised with well established techniques such as solid phase peptide synthesis, allowing facile structural manipulation that can optimise or enhance the specificity for a target.⁹⁵

However, there are still several limitations hindering the use of peptides as targeting units. These include the interaction with peptidases in complex biological environments⁹⁶, nonspecific binding for receptors⁹⁷ and low loading ratios of fluorophores.⁹⁸

Peptides offer an attractive targeting moiety for colorectal cancer related polyps. A well-developed cyclic peptide GE-137 labelled with a Cy5 dye was used to target human c-Met overexpressed in colorectal cancer (**Figure 11**). This was applied to selectively discriminate polyps from normal colorectal tissue using NIR fluorescence in an endoscopic imaging system⁹⁹ (**Figure 12**).

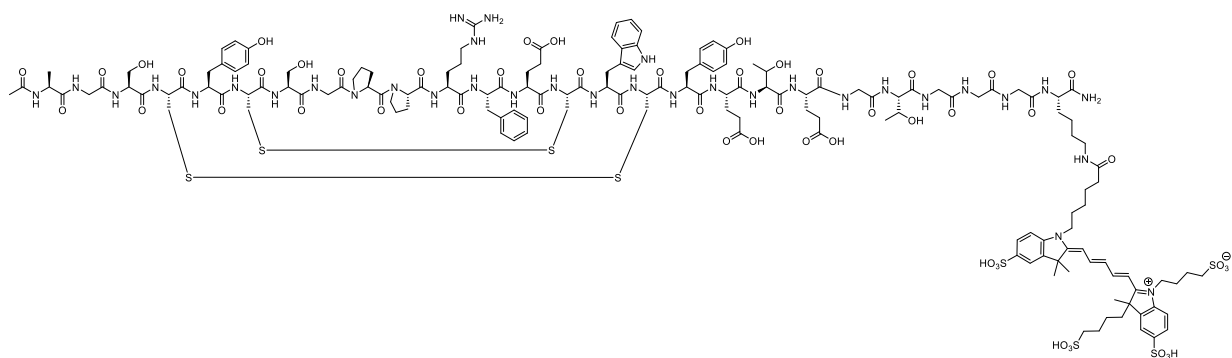


Figure 11. Chemical structure of cyclic peptide GE-137 labelled with Cy5 dye.

Although, this study displayed the peptides high affinity for c-Met, with no overlap of autofluorescence, there were limitations in the study due to the requirement for a

customised fluorescence endoscopy system and the inadequacy of the dye used, since Cy5 has a high propensity towards photobleaching, a characteristic of many cyanine dyes.¹⁰⁰

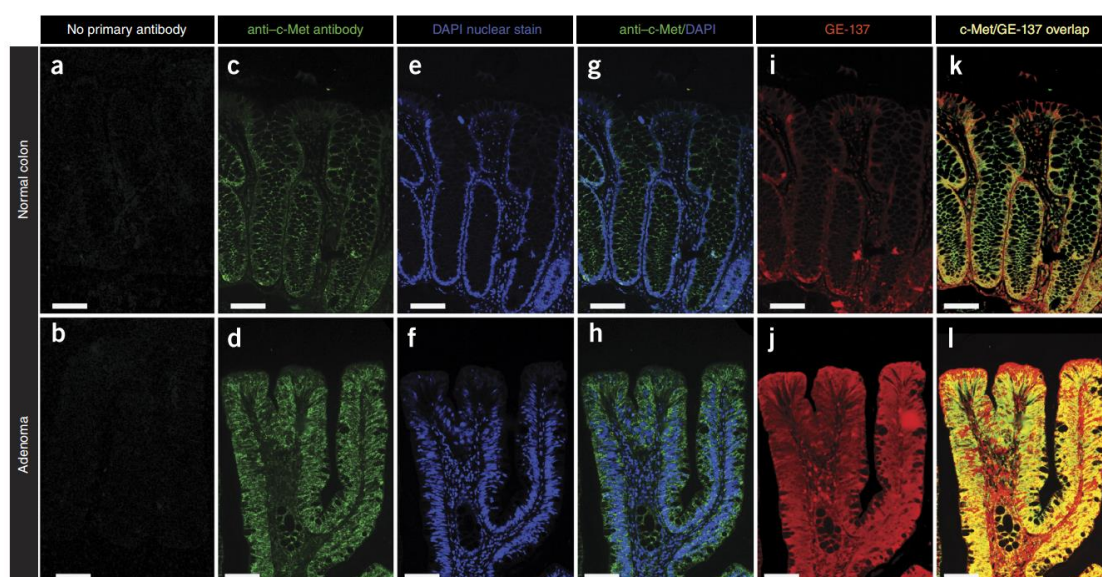


Figure 12. Microscopy imaging of c-Met expression in normal colon and adenomatous polyp targeted by GE-137 conjugate; (a,b) no staining, (c,d) c-Met labelled FITC, (i,j) NIR fluorescence of GE-137 with i – showed reduced fluorescence due to lower c-Met expression whereas j – showed higher fluorescence that corresponds to the c-Met.¹⁰⁰

Other studies of peptide conjugate imaging have also been carried in many solid tumours such as primary brain tumours¹⁰¹ and head and neck squamous carcinoma¹⁰² after promising results in canine cancer models. These are now progressing towards clinical trials with NIR fluorophores such as cyanine dyes^{101–103}

1.4.3 Protein targeting

Large biomolecules such as proteins and antibodies have also been widely investigated as potential targeting moieties. Proteins are macromolecule comprised of many amino acids (typically >50) and have been extensively studied for their ability to internalise into cells and localise to different organelles, their interesting properties prompted further investigation into the use of proteins as potential targeting units. Serum proteins such as albumin^{104,105} and lipoproteins (LDL)¹⁰⁶ can be used as endogenous carriers for selective delivery of diagnostic agents. This can be carried out by receptor mediated endocytosis targeting overexpressed receptors on tumour cells or by other means of

internalisation (**Figure 13**). Proteins are highly versatile and biocompatible for targeting cancerous tissues, and serum proteins are highly accessible as they are the most abundant blood protein in mammals.¹⁰⁷

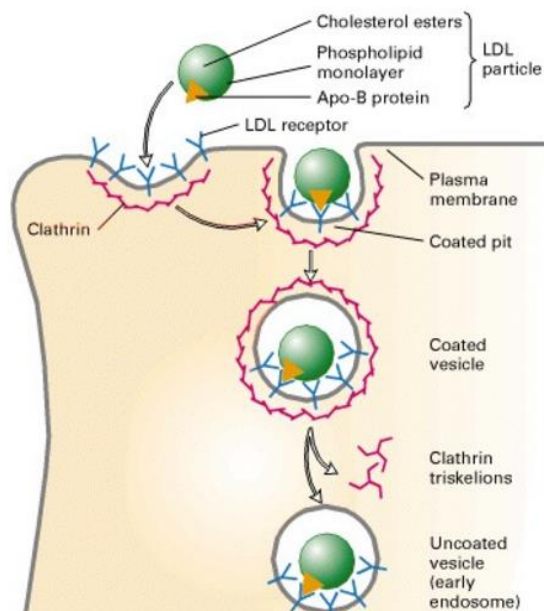


Figure 13. Receptor mediated endocytosis with LDL.¹⁰⁸

Despite the ease of targeted delivery using proteins, they have several drawbacks as targeted moieties. This is mainly due to the complex 3D structural conformation of proteins, resulting in many of the amino acids residues suitable for conjugation being internal and therefore unavailable for, bioconjugation, and leading to loss of control of loading ratios of fluorophores.¹⁰⁹ In addition, it has also been known that fluorophores such as porphyrins and their derivatives have a tendency to aggregate, resulting in non-covalent binding with the proteins.¹¹⁰ Non-covalent binding can be problematic for imaging as it results in redistributed to other proteins leading to poor contrast of margins between normal and cancerous tissue.

1.4.4 Antibodies and antibody fragments

Monoclonal antibodies (mAbs) were first described in 1975 by Köhler and Milstein as showing selective binding to specific antigen epitopes of hybridoma cells.¹¹¹ Since the discovery, mAbs has been widely used as biological tools for many scientific studies. Significant research on mAbs has led to immunoglobulins (IgG) being used to target cancer directly.^{112,113} Many antigens on cancerous tissues are tumour associated

antigens (TAA) that are overexpressed relative to normal cells. TAA expression on normal cells can reduce fluorescence contrast for cancerous tissue however if differentials in expression are sufficiently large good levels of discrimination are still possible.

Additionally, IgG are large biomolecules (>150 kDa) which can lead to non-specific tumour uptake¹¹⁴, and long circulation times¹¹⁵ (**Figure 14**). The presence of conjugatable amino acid residues in the antigen binding site can also lead to loss of specific binding affinity for the target antigen.¹¹⁶

Alternatively, to overcome the issues described above, antigen-binding fragments (Fab) could be used for targeting instead. Fab is a small antibody fragment with an average size of 25-50 kDa (**Figure 14**), it contains the paratope for selective binding, making them more attractive as targeting moieties due to decreased circulation times and higher specificity, ensuing better biodistribution profiles and lowering potential toxicities associated with antibodies.¹¹⁷ However, due to the reduction in size, the loading ratio and solubility can also be significantly reduced. In addition, the loss of the fragment crystallisable (Fc) domain can destabilise the Fab, leading to rapid degradation *in vivo*. An increased risk of aggregation can also make purification of antibody fragments conjugates more difficult¹¹⁸, hence the application of antibody targeting in FGS remains to be fully exploited.

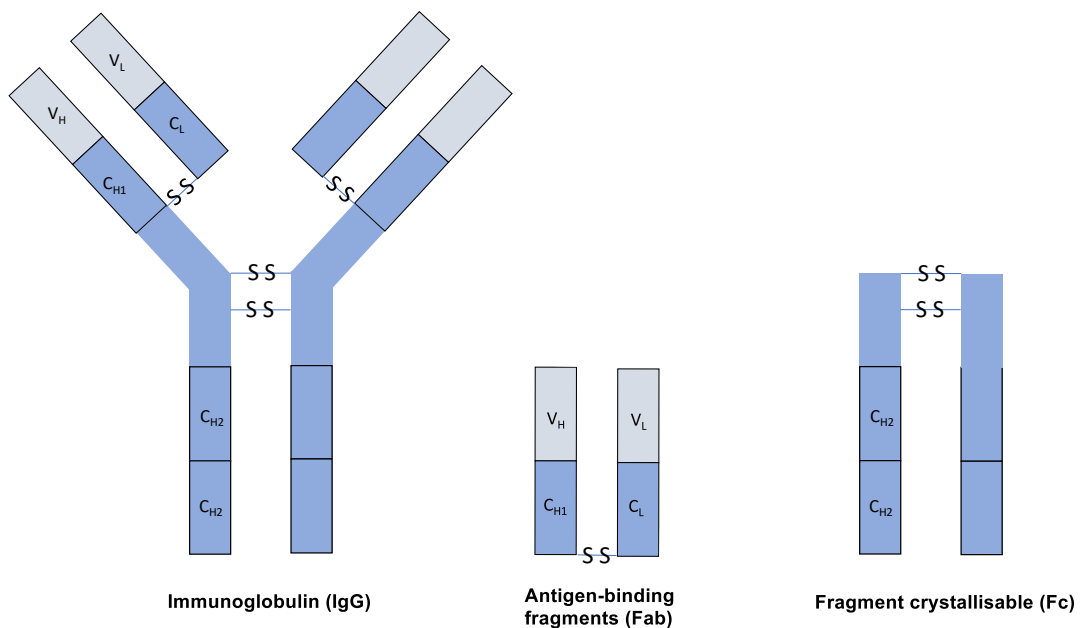


Figure 14. Structure and domains of a typical IgG.

Nevertheless, IgG antibodies have a wide range of chemodiversity and possess many amino acid residues that can be used for conjugation with fluorophores. Bioconjugation strategies employed for IgG antibodies have been well studied and developed for targeting many cancerous cell lines which overexpress corresponding antigens, so have the potential to improve diagnostic margin detection in FGS.

FDA approval for antibodies can be challenging, but once they are approved they could be repurposed for diagnostic applications, an example is Bevacizumab-800CW, an antibody targeting vascular epidermal growth factor (VEGF), which has been used for optical imaging of colorectal cancer. VEGF has been identified as an extremely selective target for human colorectal tissue with up to 96% of colorectal lesions expressing VEGF.¹¹⁹

Cetuximab is an alternative monoclonal antibody to Bevacizumab for colorectal cancer, it binds to epidermal growth factor receptor (EGFR) that is overexpressed on colorectal cancer.¹²⁰ This antibody has the ability to inhibit uncontrollable cell growth by preventing the EGFR ligand binding to EGFR through competitive binding to the receptor, thereby blocking the downstream signals for cell survival and proliferation that are caused by mutated receptors¹²¹ (**Figure 15**). This monoclonal antibody has been granted FDA approval for metastatic colorectal cancer and was studied in clinical trials for patients with EGFR expressing metastasis and it was shown that the objective response rate for combination of cetuximab and irinotecan gave a significant increase in the extended median duration response.¹²² This confirms that the receptor regulates selective binding and therefore indicates the potential of this antibody for utilisation in a fluorophore-antibody conjugate (FAC) for fluorescence guided surgery of colorectal cancers and possibly metastases. In addition, no EGF-directed antibodies other than bevacizumab have been given FDA approval for colorectal cancer, with on-going studies being carried out to suggest the potential replacement of bevacizumab with cetuximab as an adjuvant treatment.¹²²

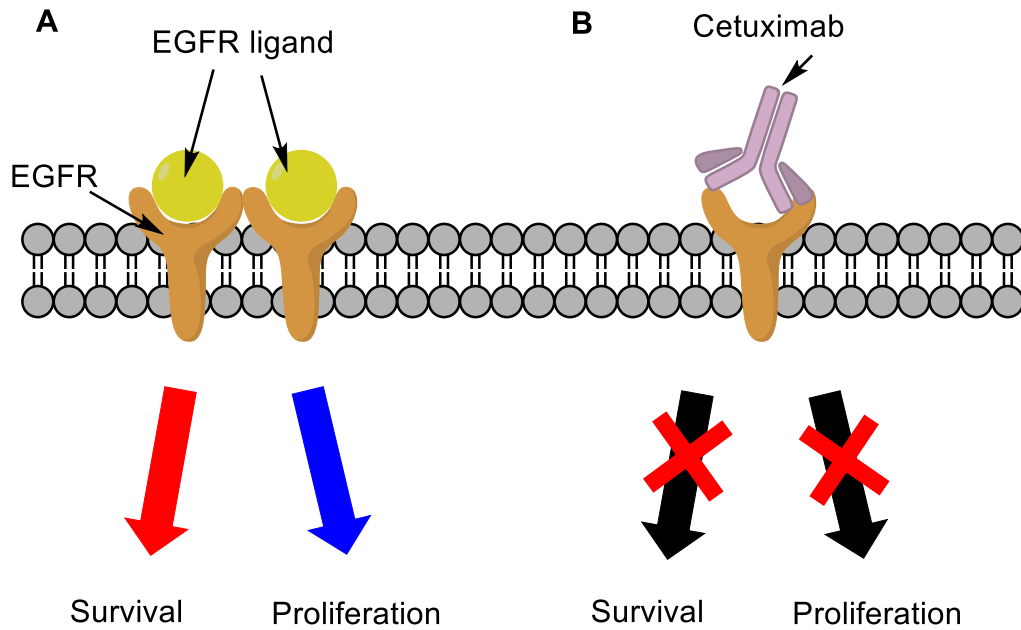


Figure 15. Mechanism of ligands and cetuximab binding. a) EGFR ligands bind to the extracellular domain of receptors and activate cell survival and proliferation. b) Cetuximab competitively binds to receptor and blocks signalling.

Several cellular studies have demonstrated the selectivity of cetuximab for head and neck cancers¹²³ and gliomas¹²⁴ for use with NIR fluorescence guided surgery, as well as providing sufficient contrast in both *ex vivo* and *in vivo* models (**Figure 16**).

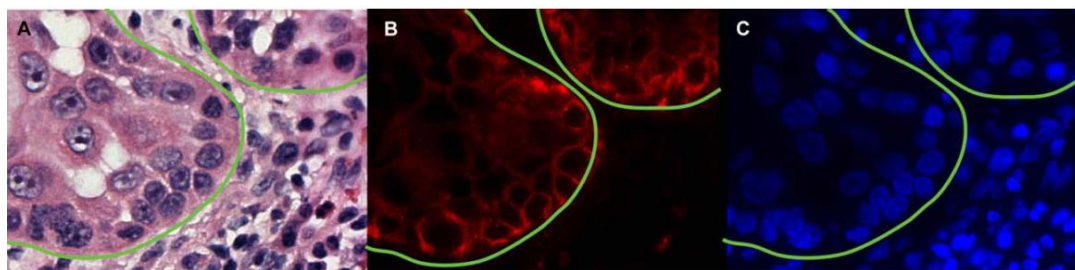


Figure 16. Microscopy images: a) white light b) fluorescence c) DAPI nuclear stain with cetuximab-IRDye800CW selectively targeting primary tumour of oral squamous cell carcinoma.¹²³

Carcinoembryonic antigen (CEA) is the most common human tumour specific antigen that is overexpressed in the vast majority of colorectal cancers, with a very low expression in healthy adult tissue. As can be seen in **Figure 17**, CEA is a glycoposphatidylinositol (GPI) anchored glycoprotein and is expressed on basal and lateral membranes allowing access to blood-borne antibodies.¹²⁵

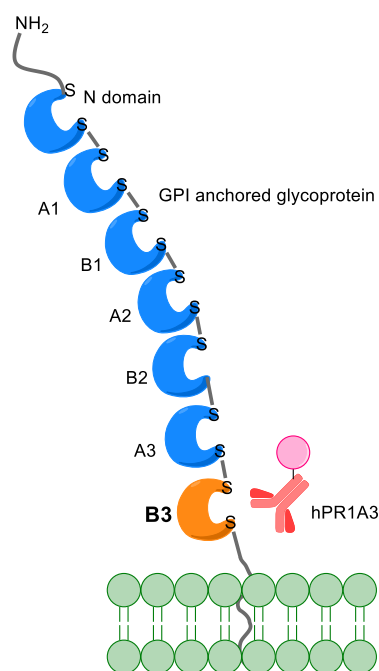


Figure 17. Antibody binding site on a GPI anchor for CEA.

Research by Jayne *et al.* has proven the selectivity of an antibody known as hPR1A3, showing an increase in lysis with increasing concentration of hPR1A3.¹²⁶ Monoclonal antibodies can be covalently bound to fluorescent probes to obtain FAC, enhancing affinity of the conjugate for colorectal tumour tissues.

Other FACs are in preclinical development featuring both approved antibodies and fluorophores. However, many unresolved challenges remain for antibody based imaging, both in their biological and photophysical properties.

1.4.5 Activatable Probes

In situ activation of fluorescence has recently been developed to improve imaging of cancerous tissues. The underlying mechanism utilises a delivery system with fluorescent probes that are self-quenched due to the close proximity of the molecules, or which show a pH dependence in fluorescence intensity. Upon delivery to the target, enzymatic cleavage or changes in pH cause the fluorescence probes to be released resulting in increased fluorescence.

The concept was demonstrated by Zheng *et al.*¹²⁷, with the use of porphyosomes and further developed for a NIR aza-BODIPY in a recent publication by O'Shea *et al.*¹²⁸ (**Figure 18**).

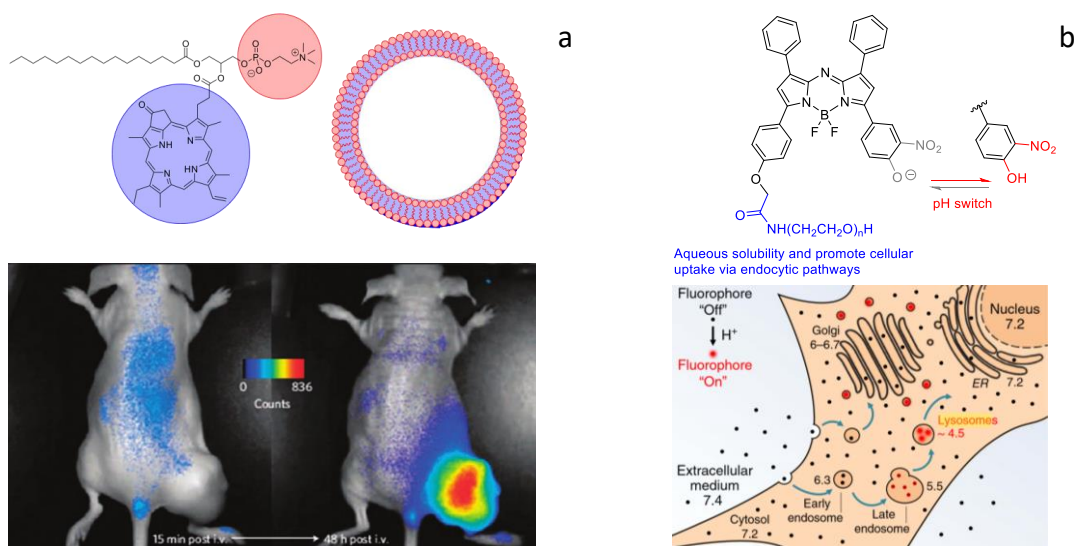


Figure 18. a) Schematic diagram of porphyrin-lipid self-assembly into porphyrinsomes and their application in *in vivo* fluorescence imaging.¹²⁷ b) Lysosomal responsive aza-BODIPY.¹²⁸

Limitations can stem from the potential for the free fluorescent probes to be released and redistributed, reducing the target to background signal to noise ratio. In addition, challenges remain for those activatable systems to be translated from model *in vitro* and *in vivo* to the more complex clinical environment.

The demand for new targeted fluorescent probes remains high, and these may lead to improvements in biodistribution, photostability, toxicity, selectivity and specificity compared to the commercial dyes currently available on the market.

1.5 Bioconjugation strategies

Targeting systems such as antibodies, proteins and peptides offer a wide range of chemodiversity that can undergo post translational synthetic modifications. Bioconjugation is a commonly used strategy to establish a stable covalent bond between a biological unit and a chemical molecule. Through bioconjugation, modified biological molecules can have a variety of applications such as targeted drug delivery, imaging biomarkers, cellular tracking and determining biodistribution.¹²⁹ Reactions involving amino acid residues are a common method for bioconjugation. Those residues include lysine (NH₂), cysteine (SH), tyrosine (OH) coupling, tryptophan (Ar) modification, N- and C- terminus modification is also common.

1.5.1.1 Lysine modification

Primary amines are commonly found in almost all proteins, these can be divided into either α -amino group from the polypeptide *N*-terminus or lysine residues. Amino group exposed at the outer surface of the protein are more easily accessible to perform conjugations.

Lysine residues have historically been the most popular reaction site in protein bioconjugation because of their nucleophilicity. However, pH is an important determining factor for conjugation involving amines, due to the potential for protonation, which leads to a dramatic decrease in reactivity. As a consequence, higher pHs are often required for these reactions.

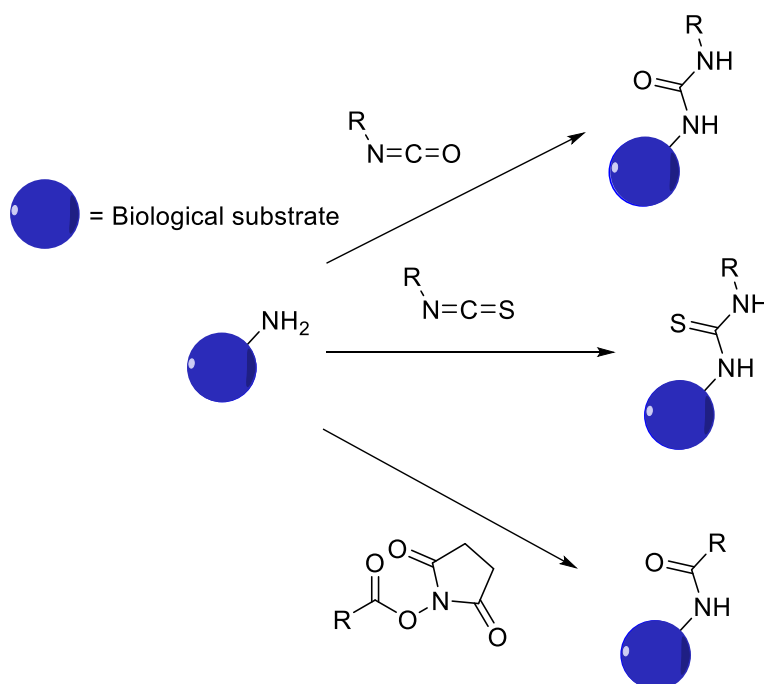


Figure 19. Common methods for lysine bioconjugation.

Lysine residues can undergo many reactions with different chemical moieties as shown in **Figure 19**. The amines can react with isocyanates to form ureas¹³⁰, however, since early studies showed complications with isocyanates due to their high reactivity and low stability, isothiocyanates, which are synthetically more versatile have largely replaced them.^{131,132}

Todrick and Walker in 1937, reported that allyl isothiocyanates are reactive with

cysteine residues under alkaline conditions.¹³³ Podhradsky *et al.*, however, demonstrated a preferential activity of isothiocyanates towards lysine over cysteine and tyrosine residues. The study found that isothiocyanates react with thiols and phenolates, but this is reversible, whereas the addition to the amine is irreversible and the equilibrium is therefore driven toward the formation of thioureas.¹³⁴ As a result, the increasing popularity of lysine residues in bioconjugation led Riggs *et al.* to develop the first fluorescent antibody conjugate formed from an isothiocyanates substituted fluorescein.¹³⁵ Fluorescein isothiocyanate has been commonly used for protein bioconjugation since its discovery and was reported separately by Tuls¹³⁶ and Burtnick¹³⁷ for selective lysine labelling, as shown in **Figure 20**.

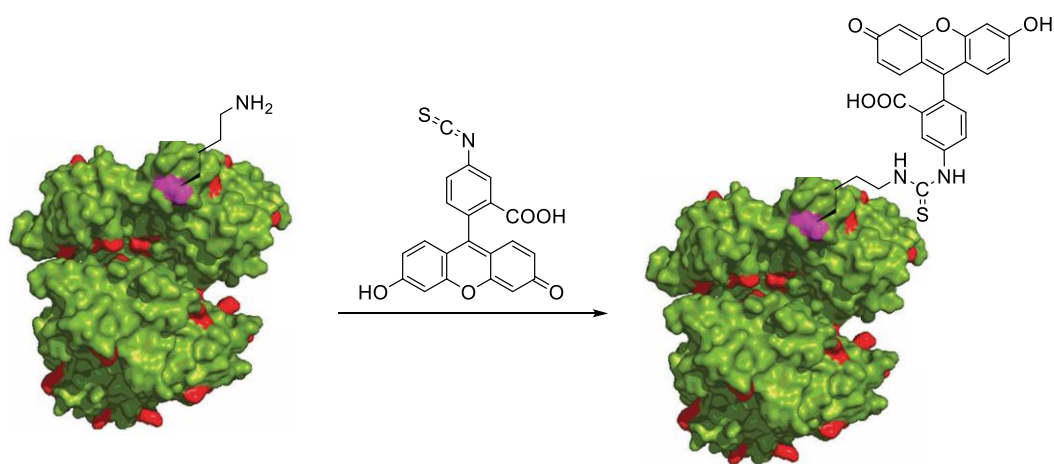


Figure 20. Selective fluorescent labelling of lysine residue of G-actin.

Activated esters are another common chemical moiety for performing bioconjugation via lysine residues. Due to the low reactivity of carboxylic acids towards amines in aqueous media, substitution is achieved by employing a better leaving group such as with succinimidyl esters, which activate the carbonyl allowing it to become more susceptible to nucleophilic substitution. NHS activated esters are arguably the most popular functional group in bioconjugation. They were first introduced by Anderson *et al.* in 1964¹³⁸, the NHS activated ester has exceptionally high selectivity towards aliphatic amines, despite some studies showing reactivity with tyrosine¹³⁹ and histidine side chains¹⁴⁰. These groups were subsequently shown to have a significantly lower reactivity in comparison to the free amines on lysine residues. However, there are several limitations including the degradation of NHS esters, which can occur through hydrolysis, and a decrease in water solubility of the carboxylate upon conversion to the

NHS ester. (**Figure 21**) Hence, sulfo-NHS derivatives are often utilised to increase water solubility.¹⁴¹ Due to the excellent biocompatibility and stability of the amide bond formed, many fluorescence probes modified with NHS esters are commercially available.

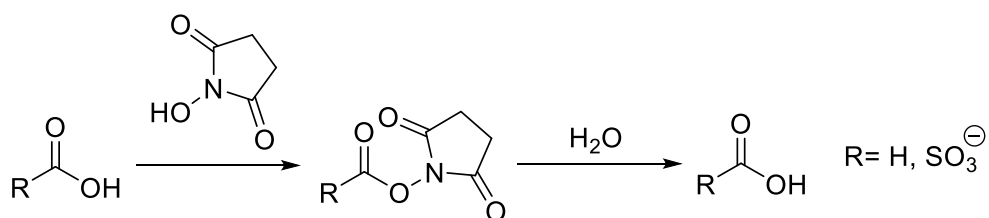


Figure 21. The conversion of carboxylate to NHS ester and subsequent hydrolysis.

1.5.1.2 Cysteine

Cysteine has been an exceptional amino acid residue in terms of chemoselective bioconjugation, due to the rarity of these residues on the protein surface. The number of cysteines residues is low in comparison to lysine residues and they are often expressed in specific locations, hence allowing site specific modification at the predetermined position of the cysteine residue.¹⁴² Sulfhydryl side chains have shown excellent nucleophilicity making them ideal for selective bioconjugation.¹⁴³ Cysteine residues are present in a range of biological molecules and especially in IgG antibodies and fragments, which are an attractive targeting unit to achieve selectivity. They are often present as disulfide bridges and are a key component for maintaining protein structure and rigidity. They are generally buried within the complex 3D structure of the protein.

In order for reactive thiols to be generated in proteins from the natural form of cysteine, selective reduction of the cysteine disulfides must be performed. This can be achieved using various reducing agents, including dithiothreitol (DTT), 2-mercaptoethanol and tris[2-carboxyethyl] phosphine (TCEP).¹⁴⁴ Thiol groups are usually reacted *via* nucleophilic addition / substitution, or through thiolate anion displacement reaction.

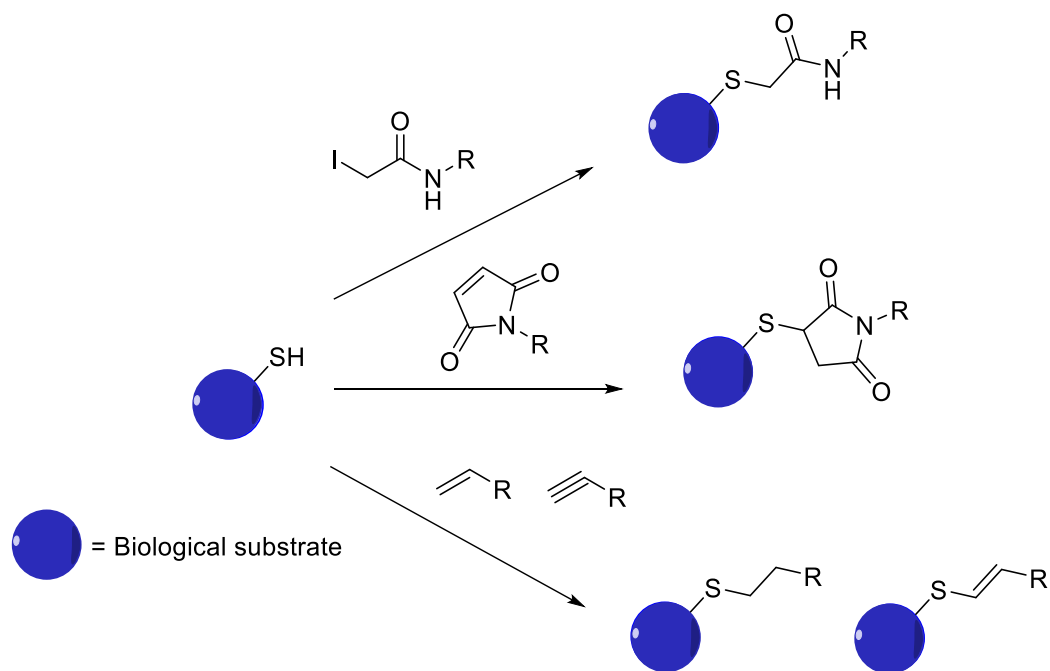


Figure 22. Common methods for cysteine bioconjugation.

α -Halocarbonyls such as iodoacetamides are electrophiles that have been widely employed for the modification of cysteine residues, due to iodide being a good leaving group, resulting in faster reaction rates and enabling use with shorter linkages, giving elevated stability. However, a major issue with this conjugation is the reaction of the iodoacetyl group with other amino acid residues present on the protein. To reduce this effect and selectively conjugate with low- pK_a cysteine residues, a neutral to slightly acidic pH is required.¹⁴⁵ In spite of advances in this bioconjugation strategy, the potential side reactions within the conjugation strategy limit applications¹⁴⁶ (**Figure 22**).

Maleimides were introduced by Friedmann in 1949 as cysteine specific reagents and were synthesised through reaction of maleic anhydride with amine derivatives.¹⁴⁷ Due to the limitations of iodoacetamides, maleimide became an extremely popular addition to the list of commonly used bioconjugation reagents. This was mainly the result of fast kinetics and high selectivity due to the susceptibility of the maleimide alkene toward nucleophilic attack by thiolates. To optimise reaction conditions for maleimide conjugation, the pH of the reaction should be maintained near 7 in order to prevent reactions with amines.¹⁴⁸ A large variety of maleimide derivatives have now been synthesised for biomedical applications, including bioimaging.¹⁴⁹

Vinyl sulfones are also popular for bioconjugations using Michael reactions under slightly basic conditions, resulting in stable thioether bonds and leading to an elevated stability in aqueous media. This is favourable compared to maleimides that are susceptible to ring opening and addition reactions at the alkene bond.¹⁵⁰ Photo- and chemical initiator induced thiol-ene and thiol-yne reactions have also been introduced over the last century.¹⁵¹ These conjugation strategies have been applied to fluorescent labelling of peptides¹⁵² and proteins.¹⁵³ However, the necessity to use initiators can lead to major side reactions such as oxidation and crosslinking.

Selective cysteine conjugation can be achieved using disulfide compounds. This reaction is similar to the formation of cysteine-cysteine bonds found in the tertiary structure of proteins and can be carried out under very mild conditions. However, this labelling strategy suffers from instability due to nucleophilic attack¹⁵⁴ (**Figure 23**).

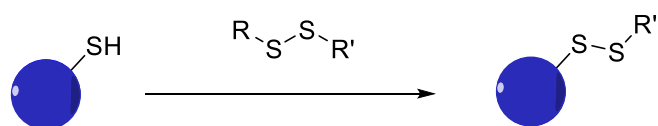


Figure 23. Schematic of disulfide exchange reaction.

Disulfide bridges can be reduced for use in conjugation using reducing agents, the most common of which is TCEP, due to its high versatility and biocompatibility. Recently, brominated maleimide was developed and employed in conjugation through disulfide rebridging^{155,156} (**Figure 24**).

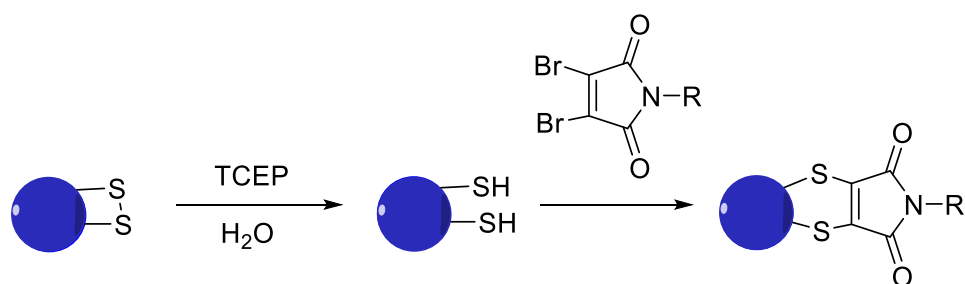


Figure 24. Schematic of disulfide rebridging with dibromomaleimide.

Bioorthogonal chemistry is also used in combination with cysteine residues. Applications utilising disulfide reactions and disulfide rebridging in conjugation with bioorthogonal ligations and click reactions have been shown to significantly improve regioselective bioconjugation on peptides¹⁵⁷, proteins¹⁵⁸ and antibodies.¹⁵⁹

1.5.1.3 Tyrosine

Tyrosine has proven to be an amino acid residue of interest in bioconjugation due to its relatively low occurrence, relative to other amino acids. However, it is often found in the inner structure of proteins due to the amphiphilic properties of phenolic groups. In order to utilise tyrosine residues as a target for conjugation, different methodologies have been employed to exploit either the electron rich aromatic ring or the tyrosine hydroxyl group, usually as a highly reactive phenolate (**Figure 25**).

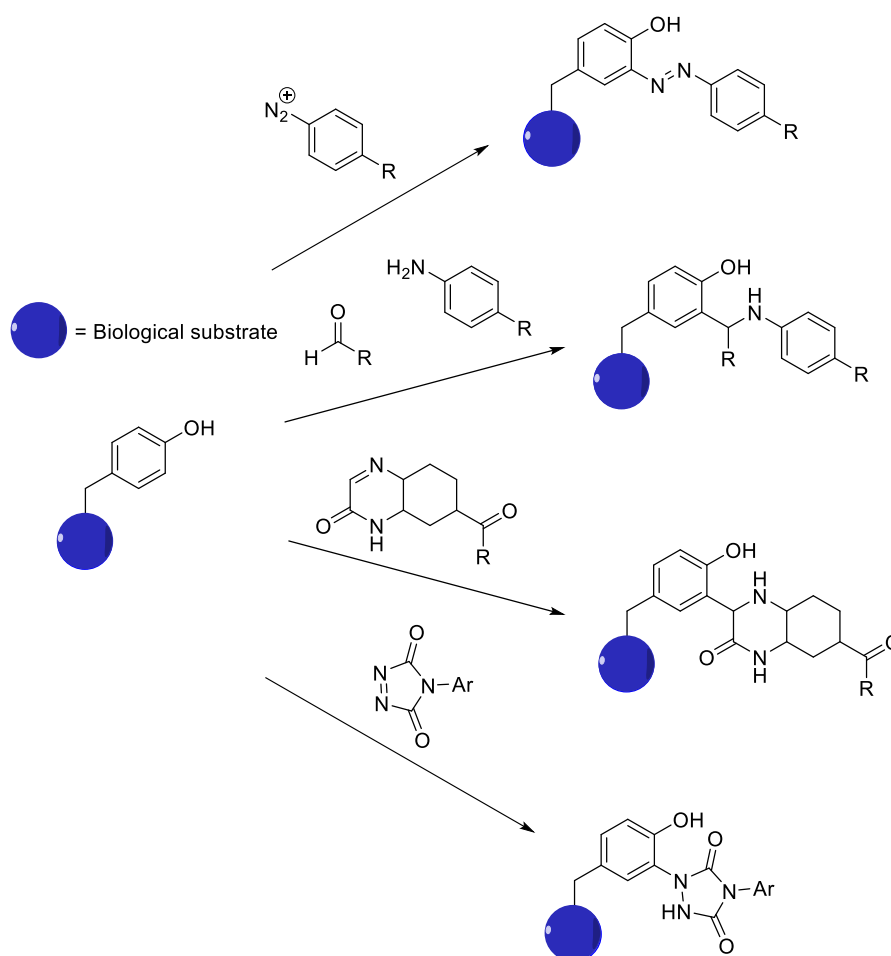


Figure 25. Common methods for tyrosine bioconjugation.

O-derivatisation is a well-known technique for tyrosine modification, especially for *O*-acetylation. In a two-step *O*-acetylation, the phenol group initially undergoes *ortho*-formylation, resulting in an aldehyde derivative, followed by the reaction with a primary amine.¹⁶⁰ This method was demonstrated by Kai *et al.*¹⁶¹ and Ishida *et al.*¹⁶², and was further elaborated by Francis *et al.* for selective *O*-and *C*-alkylation¹⁶³ (

Figure 26). However, the method was limited due to low selectivity of acylation in competition with other nucleophilic amino acid residues.

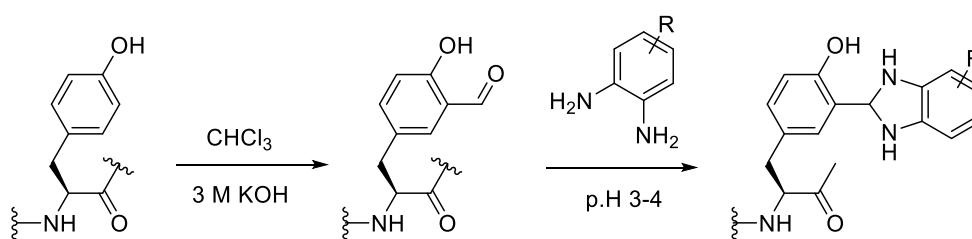


Figure 26. Two step tyrosine modification through *O*-acetylation.

A diazonium reaction for tyrosine modification was first introduced by Pauly in 1915¹⁶⁴ and ever since this discovery diazonium coupling has been of a great interest as a method for tyrosine modification. Advancement of the methodology was introduced by Higgins and Harrington and applied to a complex protein, however, the reaction was not selective and involved multiple amino acids.¹⁶⁵ With such drawbacks the methodology was not widely adopted. Francis¹⁶⁶ and Barbas¹⁶⁷ introduced a more stable and elegant way to perform tyrosine modifications, which avoided concurrent reactions with lysine and histidine residues, leading to the development of further bioorthogonal reactions with proteins and antibodies (**Figure 27**).

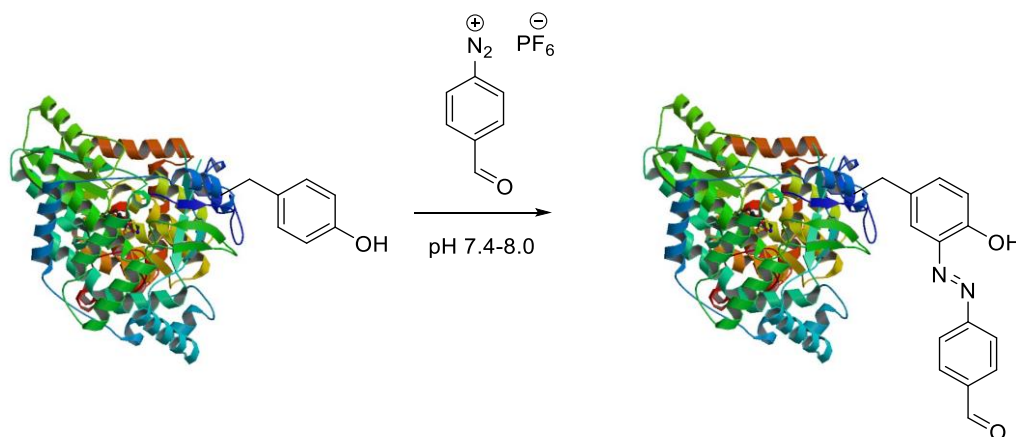


Figure 27. Selective tyrosine modification of BSA by FBDP for further bioorthogonal ligation.

Mannich reaction methodology requires the *in situ* reaction between three different components: tyrosine residue, amine and formaldehyde, and is an extension to the selective *O*- and *C*-alkylation.¹⁶⁸ Francis *et al.* used this reaction to show potential

selective modification using rhodamine, however, the reaction rate was slow for fluorescent labelling at the tyrosine residue¹⁶⁹ (**Figure 28**). Despite slow reaction kinetics and selectivity issues, Tanaka *et al.* have successfully demonstrated the potential of *in situ* formation of imines as internal fluorescence probes¹⁷⁰, yet further bioconjugation to peptide or proteins utilizing this method remains challenging.

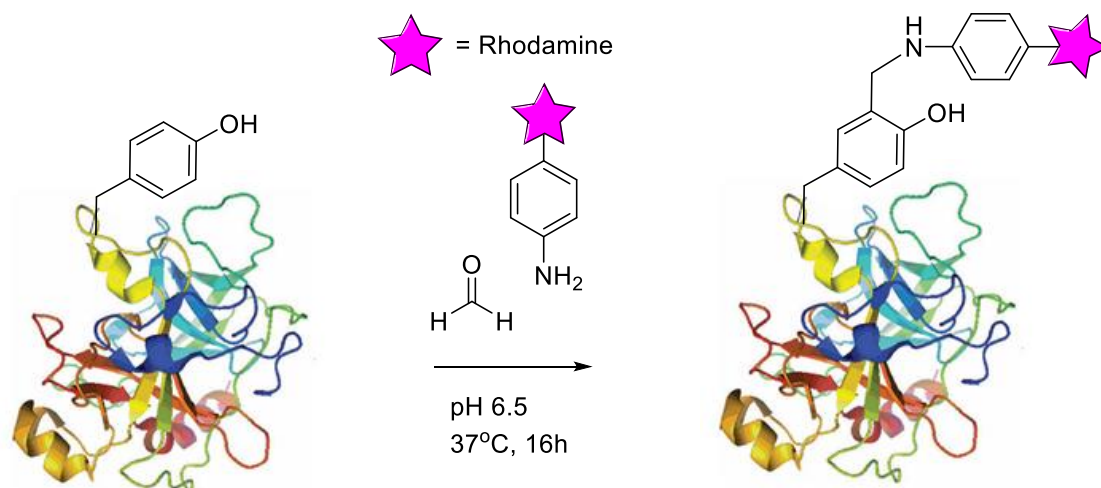


Figure 28. Mannich-type three component selective modification of tyrosine residue of α -chymotrypsinogen A with rhodamine.

Dicarboxylates and diazaodicarboxyamides have always offered potential as conjugation moieties, however, electro-deficient dicarboxylates show rapid decomposition under aqueous conditions, whereas diazaodicarboxyamides do not react with phenol group due to their high stability.¹⁷¹ Recently Barbas *et al.*, introduced the synthesis of a corresponding 4-phenyl-3H-1,2,4-triazoline-3,5(4H)dione (PTAD). This compound demonstrated a balance between stability and reactivity that could be applied to tyrosine bioconjugation. The reaction can be applied over a wide range of pHs with the optimal observed in the range of pH 7-10. Stable precursors for PTAD have shown promise for installation with different functionalities (**Figure 29**).

After success with many tyrosine bioconjugation methods, bioorthogonal chemistry, such as ligation and click chemistry, was adapted for conjugation with peptides, proteins and antibodies.¹⁷² Although, non-selective labelling of other aromatic residues can also be observed when targeting tyrosine, a high level of selectivity can still be achieved through careful tuning of the reaction conditions.

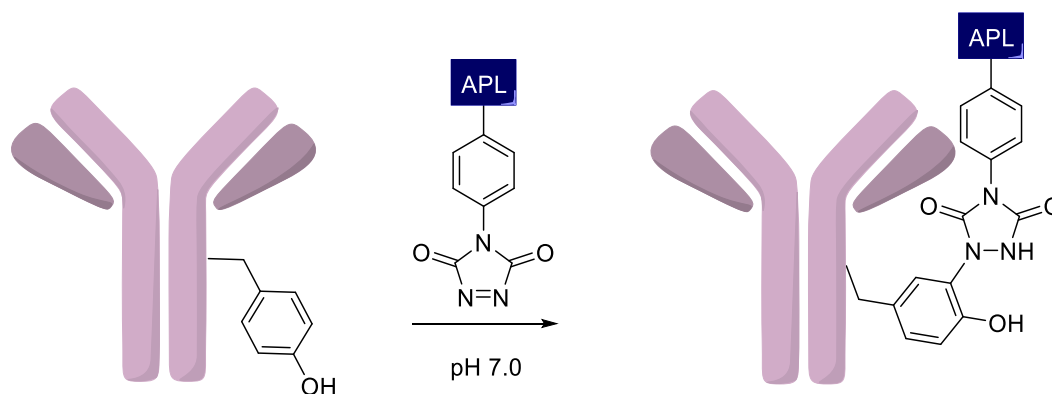


Figure 29. Bioconjugation of aplaviroc (APL) with PTAD to IgG antibody.

1.5.2 Bioorthogonal chemistry

One significant approach to successfully reproducing bioconjugation in a highly efficient and controllable way is through bioorthogonal modification of amino acid residues. Bioorthogonal chemistries are general chemical reaction that do not interfere with native biological processes and have inertly fast reaction rates.¹⁷³ This allows site-selective modification, followed by different chemical ligation strategies for a complementary probe to react with the modified functionalities. An important factor for bioorthogonal reactions is that the reactant should be stable under biological environments and yield stable covalent bonds without forming innocuous byproducts¹⁷⁴ (Figure 30).

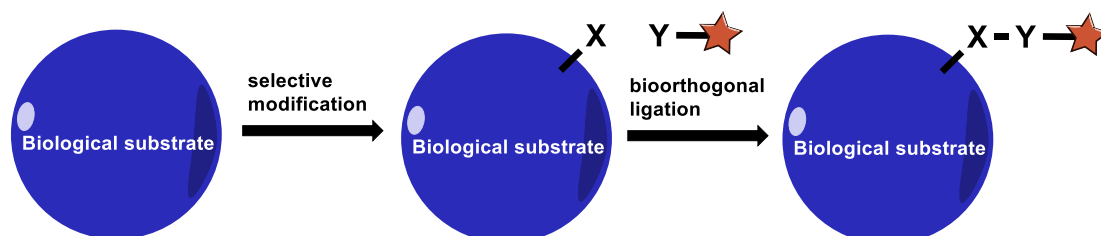


Figure 30. Bioorthogonal chemistry between modified functionality X and reactive partner Y.

In addition, bioorthogonal reactions should ideally react selectively under physiological conditions. Despite restrictions, a number of conjugation strategies have been developed such as the Staudinger ligation (**Figure 31**), ketone/hydroxylamine condensation (**Figure 32**), but the most recognised method are the click reactions.¹⁷⁵

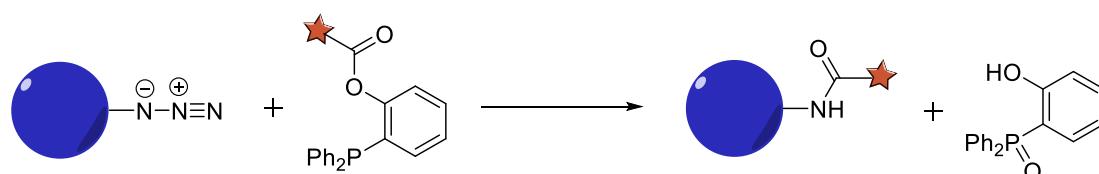


Figure 31. Schematic of Staudinger ligation.

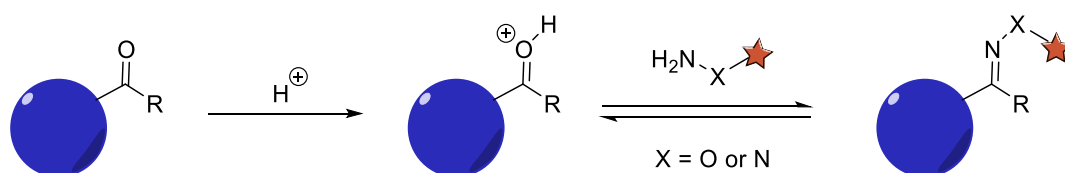


Figure 32. Schematic of ketone/hydroxylamine.

Click chemistry was first described by Sharpless in 2001 as a powerful class of reactions that would be ideal for bioorthogonal chemistry due to good biocompatibility and fast reaction kinetics. Click reactions are, ideally, facile, one pot reactions which can be performed in aqueous media with minimal generation of byproducts. Additionally, obtaining high yields with reaction specificity and simple purification methods, even in complex biological environments, characterise click reactions. With this method, bioconjugation can be performed between a fluorescent probe and a specific biomolecule of interest, this is especially useful for biomedical applications such as NIR FGS. Since the development of click chemistry, reactions such as the Huisgen 1,3-dipolar cycloaddition have been extensively reviewed, modified and optimised for use in bioconjugation.¹⁷⁶

1.5.2.1 Copper Catalysed Azide Alkyne Cycloaddition

The azide-alkyne Huisgen 1,3-dipolar cycloaddition has recently become of major interest in bioorthogonal chemistry due to its efficiency, wide applicability and low non-specific reactivity towards biomolecules. In this reaction azide moieties react with limited set of alkyne moieties on the modified protein surface to form an extremely

stable triazole unit that is resistant to oxidation, hydrolysis and enzymatic degradation, making these reactions attractive for bioconjugation.

The copper catalysed azide-alkyne cycloaddition (CuAAC) has recently become synonymous with the term “click reaction” utilising a copper (I) catalyst to yield only the 1,4-triazole from an azide and an alkyne (**Figure 33**). This reaction, discovered by Sharpless, has a significantly improved rate and yields a single product, 1,4-isomer, rather the mixture of 1,4- and 1,5-isomers that were obtained with the non-catalysed 1,3-dipolar cycloaddition.¹⁷⁶

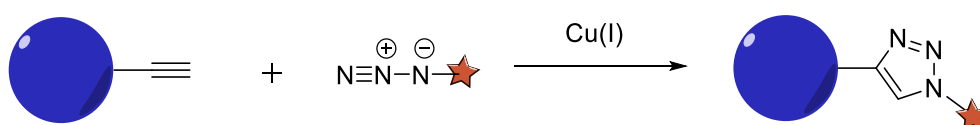


Figure 33. Schematic of Copper Catalysed Azide Alkyne Cycloaddition

The CuAAC requires a Cu(I) source to catalyse the reaction. A number of catalysts are available including CuBr, CuI or CuOTfC₆H₆ as the source of Cu(I), however it has been suggested that the formation of byproducts and sequestering of Cu by competing coordinating molecules within the solution can be problematic.¹⁷⁷ To overcome this problem Rostovtsev *et al.* stated it was possible to establish a CuAAC reaction of high yield and purity through generating the Cu(I) catalyst *in situ* by reducing Cu(II)SO₄·4.5H₂O with sodium ascorbate. This resulted in a more efficient reaction without the need for inert conditions to prevent Cu(I) from oxidising to Cu(II) by atmospheric oxygen, and a more facile purification through simply washing with water or buffer¹⁷⁸ (**Figure 34**).

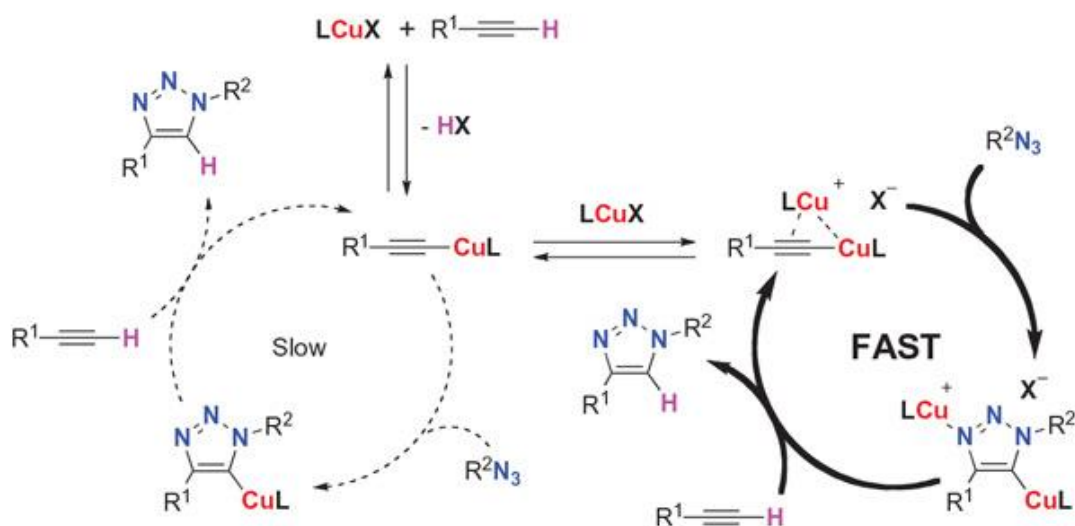


Figure 34. Possible mechanism for CuAAC reaction.¹⁷⁹

In order to maximise the reaction rate, appropriate accelerating ligands can be used in the reaction and these are especially applicable for bioconjugation, as high temperatures may not be applied. Appropriate ligands such as TBTA and THPTA are often used to promote catalysis through protection from hydrolysis by Cu(II) byproducts and to quench radical species generated during the reaction¹⁸⁰ (**Figure 35**).

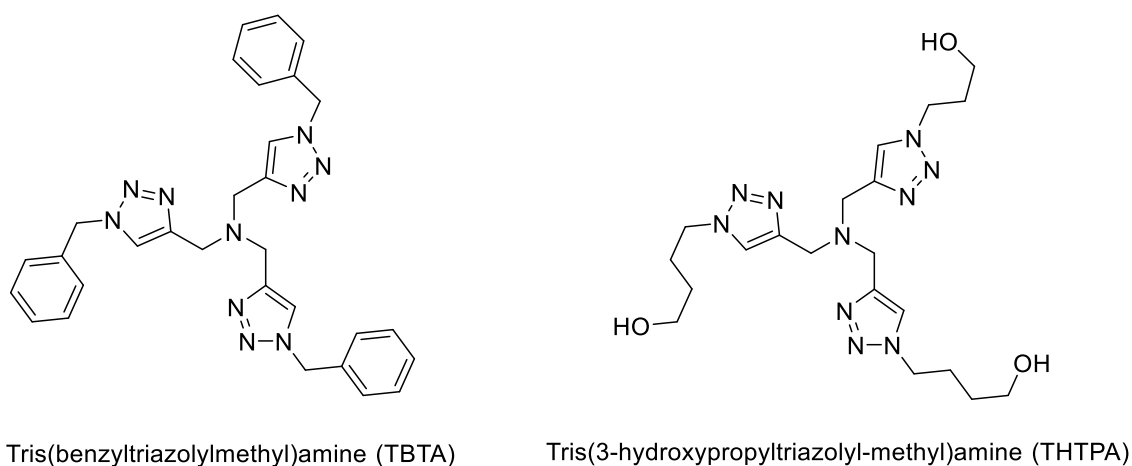


Figure 35. Structures of accelerating ligands TBTA and THPTA.

Side reactions can occur between dehydroascorbate and protein side chains as well as an induced cytotoxicity from Cu(I) derivatives. These issues can be resolved however by the simple addition of aminoguanidine and extensive washing with EDTA buffer^{180,181}. Due to the ease of synthesis utilising the azide and alkyne moieties, this reaction has inspired many bioconjugation methodologies with the CuAAC click

reaction becoming an indispensable reaction in bioorthogonal chemistry.

Many CuAAC reactions have been demonstrated for fluorophore bioconjugation to biological molecules such as oligopeptides¹⁸², proteins¹⁸³ and oligonucleotides^{184,185} as shown in **Figure 36**. The bioconjugation method using CuAAC with fluorophores have previously been used as a significant supporting protocol to aid in determining the efficiency of protein labelling, and to provide a better understanding in the mechanistic behaviour of this reaction in biological environments. These similar bioconjugation techniques can therefore be adapted in producing active targeting fluorophore conjugates for use in NIR FGS.

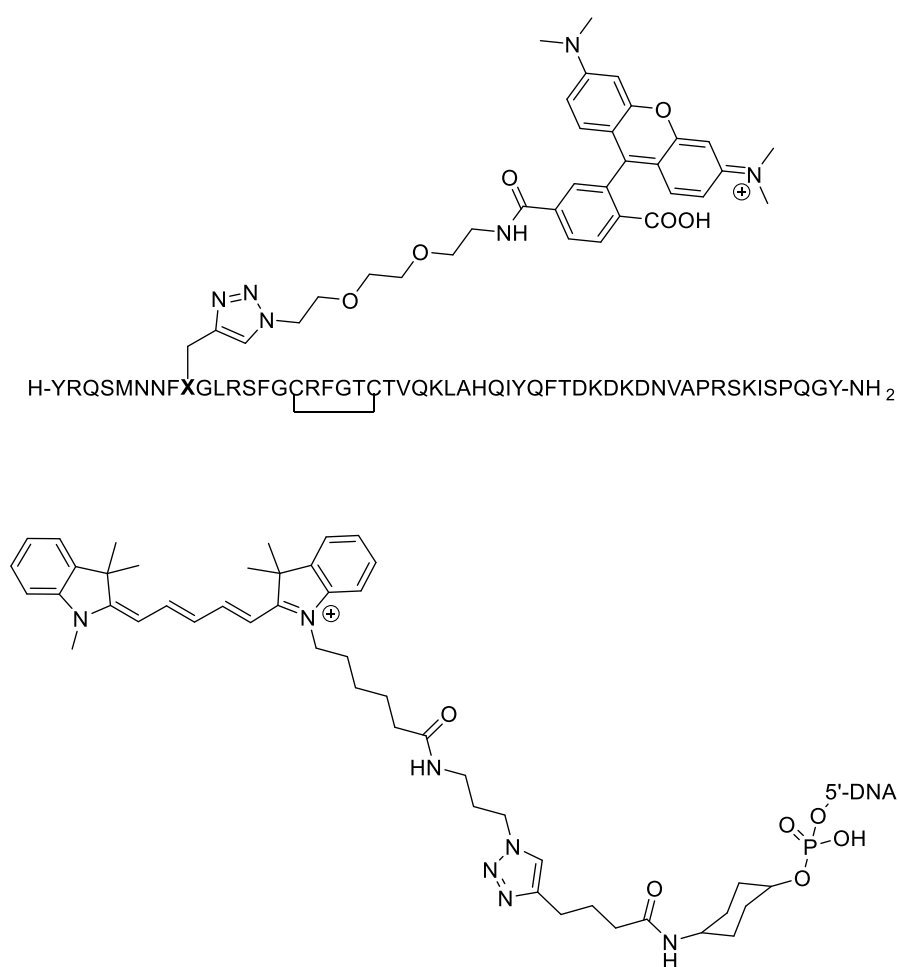


Figure 36. Examples of CuAAC of fluorophores with biological molecules.^{182,184}

1.5.2.2 Strain Promoted Azide Alkyne Cycloaddition

Strain promoted azide-alkyne cycloaddition (SPAAC) is an alternative to the Huisgen 1,3-dipolar cycloaddition click reaction, which was developed by Bertozzi's group to

overcome some of the problems associated with the CuAAC bioconjugation.¹⁸⁶ The reaction utilises a cycloalkyne and an azide; the intrinsically highly strained alkyne increasing the reactivity and accelerating formation of the triazole (**Figure 37**). This has significantly improved the biocompatibility of azide-alkyne cycloadditions and led to both *in vitro* and *in vivo* applications. Although this bioorthogonal reaction has been widely applied in bioconjugation to antibodies and peptides for therapeutic and diagnostic applications, the reaction remains limited due to slower reaction kinetics and yields, as well as the challenging synthesis of strained alkynes.^{187,188}

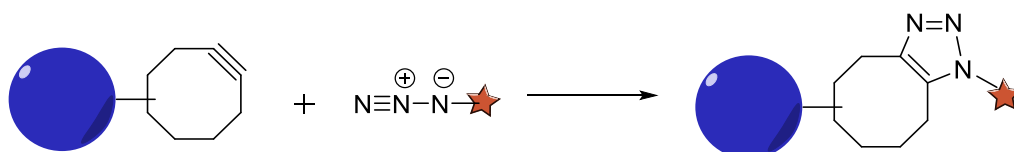


Figure 37. General schematic of strain promoted azide-alkyne cycloaddition.

Several modifications of cyclooctyne have been conducted in an attempt to increase the reactivity and reaction rate through the addition of aryl rings (DIBO, DIBAC, BARAC, BCN) or by appending electron withdrawing groups at the propargylic position (MOFO, DIFO) and use of a base such as glutathione as shown in **Figure 38**.¹⁸⁹ A range of cyclooctyne derivatives have been synthesised in an attempt to improve the stability and reaction kinetics in complex biological environments.¹⁹⁰

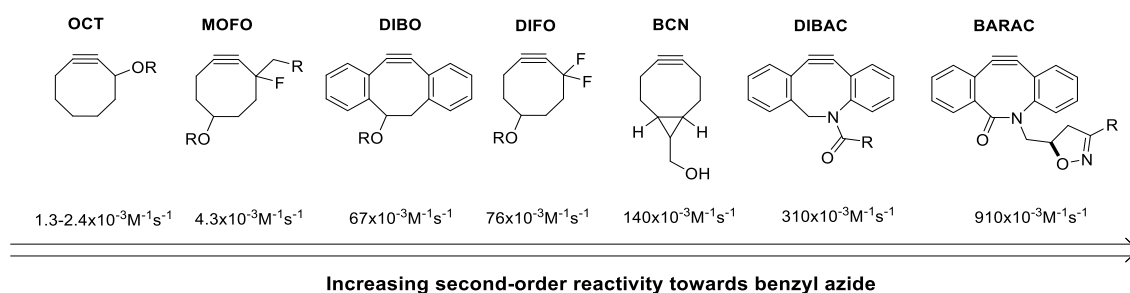


Figure 38. Reaction kinetics between different cycloalkyne derivatives.¹⁸⁹

Development of strained alkyne derivatives continue, with SPAAC becoming increasingly popular in biological applications. An example of the SPAAC biorthogonal reaction have been reported by Caddick *et al.*, utilising the method of disulfide rebridging with dibromomaleimides and dibromopyridazinediones to provide a bioconjugation platform for antibody labelling^{159,191} (**Figure 39**).

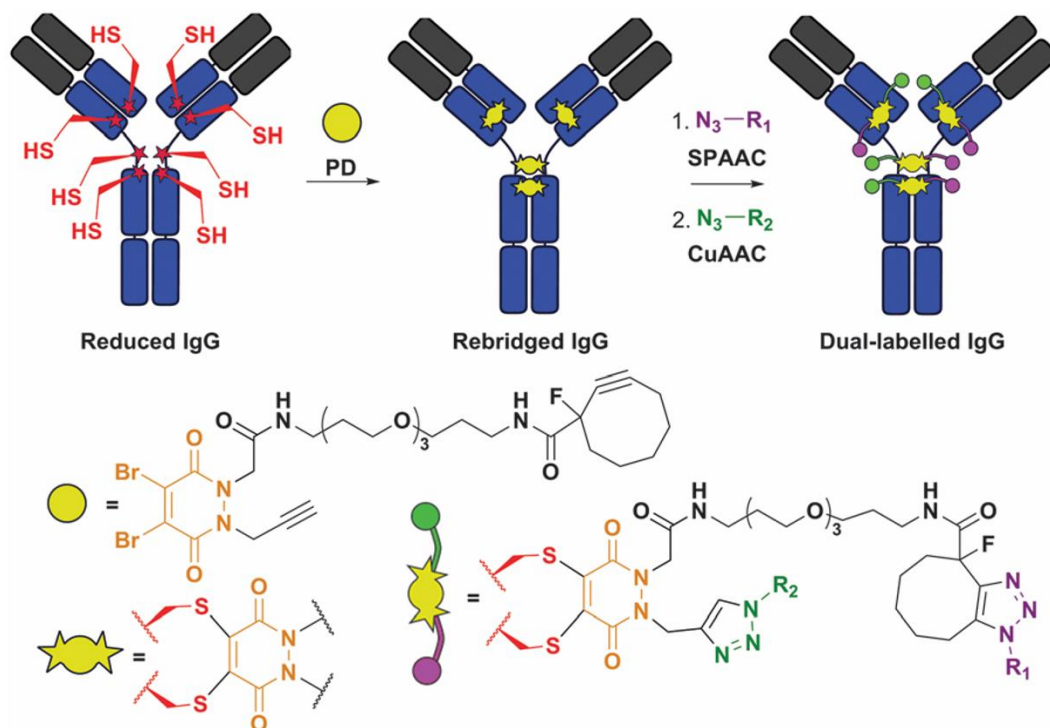


Figure 39. Disulfide rebridging of IgG antibody with dibromopyridazinediones functionalised with a strained alkyne and terminal alkyne for click reactions.

Similarly to SPAAC, strained alkynes have also been utilised for other facile bioconjugation strategies in the labelling of biological molecules with fluorophores for fluorescence imaging, Chin *et al.* have reported the used of tetrazine linkers with various fluorophores to conjugate to bicyclo[6.1.0]nonyne (BCN) to achieve site specific labelling of intracellular proteins on HEK-293 cells through fluorescence microscopy¹⁹² (**Figure 40**).

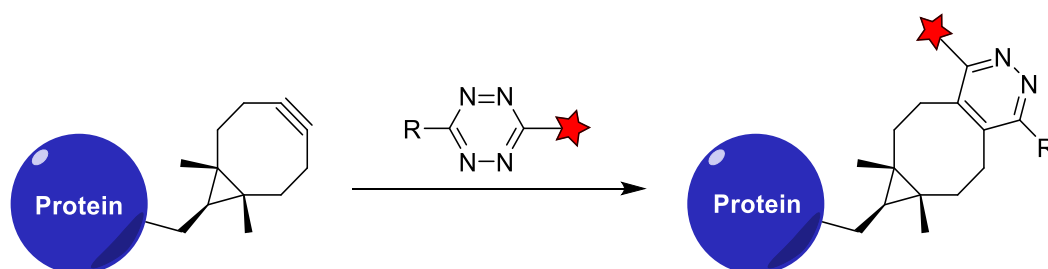


Figure 40. Bioconjugation strategy for fluorophores and BCN through the use of tetrazine linker.¹⁹²

To summarise, a range of chemical modification methods are available in the literature

to enable the construction and further investigation of an optimised bioconjugate imaging agent for use in NIR FGS.¹⁹³

1.5.3 NIR fluorophores

Due to limitations in the photophysical properties of current fluorescent probes, including photobleaching, photoinstability and lack of NIR fluorescence, alternative fluorophores are in high demand. A recent review has suggested a major factor that limits the sensitivity is the presence of blood, which significantly absorbs emitted photons and decreases excitation power¹. These issues can be overcome by the introduction of NIR fluorescent probes, as they provide deeper penetration and reduce autofluorescence. The search for the optimal fluorophore for applications in NIR FGS is ongoing, to resolve many of the issues previously described different classes of pyrrolic based organic fluorophores with potential NIR properties and high photostability have been investigated, including porphyrins, BODIPYs, aza-BODIPYs, chlorins, phthalocyanines and bacteriochlorins (**Figure 41**).

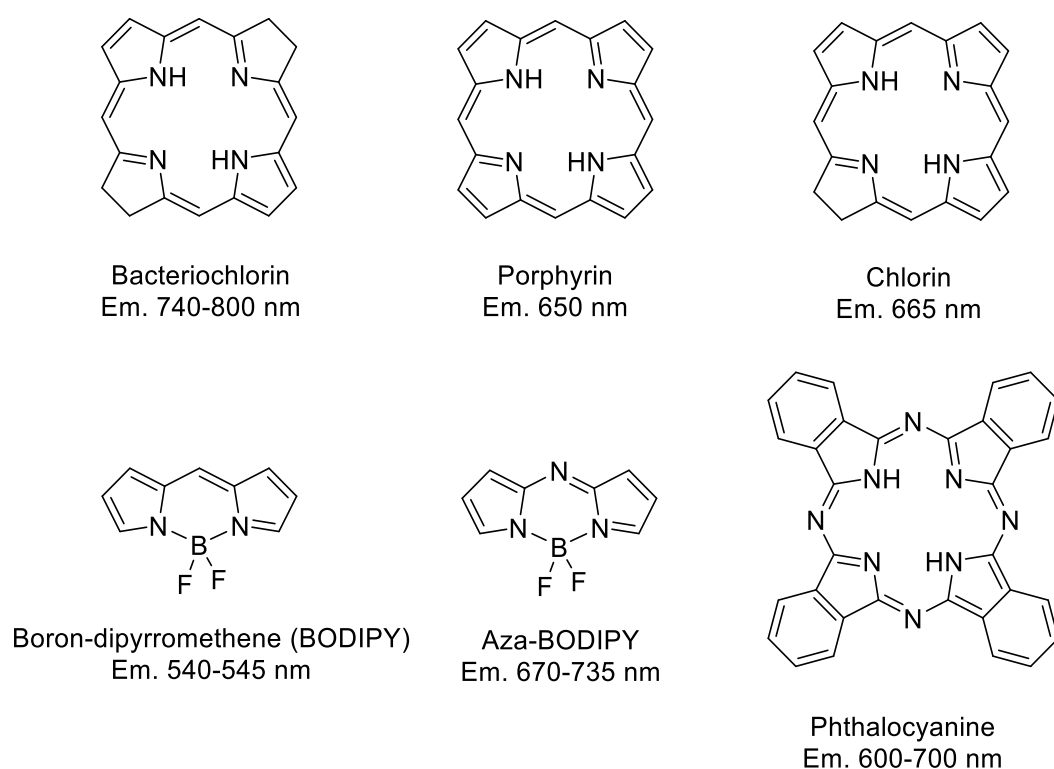


Figure 41. Alternative synthetic organic fluorophores.

In this project, BODIPYs, aza-BODIPYs and bacteriochlorins have been selected due to their distinctive advantages. (**Table 3**).

Table 3. Characteristics of an optimised NIR fluorescence probe: NIR emission, photostable, conjugatable, water soluble, low toxicity and ease of synthesis.

Properties	BODIPYs	Aza-BODIPY	Bacteriochlorin
Water-soluble	✓	✓	✓
Emission >700 nm		✓	✓
Low toxicity	✓	✓	✓
Photostability	✓	✓	✓
Conjugatable	✓	✓	✓
Easy to synthesis	✓	✓	

2. BODIPYs

BODIPYs (difluoroboron dipyrromethenes) are a class of derivatised dipyrromethene complexes. BODIPYs exhibit many advantageous photophysical properties such as high fluorescence quantum yields, definite Stoke shift, limited intersystem crossing to the triplet-state and intense emissions⁷⁷, making them very attractive as fluorophores. Since the development of the first BODIPY-based dye by Treibs and Kreuzer¹⁹⁴ in 1968, BODIPYs have been popularly used as fluorescent switches, sensors, and biological labels.¹⁹⁵ BODIPYs have especially been used in a variety of biological application, due to their relative stability against light, pH and chemicals. Also, BODIPYs have good solubility and long fluorescence lifetimes,¹⁹⁶ making them reliable fluorescence markers in biological systems. Due to the robust nature of the rigid BODIPY structure, various chemical modifications can be performed on the BODIPY core through different synthetic pathways. Both the physical and chemical properties can be finely tuned to achieve the desired fluorescence profile, making it a subject of interest for investigation of an optimised probe for FGS.

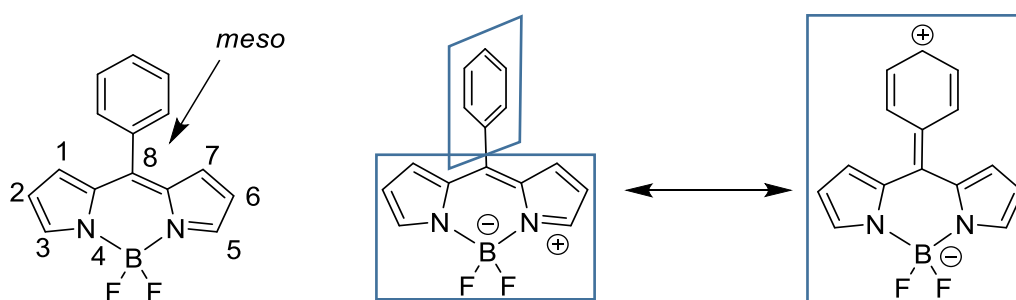


Figure 42. Schematic structure of a BODIPY core and internal quenching in 8-phenyl derivatives.

Through utilising differently substituted pyrroles such as 2,4-dimethylpyrrole and kryptopyrrole, analogues of BODIPYs can be synthesised to produce higher fluorescence quantum yields (0.70-0.81) and more intense absorption and emission bands.¹⁹⁷ Increasing substitutions on the pyrrolic part of the BODIPY can lead to a bathochromic shift for both the absorption and emission bands. For a typical BODIPY, the absorption and emission wavelengths are around 498 nm and 521 nm respectively (**Figure 43**).

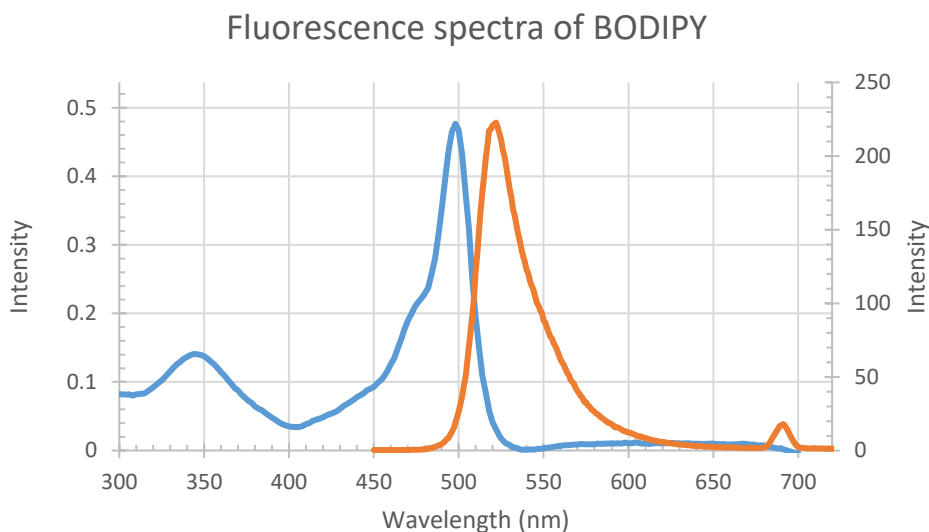


Figure 43. Typical UV-visible and fluorescence spectra of BODIPY, λ_{abs} (blue) and λ_{em} (orange).

The fluorescence of BODIPYs is also affected by intramolecular π -stacking in solution. There are two different ways that BODIPY dimers can stack, the parallel type are known as *H*-dimers, composed of parallel $S_0 \rightarrow S_1$ transition dipoles. The other type of stacking are known as *J*-dimers, consisting of 55° oriented in plane $S_0 \rightarrow S_1$ transition dipoles. The two types of dimer vary in electronic and photophysical properties, as the *H*-dimer exhibits a hypsochromic shift in absorption and emission as well as weaker fluorescence relative to the monomer, whereas the *J*-dimer shows an opposite behaviour with a bathochromic shift and higher fluorescence (Figure 44).

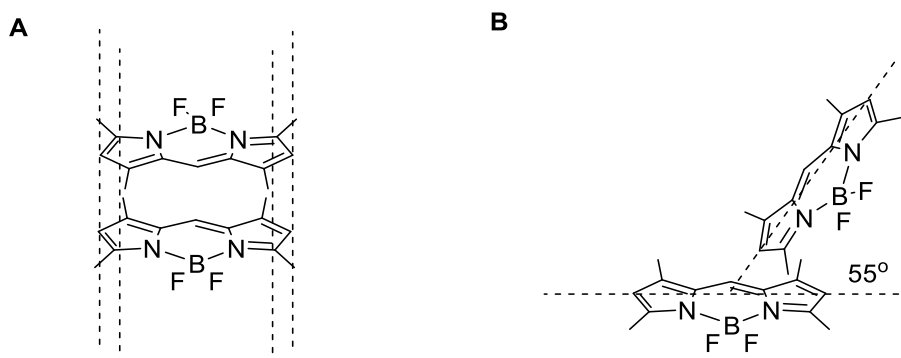


Figure 44. The proposed structure of *H*-dimer (A) and *J*-dimer (B).

Even though the *J*-dimer is fluorescent, varying the concentrations can affect the arrangement of those dimers, and the fluorescence can be significantly reduced in a

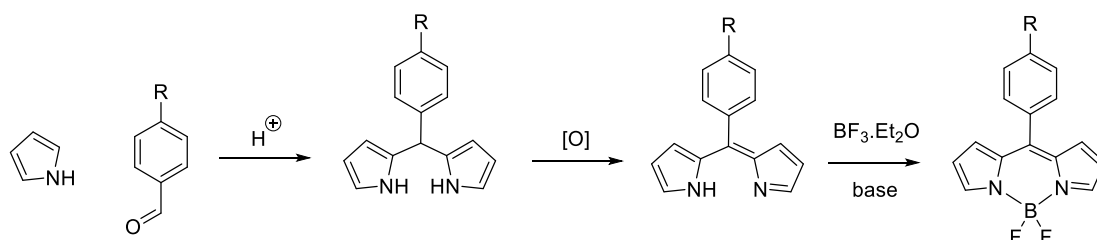
highly concentrated solution where the *H*-dimer becomes predominant. This effect was measured by Lennart B.-Å. *et al.*, using a flexible linker attaching the two BODIPYs and actively reducing the distance between BODIPYs, resulting in an increase in the probability of forming dimers.^{198–200} The formation of the dimers can be minimised by substituting the BODIPYs with bulky group as demonstrated by Trofimov *et al.* with mesityl groups at the 1-, 3-, 5- and 7- positions of the BODIPYs.²⁰¹

2.1 Synthesis of BODIPYs

Synthesis of the BODIPY framework can easily be carried out using commercially-available starting materials. Through the introduction of different electron releasing and withdrawing groups on the BODIPY core, different spectroscopic and photophysical properties can be induced.²⁰²

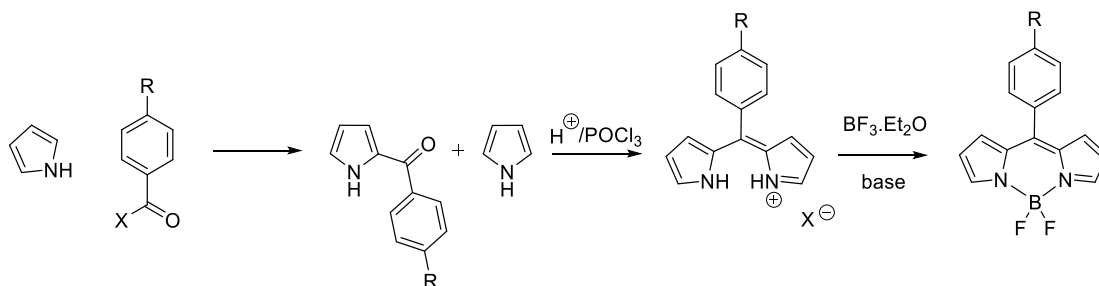
There are three well-known methods for synthesising BODIPY; one being the acid-catalysed condensation between pyrrole and aldehydes to produce dipyrromethanes.²⁰³ This reaction can be carried out with unsubstituted pyrroles (with the use of pyrrole as the solvent) or substituted pyrroles. Since the unstable dipyrromethane derivatives produced are sensitive to many environmental factors, such as light, air and acidic conditions, synthesis is often carried out as a one-pot reaction, following by oxidation using DDQ or *p*-chloranil to produce a dipyrromethene (dipyrrin).

Subsequently, this dipyrrin is treated with a base such as triethylamine or DIPEA and boron trifluoride etherate to produce a BODIPY complex. The resulting BODIPY dyes often have high stability allowing for pre- and post-synthetic modification without degrading the dye (**Scheme 1**).



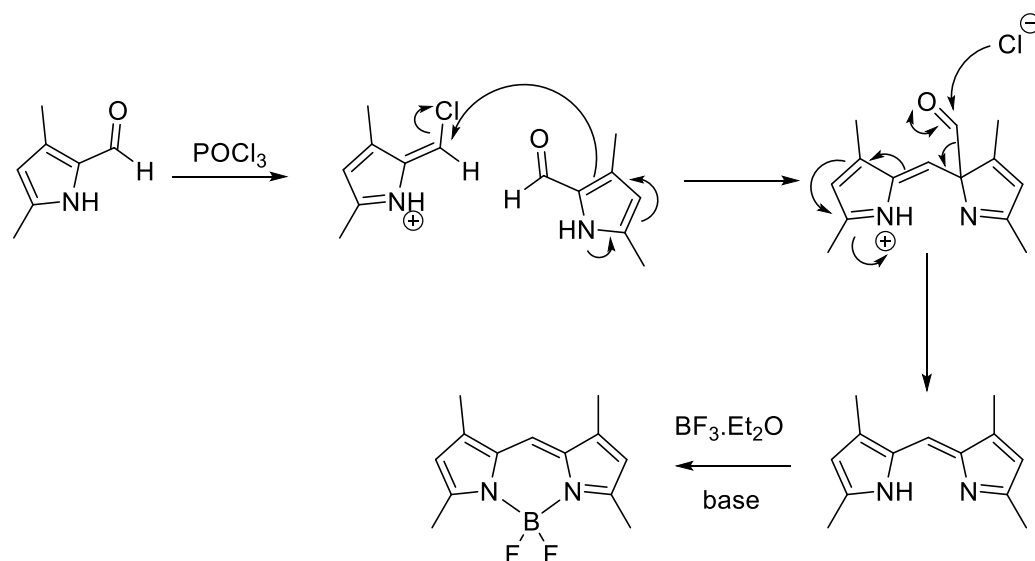
Scheme 1. Synthesis of symmetrical BODIPY *via* acid-catalysed condensation from pyrrole and aldehydes.

The other route for synthesising BODIPYs uses pyrrole and an acylium ion in a condensation reaction.^{204–207} The intermediate acylpyrrole can then react under acidic conditions with excess pyrrole to form a dipyrinium salt and hence is often not isolated due to its instability. BODIPYs are then produced through reaction with an appropriate base and boron trifluoride etherate. The main advantage of this reaction pathway is the ability to synthesise asymmetric dipyrrens, as the isolated acylpyrrole can react with a second different pyrrolic unit through an acidic condensation (**Scheme 2**).



Scheme 2. Synthesis of asymmetrical BODIPY *via* acid-catalysed condensation from pyrrole and acyl chloride.

An alternative route is the condensation of acylated pyrrole developed by Wu and Burgess²⁰⁸ as shown in **Scheme 3**. Their discovery involved the use of phosphorus oxychloride to promote self-condensation of pyrrole-2-carbaldehyde, hence a second pyrrole is not required. Phosphorus oxychloride causes the rapid substitution of the oxygen atom on the aldehyde to form a chlorinated azafulvene which is then substituted by a second pyrrole aldehyde. This reaction is followed by a nucleophilic attack with a chloride ion yielding dipyrromethene from an unstable intermediate. Through standard complexation, the dipyrromethene reacts to form symmetric BODIPYs. This one-pot method generates a product that requires little purification, and the reaction is generally higher yielding. Asymmetric systems can also be synthesised when utilising a different pyrrole.



Scheme 3. Condensation-decarbonylation of pyrrole-2-carbaldehyde with the use of a phosphorus oxychloride to yield intermediate dipyrrens and BODIPY compounds.⁷⁷

2.2 Extending wavelength

BODIPYs have been widely used as fluorescent probes and they are often linked to biological molecules to form fluorescent conjugates of proteins, antibodies and peptides for applications in biological imaging. Due to superior photostability, in comparison to other fluorescent probes such as fluorescein and rhodamine, BODIPY has become a popular substitute.¹⁹⁵ However, a notable deficiency of most BODIPYs is their short emission wavelength, which is around 500 nm, limiting *in vivo* applications, where the optimal window for transparency is 650-800 nm. Hence, the development of BODIPY dyes with an emission wavelength in the NIR region has become an area of significant research interest. Furthermore, absorption beyond 700 nm can significantly reduce problems such as autofluorescence and light scattering, allowing deeper tissue penetration, which could provide more efficient NIR FGS treatment.^{15,209,210} BODIPYs with bathochromic shifts can be synthesised through many different methods and these include halogenation²¹¹⁻²¹³, extended conjugation *via* Knoevenagel condensation^{99,214,215}, Suzuki coupling²¹⁶⁻²¹⁸, Sonogashira coupling^{218,219}, Heck reactions²¹⁸ and ring fusion²¹⁹ or the synthesis of aza-BODIPYs²²⁰⁻²²² (**Figure 45**).

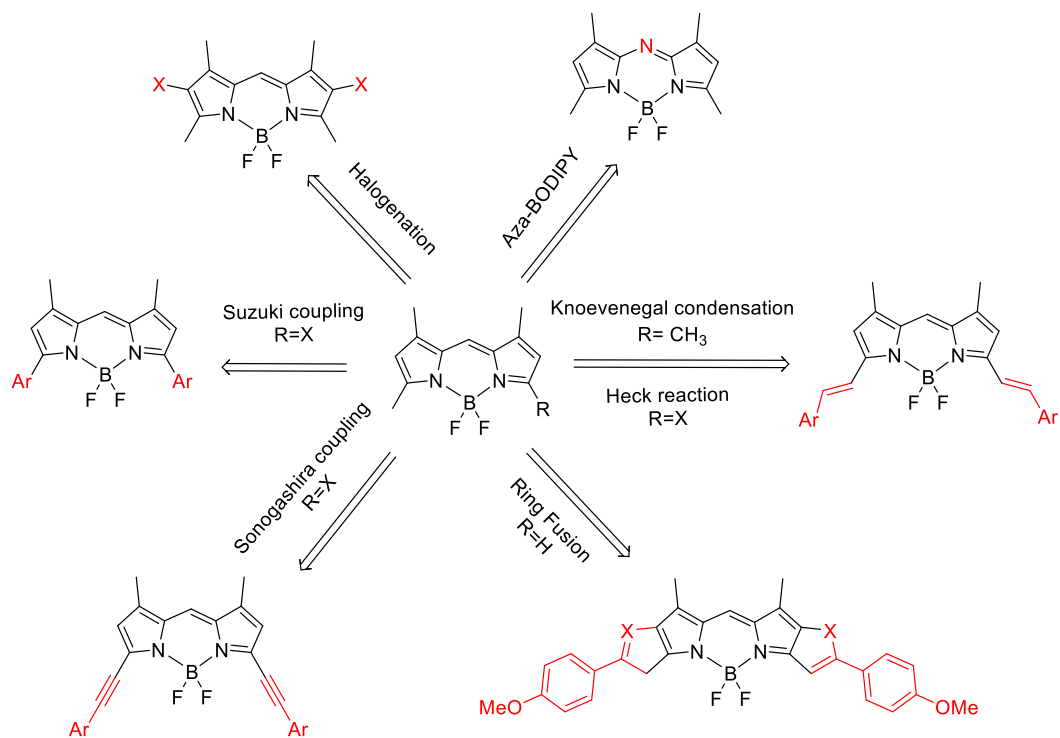


Figure 45. Methods for extending the wavelength of BODIPYs into the NIR region.

2.3 Result and discussion

A library of BODIPYs were synthesised to investigate the potential for this class of compound as NIR fluorescent probes and their biocompatibility for further bioconjugation to targeting biological molecules; three different pyrrolic units were used, allowing optimisation of the absorption and emission wavelengths. Different functionalities such as alkyne, azide, amine and NHS ester moieties were introduced that could be used for bioconjugation *via* CuAAC and peptide coupling. In addition, several different approaches were investigated in order to extend the wavelength into the NIR region, including regioselective bromination and extension of conjugation.

2.3.1 Pyrrole, 2,4-dimethylpyrrole and kryptopyrrole BODIPYs

The general method for synthesising BODIPYs was applied, with slight modifications through the use of different pyrroles. Initially, 8-phenyl BODIPYs were investigated, due to their ease of synthesis. However, it has been observed that, upon substitution of a freely rotating aryl group at the 8-position (*meso*-position), the conjugated system can become coplanar. Excited energy is then lost from the BODIPY core through radiative decay, initiating internal quenching and hence leading to a decrease in the fluorescence

quantum yield.²²³ This effect can be counteracted by restricting the rotation of the 8-position aryl ring through the insertion of bulky substituents such as methyl group to the 1,3,5,7-positions of the pyrrolic unit. Therefore, preventing the quenching of the fluorescence and resulting in higher fluorescence quantum yields (**Figure 46**).

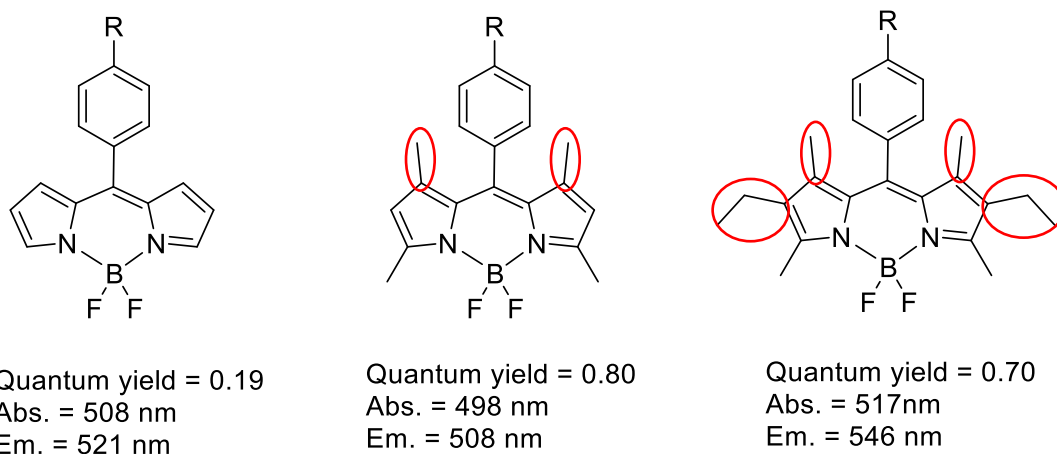


Figure 46. Alkyl- substituted pyrrolic units of BODIPYs as a possible resolution to freely rotating aryl group inducing fluorescence quenching.

Significant modifications for synthesising the library of 8-phenyl BODIPYs shown below included the use of Celite, instead of silica, to remove dipyrromethene and polypyrrole after the addition of BF_3 etherate, since it was observed that the BODIPYs adhered to silica, causing excessive losses of product. Each of the BODIPYs was synthesised with a range of functionalised groups that could be used for further conjugation. The yield of BODIPYs **1-13** ranged from 8% - 61% with varying functionalities. The yields were generally similar to literature values of around 50%, although electron withdrawing substituents generally gave lower yields (**Figure 47**).

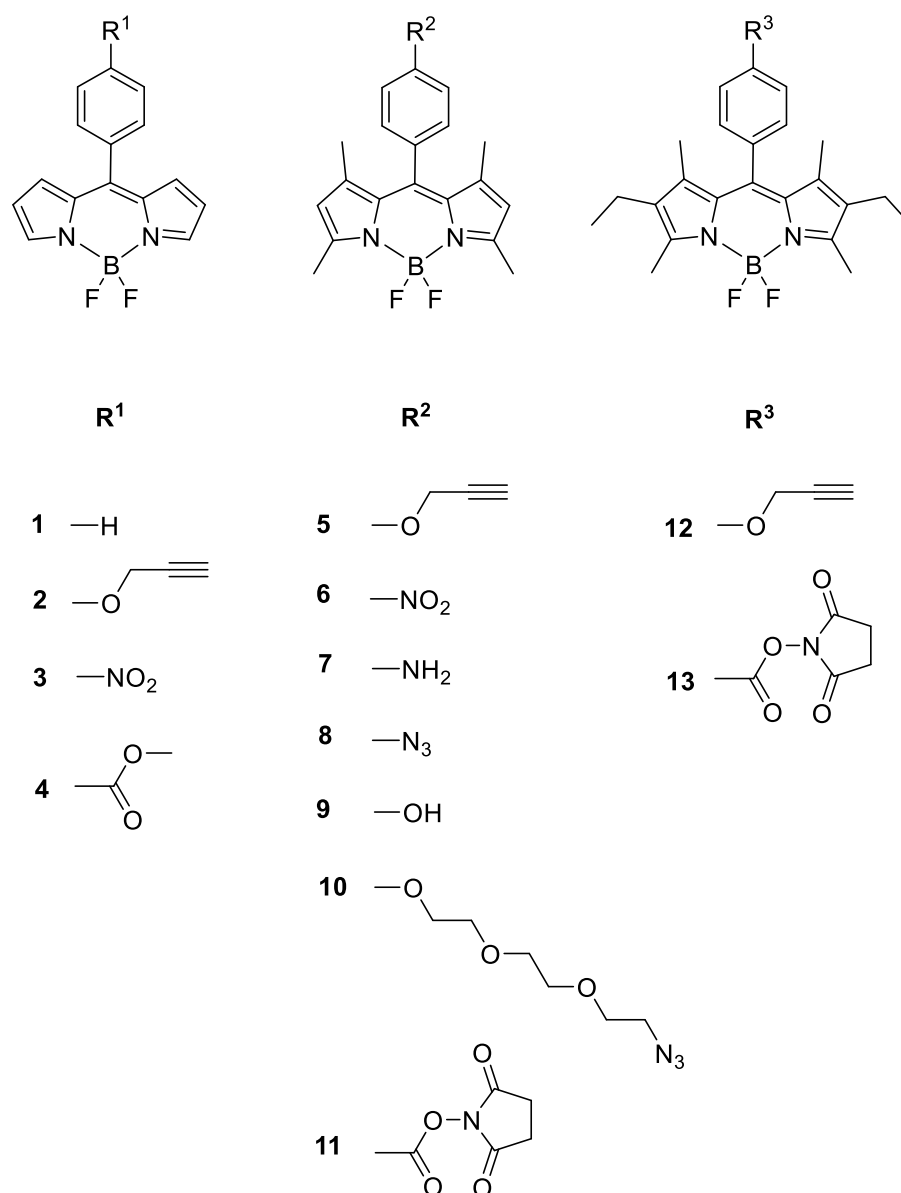
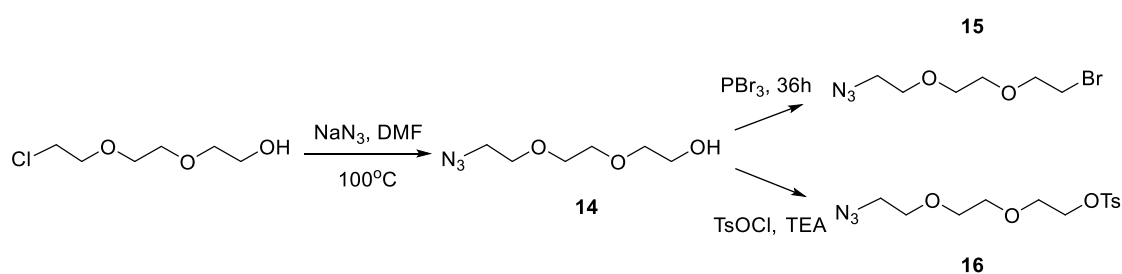


Figure 47. Library of BODIPYs with the different pyrrolic unit and conjugatable functional groups.

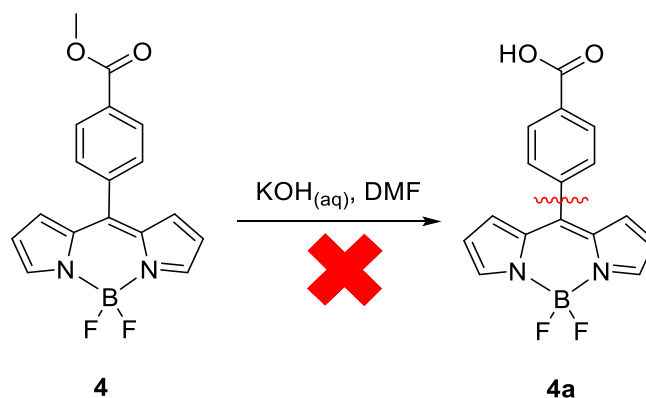
A series of azide, alkyne, amine and NHS ester BODIPYs were synthesised for further conjugation with biological targets. The azide BODIPYs were synthesised *via* two different approaches. The first approach involved a three-step reaction. The nitro BODIPY **6** was first synthesised by reacting 4-nitrobenzaldehyde with 2,4-dimethylpyrrole. This was subsequently reduced to the corresponding amino BODIPY **7**, which was immediately converted to an azide through diazotisation to obtain **8** with a yield of 67%. A second approach was also employed due to the low yield of nitro BODIPY **6**. This reaction involved the synthesis of a hydroxyl BODIPY **9**, *via* reaction

between 4-hydroxybenzaldehyde and 2, 4-dimethylpyrrole. An azide PEG chain was synthesised through a two-step reaction, in which 2-(2-(2-chloroethoxy)ethoxy)ethanol was reacted with sodium azide to afford **14** with a 99% yield. This was then brominated with PBr_3 to obtain **15**. The azide on the PEG chain **15** was difficult to identify by thin layer chromatography (TLC) using PPh_3 with ninhydrin as indicator, hence it was taken to the next step without further purification. Subsequently, **16** was synthesised through the reaction of **14** with 4-toluenesulfonyl chloride to provide a traceable azide PEG chain with a good leaving group for further nucleophilic substitution (**Scheme 4**). This was then reacted with **9** to produce **10** *via* Williamson-ether synthesis. All intermediates and BODIPYs were characterised by ^1H , ^{13}C , ^{19}F -NMR and MS.



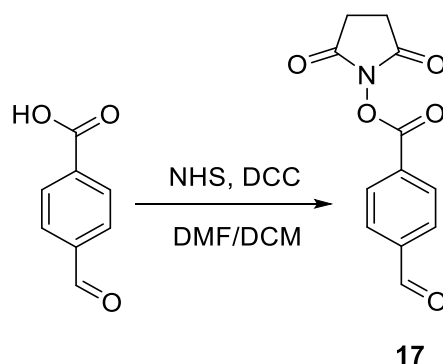
Scheme 4. Synthesis of azide PEG chains.

After the synthesis of the benzoate BODIPY **4**, a hydrolysis reaction was carried out in an attempt to synthesise a benzoic acid substituted BODIPY, with the final aim of synthesising an NHS ester substituted BODIPY. However, NMR showed the reaction had not produce the desired product, with a significant reduction in intensity of the distinctive two doublet peaks representing the phenyl ring. This suggested a rapid degradation of the compound due to the use of harsh conditions, therefore milder hydrolysis conditions or an alternative aldehyde was required (**Scheme 5**).



Scheme 5. Cleavage of benzoic acid from the *meso* position of BODIPY.

As a result, an alternative synthesis was attempted. An NHS ester benzaldehyde was therefore synthesised to be used to form the BODIPY instead. Compound **17** was synthesised from the reaction of 4-formylbenzoic acid and NHS with DCC in a mixture of DMF and DCM under an inert atmosphere. The product was collected by filtration in a yield of 66% and subsequent synthesis of the corresponding BODIPYs **11** and **13** was shown to be successful (**Scheme 6**).



Scheme 6. Synthesis of NHS ester aldehyde **17**.

The absorption and emission of each BODIPY was analysed by absorbance and fluorescence spectroscopy (**Figure 48**).

Table 4. The absorption, excitation and emission wavelength (nm) of BODIPY 1-13.

BODIPYs	Absorption wavelength (nm)	Excitation wavelength (nm)	Emission wavelength (nm)
1	498	345	522
2	499	450	518
3	508	400	543
4	506	495	530
5	501	480	510
6	505	450	514
7	500	495	511
8	504	504	515
9	500	440	513
10	499	480	512
11	504	490	521
12	525	480	539
13	529	500	550

UV-vis spectrum of BODIPYs 1-13

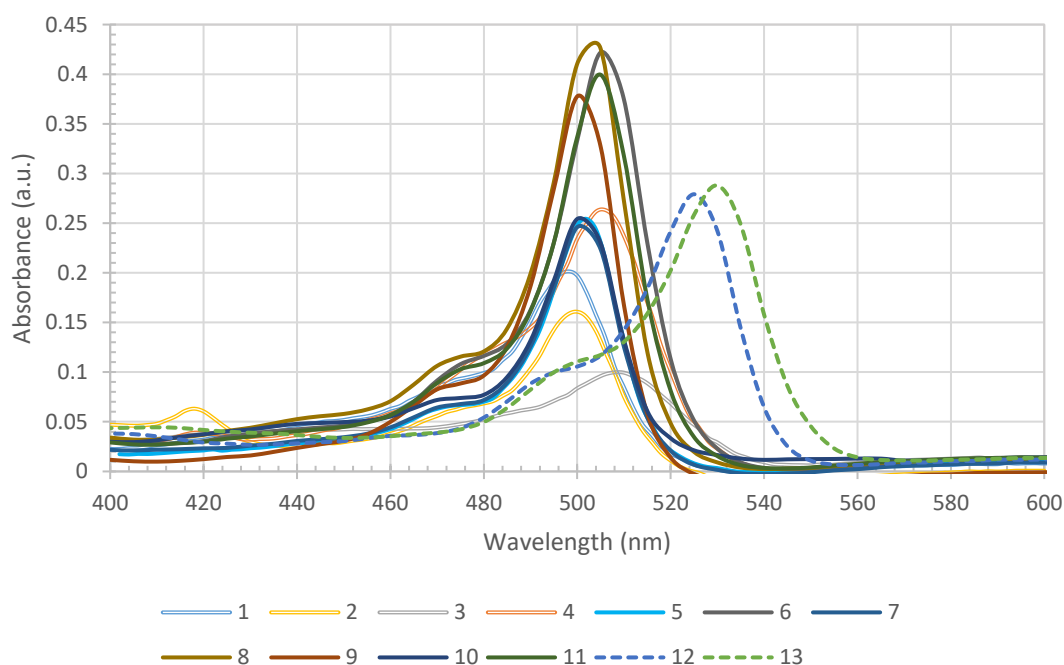


Figure 48. UV-visible spectrum showing the λ_{abs} of unsubstituted BODIPYs 1-4 (hollow lines), 1,3,5,7,8-substituted BODIPYs 5-11 (solid lines) and 1,3,5,7, 8-substituted 1,2,3,5,6,7,8-substituted BODIPYs (dash lines) in 4.8 μM solution of DCM.

2.3.2 Regioselective bromination

BODIPY has an electron rich structure suggesting it is susceptible to electrophilic aromatic substitution, therefore making them attractive for chemical modification with halogens. A commonly used method developed by Shinokubo *et al.*²¹³ to regioselectively brominate BODIPYs was first applied to the unsubstituted phenyl BODIPY **1** and benzoate BODIPY **4** with 2.4 equivalents of NBS in DCM at room temperature to produce di-brominated BODIPYs **18** and **19** with yields of 79% and 60% respectively (**Figure 49**). The structures were confirmed by ¹H, ¹³C, ¹⁹F-NMRs and MS. The atomic structure of **19** was obtained through X-ray crystallography as shown in **Figure 50**.

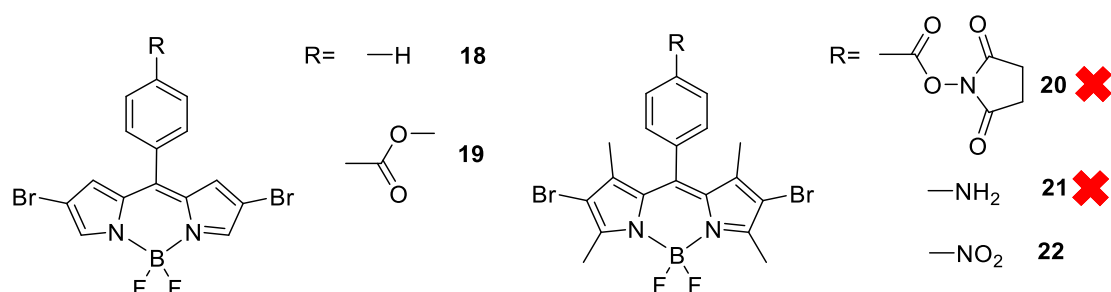


Figure 49. Schematic structure of brominated BODIPYs.

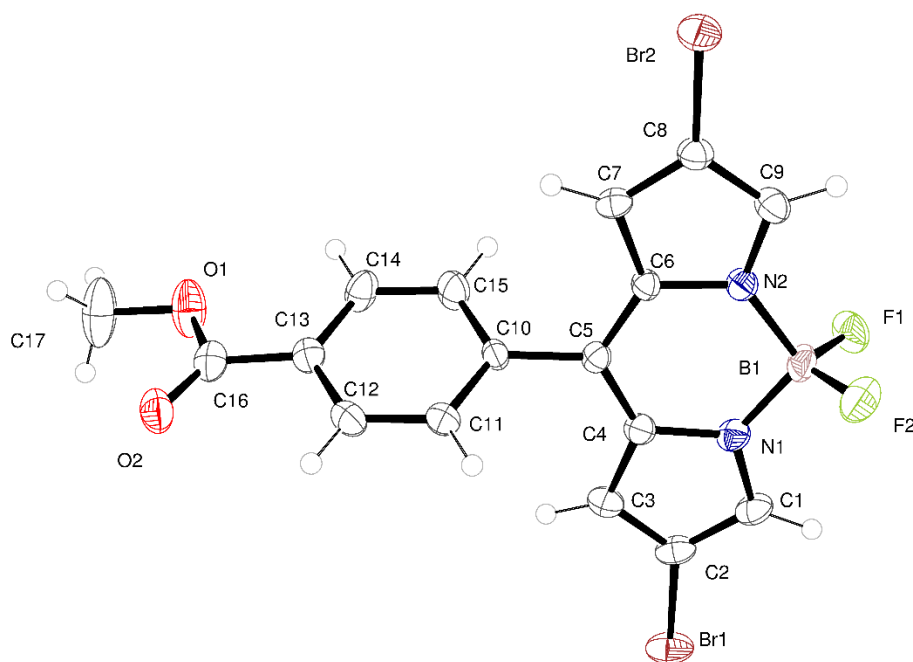


Figure 50. X-ray crystallography structure of BODIPY **19**.

Absorption and emission spectral analysis showed bathochromic shifts for both absorption and emissions peaks with λ_{abs} 42 nm and λ_{em} 41 nm red shifts for **18** and λ_{abs} 45 nm and λ_{em} 43 nm red shifts for **19** upon bromination (**Figure 51**).

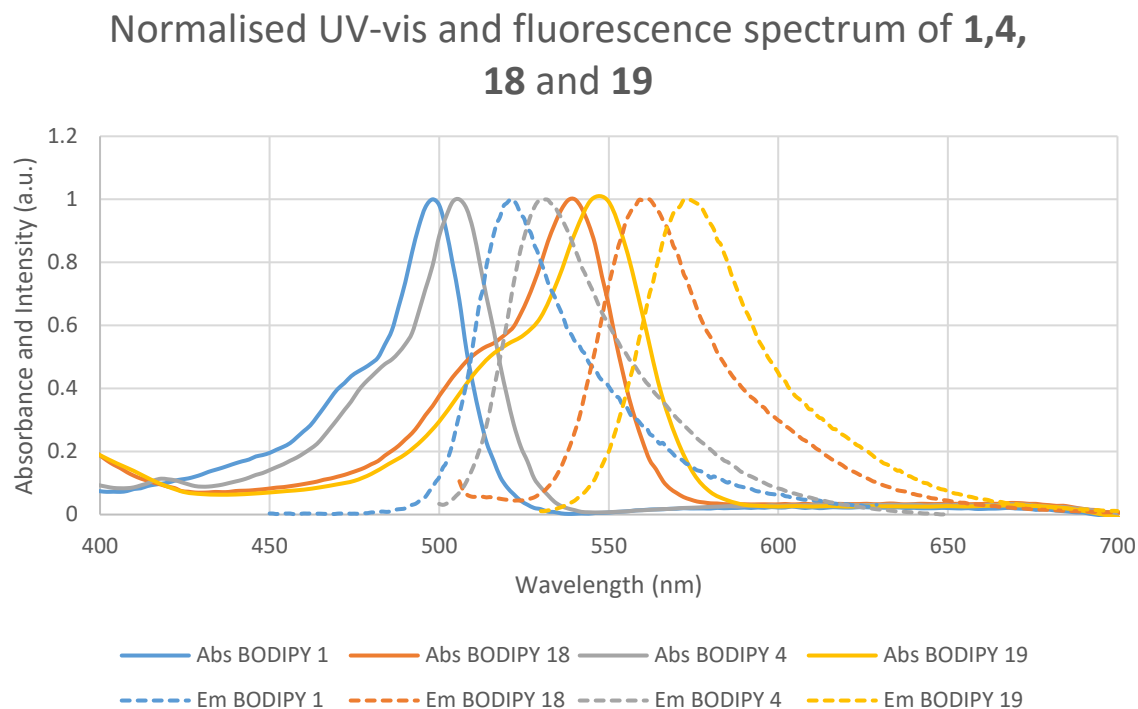


Figure 51. Normalised UV-visible and fluorescence spectra of BODIPY, **1** (blue), **4** (orange), **18** (grey) and **19** (yellow) in DCM, λ_{abs} (solid line) and λ_{em} (dash line).

The bromination of 1,3,5,7- methyl substituted NHS ester BODIPY **11** was attempted using the method of Akkaya *et al.*²¹² and was reacted with AIBN, NBS in CCl_4 . It was observed that although column chromatography with silica provided a good separation, the NHS ester began to degrade and hydrolyse on silica to give a mixture of compounds. This was confirmed by $^1\text{H-NMR}$, as a broad singlet peak at 10.28 ppm was observed, indicating the presents of a carboxylic acid, the NMRs also showed two distorted and unresolved aromatic peaks for the aryl ring indicating the present of a mixture (**Figure 52**).

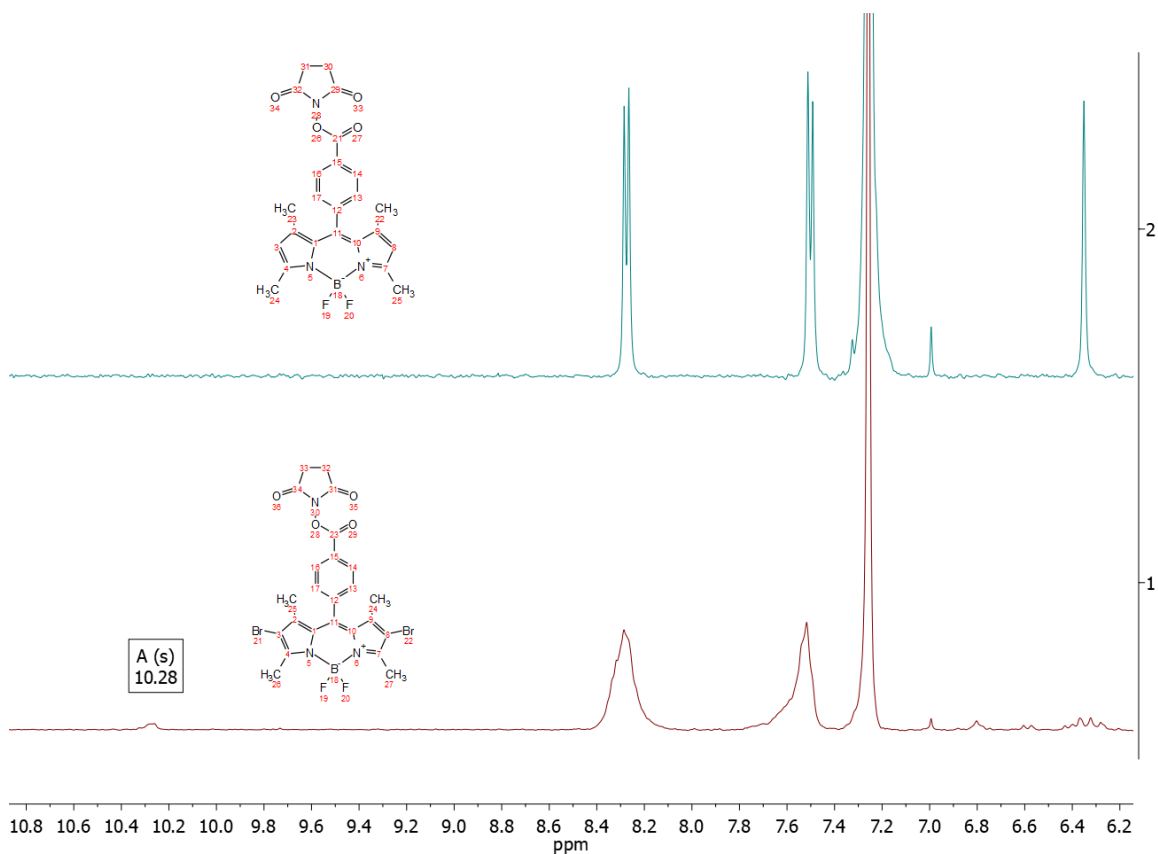


Figure 52. ¹H-NMR of attempted synthesis of BODIPY **20**, a broad singlet peak at 10.28 ppm indicating carboxylic acid formation.

Similarly, another negative result was observed for the bromination of amino BODIPY **7**. The ¹H-NMR of **21** suggested potential brominations on the phenyl ring as the aryl protons previously observed at 6.78 ppm and 7.01 ppm no longer existed in any of the fluorescent fractions collected as shown in **Figure 53**.

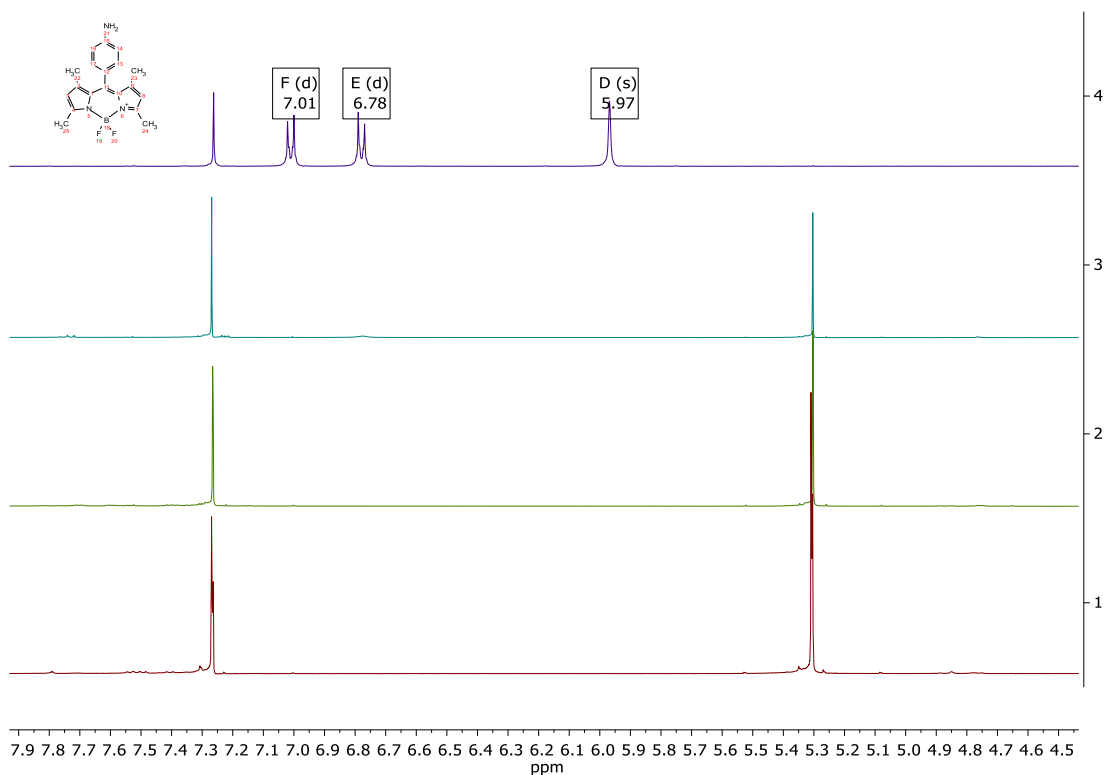


Figure 53. ¹H-NMR of attempted synthesis of BODIPY **21**, showing the absence of aryl protons previously at 6.78 ppm and 7.01 ppm for the three collected fractions from column chromatography.

Alternatively, bromination using Shinokubo *et al.*'s method²¹³ to regioselectively brominate the 1,3,5,7- methyl substituted nitro BODIPY proceeded with NBS in DCM to successfully obtain BODIPY **22** and its structure was confirmed by ¹H, ¹³C, ¹⁹F-NMRs and MS. This result reinforced the prediction regarding the deactivation effect on electron withdrawing groups when regioselectively brominating at the 2,6-positions.

Normalised UV-vis and fluorescence spectrum of **6** and **22**

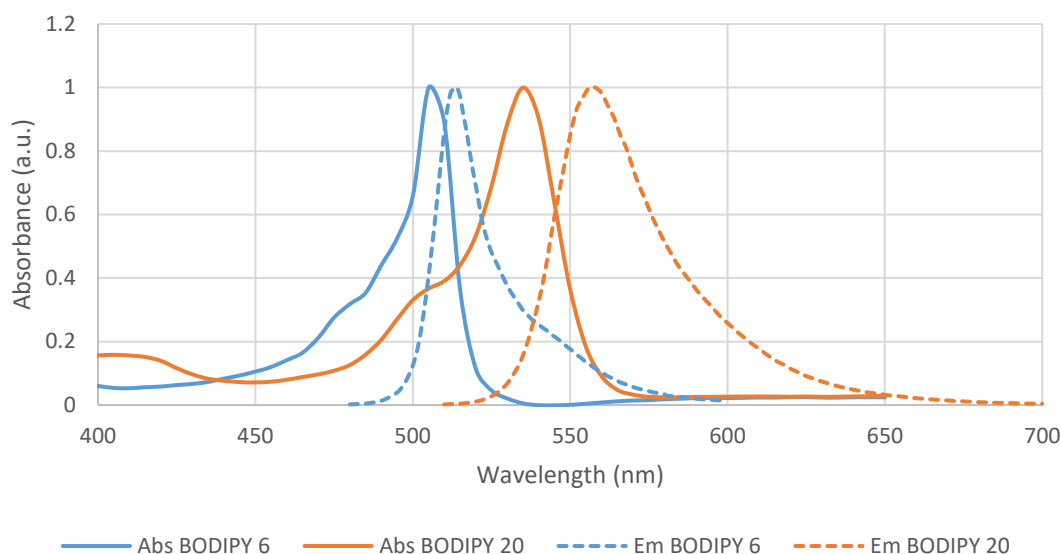


Figure 54. Normalised UV-visible and fluorescence spectrum of **6** and **22** in DCM, λ_{abs} (solid line) and λ_{em} (dash line).

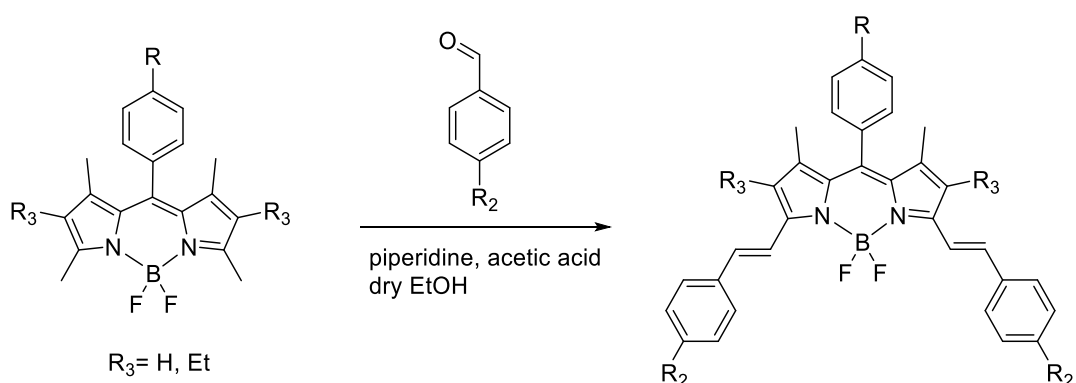
Similarly, with the 2,6-brominated nitro BODIPY **22**, a significant bathochromic shift was observed in both the absorption and emission spectrum of 30 nm and 45 nm respectively (**Figure 54**).

In general, halogenation was shown to be a difficult reaction to control for regioselective bromination of the targeted positions. Despite this, bromination did induce bathochromic shifts ranging from 30-45 nm, however this was not sufficient to reach the NIR region. The fluorescence properties of BODIPYs are affected by the heavy atom effect upon bromination. The effect increases the efficiency of intersystem crossing to the triplet state, resulting in possible loss of fluorescence. Halogenated BODIPYs may therefore be more useful as photosensitisers, rather than as NIR fluorescence probes.

2.3.3 Diaryl-Knoevenagel condensation

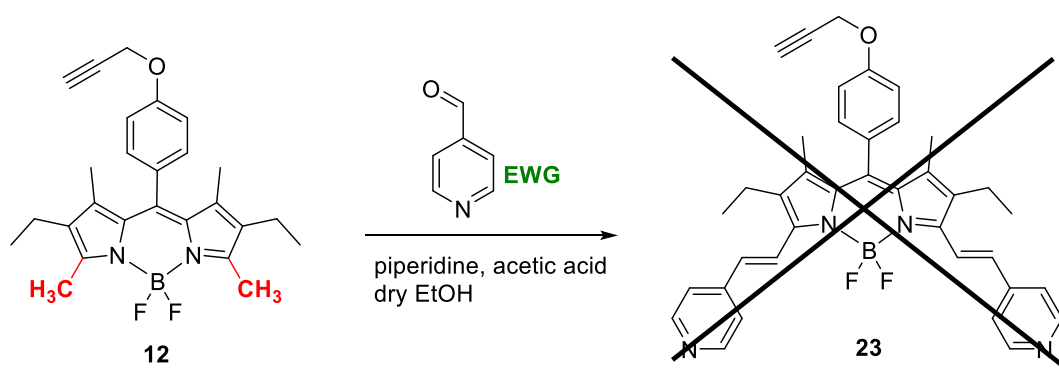
In order to extend the conjugation and induce bathochromic shifts, Knoevenagel condensation was carried out by adapting the pioneering work of Akkaya *et al.*²²⁴ The 1,3,5,7-methyl substituted BODIPYs and kryptopyrrole BODIPYs can react through Knoevenagel condensation with excess aromatic aldehydes to generate the corresponding distyryl or diaryl derivatives (**Scheme 7**). Through extending the

conjugation of the BODIPYS a large red shift for both absorption and emission wavelength can be observed into the far-red or NIR region. This has been used for several BODIPYs to induce bathochromic shifts and potentially harness their NIR fluorescence property.^{214,225–227}



Scheme 7. Synthesis of diaryl-Knoevenagel condensation.

This method was first applied to a BODIPY derived from kryptopyrrole under microwave irradiation.²²⁸ Initially, literature conditions were utilised (10 minutes, 130 °C and 1 min-pre-stirring), however, the major product obtained was the mono-aryl BODIPY. Due to the kinetics of this reaction, the length of the reaction was increased to 20-30 minutes. This method was first used with an alkyne substituted BODIPY using 4-pyridinecarboxaldehyde, but this was shown to be unsuccessful by TLC, NMR and UV-visible spectroscopy, with all data observed identical to BODIPY **12**, suggesting no reaction had taken place (**Scheme 8**).



Scheme 8. Knoevenagel condensation reaction of BODIPYs **12** with EWG.

It was later identified that the Knoevenagel condensation of 4-pyridinecarboxaldehyde with alkyl BODIPY does not proceed under the same reaction conditions.²¹² It has been

suggested that the reaction will only proceed with BODIPYs brominated at the 2,6-positions, and this was believed to be due to the associated increase in acidity of the methyl groups. Therefore, the reaction was speculated to be thermodynamically driven. Theoretically, the methyl groups should be deprotonated by piperidine forming a carbon centred anion (CH_2^-). However, without the electron withdrawing effect of bromine groups at the 2,6-position of the BODIPY, the methyl groups are insufficiently acidic. The electron withdrawing nature of 4-pyridinecarboxaldehyde would also destabilise the enolate ion of intermediate. As a result, preventing the formation of the desired mono- and di-adduct in a reversible reaction as shown in **Figure 55**.

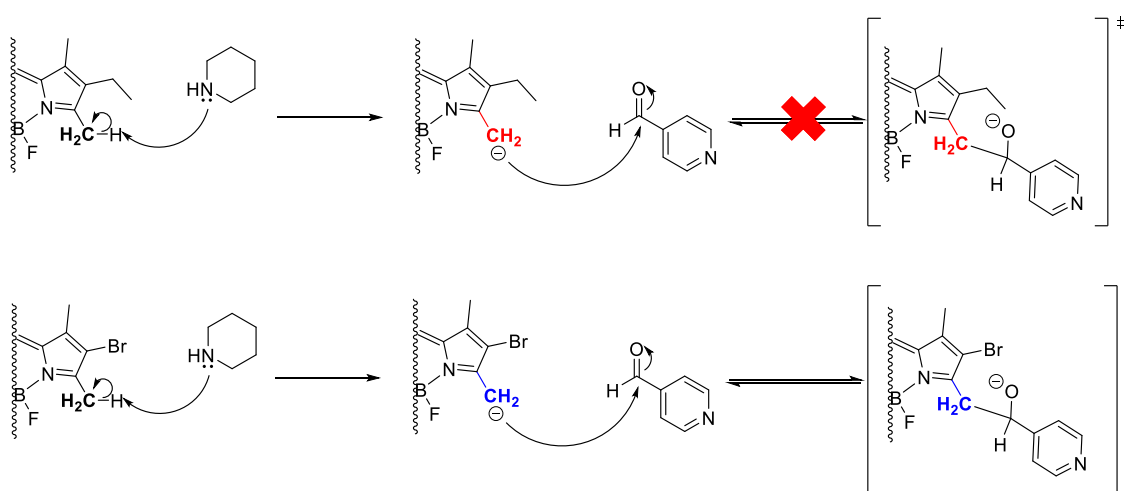
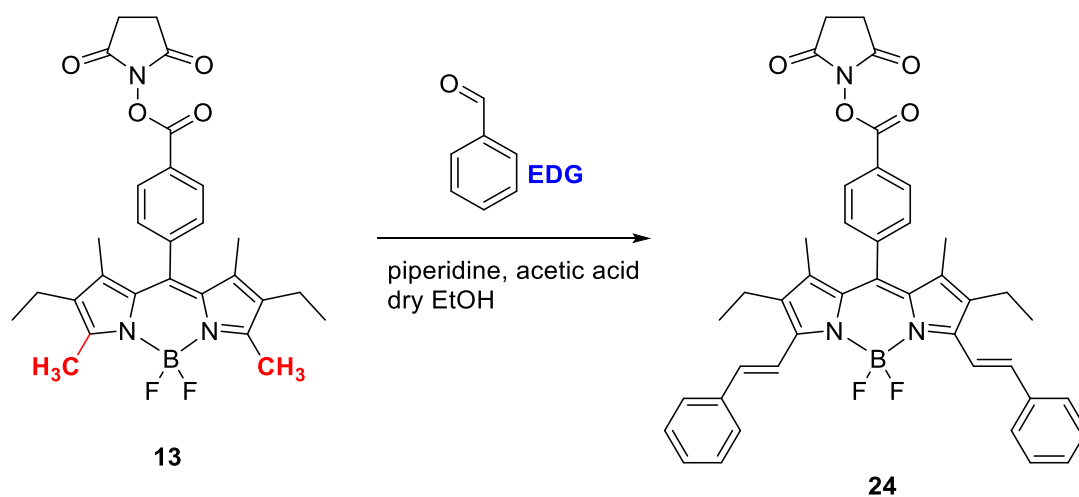


Figure 55. Proposed mechanistic explanation to the unreactive nature of 4-pyridinecarboxaldehyde with methyl BODIPY.

Hence, increasing acidity of the 1,7-methyl groups would allow the methyl groups to become more susceptible to participation in Knoevenagel condensations with a EWG.²¹² However, a non-halogenated methyl BODIPY can undergo reactions with EDG. This led to the synthesis of Red BODIPY **24**, the NHS ester BODIPY was reacted with benzaldehyde under microwave irradiation, this reaction proved to be successful. After the reaction, a distinctive colour change in the solution from pink to blue was observed and the crude mixture was purified by column chromatography to give extended conjugation and bathochromically shifted BODIPY **13** with a 27% yield. The low yield was due to incomplete reaction, giving a mixture of starting materials, mono-styryl and di-styryl BODIPYs (**Scheme 9**).



Scheme 9. Knoevenagel condensation reaction with EDG to produce BODIPYs **24**.

Although this shifted the wavelength for both absorption and emission peaks to the red region, from λ_{abs} 529 nm to 640 nm, and λ_{em} 550 nm to 656 nm respectively, the wavelength did not reach the NIR regions. The Stokes shift remained small and two peaks were observed for both absorption and emission spectrum and with excessive overlap between the peaks. This compound did not provide a clear excitation wavelength and two absorption bands can be a major limitation against both band pass and long pass filters that are commonly used for fluorescence imaging. When the first absorption peak at 580 nm was excited, two emission peaks at around 600 nm and 658 nm were observed, the first emission was the result of the first absorption band at 580 nm and *vice versa* for the second emission band observed (**Figure 56**).

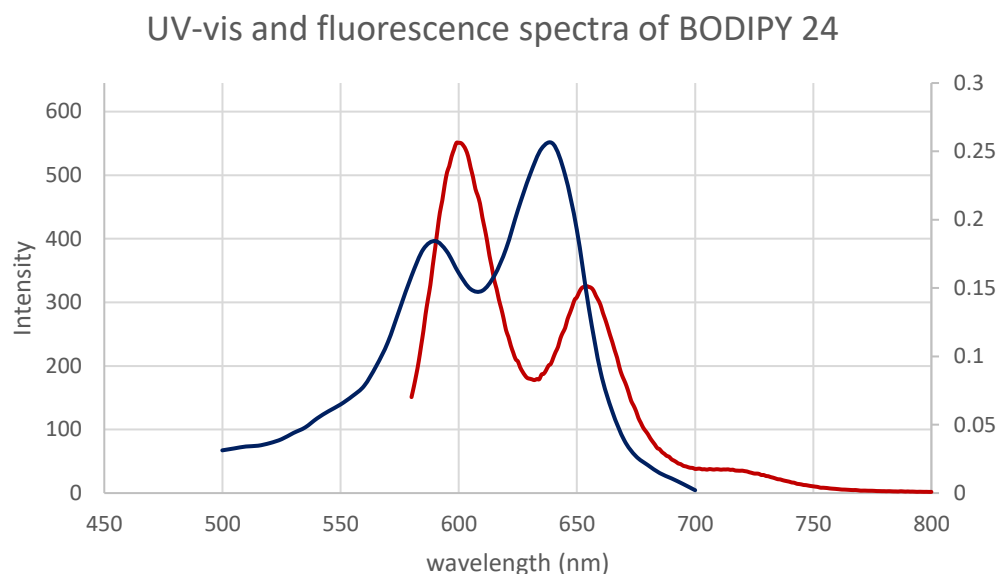
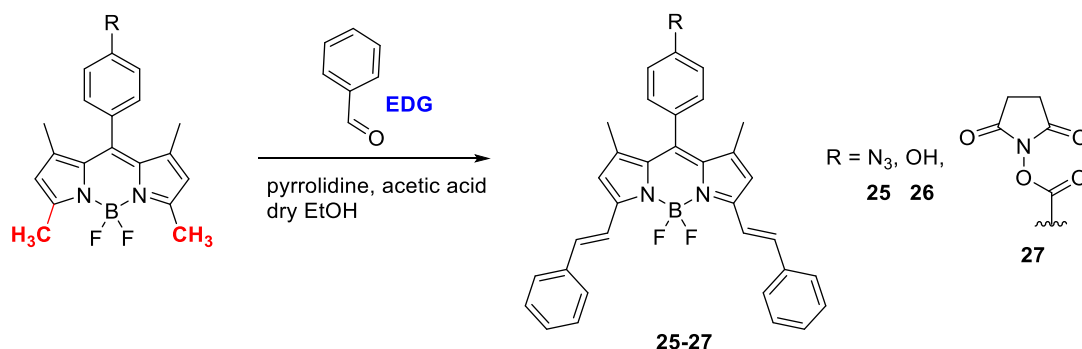


Figure 56. UV-visible and fluorescence spectra of **24** in DCM, λ_{abs} (blue) and λ_{em} (red).

The same synthetic conditions were then applied to the 2,6-unsubstituted BODIPYs. However, the reaction did not reach completion, even with extensive heating and longer reaction times, as the reaction kinetics were slow, this resulted in a lower yield overall. To increase the rate of reaction, an alternative base to piperidine was investigated. Adapting a previously developed method,²²⁹ the reaction was conducted with benzaldehyde, acetic acid and pyrrolidine and heated under reflux, the progress was constantly monitored by TLC and was subsequently purified by column chromatography. Thus, distyryl Red BODIPYs **25-27** were synthesised with yields ranging from 20-74%. The yield for NHS ester substituents **27** was found to be much lower at 20% compared to **25** and **26**. This was likely due to rapid hydrolysis on column chromatography using silica. The compounds obtained were characterised using ^1H , ^{13}C , ^{19}F -NMRs, MS, UV-visible spectroscopy and fluorescence spectroscopy. (**Scheme 10**)

Pyrrolidine was used to replace piperidine, in an attempt to increase the rate of reaction. Pyrrolidine has a more basic nature, it has a smaller ring and higher electron density at the nitrogen atom that contributes to stabilising the pyrrolidine cationic form in a polar solvent. As a consequent, the changes in the base significantly improved the reaction rate of the Knoevenagel condensation reaction with the 3,5-dimethyl positions.



Scheme 10. Knoevenagel condensation reaction of BODIPYs and benzaldehyde to form distyryl adducts.

The UV-visible and fluorescence spectra of those compounds were analysed to observe a general trend of bathochromic shift for both absorption and emission peaks. Similar to Red BODIPY **24**, 2,6-unsubstituted Red BODIPY **25-27** also suffers from the extensive overlap for both absorption and emission peaks. To circumvent this, a more precise excitation wavelength was required for each of the Red BODIPYs, hence excitation wavelength at 570 nm or above was used to discriminate the emission peak at around 580 nm resulting from the excitation of a lower wavelength. (**Figure 57**)

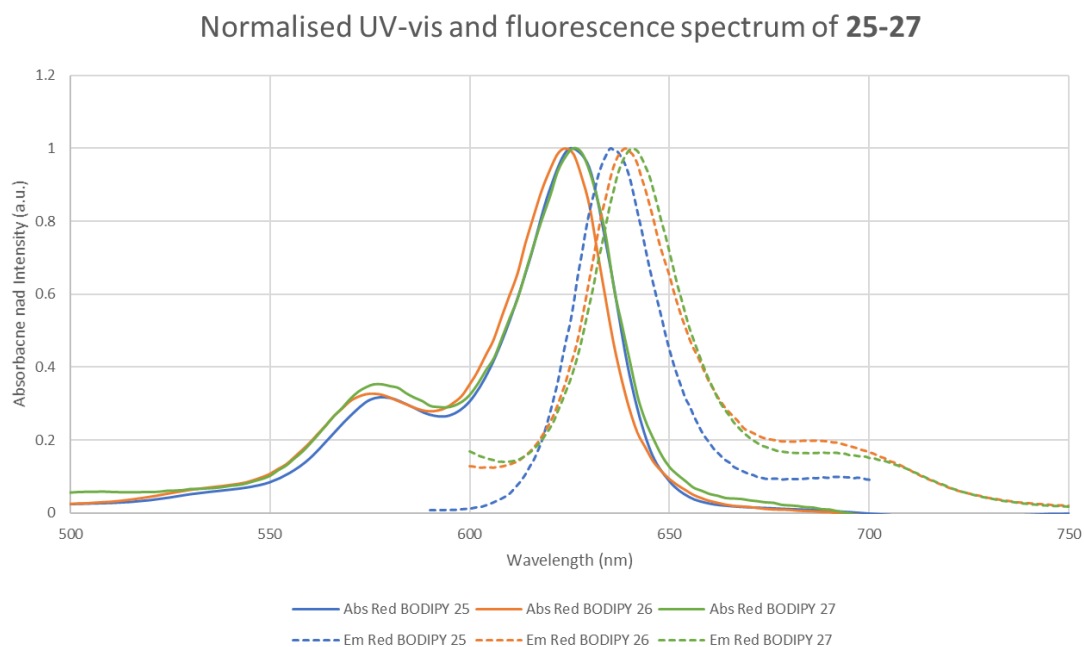


Figure 57. Normalised UV-visible and fluorescence spectra of **25-27** in DCM, λ_{abs} (solid line) and λ_{em} (dash line).

The fluorescence spectrum of the Red BODIPYs were compared to the corresponding BODIPYs to reveal a significant red shift of approximately 120 nm. This modification through extended conjugation has been demonstrated to be one of the most efficient and effective ways to induce red shifts in BODIPYs. (**Figure 58**)

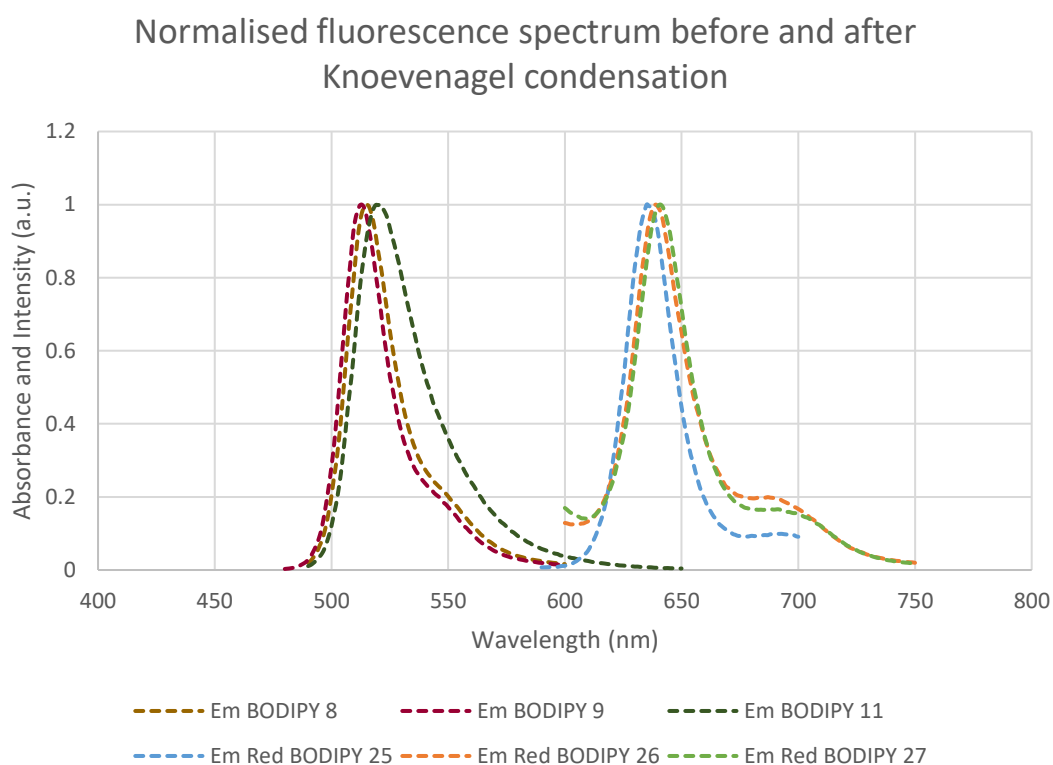


Figure 58. Normalised fluorescence spectrum of BODIPY **8, 9, 11** and corresponding red BODIPYs **25-27** in DCM after Knoevenagel condensation.

Overall, despite a clear and significant bathochromic shift observed in both absorption and emission wavelength for Red BODIPYs, the Stoke shift for these compounds was again relatively small, as well as the emissions observed being only in the far-red region rather than NIR region as desired. Along with significant overlap of absorption and emission peaks, accurate excitation of those compounds is made more challenging and is generally limiting in their application in a surgical environment. Therefore, in conclusion, the extended conjugation BODIPYs were found to not be ideal NIR fluorophores for application in NIR FGS.

3. Aza-BODIPY

Aza-BODIPYs have the core structure of a BODIPY with the *meso* carbon atom replaced by a nitrogen atom. This change causes a reduction in the band gap, giving aza-BODIPYs their characteristic NIR absorption and emission wavelengths with a high extinction coefficient and an adequate fluorescence quantum yield at around 0.3 (Figure 59).²²¹

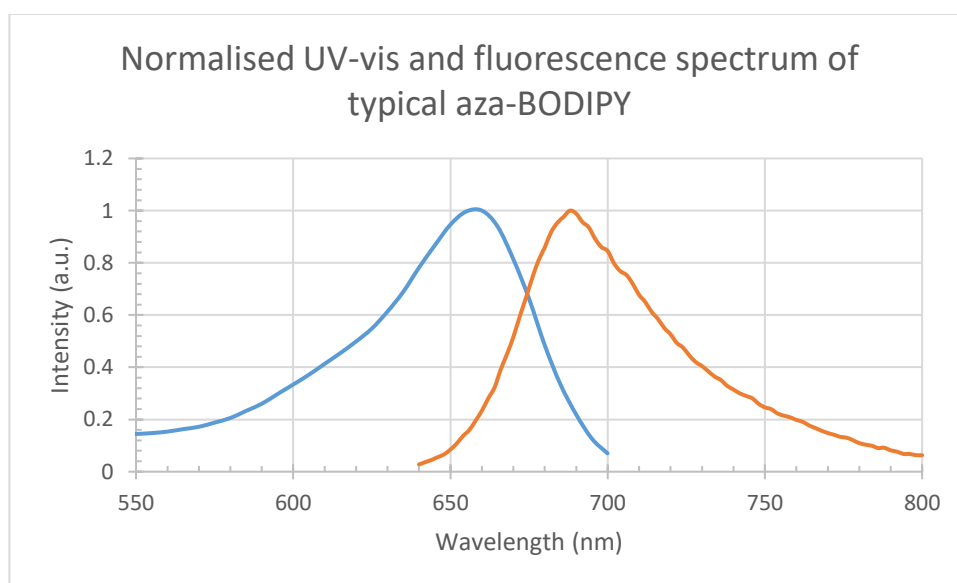
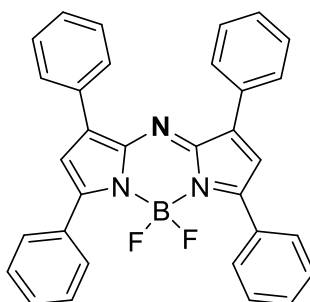


Figure 59. Chemical structure of aza-BODIPY and typical UV-visible and fluorescence spectrum, λ_{abs} (blue) and λ_{em} (orange).

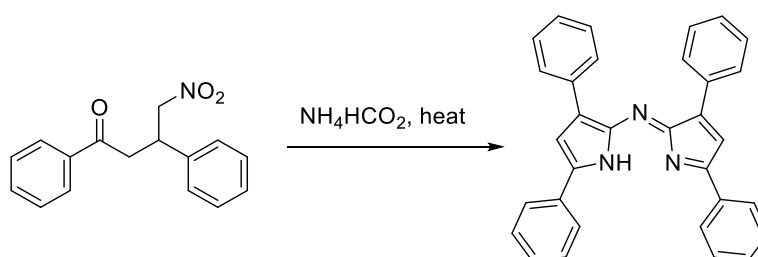
This class of compound was first described in the 1940s,²³⁰ however, its applications were not widely explored until O'Shea *et al.* developed an optimised reaction for the facile synthesis of symmetrically substituted aza-BODIPYs. The optimised reaction provided a more synthetically friendly pathway to obtain aza-BODIPYs and eventually led to an increase in interest in this new class of dye. Like their BODIPY counterparts, aza-BODIPYs exhibit relative insensitivity toward changes in pH and solvent polarity.

Due to many of their physical and chemical advantages, these molecules have recently been the subject of many biological studies^{231,232} and materials based applications^{233,234}. The strong absorption and emission in the NIR diagnostic window have allowed this class of compounds to become extremely promising as fluorescence agents for NIR FGS.

Since one of the major concerns with NIR fluorescence probes is the extent of photobleaching under constant light illumination, Aza-BODIPYs were suggested to be a superior alternative, as research has demonstrated their excellent photostability, when compared with many commercial dyes such as ICG²³⁵, seminaphthorhodaflor decyl ester (SNARF-DE)²³⁶, thymol-blue and m-cresol-purple²³⁷. From those results, aza-BODIPYs showed significantly better photostability profiles under the same condition, making it more suitable as an optimised NIR fluorescence probe.

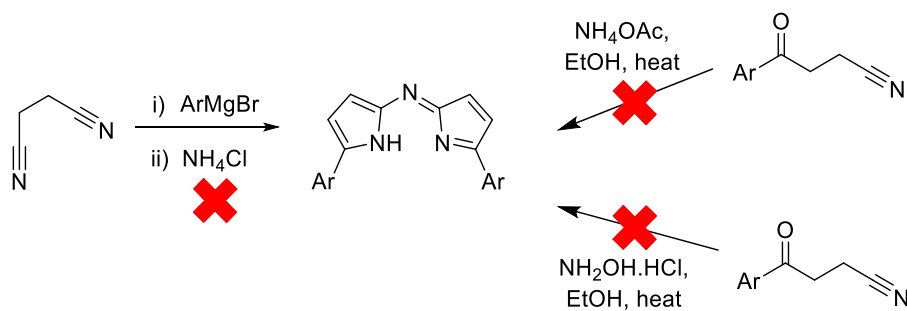
3.1 Synthesis of Aza-BODIPY

The first aza-dipyrrin was synthesised as a dye by Rogers in 1943²³⁸, the synthetic strategies involved an aldol condensation with an aldehyde or ketone, followed by Michael addition, and a solvent-free Leuckart reaction with ammonium formate at 180-200°C for 15 to 30 min. However, this method produced a relatively low yield of 37% using a difficult synthetic procedure and a harsh environment (**Scheme 11**).



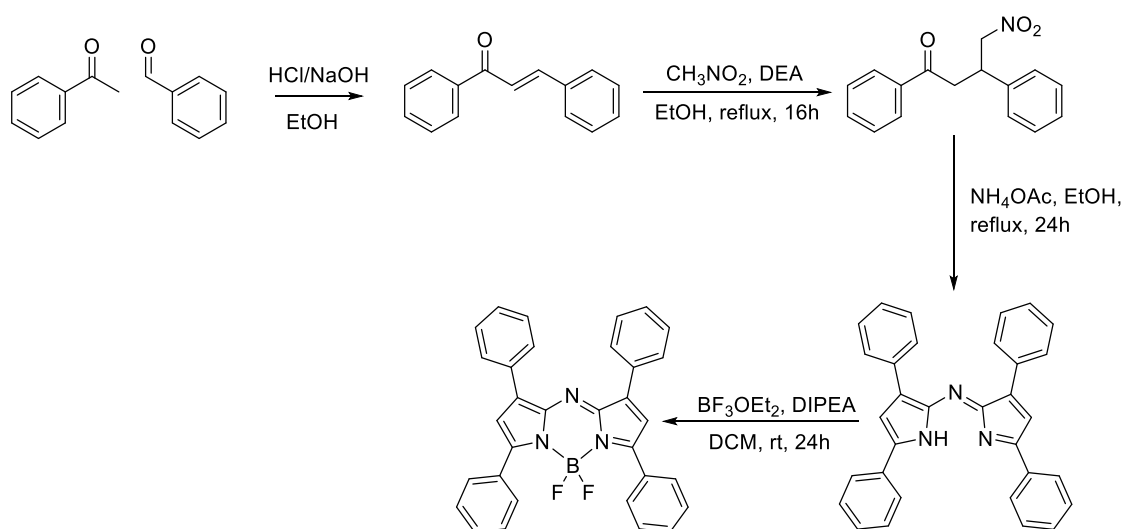
Scheme 11. Synthesis of aza-dipyrrin by Roger *et al.*²³⁸.

Despite many groups claimed the syntheses of aza-dipyrrin through using nitrile derivatives, the report by O'Shea *et al.* in 2013 established the difficulty to obtain the desired aza-dipyrrin through these methods (**Scheme 12**).²³⁹ Therefore, further development of aza-BODIPY was not of great interest until 2002 and 2004 when O'Shea *et al.* released a structurally constrained aza-BODIPY²²⁰ and introduced a much more synthetically friendly reaction.



Scheme 12. Attempted syntheses 5,5'-diarylaza-dipyrin from nitrile derivatives.²³⁹

Recent developments by O'Shea *et al.* revealed a number of different synthetic strategies to substitute aza-BODIPYs with different functionalised groups.^{221,222} A simple strategy for two sets of functionalities was developed using an aldehyde and acetophenone through an aldol/dehydration reaction²²¹, to form the corresponding α,β -unsaturated ketone which, with the further addition of nitromethane accompanied by a base such as diethylamine (DEA), gave 1,3-diaryl-4-nitrobutan-1-ones. These organic reactions have been shown to be efficient at providing a series of precursors for the formation of tetraarylazadipyrromethenes in reactions with ammonium acetate and ethanol for 24 hours under reflux. A typical yield for this reaction ranges from 30-45% with the nitroketone reacting to form a C_2 symmetrical product with the same substituents on the opposing aryl rings. Another reaction utilises tetraarylazadipyrromethenes with boron trifluoride etherate and DIPEA at room temperature to yield the aza-BODIPY product, as shown in **Scheme 13**.

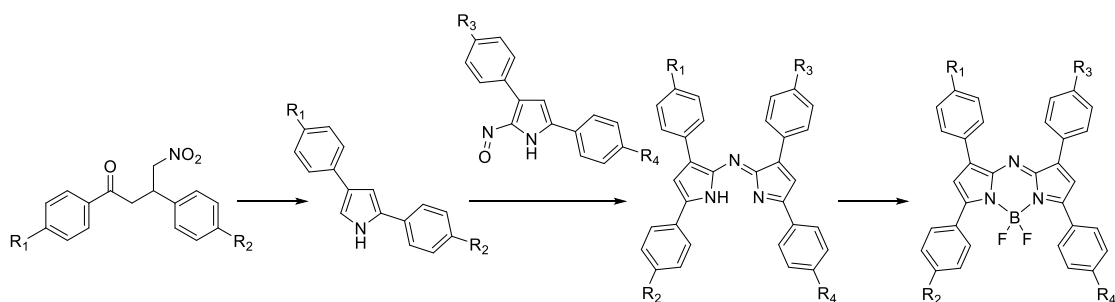


Scheme 13. Synthetic approach to symmetrical aza-BODIPY.

3.1.1 Synthetic approach to asymmetrically substituted aza-BODIPY

Although, the approach previously discussed had an easy synthetic pathway, there are limitations with this route as the number of different substituents on the aryl rings are restricted. Therefore, the route could only lead to the formation of C_2 symmetrical derivatives with the two pairs of substituents.

An alternative approach is to adapt different aryl substituents giving non C_2 symmetrically derived tetraarylazadipyrrmethenes as reported by O'Shea *et al* in 2005, through condensation of 2,4-diarylpyrroles with 2,4-diaryl-5-nitroso-pyrroles.²⁴⁰ This sectional approach allows flexibility for introducing up to four different aryl substituents on the azadipyrrmethene, while maintaining mild conditions allowing the reaction to be applied to sensitive substituents. Through the Nef reaction the 2,4-diarylpyrroles can be synthesised from 1,3-diaryl-4-nitrobutan-1-one and further condensation with ammonium acetate results in an asymmetric azadipyrrmethene with four different substituents (**Scheme 14**).



Scheme 14. Synthetic approach of asymmetrically substituted aza-BODIPY

3.2 Structure modification of aza-BODIPY

The 5-6-5 fused ring system of a conjugated aza-BODIPY has provided the rigidity required for the molecule to undergo structural modification. This can often change the inherent conjugate system of the fluorophore and hence impacts on the fluorescence spectra. Due to the facile nature of the syntheses that have been pioneered by the O'Shea's group, research interest has grown significantly over the last decade. This interest has led to numerous approaches being developed for post-synthetic structural modification including β -thiophene substitution,^{241,242} conformationally restricted derivatives,²³⁵ PO_2 chelated PODIPY,²³⁵ and aza-dipyrrmethene metal complexes.²⁴²⁻

²⁴⁵ These new compounds led to many applications, including NIR optical sensors, light activating therapeutics and diagnostics, supramolecular building blocks, photoredox catalysts, solar energy and optoelectronic materials (**Figure 60**).²⁴⁶ In this project, the potential modifications for conjugating moieties and bioconjugation to a targeting system are investigated.

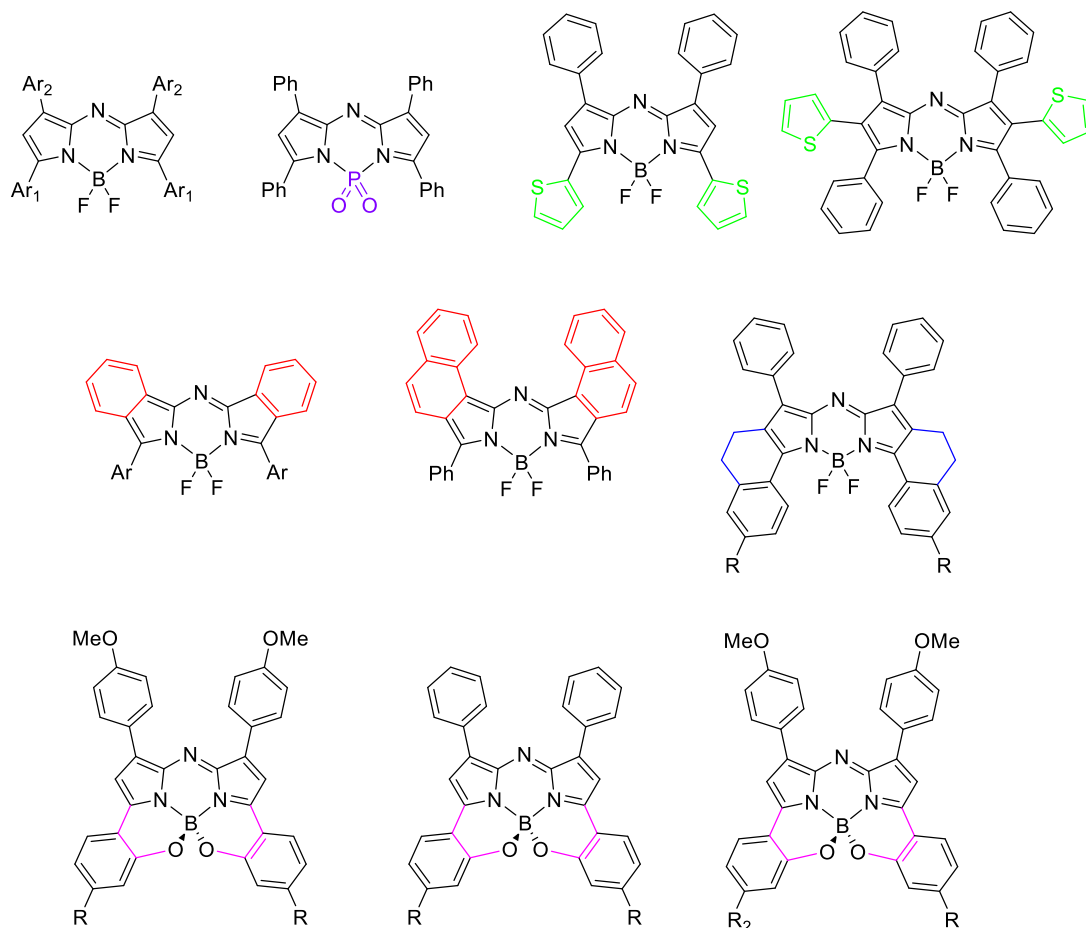


Figure 60. Structural modification of aza-BODIPY core.

3.2.1 Fluoride displacement

Due to the limited positions available for modification on the aza-BODIPY core, nucleophilic substitution of fluoride from the BF₂ has been investigated to introduce various moieties on to aza-BODIPY for structural elaboration. The two commonly known fluoride displacement methods are B-O complexation and the C-nucleophilic substitution.

B-O -chelation was first introduced by the reaction of aza-BODIPY with sodium

hydride and sodium methoxide at room temperature.²⁴⁷ The introduction of alkoxy groups *via* B-O bonds was explored for many applications such as on-bead NIR fluorescent sensors²⁴⁷, fullerene dyads²⁴⁸, and benzo-fused high quantum yield NIR fluorescence probes²⁴⁹ as shown in **Figure 61**.

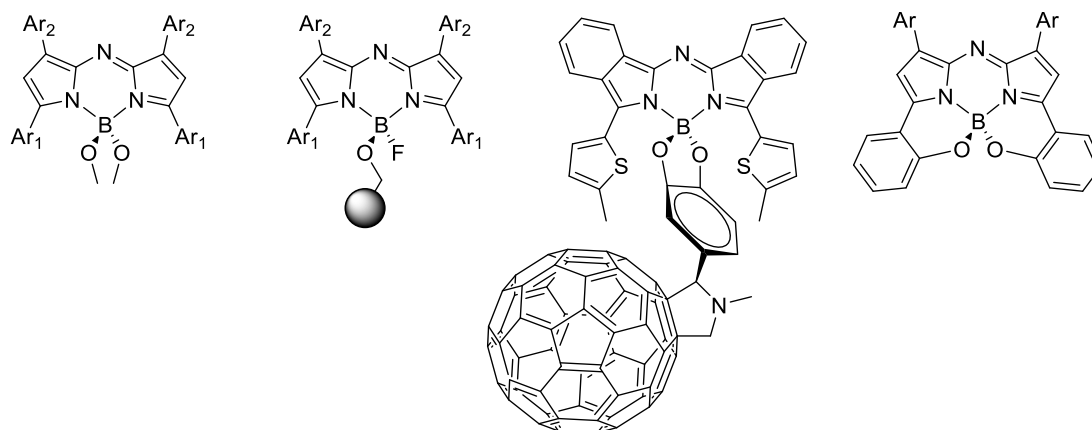


Figure 61. B-O chelation of aza-BODIPY.

Fluoride displacement has also been accomplished with aryl and alkynyl C-nucleophiles. The method requires the use of organometallic reagents to perform nucleophilic substitutions to form boron-aryl and alkynyl substituted derivatives.

A ferrocene-azadipyrromethene triad has been reported via fluoride displacement based on a reaction with an alkynyl-ferrocene Grignard reagent (**Figure 62**). However, fluoride displacement with a conjugatable moiety and water-solubilisation are yet to be reported in either method.

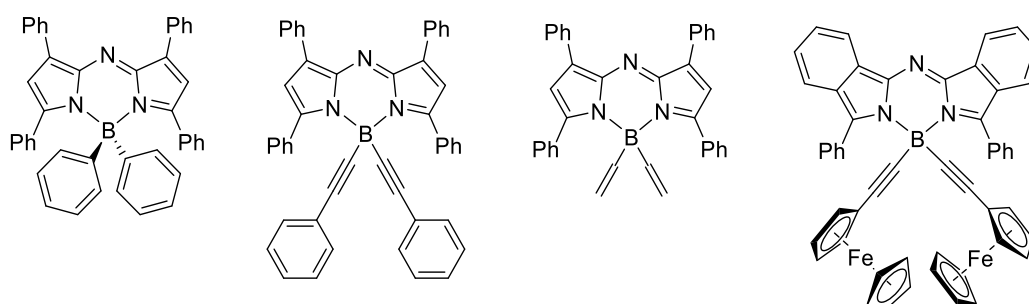


Figure 62. Aryl and alkynyl C-nucleophilic substitution of aza-BODIPY

3.2.2 Water solubilisation

The importance of aqueous solubility in biological applications is widely recognised.

Although aza-BODIPYs exhibit NIR properties, the aryl substituents also introduce a high hydrophobicity and encourage aggregation in aqueous media. In order to minimise aggregation and optimise BODIPYs for the various bioconjugation methods, the fluorescent probes must have high stability and solubility in aqueous solution. Despite many attempts involving sulfonation reactions, the electron deficient character of aza BODIPY significantly changes the reactivity and results in loss of the BF₂ fragments under a variety of conditions.²⁵⁰ Several alternative different approaches to water solubilisation have been recently reported. Recently, O'Shea *et al.* reported an increase in aqueous solubility *via* the reaction of the phenol substituents with functional groups such as carboxylic acids and sulfonic acids to introduce bis-anionic derivatives. Another synthetic approach was also described for bis-cationic derivatives through the introduction of ammonium groups at the precursor stage, followed by methylation to achieve water solubility²⁵¹ (**Figure 63**).

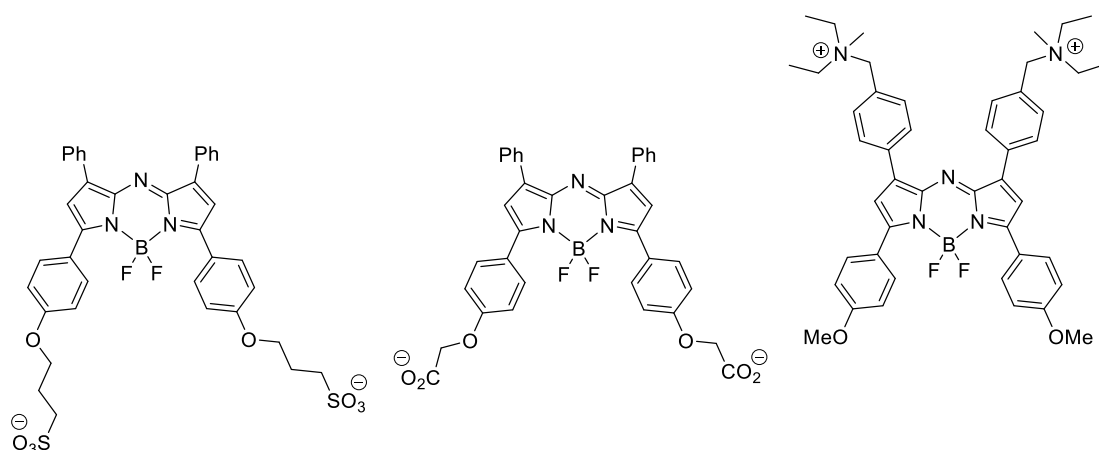
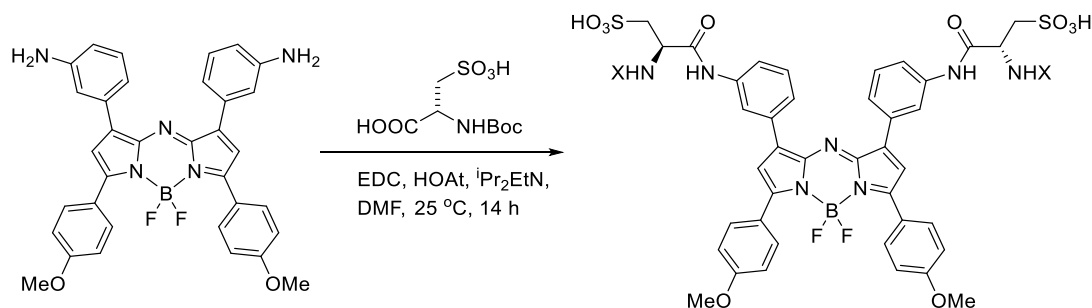


Figure 63. Water-soluble aza-BODIPYs

Another method for water solubilisation was developed by Burgess *et al.* by coupling a negatively charged di-cysteic acid to *meta*-diamine substituents (**Scheme 15**).²⁵⁰



Scheme 15. Synthesis of aza-BODIPY containing cysteic acid.

3.2.3 Functionalisation for bioconjugation

The success of introducing water-soluble groups for aza-BODIPY has inspired the synthesis of conjugatable aza-BODIPYs for further bioconjugation. Despite the range of functionalised moieties available for aza-BODIPY, the limited modifiable sites hindered the development of aza-BODIPYs for bioconjugation to a range of targeting units. Currently, there are several examples of aza-BODIPY bioconjugation with small biological molecules such as sugars²⁵² and peptides²⁵³ (**Figure 64**).

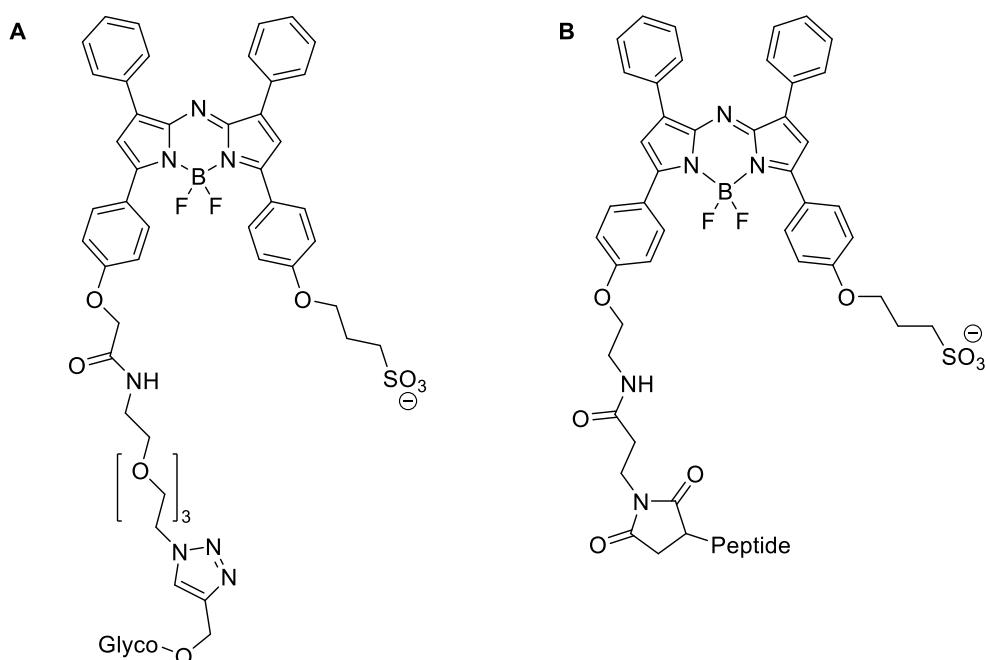


Figure 64. Glycoconjugated aza-BODIPY (A). Amino acid and peptide conjugates from maleimide aza-BODIPY(B)

Although the bioconjugation of small biological molecules has been successful, bioconjugation of antibodies and proteins remains challenging with an intrinsically targeting aza-BODIPY probe yet to be reported.

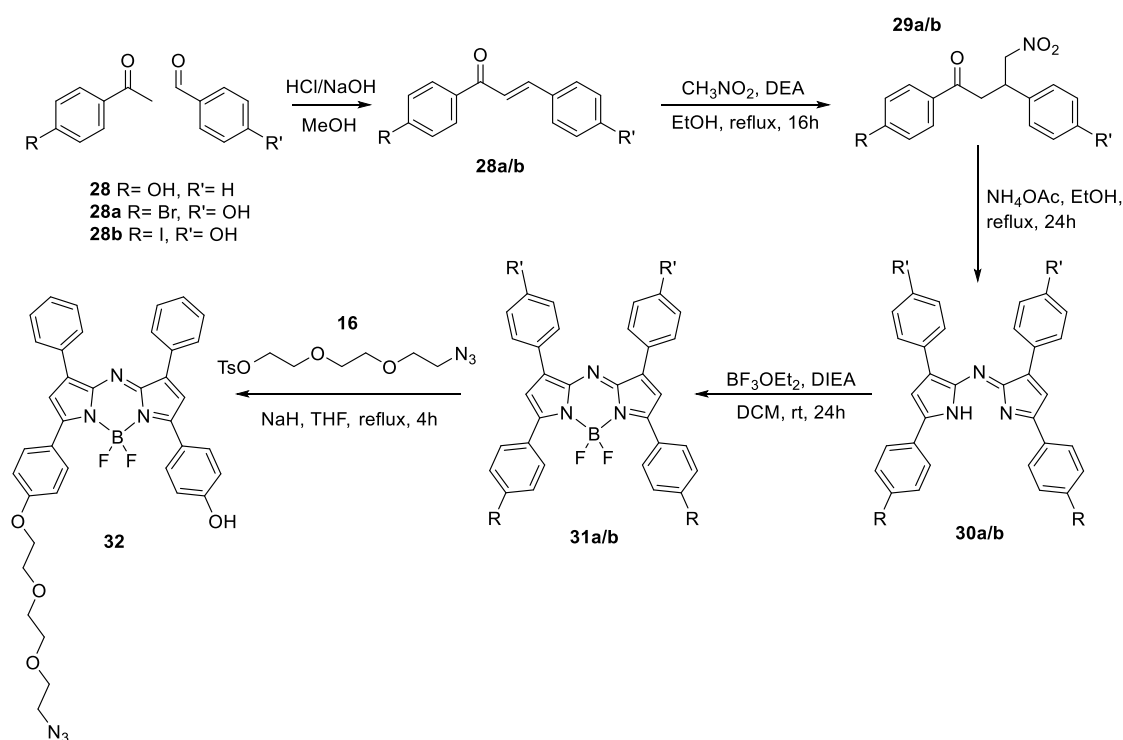
3.3 Results and discussion

Several aspects of aza-BODIPYs have been investigated, primarily the introduction of conjugatable moieties was investigated utilising different synthetic approaches such as F-displacement through B-O complexes and S_N2 reactions at phenolic substituents. Furthermore, water-solubilisation was carried out for symmetrical and asymmetrical aza-BODIPY using anionic substituents. A library of aza-BODIPYs with both bioconjugate groups and water-solubilising units were synthesised and analysed. However, spectroscopic data suggested instability and limited water-solubility in water. Therefore, an enhanced water-soluble aza-BODIPY was developed. Initially, attempts to synthesise multiply functionalised aza-BODIPYs were carried out with two different protecting groups introduced into the precursors. Due to the instability of aza-BODIPY however, the deprotections were unsuccessful. Eventually a successful synthesis of a PEG substituted azido aza-BODIPY with excellent water-solubility in aqueous solution was achieved.

3.3.1 Clickable hydrophobic azido aza-BODIPY

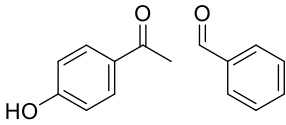
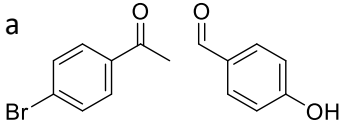
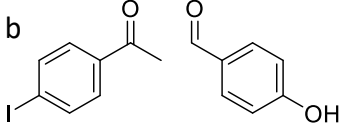
An azido aza-BODIPY was successfully synthesised using a modification of the method developed by O'Shea *et al.*^{251,254} The method was followed initially from the reaction of 4-hydroxybenzaldehyde and acetophenone under catalytic acidic conditions with conc. sulfuric acid to yield the respective chalcone **28** in 64% yield, which was found to be similar to the literature. The compound was characterised by NMR and MS, with the ¹H-NMR showing two distinctive peaks for the alkene at 7.67 and 7.75 ppm. It was subsequently nitrated with nitromethane and DEA, and purified by recrystallisation from cold diethyl ether to obtain nitrochalcone **29** in 73% yield, this was found to be the same as the literature value. This was then refluxed for 24 hours with ammonium acetate in ethanol, and the precipitant was isolated and washed with cold ethanol to afford aza-dipyrrromethene **30** as a blue/black solid in 75 % yield. The yield was lower than the literature value due to an insufficient precipitation from the excessive amount of solvent used. The aza BODIPY **31** was then produced by reacting **30** with BF₃.Et₂O and DIPEA, the product was isolated using column chromatography on silica with a relatively high yield of 72%.

For the synthesis of the PEG chain **16**, modifications to the literature method²⁵⁴ were made. An azide PEG chain **14** was synthesised as previously reported, in which 2-(2-(2-chloroethoxy)ethoxy)ethanol was reacted with sodium azide to afford **14** with a 99% yield. The synthesis of a tosylated PEG azide chain **16** was achieved by the reaction of tosylchloride with the azide PEG chain **14** that was previously synthesised affording an 87% yield. This reaction between aza-BODIPY **31** and **16** produced mono and di-substituted derivatives and upon column chromatography **32** was isolated in 46% yield, with characterisation carried out by ¹H, ¹³C, ¹⁹F-NMR and MS. Synthesis of brominated and iodinated aza-BODIPY was also attempted using the method described above started with the reaction of halogenated acetophenone and 4-hydroxybenzaldehyde forming the subsequent nitrochalcone. However, the resulting halogenated aza-dipyrrins **30a** and **30b** were found to be insoluble in most commonly used solvents, such as DCM, chloroform, acetone, ethyl acetate, methanol and ethanol. BF₂ insertion was carried out in attempt to improve the solubility of aza-BODIPY **31a** and **31b**, the solubility was found to improve when dissolved in a coordinating solvent such as acetone, but overall the resulting products had poor solubility making purification difficult and hence prohibited further modifications and characterisations to take place (Scheme 16 and Table 5).



Scheme 16. Synthesis of aza BODIPY **32** with azide PEG chain.

Table 5. Stages of successful synthesis of aza-BODIPYs and their relevant precursors.

Starting materials	Chalcone (28)	Nitro- chalcone (29)	Aza-dipyrrin (30)	Aza-BODIPY (31)
	✓	✓	✓	✓
a 	✓	✓	✓	X
b 	✓	✓	✓	X

Through UV-visible and fluorescence spectroscopic analysis, absorption and emission wavelengths of 654 nm and 690 nm were observed from the azide functionalised aza BODIPY (**Figure 65**). This class of BODIPY was shown to generally provide better red shifts toward the desired NIR regions as well as better Stokes shift for excitation in comparison to other BODIPY derivatives.

UV-vis and fluorescence spectrum of azide conjugated aza-BODIPY 32

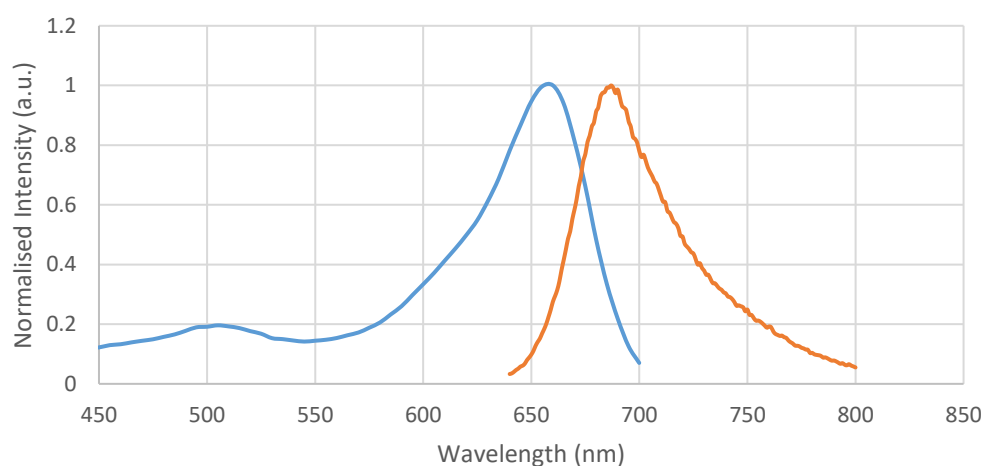


Figure 65. Normalised UV-visible and fluorescence spectra of **32** in DCM, λ_{abs} (blue) and λ_{em} (orange).

3.3.2 B-O aza-BODIPY complexes

Several groups have reported methods to synthesise B-O BODIPYs that can be functionalised with different alkoxy or diarylalkoxy derivatives.^{255,256} The reaction involved a Lewis acid, for example, AlCl₃ reacting with the BODIPY in dry DCM, allowing activation of the B-F bonds, followed by nucleophilic substitution with various alcohols (**Figure 66**).

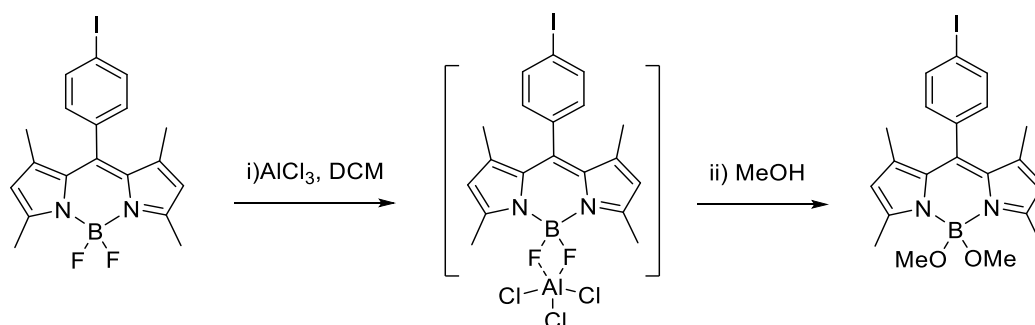
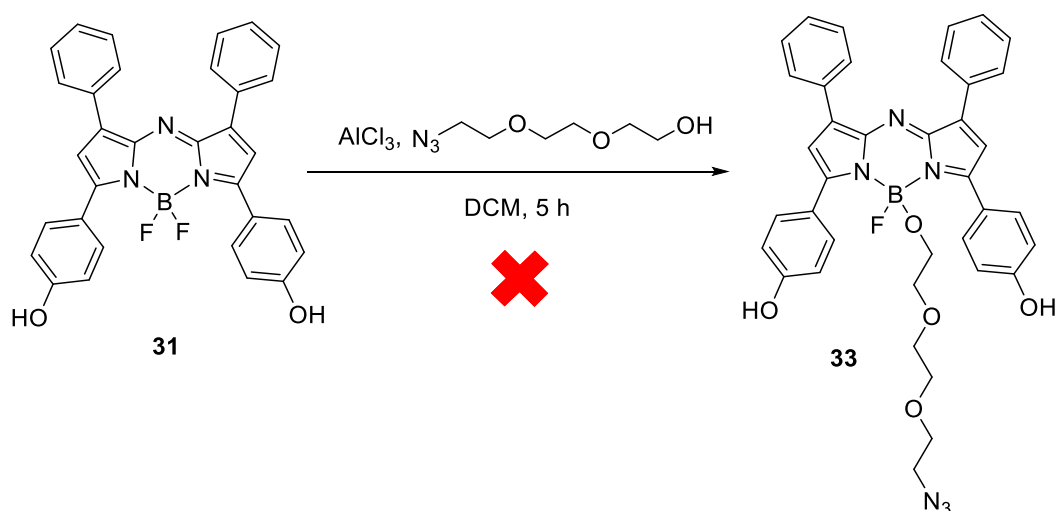


Figure 66. Proposed mechanism for the formation of alkoxy-BODIPY with AlCl₃.

Although the reaction was not optimised to produce a mono-substituted aza-BODIPY, there was evidence in the literature for the successful F-displacement from BODIPYs and this could potentially be applied to aza-BODIPY to access a mono-substituted adduct. Aza-BODIPY **31** was treated with AlCl₃ in dry DCM and heated under reflux for 20 minutes, and upon cooling to room temperature, the subsequent azide PEG chain was added and stirred for a total of 5 hours (**Scheme 17**). TLC after 30 minutes showed the progress of the reaction, which revealed three bands, postulated to be starting material, or the aza-dipyrrin, and the mono and di-boron substituted compounds. The formation of the aza-dipyrrin was suspected due to the use of the Lewis acid AlCl₃, which may potentially remove the BF₂ from the complex before substitution of the fluorine atom could take place.



Scheme 17. Attempted B-O chelation reaction of aza BODIPY with azide PEG chain moiety and Lewis acid – AlCl₃.

However, the mixture was suspected to consist mainly of the starting material after 2 hours of stirring at room temperature, and with further stirring, for another 3 hours, the relative level of the di-substituted adduct decreased with an increase in the band that was considered to be the starting material. A possible explanation for this observation was the difference in relative bond strengths, since the B-O is a weaker bond (typical bond energy of 536 kJmol⁻¹) compared with the B-F bond, which has a bond energy of 613 kJmol⁻¹, suggesting that, with enough energy and time, the B-F bond can reform, if fluoride anion is present. Therefore, reversibility of the reaction could explain the observed decrease in the boron substituted adducts after extended reaction times.

Purification by column chromatography was performed to separate the product for further analysis, however, this aza-BODIPY adheres strongly to the silica. And even with deactivation with TEA, purification was unsuccessful. The problematic purification was believed to be due to the extremely adhesive nature of the aza-BODIPY toward silica, so a possible solution was to perform the column chromatography on neutral alumina instead. However, it was observed by Tahtaoui *et al.*, that the presence of moisture would deactivate basic alumina leading to formation of dihydroxy derivatives from the dimethoxy product.²⁵⁶ As a result, the overall evidence above suggests this method can be problematic (**Figure 67**).

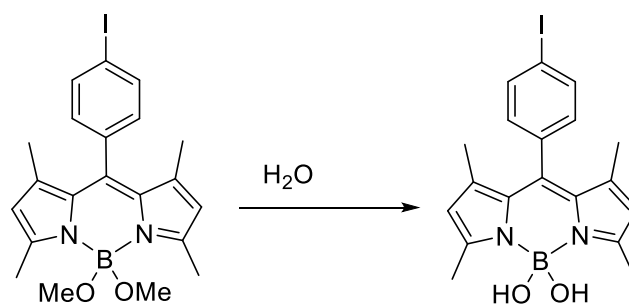


Figure 67. Hydrolysis of B-dimethoxy BODIPY derivatives. ²⁵⁶

Another method was reported by Mazitschek *et al.* ²⁵⁷. This reaction was first described for the reaction of BODIPY with trimethylsilyl trifluoromethane-sulfonate (TMSOTf) to form a BODIPY-OTf intermediate. The formation of this intermediate allowed for a direct reaction with alcohols. The reaction time was optimised to yield the desired monoalkoxy-BODIPY, without the formation of the dialkoxy BODIPY. This was suggested to be a cleaner reaction, as it substitutes a single fluoride from the BF_2 to generate a borenium intermediate (**Figure 68**).

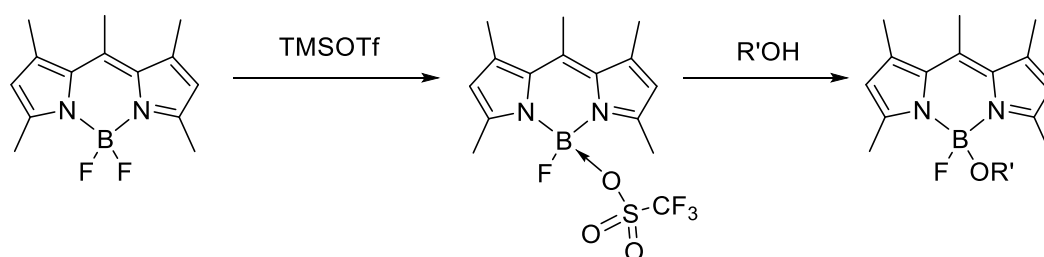
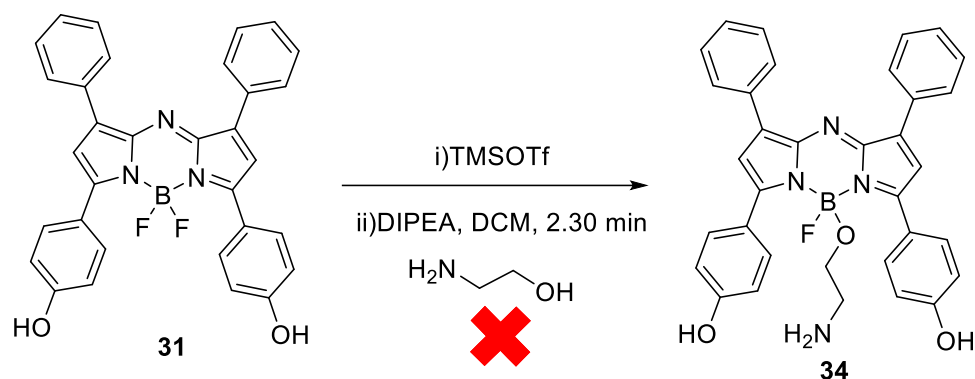


Figure 68. Formation of monoalkoxy BODIPY with TMSOTf.

As this reaction improved the selective substitution of only one fluorine position, it provided a cleaner alternative to the previous Friedel Craft type reaction.

However, due to instability of the intermediate under the reaction conditions, the intermediate can slowly degrade. For this reason, aminoethanol was concurrently added and stirred for 2.30 minutes, the time found to optimise simultaneous formation of the monoalkoxy product **34** under mild condition, with the use of a non-nucleophilic base DIPEA to buffer and stabilise the acidity of the reaction mixture (**Scheme 18**).

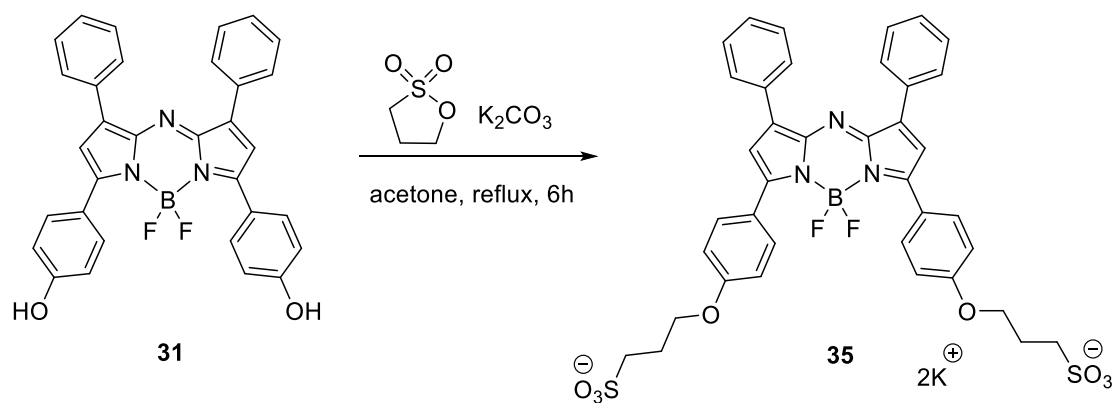


Scheme 18. Attempted B-O chelation reaction of aza BODIPY with aminoethanol using reactive leaving group - TMSOTf.

Unfortunately, the reaction did not proceed as expected due to its poor solubility. A clear NMR was not obtained, and MS analysis showed no monoalkoxy-aza BODIPY **34** was present, the only significant peak observed was at m/z 529, corresponding to the starting material.

3.3.3 Water soluble aza-BODIPY

Water solubility of a compound is an important factor for successful bioconjugation with antibodies and proteins. Methods of water solubilisation with a diphenolate aza-BODIPY were first developed by O'Shea *et al.* to produce cationic and anion aza-BODIPYs.²⁵¹ In this project, an anionic aza-BODIPY was investigated, as a negatively charged fluorescent probe exhibits intrinsic repulsion with the negative head groups on the cell membrane, thus minimising non-specific binding. The reaction required an aza-BODIPY with a phenolate group to react with 1,3-propanesultone at 60 °C for 6 hours under an inert atmosphere to yield aza-BODIPY **35** (**Scheme 19**). The purification method in the literature described by O'Shea *et al.* required the use of a preparative HPLC and reverse phase silica column chromatography, making the scale and cost of the purification process prohibitive.



Scheme 19. Synthesis of anionic water-soluble aza-BODIPY.

To overcome these issues, a novel counter ion exchange method was developed. The initial counter ions were potassium ions, which gives the molecule hydrophilicity and allowed the product to be washed with acetone to remove excess 1,3-propanesultone and the starting aza-BODIPY. After washing with acetone, the crude product remains a mixture of aza-BODIPYs, tetrabutylammonium chloride (TBAC) was then added to initiate the counter ion exchange to NBu_4^+ to further purify the product. This allowed the aza-BODIPY **36** to become soluble in DCM and provided a way to remove any water-soluble impurities. Also, further purification is possible by column chromatography using normal phase silica, due to the change in polarity. After purification, the NBu_4^+ counter ions were exchanged for Na^+ through the addition of NaI to allow the molecule to regain water-solubility. The product was filtered and washed with acetonitrile since the resulting NBu_4I salt was soluble in this solvent, whereas the anionic aza-BODIPY **37** was not. This provided a more feasible and elegant purification approach for anionic aza-BODIPY (**Figure 69**).

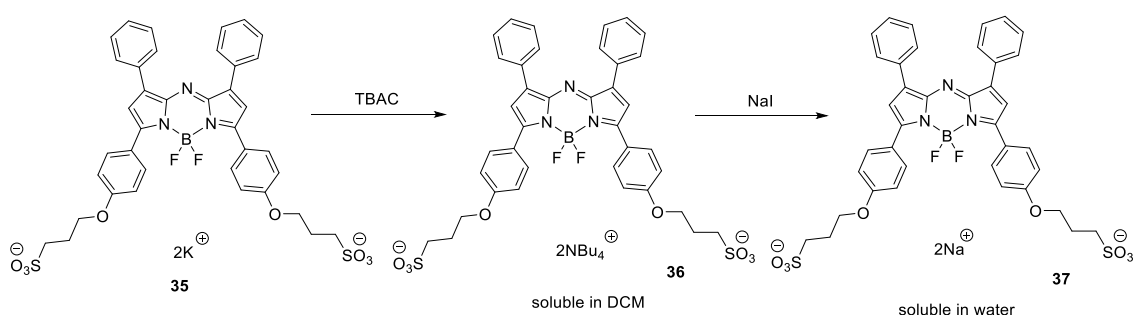


Figure 69. Novel counter ion exchange method for disulfonated aza-BODIPY.

Further characterisations were carried out by NMRs and MS to confirm the structure. The purity was confirmed by HPLC chromatography, showing a single peak of the major product, for a retention time of 13.3 min. UV-visible and fluorescence spectroscopic analysis showed an NIR emission (**Figure 70**); for the anionic aza-BODIPY with NBu_4^+ , $\lambda_{\text{abs}} - 665 \text{ nm}$ and $\lambda_{\text{em}} - 713 \text{ nm}$ upon excitation at 660 nm.

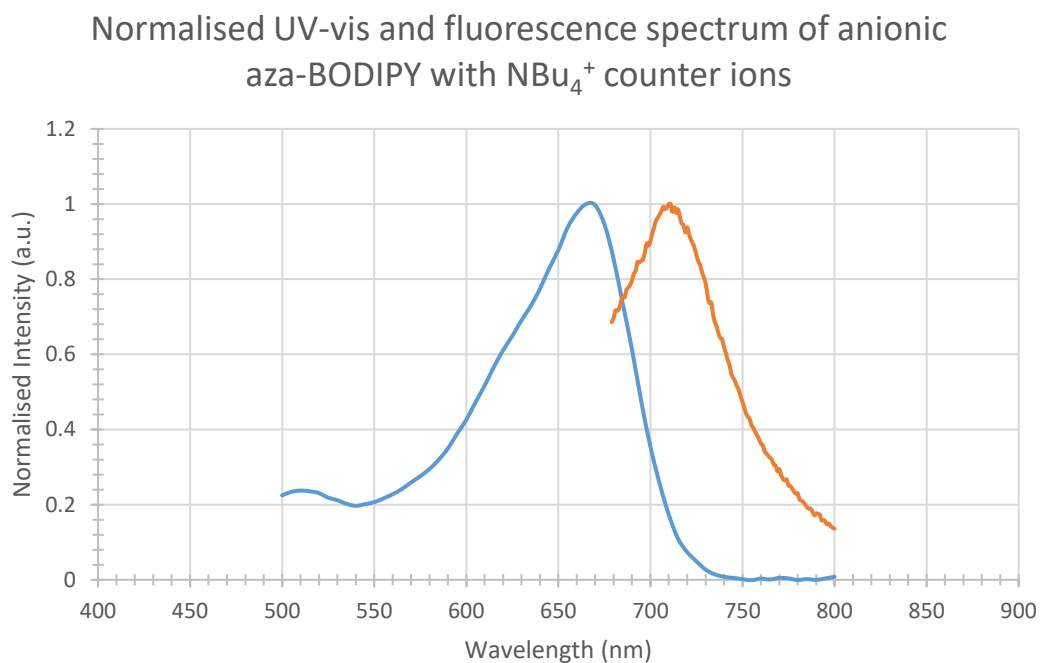


Figure 70. Normalised UV-visible (blue) and fluorescence (orange) spectra of **36** in DCM.

UV-visible and fluorescence spectra for the anionic aza-BODIPY with Na^+ shown in **Figure 71**, suggested a bathochromic shift in the more polar solvent due to solvent effects²⁵⁸, with an absorption of $\lambda_{\text{abs}} - 735 \text{ nm}$ and emissions at $\lambda_{\text{em}} - 767$ and 822 nm upon excitation at 640 nm .

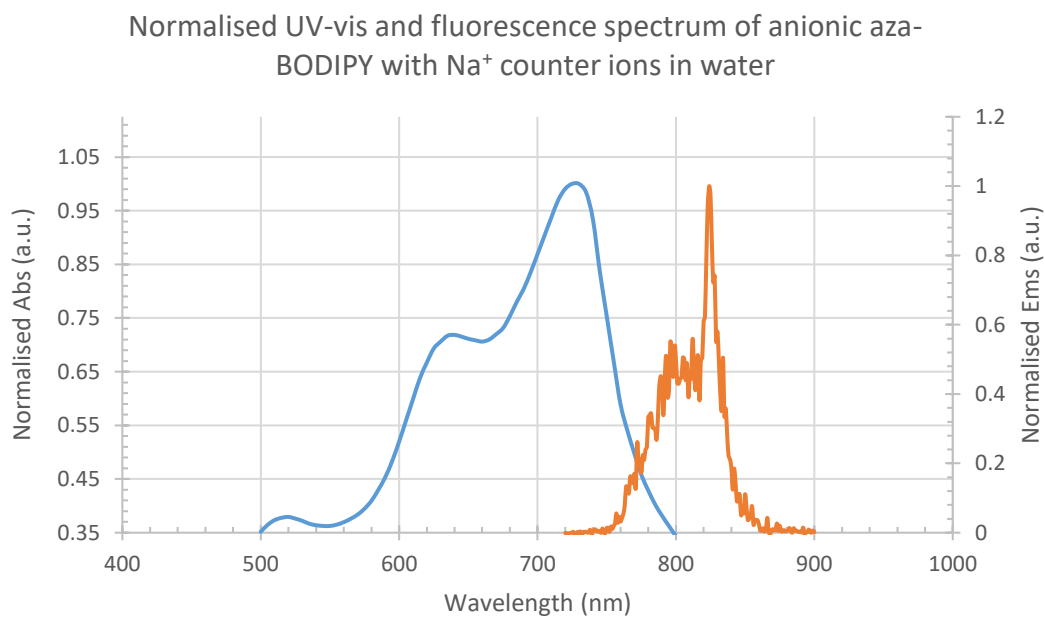


Figure 71. Normalised UV-visible (blue) and fluorescence (orange) spectra of **37** in water.

The low intensity obtained from the fluorescence spectrum in water suggested aggregation of the compound in the aqueous media leading to fluorescence quenching. The planarity of the hydrophobic aza-BODIPY core contributes to the aggregation as it causes stacking and the formation of H-dimers. This speculation was further confirmed by the comparison of the fluorescence spectrum in methanol (**Figure 72**), through the observation of a higher intensity spectrum with a maximum emission λ_{em} – 713 nm upon excitation at 640 nm.

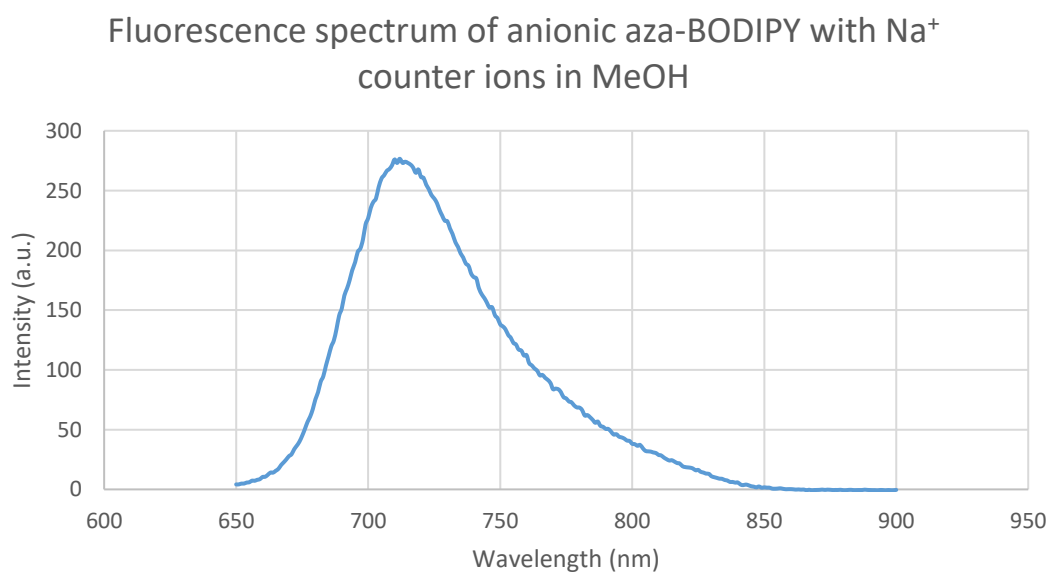
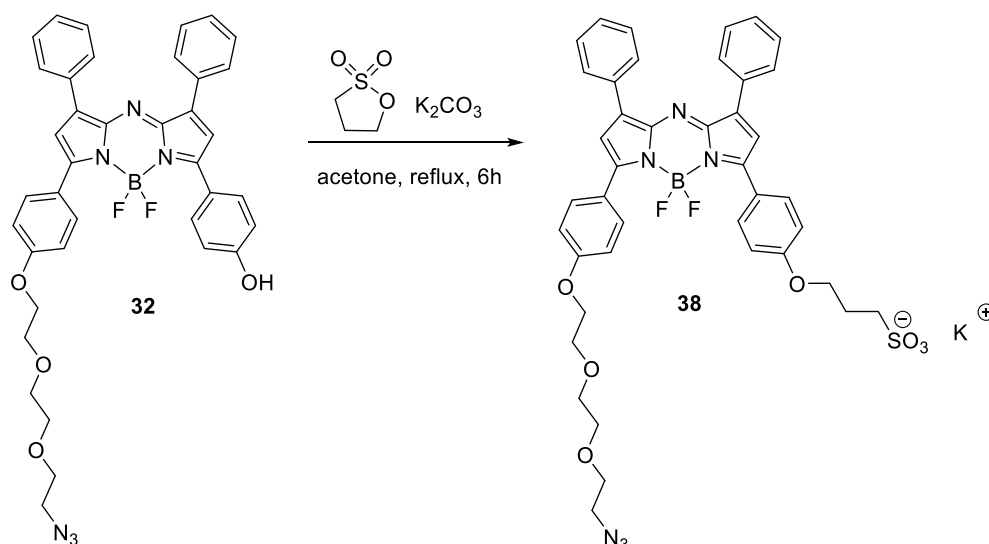


Figure 72. Fluorescence spectra of **37** in methanol.

The anionic aza-BODIPY demonstrates potential as a fluorescence probe due to its relatively wide Stokes shift and hydrophilicity, offering the possibility for further bioconjugation.

3.3.4 Clickable water-soluble azido aza-BODIPY

In order to increase the selectivity towards tumour tissue and become biologically compatible for *in vivo* imaging, a water-soluble and bioconjugatable aza-BODIPY was required. However, the limited number of substitutable positions available on an aza-BODIPY limits the methods that can be employed. Herein, a propanylsulfonic acid group and a pegylated azide chain were introduced on each of the aryl rings adapting a recently published method.²⁵²



Scheme 20. Synthesis of azido anionic aza-BODIPY.

The synthetic route followed an S_N2 reaction of the tosylated PEG azide to form the mono-substituted product **32** as previously reported in this chapter. To introduce water solubility, 1,3-propanesultone was reacted with the other phenol ring present on compound **32** and heated under reflux in acetone with the catalytic K_2CO_3 (**Scheme 20**) to initially obtain **38**. Purification of **38** was immediately followed by the counter ion exchange method previously described to purify the product and to obtain an azido anionic aza-BODIPY **40** in 57% yield (**Figure 73**). Confirmation of the desired compounds was obtained by 1H , ^{13}C , ^{11}B and ^{19}F -NMR and MS. HPLC analysis was also carried out to ensure the purity and a single peak was obtained with a retention time of 7.5 min.

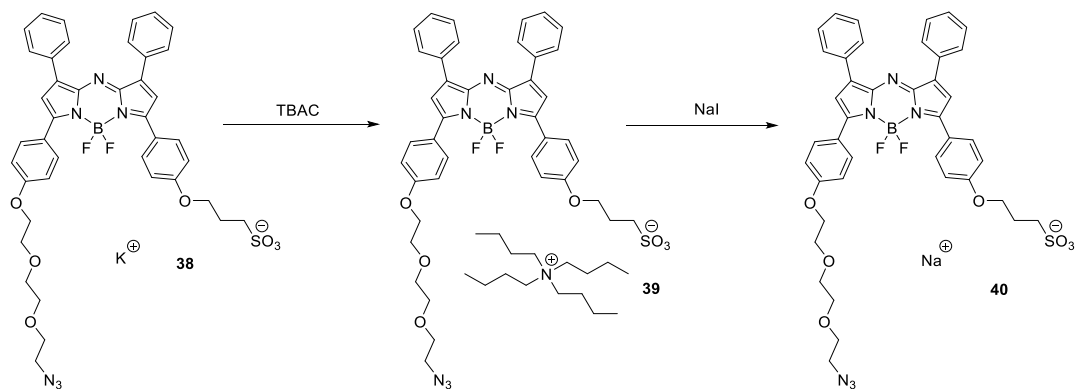


Figure 73. Counter ion exchange method for azido anionic aza-BODIPY isolation.

UV-visible and fluorescence analysis of compound **40** were performed with two different polar solvents. **Figure 74** shows the spectrum of azido anionic aza-BODIPY in methanol with an absorption at 665 nm and a fluorescence emission at 708 nm.

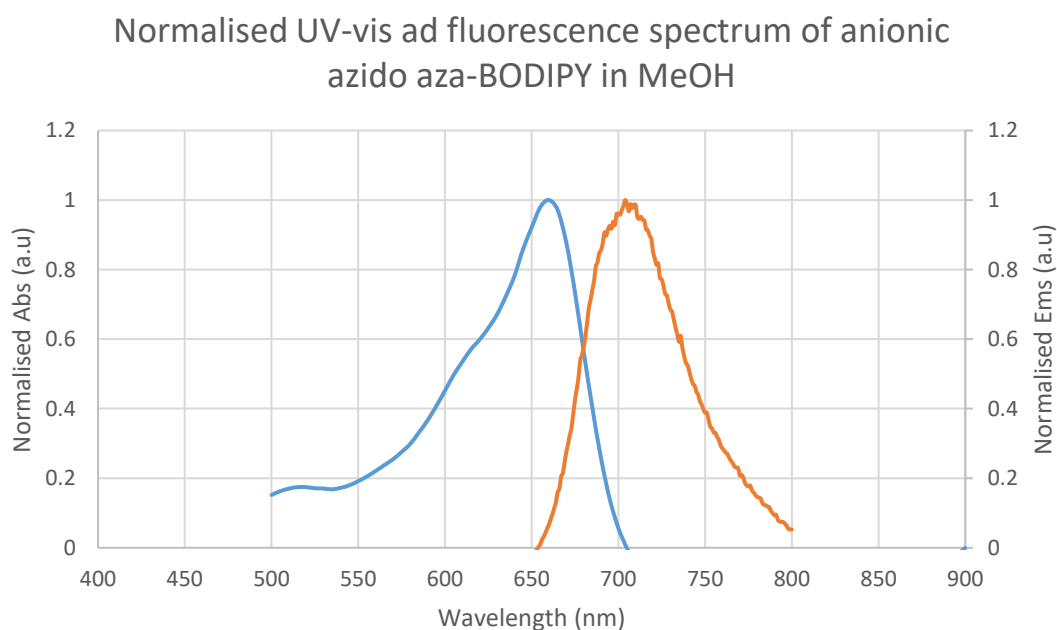


Figure 74. Normalised UV-visible (blue) and fluorescence (orange) spectra of **40** in methanol.

A small bathochromic shift was observed in aqueous solution with an absorption at 740 nm and upon excitation at 680 nm a fluorescence emission was observed at 750 nm. (**Figure 75**)

Normalised UV-vis and fluorescence spectrum of anionic azido aza-BODIPY in water

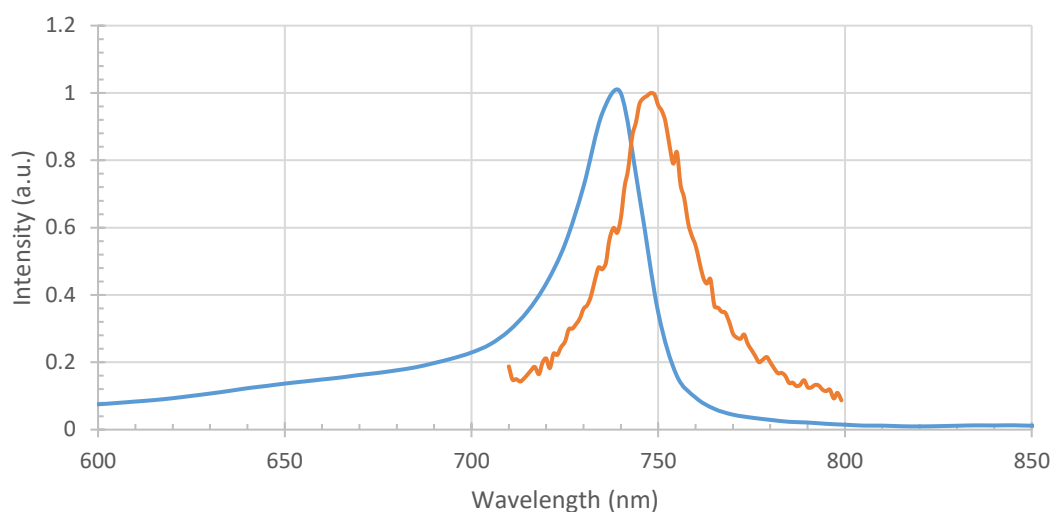
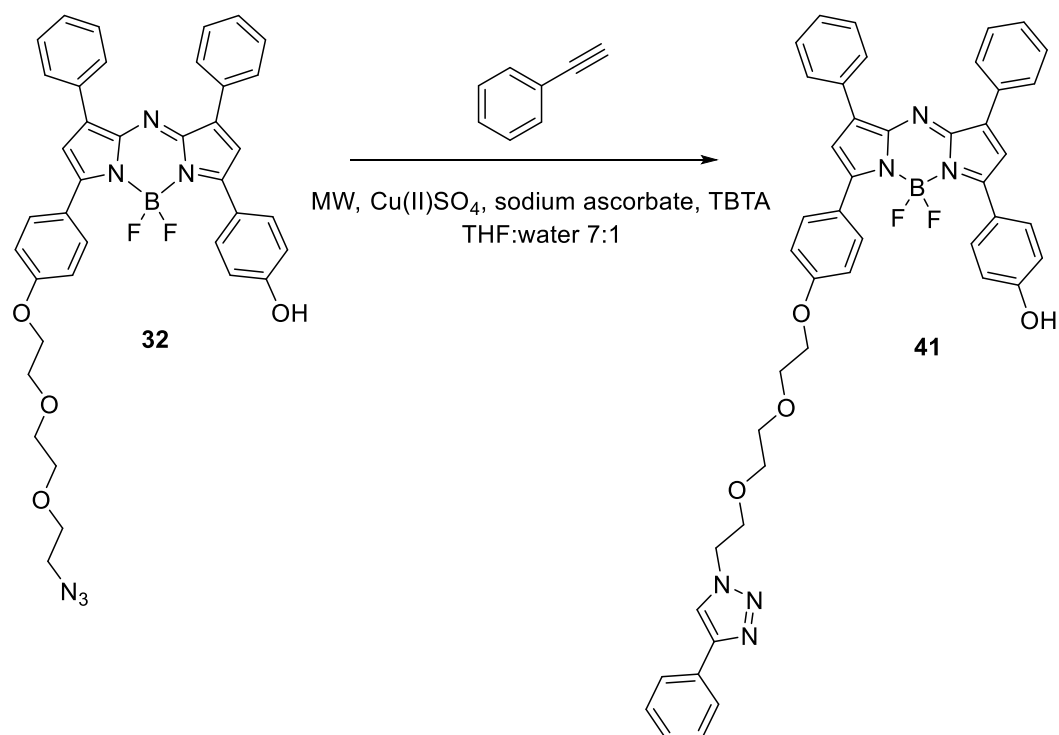


Figure 75. Normalised UV-visible (blue) and fluorescence (orange) spectra of **40** in water.

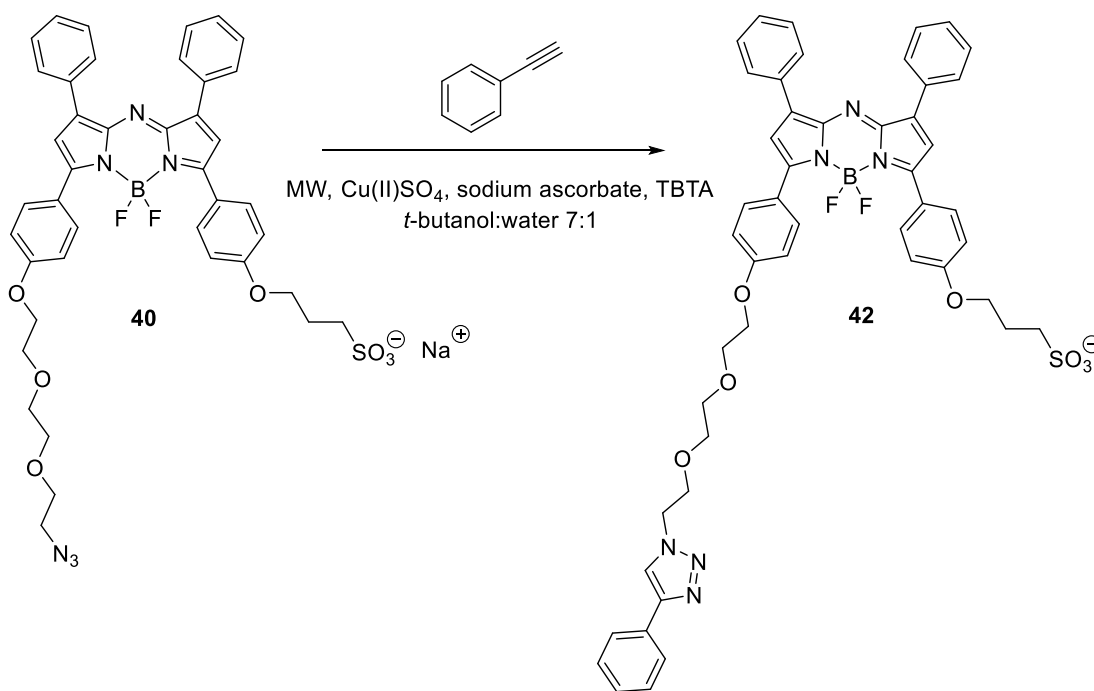
3.3.5 Synthesis of aza-BODIPY conjugate by click chemistry

In order to prove the compatibility of aza-BODIPY and CuAAC click conjugation conditions, and to develop an optimised method, conjugation was first attempted using simple aromatic alkynes. Two azido aza-BODIPYs previously synthesised were used to validate the CuAAC reaction with phenylacetylene.



Scheme 21. CuAAC reaction of lipophilic aza-BODIPY **32** with phenylacetylene.

The click chemistry conjugation was first carried out in a biphasic solution of THF: water, for the lipophilic aza-BODIPY **32**, and was catalysed by Cu (I) obtained from the *in-situ* reduction of copper (II) sulphate by sodium ascorbate. This reaction was first carried out under microwave irradiation, heating to 80°C for 30 minutes, however very little product formation was observed in this process, even upon further heating to 80°C for 2 hours or 90°C for 4 hours. Although there was some evidence from TLC to suggest the reaction was progressing, the reaction rate was extremely slow even under microwave irradiation. To increase the rate of reaction the catalyst TBTA was added in order to stabilise the copper (I) oxidation state and to catalyse the 1,2,3-triazole formation. Upon addition of TBTA, the reaction went to completion under microwave irradiation at 80°C for 40 minutes, and **41** was purified by column chromatography to afford a 93% yield (**Scheme 21**).



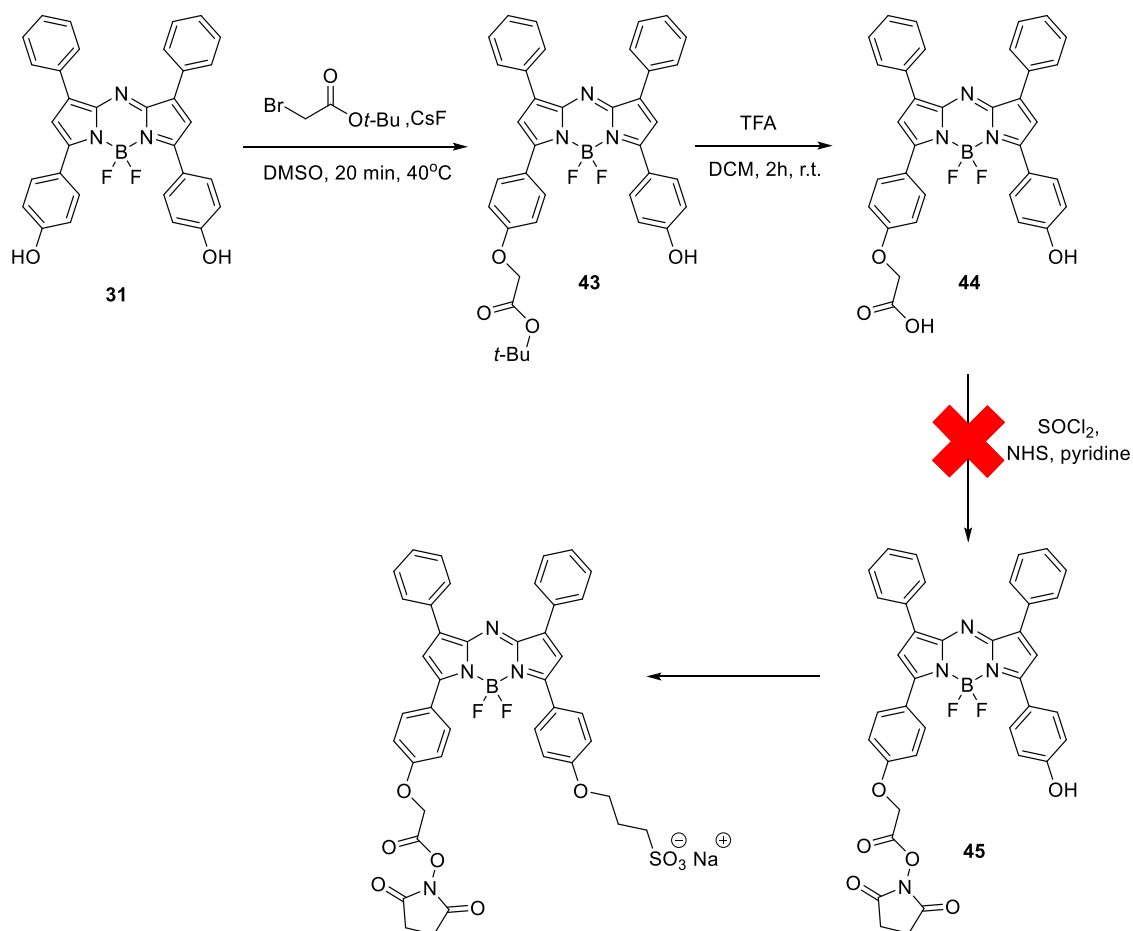
Scheme 22. CuAAC reaction of hydrophilic aza-BODIPY **40** with phenylacetylene.

To further ensure the validity of the CuAAC reaction for possible biorthogonal reactions, a reaction with the water-soluble aza-BODIPY was attempted. This was first carried out with the same conditions as for the lipophilic aza-BODIPY. However, the reaction proved to be unsuccessful due to poor solubility in the bi-phasic solution of THF: water, as compound **40** was not fully soluble in either THF or water. Upon changing to a more polar solvent of *t*-butanol the aza-BODIPY became more soluble in the reaction mixture and the reaction proceeded under microwave heating at 80°C for 40 minutes. After purifying **42** a yield of 47% was obtained and its structure was confirmed by ¹H, ¹³C, ¹¹B and ¹⁹F-NMR (**Scheme 22**).

3.3.6 Peptide coupling carboxylic acid functionalised aza-BODIPY

Smaller targeting systems such as peptides and small molecule antagonists can undergo peptide coupling reactions with activated carboxylic acid moieties to selectively conjugate to a primary amine such as a lysine residue. This bioconjugation synthetic route, utilising a carboxylic acid functionality, began when aza-BODIPY **31** Aza-BODIPY **31** were treated with *tert*-butyl bromoacetate and caesium fluoride in anhydrous DMSO. The resulting crude product was purified by column chromatography to obtain a mono *tert*-butyl ester aza-BODIPY **43** in 37% yield, a

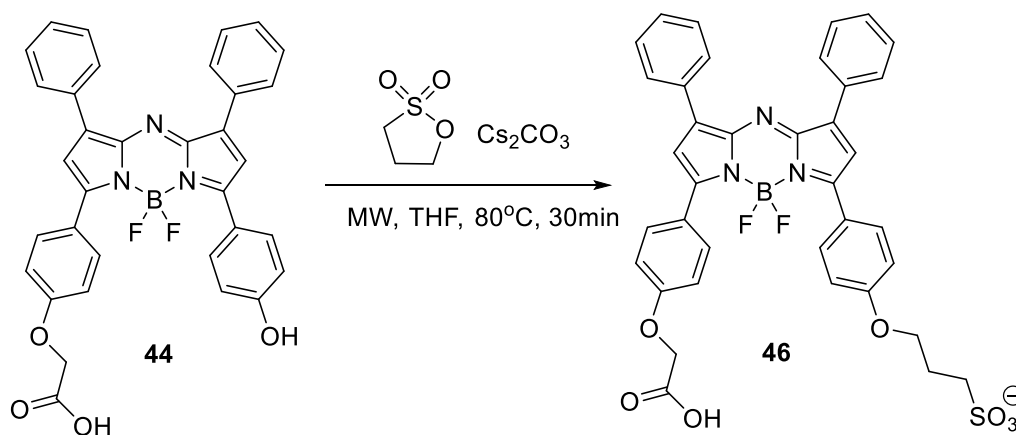
relatively low but acceptable yield. This was then followed by ester deprotection with TFA in dry DCM to give a 95 % yield of the carboxylic acid derivative **4** (**Scheme 22**).



Scheme 23. Synthesis of NHS ester aza-BODIPY.

Synthesis of aza-BODIPY **45** with an activated NHS ester was attempted in order to perform further reactions under mild conditions with lysine residues. The introduction of the activated NHS ester was carried out as a one pot, two steps reaction. Thionyl chloride was used to form the acyl chloride, which was then treated with NHS to obtain the activated ester. TLC analysis suggested this reaction produced many unwanted by-products, with aza-BODIPY instability under these reaction conditions being a possible factor. The data suggested the product was not formed as the $^1\text{H-NMR}$ showed no signals associated with the NHS ester. This is likely to be the consequence of poor separation and possible hydrolysis of the activated ester from the purification process using column chromatography on silica.

After several unsuccessful reactions to access the activated ester, carboxylic acid functionalised aza-BODIPY was synthesised with an anionic moiety to induce water-solubility. The method utilised the water-solubilisation method previously described, but with microwave irradiation to improve the reaction rate. The reaction between **44** and 1,3-propanesultone was carried out in THF with microwave heating at 80°C for 30 minutes with Cs₂CO₃ instead of K₂CO₃. The reaction was monitored by TLC every 10 minutes and showed no sign of further product formation or starting material consumption after 30 minutes. Initially, the product was purified by precipitation with diethyl ether over methanol, followed by extensive washing with diethyl ether and ethanol, but, only small amounts of impurity were removed through rapid precipitation. Hence, the counter ion exchange approach was applied to purify the crude product to obtain a carboxylic acid anionic aza-BODIPY **46** with a yield of 91%. The counter ion exchange method showed significant improvement in purity by TLC, and HPLC chromatography showed a single peak with a retention time of 4.1 min. This compound was characterised by ¹H, ¹³C and ¹⁹F-NMR and MS (**Scheme 24**).



Scheme 24. Synthesis of water soluble anionic aza-BODIPY with carboxylic acid functionality.

The UV-visible and fluorescence spectra for compound **46** were obtained in acetonitrile, to show an absorption band at 660 nm and an emission band at 710 nm as shown in **Figure 76**.

Normalised UV-vis and fluorescence spectrum of carboxylic acid functionalised anionic aza-BODIPY in MeOH

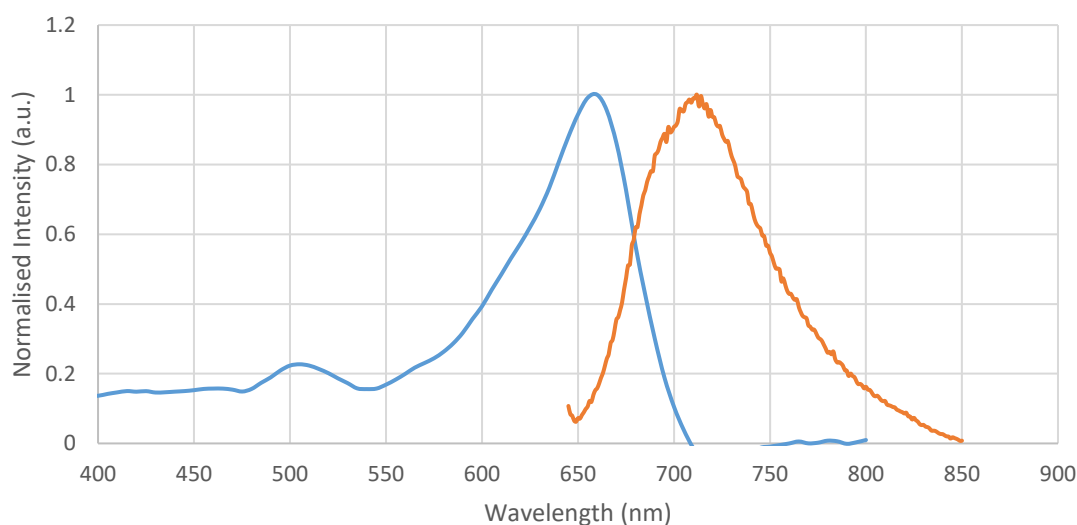
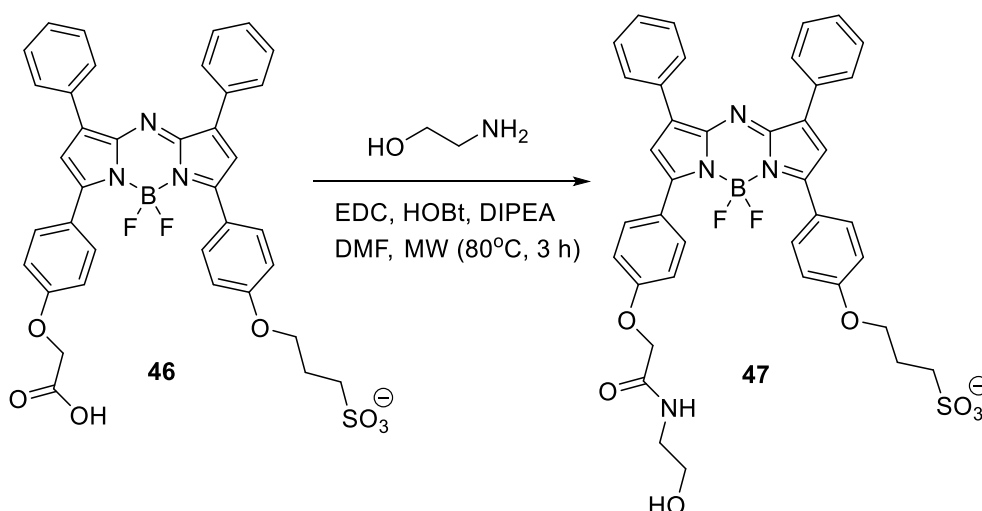


Figure 76. Normalised UV-visible (blue) and fluorescence (orange) spectra of carboxylic acid functionalised anionic aza-BODIPY **46** in methanol.

3.3.6.1 Synthesis of peptide coupled aza-BODIPY conjugate

Formation of the water soluble carboxylic acid functionalised aza-BODIPY was followed by a one-pot peptide coupling reaction with a simple aliphatic amine chain, aminoethanol, to demonstrate the viability of using the aza-BODIPY **46** in a peptide coupling reaction. The synthesis was carried out *via* a microwave reaction in DMF with the coupling reagents HOBt, EDC and DIPEA, while heating to 80°C for 3 hours (**Scheme 25**). The reaction generated the activated ester *in situ* for subsequent coupling with the primary amine of aminoethanol.



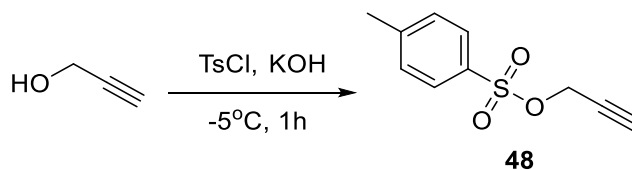
Scheme 25. Peptide coupling reaction of carboxylic acid functionalised aza-BODIPY and aminoethanol.

The reaction was closely monitored by TLC every hour. Initially, three bands were shown, after the first hour of the reaction, the three bands corresponding to unreacted starting material, NHS ester derivative, and desired product. The reaction was continued for another two hours until no further reaction was observed. Purification with the counterion exchange technique was applied to afford conjugate **47** in 71% yield. This compound was characterised by ¹H, ¹¹B-NMR.

3.3.7 Clickable water-soluble alkyne functionalised aza-BODIPY

Another functionality was also investigated for the water soluble anionic aza-BODIPY, to demonstrate the facile modification and applicability of the novel counterion exchange method to a range of functionalised aza-BODIPY.

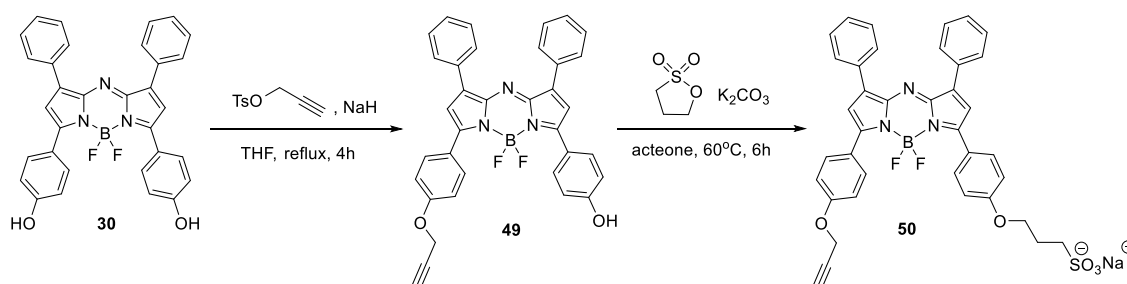
For the precursor to introduce an alkyne moiety, propargyl tosylate **48** was first synthesised through the reaction of propargyl alcohol and *p*-toluenesulfonyl chloride under a basic condition to afford **48** with 85% yield. (**Scheme 26**)



Scheme 26. Synthesis of propargyl tosylate **48**.

Similar to the previous S_N2 reactions to introduce functionalities, **48** was reacted with

aza-BODIPY with NaH for 5 hours to obtain an alkyne functionalised aza-BODIPY **49**. This reaction produced mono and di-substituted derivatives and upon column chromatography, **49** was isolated in 32% yield. Subsequently, **49** was subjected to water solubilisation with 1,3-propanesultone and purified through the counter ion exchange method to obtain the desired alkyne functionalised anionic aza-BODIPY **50** in an excellent yield of 90% (**Scheme 27**).



Scheme 27. Synthesis of alkyne functionalised aza-BODIPY **49** and corresponding anionic aza-BODIPY **50**.

Upon modification, the UV-visible and fluorescence properties in the red/NIR region were also confirmed. **Figure 77** shows an absorption of aza-BODIPY **50** at 660 nm and its corresponding fluorescence emission at 695 nm.

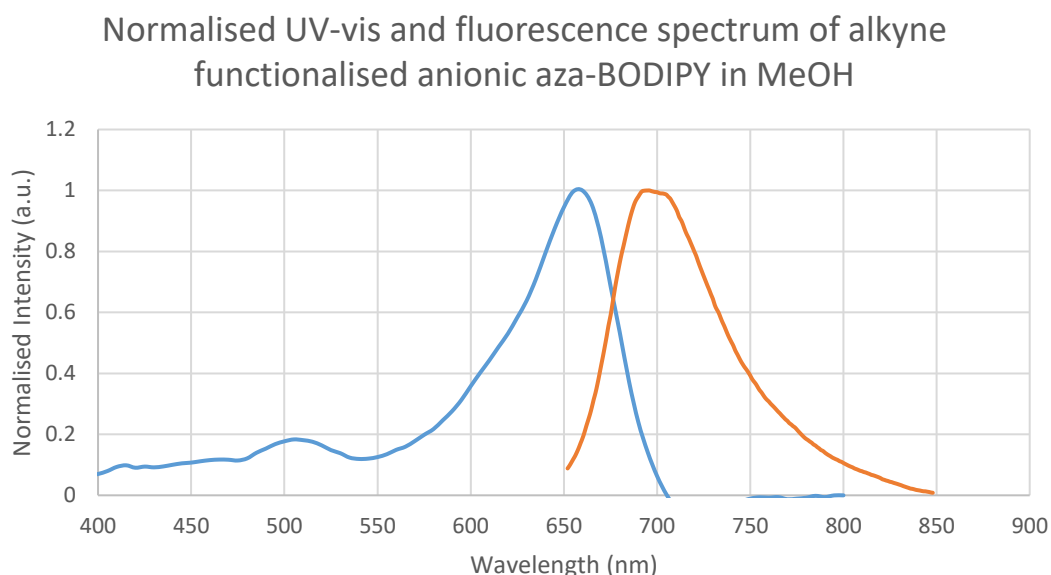


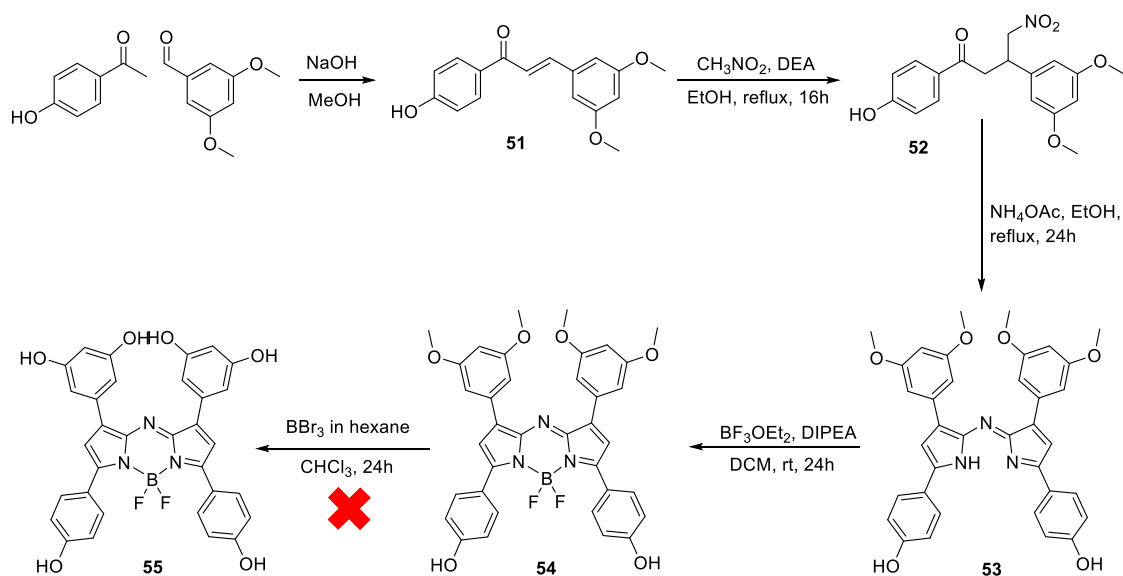
Figure 77. Normalised UV-visible (blue) and fluorescence (orange) spectrum of alkyne functionalised anionic aza-BODIPY **50** in methanol.

The application of this water-solubilisation method and subsequent purification approached was applied to three different conjugable moieties with the counterion

exchange method applicable to the library of anionic aza-BODIPY synthesised. This purification enabled scaling up of the reaction to obtain the product in high yield and purity. However, the fluorescence spectra in water indicated the occurrence of aggregation from stacking of the hydrophobic core. This could potentially lead to further complications in the process of labelling biological molecules using different bioconjugation techniques.

3.3.8 *Synthesis of enhanced water-soluble aza-BODIPY through methyl ether protection*

To enhance the water solubility of aza-BODIPYs several approaches were attempted. The first approach utilised an aza-BODIPY structure to introduce moieties at multiple modification sites. Hence, 3,5 dimethoxybenzaldehyde was first reacted with 4-hydroxyacetophenone in a base catalysed aldol reaction to obtain the corresponding chalcone **51** in 45% yield. **51** was then reacted with nitromethane under a nitro aldol reaction and the crude was purified by rapid extraction with EtOAc and diethyl ether to obtain **52** in 45% yield. Due to difficulty in purifying this compound, **52** was reacted with ammonium acetate in ethanol without further purification for 48 hours and heated under reflux. The resulting precipitant was purified through washing with cold ethanol and recrystallised from CHCl₃ to afford aza-dipyrrromethene **53** as a blue/black solid in 39% yield. The lower yield was because of the impure precursor from the previous step, hence, excess purification was required. Aza BODIPY **54** was synthesised by reacting **53** with BF₃.Et₂O and DIPEA, the product was isolated by column chromatography to obtain **54** with a yield of 30%. The inherent low yield was a result of incomplete reaction as a significant amount of starting aza-dipyrrin **53** was observed. (**Scheme 28**)



Scheme 28. Attempted synthesis of hexahydroxy aza-BODIPY **55**.

UV-visible and fluorescence spectra were acquired and red/NIR absorption and emission bands were observed for aza-BODIPY **54**, with the λ_{abs} at 680 nm and λ_{em} at 717 nm as shown in **Figure 78**.

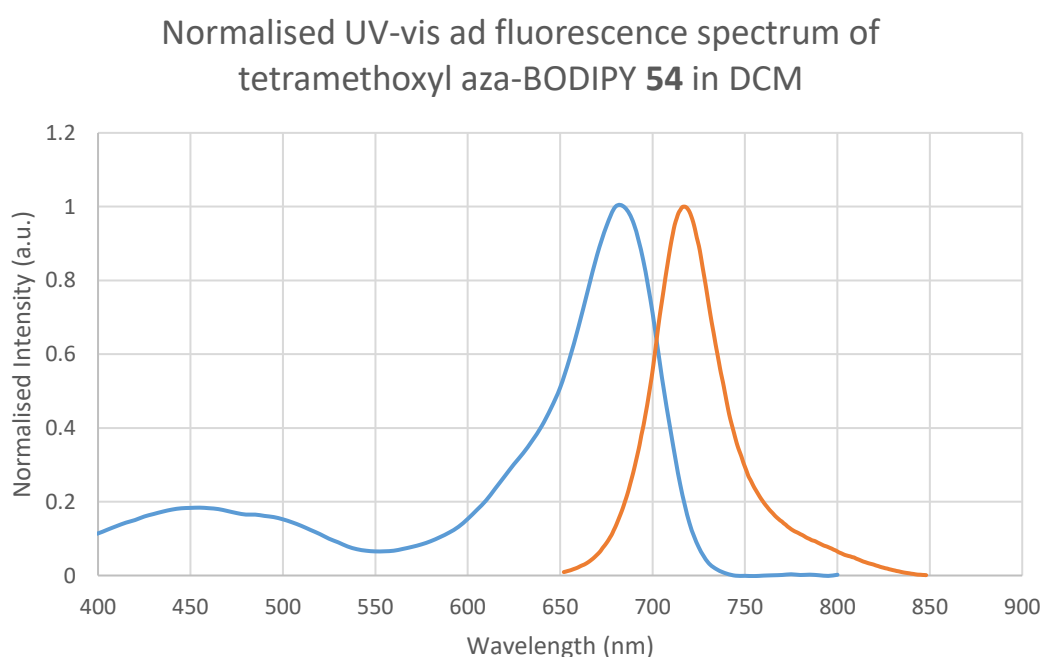


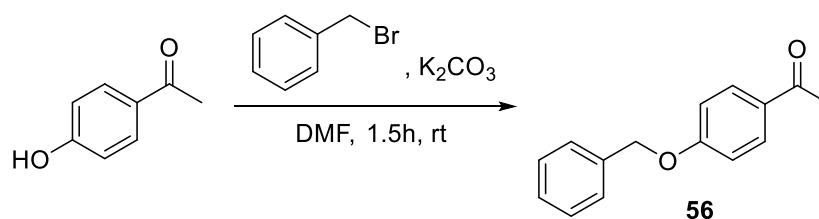
Figure 78. Normalised UV-visible (blue) and fluorescence (orange) spectrum of methyl ether protected aza-BODIPY **54** in DCM.

Deprotection of the four methyl groups was attempted using a stoichiometric quantity

of BBr_3 in hexane to selectively cleave the methyl ether group ($\text{H}_3\text{C-O}$) without removal of BF_2 . However, this reaction did not proceed as expected, the material recovered after chromatographic purification for **55** was identified as the starting aza-BODIPY **54**. This was believed to be a result of insufficient molar quantities used to achieve complete cleavage. Since aza-BODIPYs are sensitive to harsh acidic conditions, it was difficult to optimise reaction conditions for selective cleavage of methyl ether ($\text{H}_3\text{C-O}$) bond. Therefore, a different protecting group was required.

3.3.9 Synthesis of enhanced water-soluble aza-BODIPY through benzyl ether protection

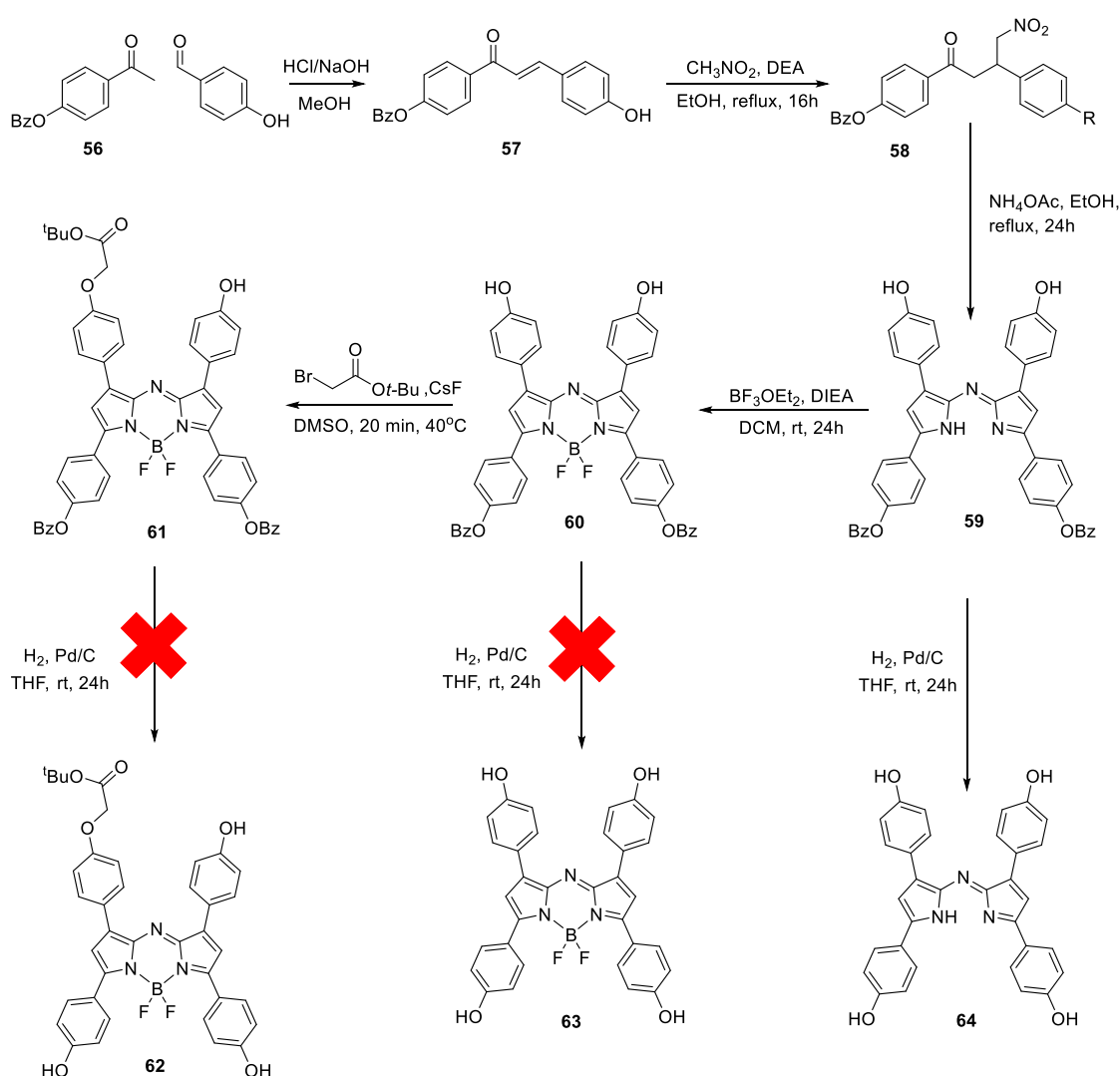
The use of benzyl protecting groups was investigated, since benzyl deprotection does not require the use of acidic reagents, making it more suitable for the selective deprotection of an aza-BODIPY. The synthesis of dibenzyl aza-BODIPY was carried out using the general method previously described, but started from the corresponding acetophenone precursor. 4-Benzyloxyacetophenone **56** was synthesised by the protection of the hydroxyl group of 4-hydroxyacetophenone with benzyl bromide and K_2CO_3 to obtain **56** in 88% yield (Scheme 29).



Scheme 29. Synthesis of 4-benzyloxyacetophenone **56**.

Subsequently, 4-benzyloxyacetophenone was reacted with 4-hydroxybenzaldehyde through an acid catalysed aldol condensation reaction with concentrated sulfuric acid to obtain the respective chalcone **57** with 64% yield. It was then nitrated with nitromethane and DEA, and purified by column chromatography to obtain nitrochalcone **58** in 86% high yield. **58** was further refluxed for 24 hours with ammonium acetate in ethanol and the precipitant was isolated and washed with cold ethanol to afford aza-dipyrromethene **59** as a blue/black solid in 49% yield. Aza-BODIPY **60** was then produced by reacting **59** with $\text{BF}_3\cdot\text{Et}_2\text{O}$ and DIPEA and purification by column chromatography to obtain a yield of 56%. Aza-BODIPY **60** was

initially found not to be soluble in most non-polar solvents and some aprotic solvents. The general solubility improved when dissolved in a coordinating solvent such as THF, this is similar to the behaviour observed for halogenated aza-BODIPY. After the synthesis of the dibenzyl protected aza-BODIPY, a *t*-butyl ester was introduced at the available phenolates through the reaction with CsF and *t*-butylbromoacetate for 20 minutes. Chromatographic purification was carried out to obtain the mono-adduct aza-BODIPY **61**, but only a low yield of 13% was obtained due to the formation of both mono and bis- adducts as a mixture. (Scheme 30)



Scheme 30. Attempted synthesis of the 3+1 aza-BODIPY.

Through UV-visible and fluorescence analysis, a bathochromic shift was observed for aza-BODIPY **61** in the red/NIR region, with λ_{abs} at 690 nm and λ_{em} at 722 nm observed (Figure 79).

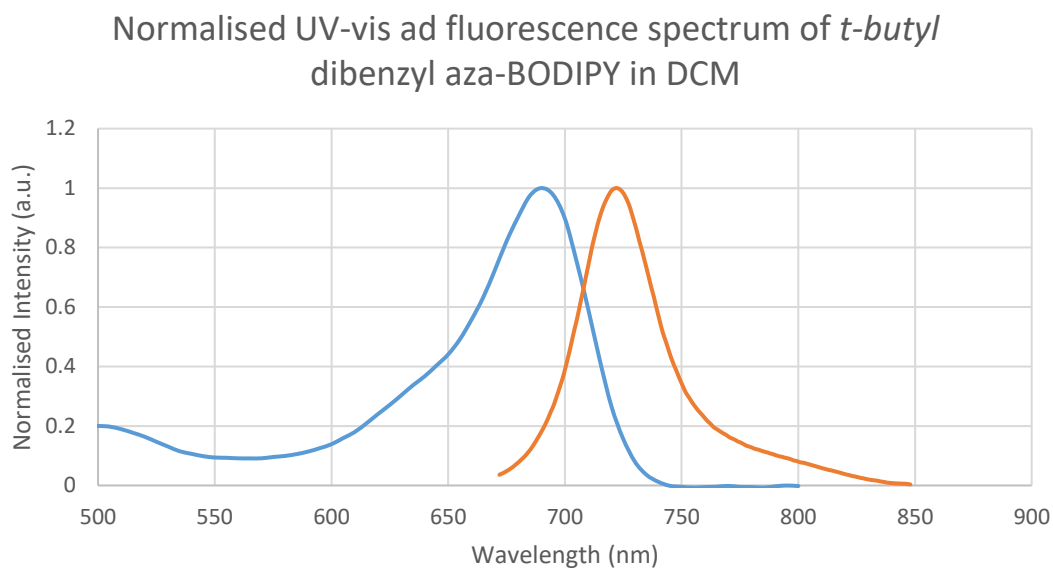


Figure 79. Normalised UV-visible (blue) and fluorescence (orange) spectra of *t*-butyl dibenzyl aza-BODIPY **61** in DCM

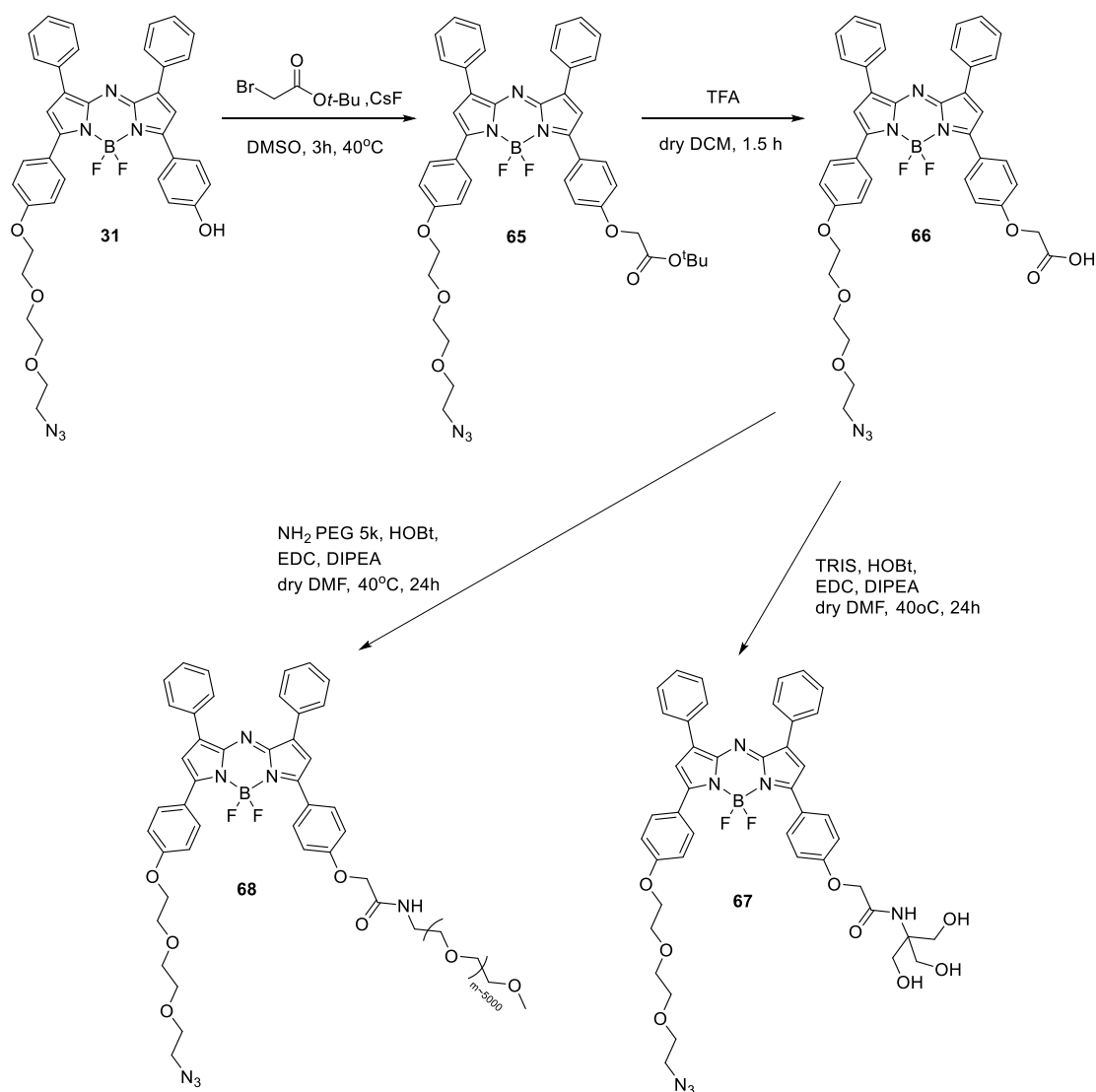
The pure product **61** was then subjected to catalytic hydrogenation in an attempt to deprotect the benzyl group. From the TLC analysis, a mixture was obtained after the reaction, this was initially suspected to be multiple and uncontrolled cleavages of the *t*-butyl ester functionality and the benzyl groups. However, the mixture consisted of mainly a less polar specie suggesting formation of the corresponding aza-dipyrrin due to the removal of BF₂. Unfortunately, this speculation could not be validated through the analysis of the less polar species due to difficulty in separating the mixture. To investigate this, hydrogenation reactions with aza-BODIPY **60** and aza-dipyrrin **59** were also carried out. Hydrogenation with aza-BODIPY **60** showed the same mixture consisting of a less polar species similar to that observed from the previous reaction. This less polar species corresponded to aza-dipyrrin **59** as identified by TLC analysis (R_f value of 0.57 (silica, 50% THF: hexane)). Whereas for aza-dipyrrin, the hydrogenation went to completion to obtain tetrahydroxyl aza-dipyrrin **64** in 56%.

Although the benzyl deprotection of a dibenzyl BODIPY has previously been reported in the literature²⁵⁹, the hydrogenation reaction did not behave in the same way for aza-BODIPY. The hydrogenation of aza-BODIPYs resulted in the loss of the BF₂ fragment from the core rather than the cleavage of benzyl groups. The electron deficient properties of aza-BODIPY could have contributed to this phenomenon, as this could

result in significantly changes to the reactivity toward the aza-BODIPY core. Therefore, making the loss of the BF₂ fragment more susceptible. With the unexpected limitation to this approach, another method was developed to significantly enhanced the water solubility.

3.3.10 *Synthesis of enhanced water-soluble aza-BODIPY through PEG conjugation*

A more facile method with less variability was developed to synthesise an azido aza-BODIPY with enhanced water solubility to enable further bioconjugation strategies for the labelling of proteins and antibodies. An azide functionalised aza-BODIPY **32** was synthesised by adapting a method previously reported in this chapter. Briefly, S_N2 Williamson ether synthesis was performed at the available phenolate of **32** to introduce a *t*-butyl ester. Followed by chromatographic purification to afford **65** in a yield of 78 %. Deprotection of the *t*-butyl group was achieved using TFA and the reaction was carefully monitored to circumvent removal of BF₂ under acidic conditions. The optimised deprotection time was found to be 1.5 hours and the crude was purified by column chromatography to obtain the carboxylic acid **66** in 34 % yield. Initially, the carboxylic acid moiety was reacted with TRIS using peptide coupling reagents; HOBt, EDC, and DIPEA in dry DMF at 40 °C for 24 hours, the resulting crude was purified by column chromatography to obtain **67** in 36% yield. The low yield was due to the modification of introducing the trihydroxyl group, which increased the adhesiveness towards silica, making the purification process more challenging. The addition of the TRIS moiety did not significantly enhance the water solubility. Therefore, an amine substituted PEG chain (5k) was reacted with the corresponding carboxylic acid **66** through peptide coupling using the same set of coupling reagents as previously described in dry DMF at 40 °C for 24 hours. The crude product was purified using a Sep-Pak C18 cartridge to obtain the water soluble aza-BODIPY **68** in an excellent 98 % yield (**Scheme 31**).



Scheme 31. Synthesis of the enhanced water-soluble azido aza-BODIPYs.

UV-visible and fluorescence analysis of the aza-BODIPY **68** in aqueous media was carried out and showed absorption and emission maxima in water at 635 nm and 713 nm respectively. Due to the higher solubility and stability in aqueous media, the low-intensity fluorescence spectrum in water was no longer observed, indicating the absence of aggregation (**Figure 80**).

Normalised UV-vis and fluorescence spectrum of azido
PEG 5k aza-BODIPY in water

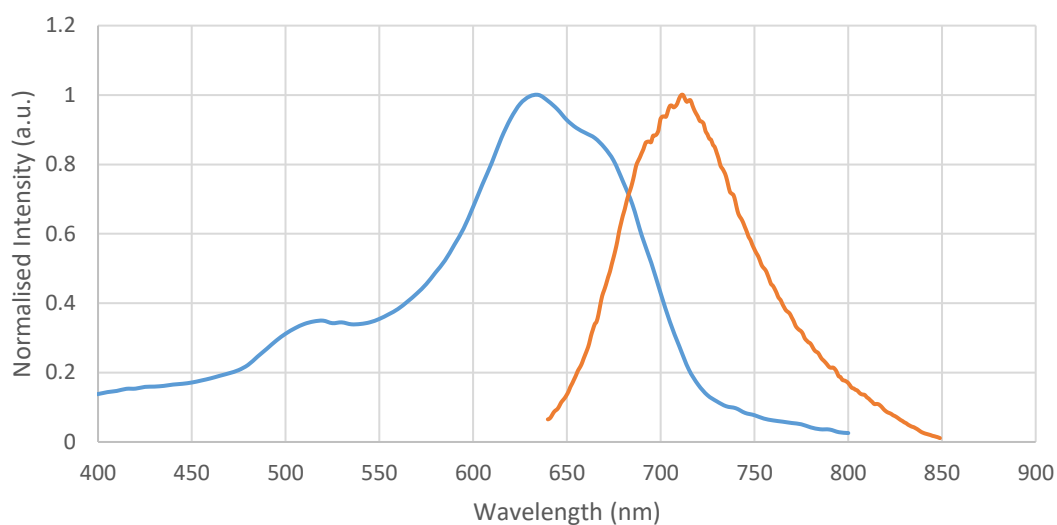


Figure 80. Normalised UV-visible (blue) and fluorescence (orange) spectrum of azido PEG 5k aza-BODIPY **68** in water.

To conclude, several different synthetic strategies were investigated in order to synthesise a range of aza-BODIPYs with different groups suitable for bioconjugation and water-solubilising groups. Throughout the project, a novel purification method was developed for the sulfonated aza-BODIPYs to provide an inexpensive and facile technique, as well as allowing scale up of the water-solubilisation reaction.

4. Bacteriochlorins

Bacteriochlorins are a class of tetrapyrrolic macrocycles and form the core structure of bacteriochlorophylls. Bacteriochlorophyll *a* was first found in photosynthetic bacteria as a natural light absorbing pigment by Eisner in 1957²⁶⁰ and first isolated and purified by Omata and Murata in 1983 from chromatophores found in the bacterium *Chromatium vinosum*.²⁶¹ Bacteriochlorins are often found in nature, for example tolyporphin is a naturally occurring bacteriochlorin isolated from blue green alga *Tolypothrix nodosa* as was discovered by Prinsep *et al.*²⁶²

Upon the discovery of bacteriochlorophyll *a*, two corresponding derivatives were found by Beems *et al.* through saponifying bacteriochlorophylls *a* to obtain bacteriochlorophyllin *a* and subsequent Mg metal removal to obtain bacteriochlorin *a*, with no significant changes in optical properties being observed; opening up new research areas due to the robust nature of bacteriochlorin for chemical modifications²⁶³ (**Figure 81**).

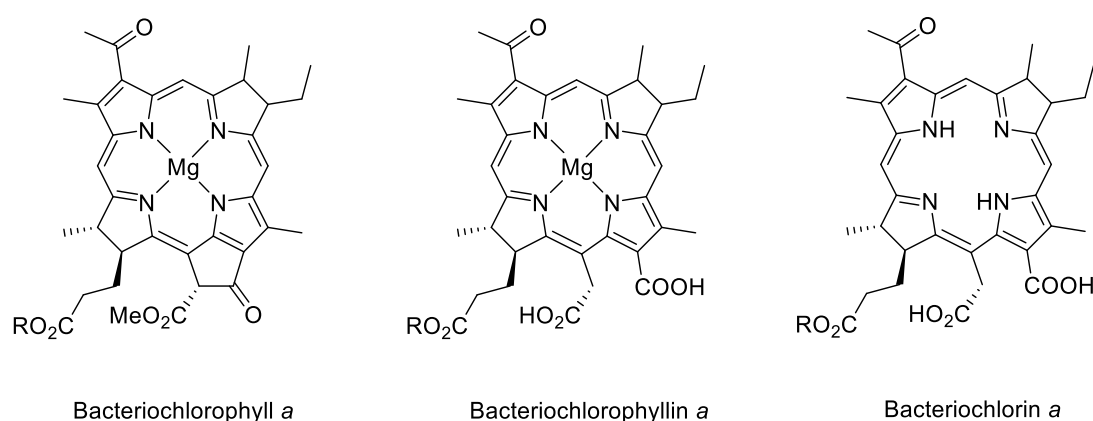


Figure 81. Structure of bacteriochlorophyll *a* and its derivatives.

The chemical and physical properties of bacteriochlorin are dependent on the presence of the conjugated aromatic 18π system, that is cross-conjugated with two reduced β,β' -double bonds on opposing pyrroles as shown in **Figure 82**. This difference in the tetrapyrrolic structure, relative to the porphyrins, leads to an increase in flexibility of the conjugated π system resulting in bathochromic shift, as well as a decrease in basicity of the inner nitrogens.^{264,265}

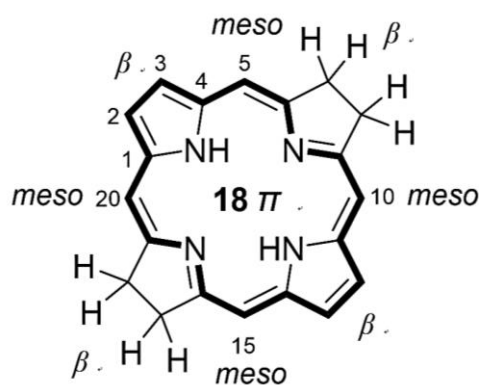


Figure 82. Schematic structure of bacteriochlorin and its 18 π aromatic system.

Bacteriochlorins display significant differences in their optical properties in comparison to porphyrins and chlorins. The spectrum of a bacteriochlorin typically has three distinctive bands, those include the hypsochromically shifted Soret band (B_x and B_y) in the near UV region, a small Q_x band in the visible region, and most significantly an intense absorption band known as the Q_y band in the NIR region at ~ 730 nm²⁶⁶ (**Figure 83**).

Many spectroscopic studies of bacteriochlorins have been carried out; and, with their emissions in the NIR region, these compounds are clinically favourable for FGS as they allow for deeper penetration into tissue. Furthermore, they have a large effective Stokes shift, high photostability and low dark toxicity making them an attractive class of NIR fluorophores.²⁶⁷

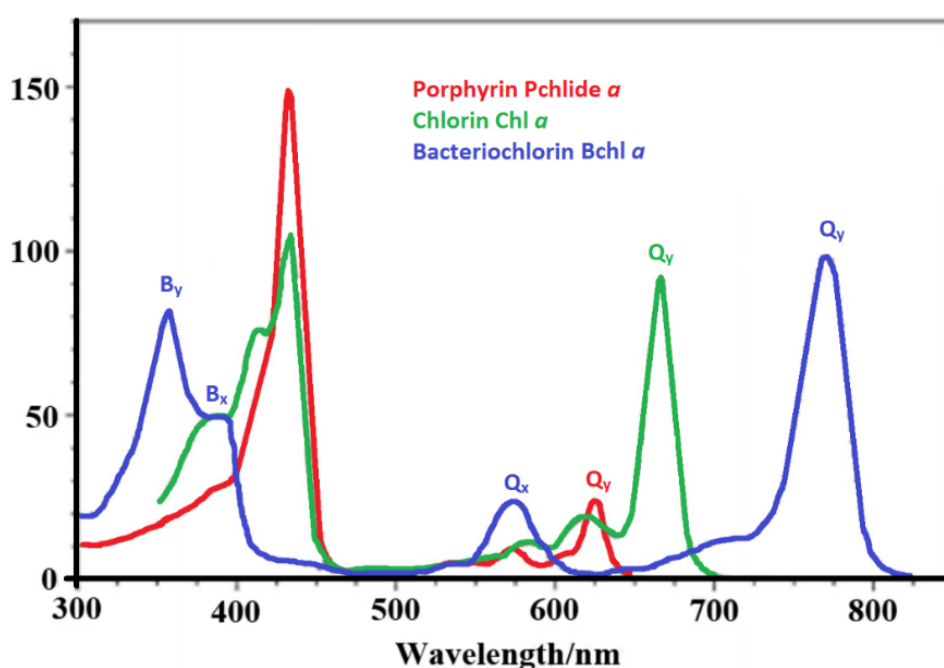
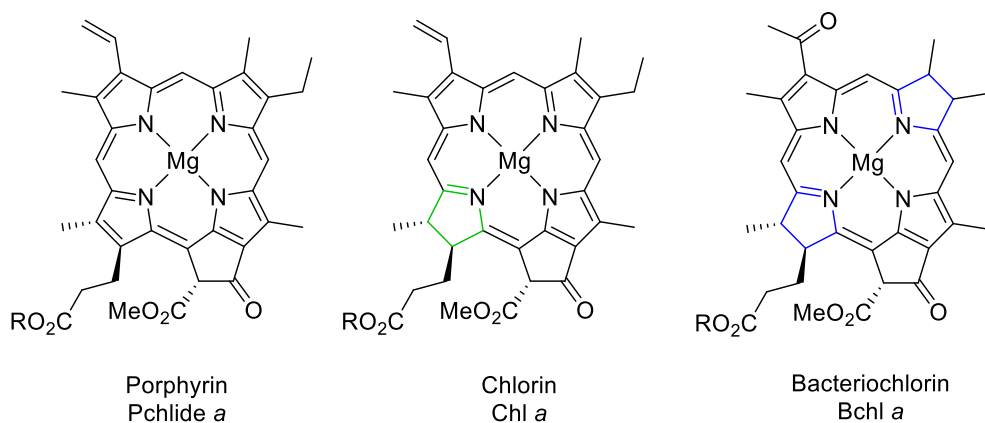


Figure 83. Schematic structures and absorption spectrums of Pchl *a*, Chl *a*, and Bchl *a*.

However, bacteriochlorins have tendency to oxidise back to chlorins and porphyrins, significantly affecting their use in biomedical applications. This instability can result in limitations in *in vivo* application and was first described by Henderson *et al.* in 1991.²⁶⁸ The synthesis of a stable bacteriochlorin has been extremely challenging, leading to limited investigations into their fluorescence properties in the NIR region. Therefore, fewer investigations toward their applications for clinical, diagnostic and biomedical imaging.²⁶⁹

4.1 Synthesis of bacteriochlorin

Due to the synthetic challenges of bacteriochlorins, there are currently only a limited number of synthetic routes available to achieve bacteriochlorins through chemical manipulations. From those, there are five distinctive approaches that are widely used: the modification of natural bacteriochlorophylls, reductive hydrogenation of porphyrins, oxidative dihydroxylation of porphyrins, 1,3-dipolar cycloaddition of porphyrins and *de novo* synthesis of bacteriochlorins.

4.1.1 Modification of natural bacteriochlorophylls

Currently, the most prevalent route to bacteriochlorin is to extract *Behl a* and to perform chemical modification at multiple positions. Many modifications could be carried out to tune optical properties, improve solubility and enhance chemical stability. These include the derivatisation of the 3-position acetyl group at ring **A** as it is susceptible to reduction and dehydration to give 2-hydroxyethyl and vinyl substituents.²⁷⁰ The most common modification is transesterification or acid catalysed hydrolysis that can occur at the 17-position propionate moiety of ring **D**, and are often followed by transamination reactions.²⁷¹ In addition, the keto ester functionality in ring **E** can be readily enolized and lead to ring opening, such as alkaline hydrolysis and transformation of the isocyclic ring into the six membered imide, and further functionalisation at the *N*-imide group.²⁷² Other modifications such as demetallation and remetallation can also occur at the central cavity²⁷³ (**Figure 84**).

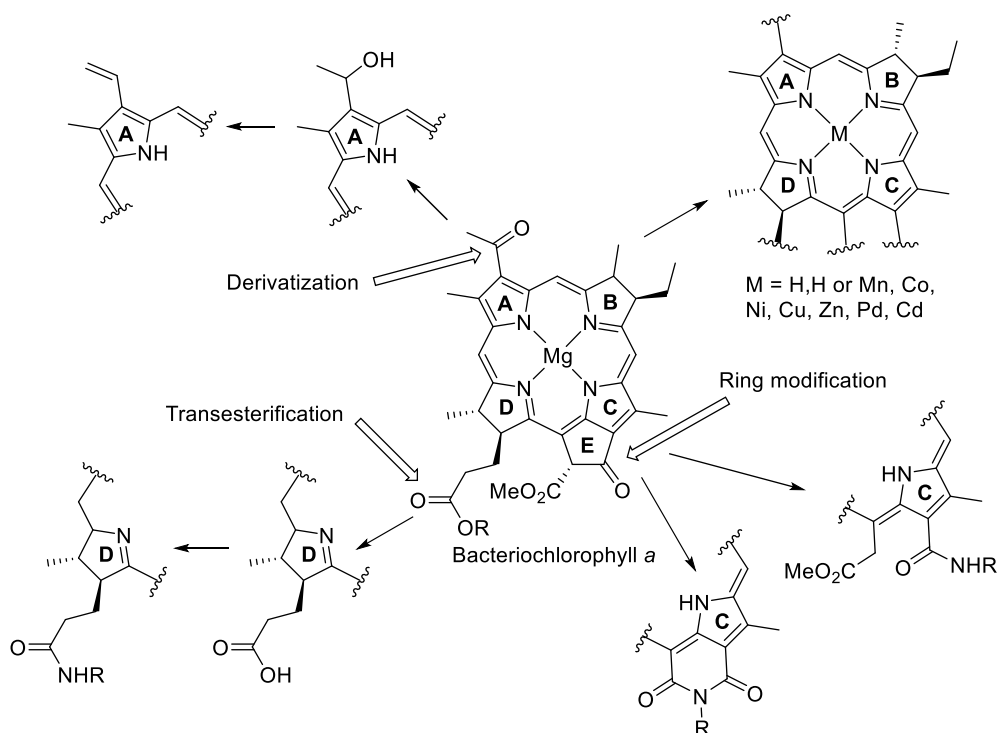


Figure 84. Chemical modifications of bacteriochlorophyll *a*.

Despite this method allowing simple modifications of the bacteriochlorin core, the chemodiversity is often limited to the pre-existing moieties at specific sites. Therefore, restricting the overall functionalities that can be introduced for such bacteriochlorins.

4.1.2 Reductive hydrogenation of porphyrins

Bacteriochlorins can be synthesised through reduction of porphyrins and chlorins. Diimide, being an excellent reductant, is most often used to selectively reduce the porphyrin β,β' -double bond *via* the Whitlock diimide reduction, typically through syn-addition of hydrogen to form the corresponding *cis* bacteriochlorin adducts²⁷⁴ (**Figure 85**).

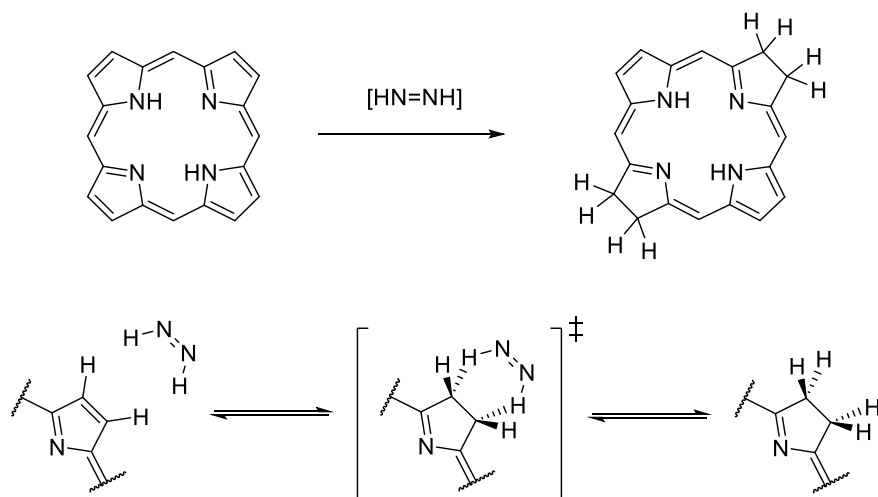


Figure 85. Whitlock diimide reduction²⁷⁴ of porphyrin through *syn*-hydrogenation.

The subsequent crude product can be purified utilising the differences in solubility as the basicity decreases from a porphyrin to a bacteriochlorin. Porphyrin and chlorin are more basic molecules and can be extracted from acidic aqueous solution. Therefore, bacteriochlorin being, less soluble in aqueous solution, can be easily separated as it remains in the organic phase.²⁶⁵

However, there are several drawbacks to this approach, firstly this reaction causes the formation of a mixture of porphyrin, chlorin and bacteriochlorin making purification a challenge. Secondly, the substitution pattern of the macrocycle can cause the formation of regioisomers. Lastly, there are possible reaction pathways that can lead to dehydrogenation allowing the formation of unwanted porphyrins and chlorins.²⁶⁶

4.1.3 *OsO₄ mediated oxidative dihydroxylation of porphyrin*

Other relatively more stable bacteriochlorins have been synthesised using osmium(IV) tetroxide to mediate vicinal dihydroxylation of porphyrins and chlorins.^{275,276} This was first conducted by Fischer in 1940 through the dihydroxylation of a β,β' -double bond of an octaalkylporphyrin.²⁷⁷ Dihydroxylation has been demonstrated on a variety of porphyrins^{278–282} and been recognised as a versatile method with the corresponding bacteriochlorin having relatively high chemical stability.²⁸³ However, the reaction suffers from the production of stereoisomers, due to bis-osmylation that generates two isomeric bacteriochlorin; the *cis*-tetrahydroxybacteriochlorin and the *trans*-tetrahydroxybacteriochlorin. The presence of four very polar hydroxyl groups also

adds further complexity to separation of diastereomerically pure compounds from the corresponding mixture.²⁸² (**Figure 86**).

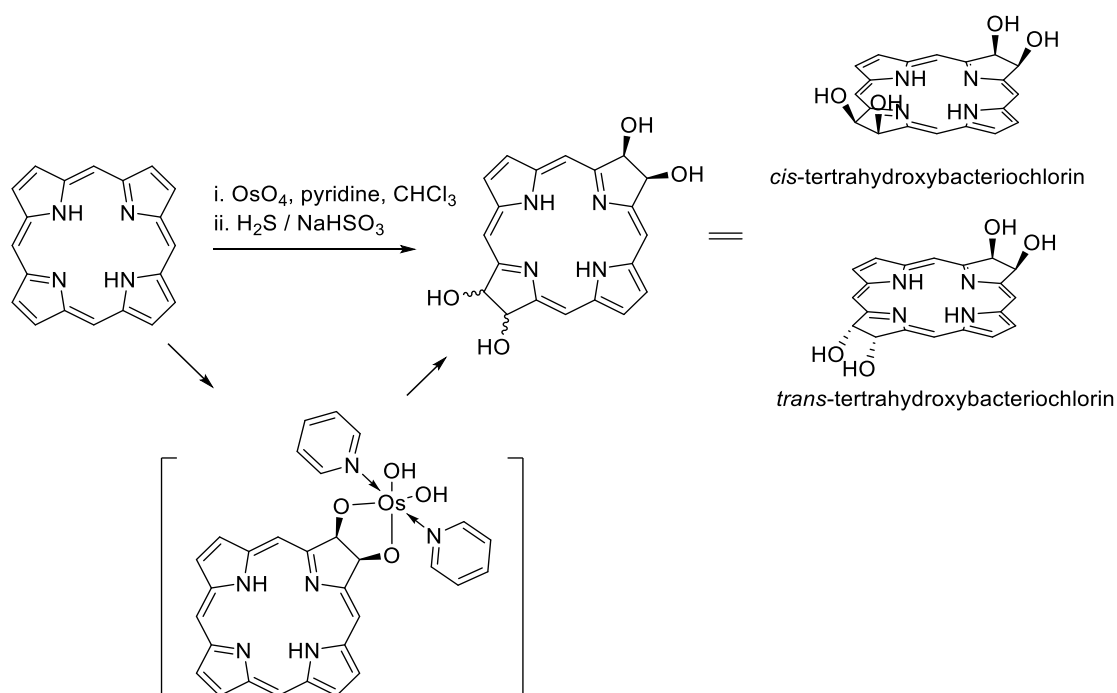


Figure 86. Bacteriochlorin diastereomers generated from OsO_4 mediated oxidation of porphyrin.

The development of this methodology led to a significant increase in the yield of bacteriochlorin²⁸⁴ and gained in popularity. Bacteriochlorins generated with this method have subsequently been subjected to various of biological studies.^{276,285} However, the method utilised an undesirable reactant, OsO_4 which has been considered as highly toxic and expensive to use.

4.1.4 1,3 Dipolar cycloadditions to porphyrins

1,3-Dipolar cycloaddition with porphyrins was first investigated by Cavaleiro *et al.* in 1999²⁸⁶ to generate corresponding chlorins, isobacteriochlorins and bacteriochlorins. Due to the discovery, many reactions employed the cycloaddition approach for porphyrin conversion to chlorins and to bacteriochlorins. This methodology has since been reported with the use of several different 1,3-dipoles such as azomethine ylides^{287,288}, nitrile oxide^{289,290} and nitrones²⁹¹ (**Figure 87**).

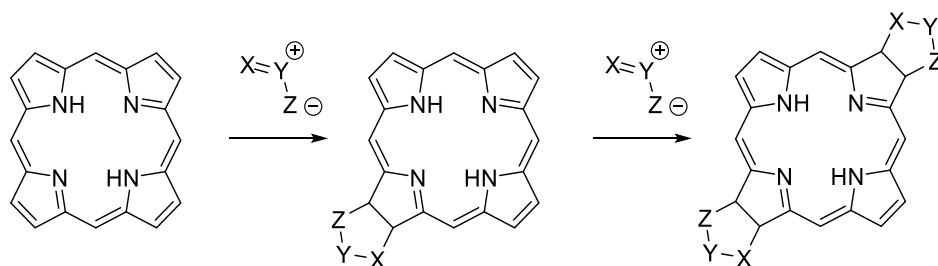


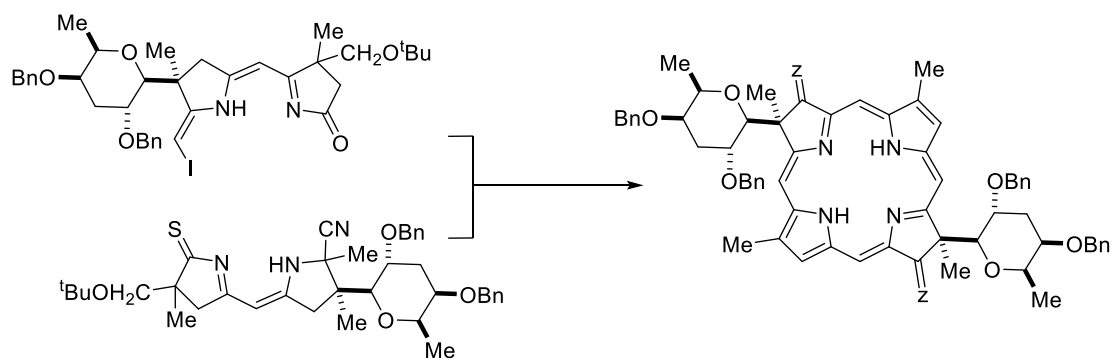
Figure 87. Generalised scheme of 1,3-dipolar cycloaddition of porphyrins and chlorins to bacteriochlorins.

Arguably, cycloaddition is currently one of the simplest methods for producing a stable bacteriochlorin, as it requires very few steps and prevents oxidation to unwanted porphyrins and chlorins, making this approach very attractive. However, these types of reaction have several disadvantages such as the fact that the reactions are limited to certain specific porphyrins and 1,3-dipoles, as well as slow reaction rates and low yields.^{287,292} Purifications are also considered to be difficult due to the production being a mixture containing 1,3-dipolar regio- and stereoisomers.^{291,293}

4.1.5 *De novo synthesis of bacteriochlorin*

De novo synthesis is a complementary approach utilising simple precursors to form stable products, avoiding dehydrogenation and ensuring no oxidation takes place. There are currently two well-known *de novo* routes for the synthesis of bacteriochlorins, one being the total synthesis of tolyporphyrins by Kishi *et al.*^{294,295} and the other being the introduction of the geminal dimethyl group at the reduced pyrroline ring position by Lindsey *et al.*^{296–299}

Kishi *et al.* investigated the structure of tolyporphyrin *a* and found that the structure consists of an unsymmetrical dioxobacteriochlorin core. Upon investigation, the group developed a synthetic pathway for tolyporphyrins from monocyclic precursors. This synthetic pathway involved a more than 20 steps reaction sequence, producing less than 5 mg of the final product.^{294,295} (**Scheme 32**)



Scheme 32. Kishi *et al.*'s *de novo* synthesis of tolyporphyrins from dipyrin precursors.

Lindsey's group recently employed a *de novo* synthesis, whereby a geminal dimethyl acetal moiety was introduced on the pyrrolic unit of the dihydrodipyrin to ensure stability against oxidation. The yield was significantly improved to obtain around 30% in comparison to less than 1% in Kishi's reaction. This reaction has now been shown to be a more stable and efficient bacteriochlorin synthetic pathway²⁹⁹ (**Figure 88**).

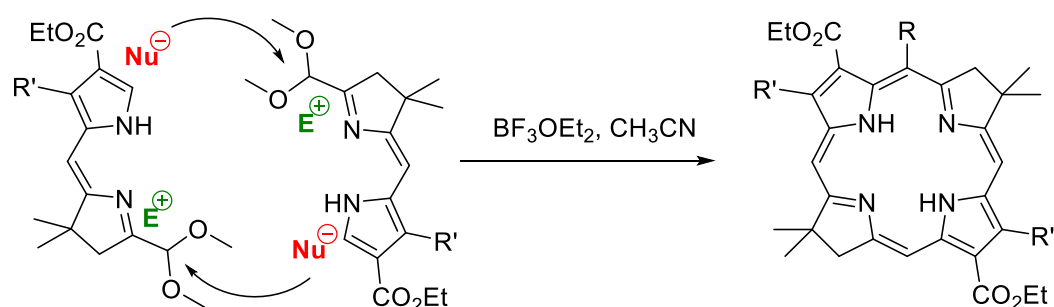


Figure 88. Lindsey approach of *de novo* synthesis using geminal dimethyldipyrin to generate oxidation stable bacteriochlorin.

From the *de novo* synthesis, bacteriochlorins can be elaborated with several different methods including coupling reactions, aldol condensation and a regioselective bromination reaction at the 15 position.^{300,301}

4.2 Imaging with bacteriochlorin

Although bacteriochlorins have not been widely applied for the purpose of fluorescence imaging, there are several examples of *in vivo* imaging demonstrating the possibilities for bacteriochlorin as an NIR fluorescence imaging probe. Kobayashi *et al.* employed

Lindsey's method of introducing geminal dimethyl groups in the bacteriochlorins to develop a class of bacteriochlorin (λ_{Qy} 710 and 820 nm) with an NHS ester moiety that was used in detecting ovarian cancer metastases.³⁰²

Other methods employing bacteriochlorin dyads have also been investigated for fluorescence imaging. One was conducted by Holten *et al.* through the design of an up regulated system with the assembly of chlorin-bacteriochlorin dyads.^{303,304} The NIR fluorescence could be obtained through energy transfer from the lower wavelength and well resolved chlorin absorption band to the bacteriochlorin emission band. The fluorescence properties have been demonstrated through multicolour imaging to show the potential of bacteriochlorins in fluorescence imaging³⁰⁵ (**Figure 89**).

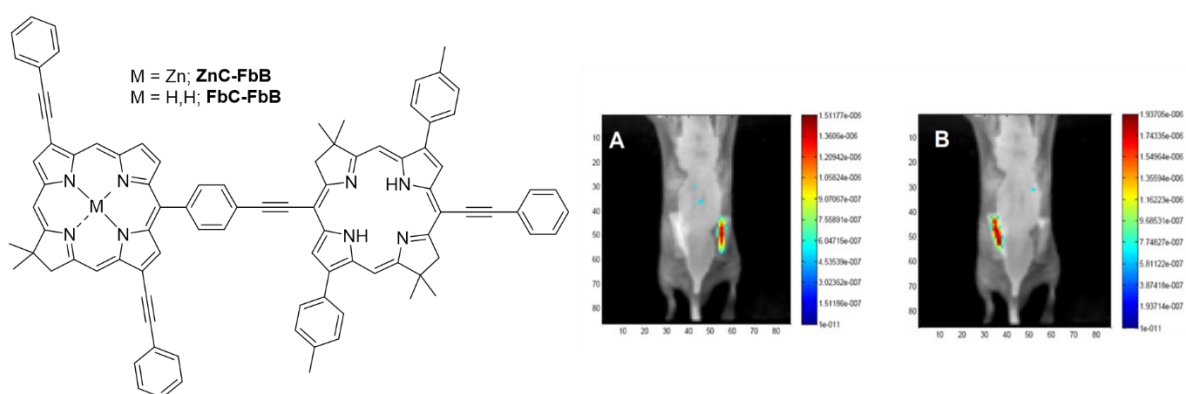


Figure 89. Structure of chlorin-bacteriochlorin dyads and optical reconstructions of fluorescence for ZnC-FbB (A) and FbC-FbC (B) with excitation at 650 or 675 nm and detection at 760 nm.

A combination of nanotechnology incorporating bacteriochlorins was developed by Zheng *et al.* through the incorporation of bacteriochlorophyll into high-density lipoprotein nanoparticles for application in a drug delivery system for tumour imaging. It was shown that bacteriochlorophyll nanoparticles retained stable NIR fluorescence properties and were used as both a delivery vehicle and NIR fluorescence probe for use in NIR fluorescence imaging.³⁰⁶

Recent research has displayed the potential of bacteriochlorins for the targeting of probes for NIR fluorescence imaging, and has highlighted the interest in further development of bacteriochlorin based NIR fluorescence probes in an NIR FGS.

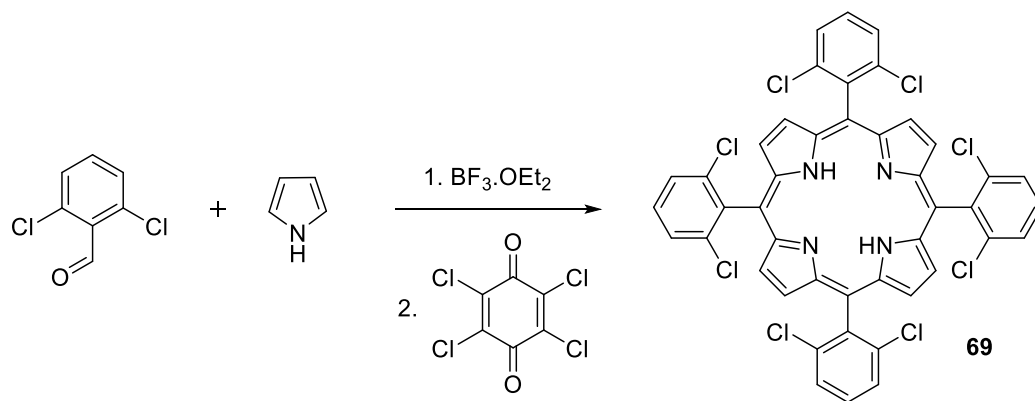
4.3 Result and discussion

Despite the synthetic challenges of current methodologies for generating stable bacteriochlorins, their NIR fluorescence properties remain interesting in the field of FGS, and for this reason, they were investigated in this project. After consideration of the potential methods for bacteriochlorin synthesis, Whitlock's diimide reaction was first employed due to its comparative simple nature. However, the reaction did not reach completion and the resulting mixture of porphyrin, chlorin and bacteriochlorin was difficult to separate using chromatography. Subsequently, bacteriochlorin synthesis following 1,3-dipolar cycloaddition was attempted using azomethine ylides, the reaction was found to be hindered by the reaction rates. Hence, the more synthetically challenging Lindsey approach to the germinal dimethyl substituted dipyrin was investigated to successfully synthesise a stable bacteriochlorin for further study.

4.3.1 Synthesis of bacteriochlorin through diimide reduction

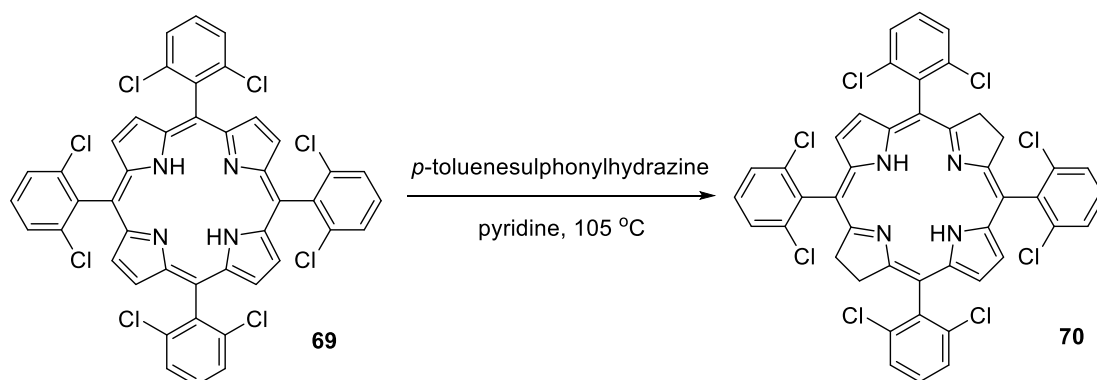
Arnaut *et al.* proposed that the introduction of halogens at the ortho positions on the phenyl ring of a *meso*-tetraphenylporphyrin can successfully produce a stable bacteriochlorin *via* diimide reduction, without the need for complex purification procedures. It is believed that the introduction of these electron withdrawing groups greatly increases the oxidation potential of the porphyrins as well as providing steric protection to the labile bonds that could undergo re-oxidation.³⁰⁷

The Lindsey method was first used to synthesise an *ortho*-substituted tetraphenylporphyrin under mild conditions. This was carried out by reacting 2,5-dichlorobenzaldehyde and pyrrole with catalytic BF₃.OEt₂ at room temperature in chloroform. After 1 hour, the porphyrinogen was oxidised to the corresponding porphyrin through addition of *p*-chloranil and refluxing for 1 hour. The crude product was washed with excess methanol to remove any pyrrolic impurities. (**Scheme 33**) The compound **69** was obtained in a yield of 5 %.



Scheme 33. Synthesis of ortho-substituted 5,10,15,20-tetrakis(2,6-dichlorophenyl)porphyrin.

A Whitlock diimide reduction was employed with an *ortho*-octachloroporphyrin. The reaction involved a reductive precursor and an organic base such as *p*-toluenesulphonylhydrazine and pyridine as the co-solvent to generate diimide gas *in situ* and initiate porphyrin reduction through hydrogenation.²⁶⁵ (**Scheme 34**)



Scheme 34. Attempted synthesis of ortho-substituted 5,10,15,20-tetrakis(2,6-dichlorophenyl) bacteriochlorin.

The reaction was monitored by TLC and UV-visible spectroscopy every 30 minutes following each addition of *p*-toluenesulphonylhydrazine in pyridine. The need for repeated additions and constant monitoring was due to rapid consumption of the reductive precursor. Adding the reductive precursor every 30 minutes ensured a steady state of diimide gas generation in the system. Before the reaction, the Soret band of the porphyrin could clearly be observed at 420 nm with three smaller Q bands observed at 515 nm, 590 nm and 659 nm. After 4 hours the rate of addition was reduced to hourly

until 6 hours. Throughout the reduction, the UV-visible spectrum displayed formation of the corresponding chlorin with characteristic absorption bands at 605 nm and 660 nm. In addition, characteristic bacteriochlorin bands were observed at 350 nm, 375 nm, 515 nm and 745 nm respectively and increased over time, accompanied by a decreasing intensity in the Soret band at 420 nm (**Figure 90**). After 6 hours the solution of *p*-toluenesulphonylhydrazine in pyridine was no longer added and the reaction was left heating for a further 15 hours.

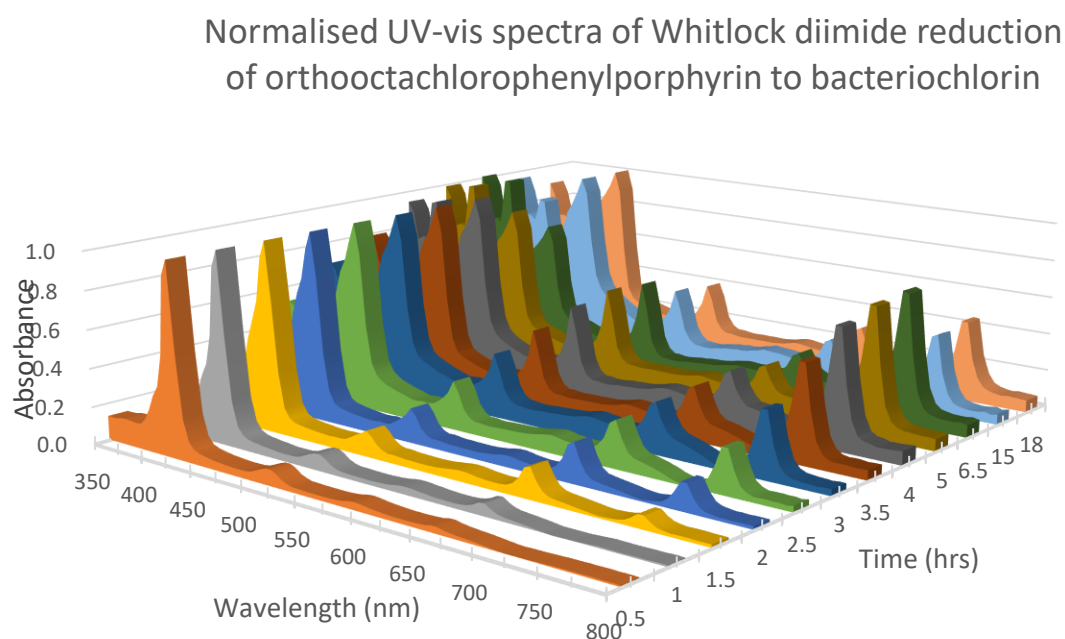


Figure 90. UV-visible spectra of Whitlock diimide reduction of ortho-substituted 5,10,15,20-tetrakis(2,6-dichlorophenyl)porphyrin to its relative bacteriochlorin **70** in DCM over a duration of 18 hours.

Even within a sealed system under an inert atmosphere, the UV-visible spectrum showed a slow oxidation from the bacteriochlorin back to the corresponding chlorin and porphyrin, once addition oxidant was stopped. This was shown through a relative increase at the intensity of the Soret band at 420 nm and a reduction in all three bands for the bacteriochlorin after 15 hours. The reaction could therefore not be driven to completion, this could be due to the modified method used, as under a highly pressurised system there could be no possible escape of the diimide gas generated *in situ*.

Despite incomplete nature of the reaction, isolation of the bacteriochlorin **70** was attempted by column chromatography, however the separations were poor, as the R_f values of porphyrin, chlorin and bacteriochlorin were extremely close. After an attempt at separation, the UV-visible spectrum suggested the product was still a mixture, and there was evidence of oxidation occurring during purification, as the relative peaks for the bacteriochlorin decreased while the Soret band of the porphyrin increased as shown in **Figure 91**.

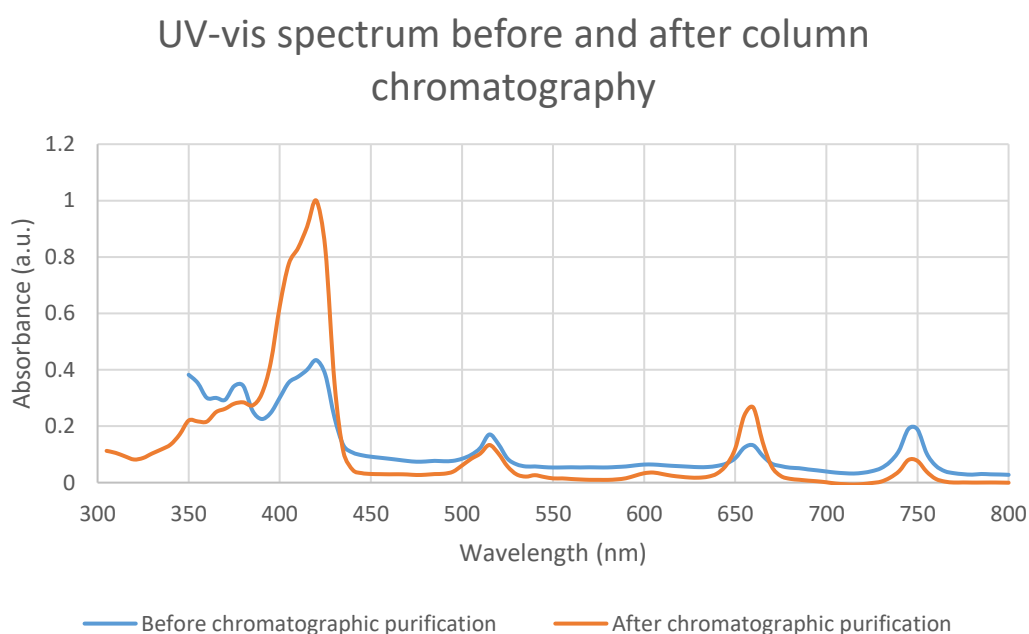


Figure 91. UV-visible spectrum of octachlorobacteriochlorin **70** in DCM before and after column chromatography.

Although the UV-visible spectrum showed reduction occurring, and formation of the corresponding bacteriochlorin, as indicated by an increased relative intensity in the Q_y band at 745 nm, the reaction, unfortunately, did not proceed as described in the literature. Due to the resulting mixture of products, the purification by column chromatography was again rather problematic and the desired product could not be isolated.

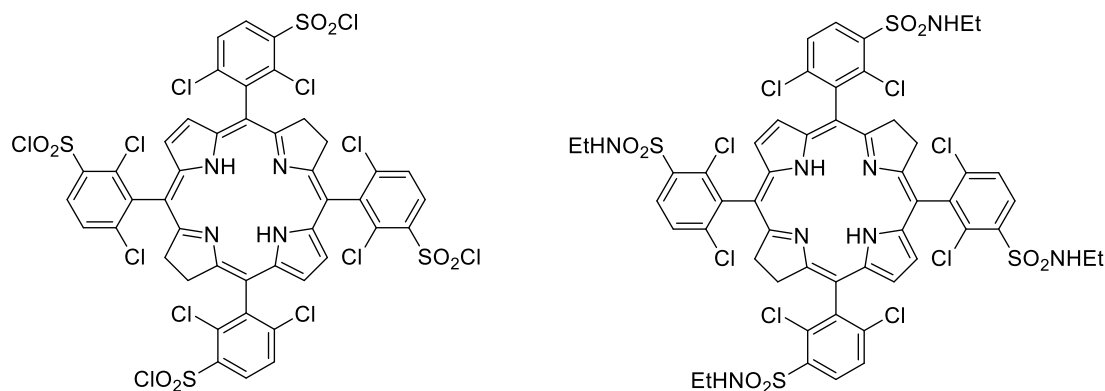


Figure 92. Examples of sulfonated and halogenated tetraaryl bacteriochlorins.³⁰⁷

Increasing the oxidation potential *via ortho*-halogenated porphyrin under the conditions of Whitlock diimide reduction has been shown to have limited potential for pre-modification and was unsuccessful in forming a stable bacteriochlorin. This method may therefore be limited to very specific porphyrins with certain substituents such as *ortho*-halogens and *meta*-sulfonyl group (sulfonyl halides and sulfonamides) as shown in **Figure 92**. As these preconditions were essential in maintaining sufficient oxidation potential. Further modification of the porphyrin may have a detrimental effect on its oxidative stability, limiting opportunities for different substituents to be introduced.³⁰⁷ Therefore, the more reliable 1, 3-dipolar cycloaddition reaction and Lindsey's *de novo* method were investigated.

4.3.2 Synthesis of bacteriochlorin via 1,3-dipolar cycloaddition reactions

One of the most facile methods for synthesising a stable bacteriochlorin is 1,3-cycloaddition reaction of porphyrin with azomethine ylides, and this method has been employed successfully to 5,10,15,20-tetrakis(perfluorophenyl) porphyrin. The corresponding chlorin, isobacteriochlorin and bacteriochlorin could be acquired through reacting with azomethine ylides generated *in situ* through the reaction of paraformaldehyde and *N*-methylglycine.

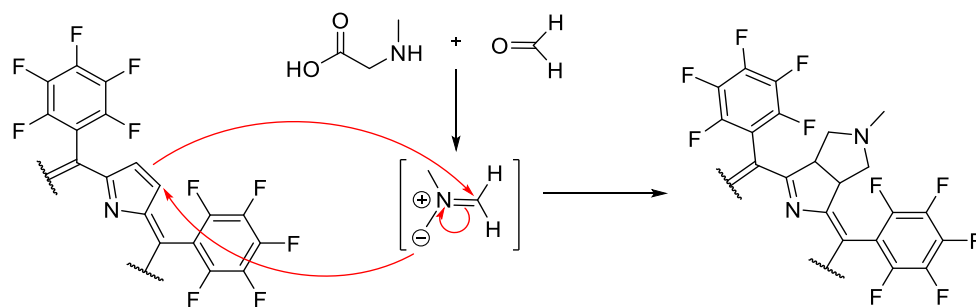
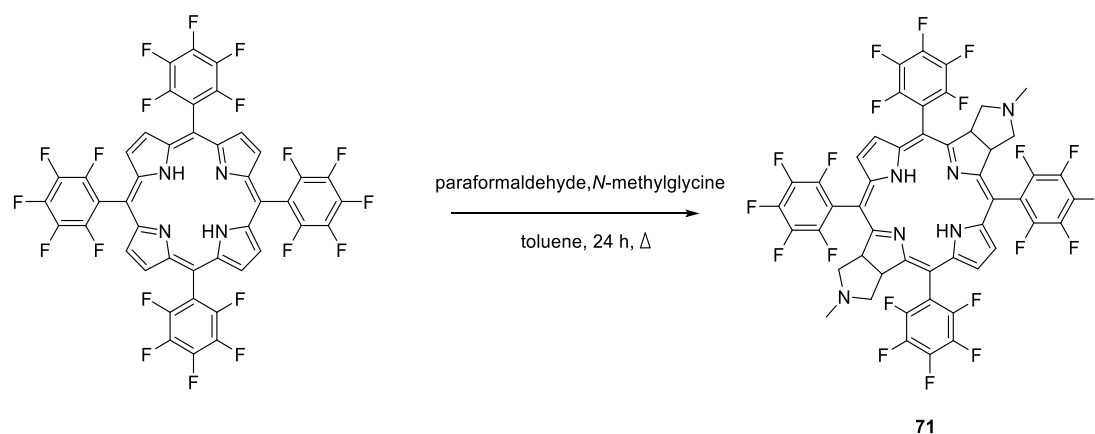


Figure 93. Mechanism of 1,3-cycloaddition reaction of ,10,15,20-tetrakis(perfluorophenyl) porphyrin with azomethine ylides.

The reaction was initially explored using the original method, the porphyrin being reacted with 2 equivalents of *N*-methylglycine and 5 equivalents paraformaldehyde, and heated under reflux for 5 hours under an inert atmosphere. After 5 hours, TLC indicated formation of the corresponding chlorin, hence a ten-times excess of the reactants were added and the reaction was heated under reflux overnight. After 20 hours of reaction, the majority of the porphyrin was converted to the corresponding chlorin with unchanged starting porphyrin remaining and a small fraction of isobacteriochlorin observed by TLC, indicated a longer reaction time was required to achieve bacteriochlorin **71** as shown in **Scheme 35**.

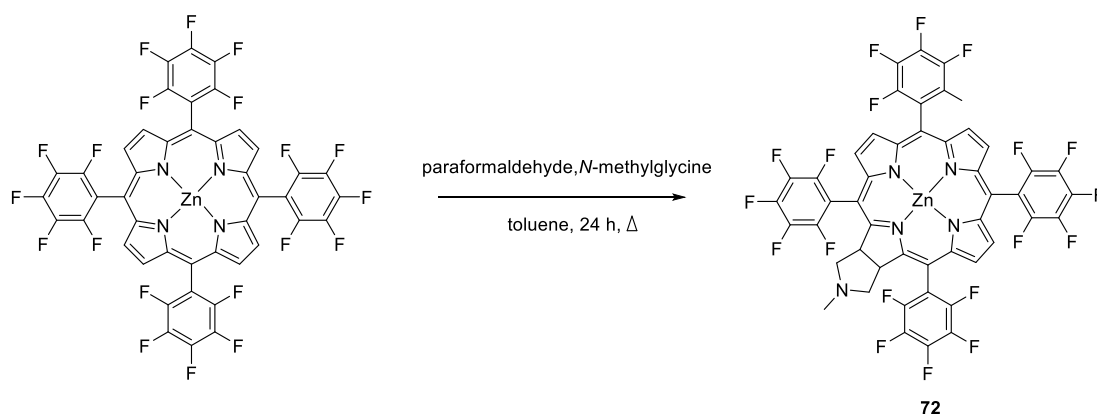


Scheme 35. Attempted synthesis of bacteriochlorin **71** through 1,3-cycloaddition reaction with azomethine ylides.

The slow reaction indicated a kinetic factor was involved and hence an attempt to increase the rate of reaction was investigated with the use of microwave irradiation. However, the reaction did not proceed and no evidence was shown for the formation of

the corresponding chlorin, isobacteriochlorin or bacteriochlorin. This was suspected to be due to the use of a pressurised microwave system, at which the reaction was heated at a higher temperature and as paraformaldehyde is very reactive, it could potentially have vaporised from the reaction with the lack of an appropriate coolant system.

Another attempt to improve the rate of reaction was carried out by metal coordination, by repeating the reaction with the zinc complex of 5,10,15,20-tetrakis(perfluorophenyl) porphyrin. Initially, 2 equivalents of *N*-methylglycine and 5 equivalents of paraformaldehyde were heated under reflux for 5 hours under an inert atmosphere, this was then monitored by TLC every hour and further portions of *N*-methylglycine and paraformaldehyde (10× excess) were added and the reaction was refluxed overnight. The resulting mixture showed primarily chlorin and with a negligible amount of bacteriochlorin being observed, the chlorin **72** was isolated and purified by column chromatography, with a yield of 23% (**Scheme 36 and Figure 94**).



Scheme 36. Synthesis of corresponding zinc chlorin **72** through 1,3-cycloaddition reaction with azomethine ylides.

been reduced. Secondly, the Zn(II) complex could induced coordination of the azomethine ylides which would effectively reduce the concentration available for cycloaddition. (**Figure 95**)

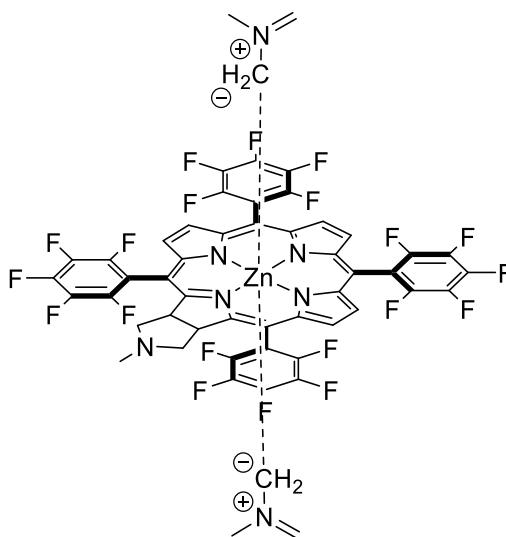


Figure 95. Possible Zn coordination forming a strong octahedral complex with azomethine ylide.

Despite the fact that this reaction could produce an oxidatively stable bacteriochlorin, the overall reaction rates were very slow and the formation of a mixture of porphyrin, chlorin, isobacteriochlorins and bacteriochlorin, as well as corresponding distereoisomers, would require complex separation procedures. The variation in different functionalities of the bacteriochlorins was also limited as azomethine ylide is a type I nucleophilic dipole. Therefore, the porphyrin acted as the dipolarophile and the reaction would only be accelerated for electron deficient porphyrins such as 5,10,15,20-tetrakis(perfluorophenyl)porphyrin, thus significantly reducing the variety of porphyrins that could undergo this reaction (**Figure 96**).

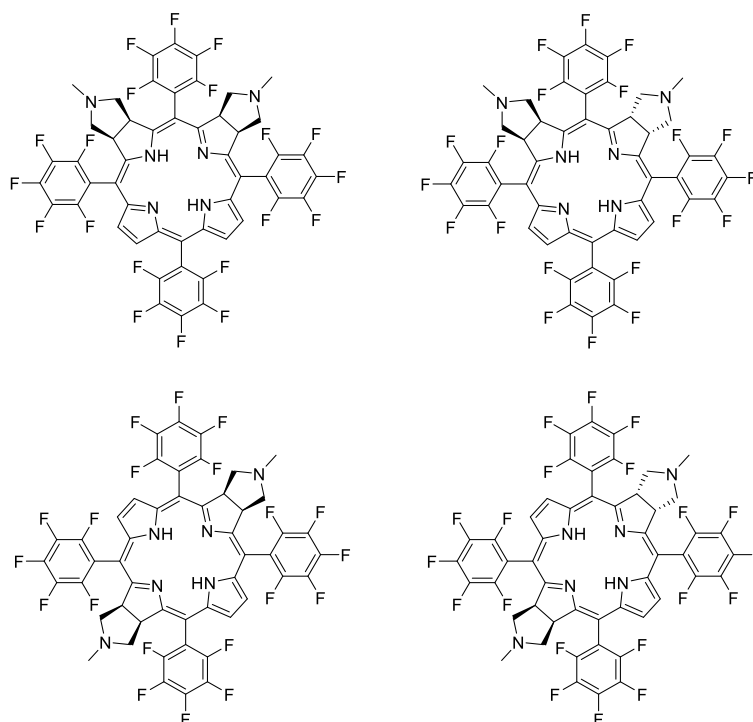


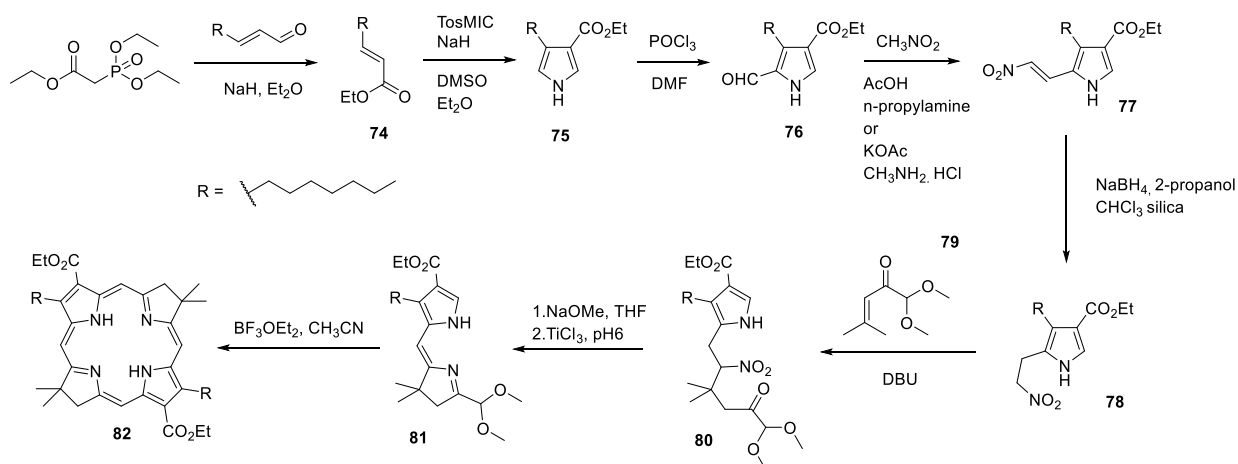
Figure 96. All known bis-adducts of isobacteriochlorins and bacteriochlorins generated through 1,3-dipole cycloaddition.

4.3.3 Synthesis of lipophilic bacteriochlorin via Lindsey's Method

After several unsuccessful attempts to synthesise bacteriochlorins from porphyrins, Lindsey's method of *de novo* synthesis was finally employed starting from pyrrolic precursors as building blocks. The first precursor was produced by reacting triethyl phosphonoacetate with octanal in a Horner-Wittig reaction to form the, α , β -unsaturated ester **74** with a yield of 98%. This was then followed by the Lindsey's *de novo* method to synthesise bacteriochlorin precursors.²⁹⁸ Through a van Leusen reaction, the α , β -unsaturated ester **74** was reacted with *p*-toluenesulfonyl methylisocyanide (TosMIC) to form the corresponding pyrrole derivative **75** with a 52 % yield. This was followed by Vilsmeier-Haack formylation, yielding a mixture of regioisomers, as substitution occurred at the 2- and/or 5-position of the pyrrole derivative. A series of purifications via column chromatography were carried out and the major regioisomer was eventually isolated to afford pyrrole-2-carboxaldehyde **76** in a yield of 54%. After extensive purification, the yield was still very similar to the literature. Henry condensation was then performed with nitromethane to afford 2-(2-nitrovinyl) pyrrole **77**. This was not isolated and was subsequently reduced with NaBH₄ to produce β -substituted

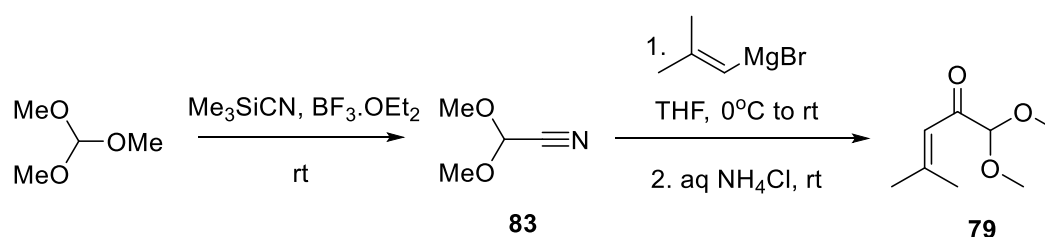
nitroethylpyrrole **78** with a 39 % yield. Compound **78** was reacted with α, β -unsaturated ketone-acetal **79** and DBU in a Michael reaction to form nitrohexanone-pyrrole **80** with a yield of 38%. However, some deviations from the literature NMR values were observed. From the chiral centre present on nitrohexanone-pyrrole **80** it was speculated this was due to possible formation of enantiomers from the Michael addition. A McMurry reaction was then performed to reductively cyclise **80** using titanium (III) chloride under argon. This was carried out using a cannula transfer technique to produce the dihydrodipyrin-acetal **81**. However, the compound was air sensitive and degradation of the compound was observed during column chromatography. This caused a significant reduction in the yield after the first purification and, due to the difficulty in separation, the compound was taken on to the next reaction without further purification before being characterised by using ^1H , ^{13}C -NMRs and MS. Bacteriochlorin **82** was then synthesised from a catalytic self-condensation using $\text{BF}_3\cdot\text{OEt}_2$ at room temperature. Purification of the bacteriochlorin by column chromatography was relatively simple as only one product was observed. The schematic of this *de novo* reaction can be followed in **Scheme 38**. Despite the successful synthesis of a lipophilic bacteriochlorin, the yield remains lower than the literature value, with the final yield being 2%. This was mainly due to the number of steps required and the difficulty in the handling and purification of air-sensitive compounds.

All steps for the synthesis of the lipophilic bacteriochlorin were confirmed using ^1H , ^{13}C -NMRs and MS.



Scheme 38. Synthesis of lipophilic bacteriochlorin **82**.

The α , β -unsaturated ketone-acetal **79**, required for conversion of compound **78** to **80** (Scheme 38) was synthesised *via* the nitrile method, a catalysed reaction of trimethyl orthoformate and TMS cyanide was performed with $\text{BF}_3 \cdot \text{Et}_2\text{O}$ affording 2,2-dimethoxyacetonitrile **83** and was purified by distillation at 150°C obtaining the product in a 46% yield. The reaction of **83** and 1.2 molar equivalents of 2-methyl-1-propenylmagnesium bromide solution (0.5 M in THF) and subsequent hydrolysis with aqueous NH_4Cl was then carried out to yield product **79** as the major product. (Scheme 39)



Scheme 39. Reaction of 2,2-dimethoxyacetonitrile with the Grignard reagent to form 1,1-dimethoxy-4-methylpent-3-en-2-one.

However, the α , β -unsaturated ketone-acetal **79** was obtained in poor yield (6%) after purification by column chromatography with silica. Hence, this was then used without further purification as the acceptor for the Michael reaction with the 2-(2-nitroethyl)-pyrrole **78**.

This method was employed due to many disadvantages associated with the alternative method using diphenyl diselenide and ammonium peroxydisulfate. These include demanding purification, cost and toxicity of diphenyl diselenide.³⁰¹

UV-vis and fluorescence spectra of lipophilic bacteriochlorin **82**

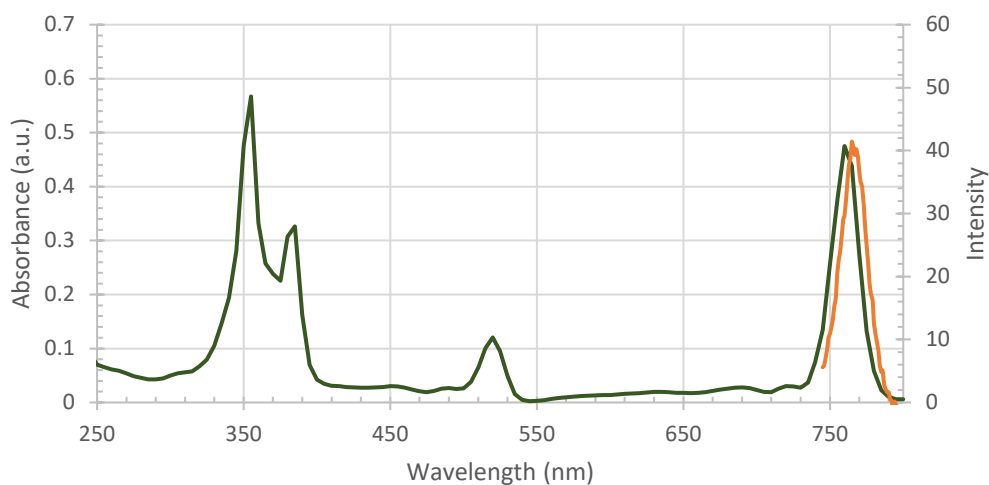


Figure 97. UV-visible (green) and fluorescence (orange) spectra of **82**.

UV-visible and fluorescence analysis of the product was carried out, confirming the distinctive characteristics of the bacteriochlorin with the absorption covering a wide range of the spectrum. B_y , B_x bands were observed at λ_{abs} 355 nm, 384 nm and the Q_x band was observed at λ_{abs} 519 nm. The Q_y absorption in the NIR was observed at λ_{abs} 759 nm. The NIR fluorescence was also observed with an emission of λ_{em} 767 nm (**Figure 97**).

Although there were some difficulties with synthesis of the precursors, they were eventually overcome, and all were synthesised successfully. Despite this synthetic method requiring multi-step reactions of the building blocks, it offers many advantages over other methods, such as the self-condensation requiring only one dipyrrolic intermediate without the need for further redox reactions. Also, enabling further post-synthetic functionalisation through the β and *meso* pyrroles to provide a highly tuneable and truly regio- and stereo-chemically pure bacteriochlorin. Spectral analysis alludes to the potential of the bacteriochlorin as an NIR fluorescence probe, with the eventual aim of synthesising a bacteriochlorin with NIR properties that can be conjugated with a targeting system.

Bacteriochlorins have shown themselves to be interesting as potential NIR fluorescent probes. However, the overall application of conjugatable and water soluble

bacteriochlorins is limited due to the complex synthetic strategies and multi-step reactions required to access them. In addition, scaling-up these reactions to a reasonable level remains problematic as bacteriochlorins can often be compromised by at least one of these issues: inherently low yields, troublesome purification, limited stability and cost. Therefore, this investigation suggested that bacteriochlorins may not be the optimal compounds as NIR fluorescence agents in comparison to the BODIPY and aza-BODIPY also synthesised in this investigation.

After assessing both the synthetic and photophysical results of the three class of NIR fluorophores, it was concluded that aza-BODIPYs provide the most desired properties as a scalable, conjugatable and biocompatible NIR fluorescence probe.

5. Bioconjugation to targeted moieties

Specificity of fluorescence detection is an important aspect for imaging cancerous tissue, and this can often be achieved through conjugation of a fluorophore to a biological targeting moieties⁸⁹ such as antibodies, peptides and proteins. A range of different ligation strategies has been developed to modify endogenous amino acid residues, based on their robustness and ability to undergo chemical modifications. Therefore, bioconjugation to amino acid residues has been commonly carried out in the design of complex antibody drug conjugates. Many studies have shown the modification of amino acid residues for bioconjugation and the application of the resulting conjugates as diagnostic units for MRI, PET and fluorescence imaging.¹⁹³ Among many different bioconjugation methodologies, bioorthogonal modification has become increasingly popular and the most commonly modified amino acid residues are lysine, cysteine and tyrosine residues¹⁶⁴ (**Table 6**). These residues have been extensively investigated in this chapter for aza-BODIPY bioconjugation with peptides, antibodies and proteins respectively.

Table 6. Overview of functionalities investigated for aza-BODIPY conjugation to biological molecules.

Functionality	Targets	Linkage type
Activated Ester	Amine (Lysine residue)	Amide
Pyridazinedione	Sulphydryl group (Cysteine residue)	Mercaptopyridazinedione
Diazonium agent	Phenol (Tyrosine residue)	Azo linkage
Alkyne	Azide (CuAAC/SPAAC)	1,2,3-triazole
Azide	Alkyne (CuAAC/SPAAC)	1,2,3-triazole

5.1 Bioconjugation to tyrosine residues on peptides and proteins

In labelling techniques currently used for fluorescent molecules the most commonly modified sites are lysine residues, due to both their high abundance on proteins, and the ease of synthesis of the corresponding reactive fluorescent probes.¹⁶⁴ Fluorescein isothiocyanate (FITC) is a popular fluorescent dye for protein labelling at lysine

residues, but despite the high fluorophore/protein (F/P) ratios achieved, the resulting fluorescence remains relatively low due to fluorescence quenching, resulting in unreliable measurements.³⁰⁸

As an alternative to lysine residues, tyrosine residues allow control and selectivity of labelling of proteins and peptides due to its lower abundance. Tyrosine conjugations using diazonium salts have recently been reported by Francis *et al.*¹⁶⁶ and Barbas *et al.*¹⁶⁷ through the development of a stabilised diazonium salt to perform selective and efficient bioconjugation. These bioconjugations were carried out through selective electrophilic aromatic substitution to the *ortho* position adjacent to the hydroxyl group of the phenol ring, and the same studies have reported the potential for modification at tyrosine residues to introduce functional groups such as aldehydes, ketones,¹⁶⁷ and more recently alkynes³⁰⁹ at the position *para* to the azo linkage. These developments allow further bioorthogonal reactions for the synthesis of diagnostic agents, including fluorescent probes.

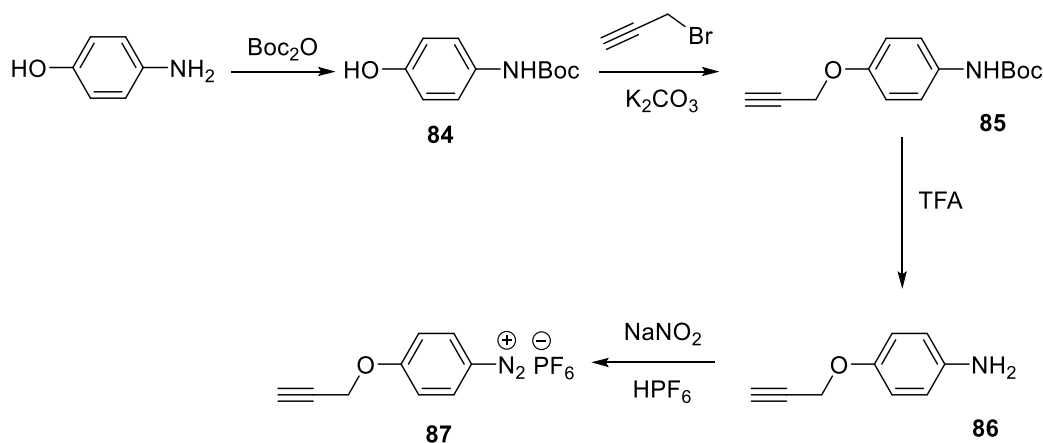
Recognising the challenges summarised above we set out to develop a versatile system for labelling peptides and proteins with a set of multiwavelength BODIPY fluorophores.

5.1.1 Synthesis of alkyne functionalised diazonium linker

The facile and flexible nature of bioorthogonal reactions, especially CuAAC, has been shown to be particularly applicable to bioconjugation, providing mild reaction conditions.¹⁷⁵ For this reason, a simple synthetic route to produce an alkyne-functionalised diazonium salt, utilising low-cost and readily available reagents, was investigated.

The method began with a Boc protection reaction at the primary amine of 4-aminophenol using di-*tert*-butyl dicarbonate to produce *tert*-butyl (4-hydroxyphenyl)carbamate **84** with a high yield of 98%. This was followed by a Williamson ether synthesis with propargyl bromine catalysed by K₂CO₃ to afford *tert*-butyl (4-(prop-2-yn-1-yloxy)phenyl)carbamate **85** in 89% yield. Boc deprotection with TFA was then carried out initially for 3 hours, but TLC analysis showed unreacted starting material. Therefore, the resulting solution was stirred overnight to obtain **86** in near quantitative yield. Diazotisation of the free amine was carried out with sodium

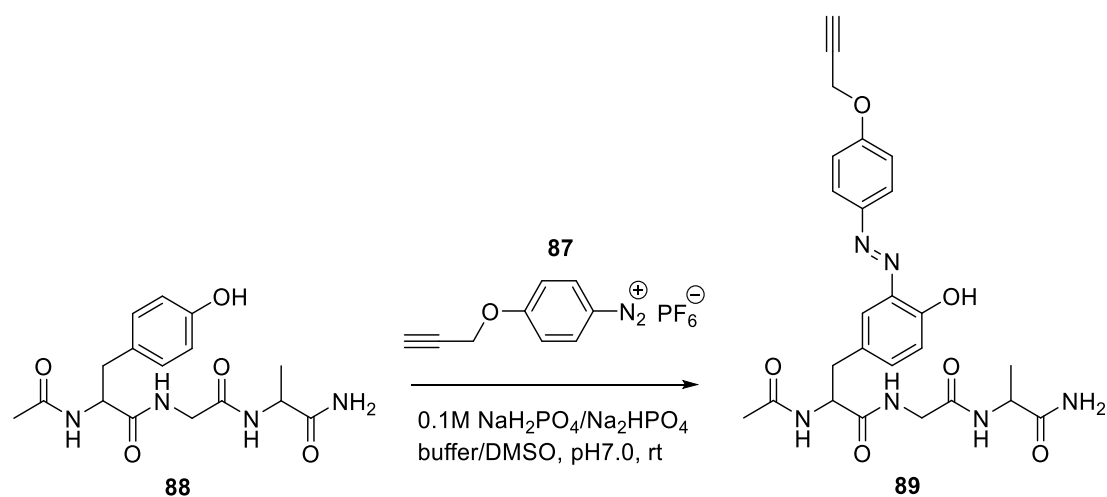
nitrite in TFA at -10°C for 1.5 hours. The diazonium product was stabilised as the hexafluorophosphate salt by adding HPF_6 , which offers shelf stability and improved storage in comparison to the tetrafluoroborate analogue.¹⁶⁷ Finally simple filtration gave the 4-(prop-2-yn-1-yloxy)benzenediazonium hexafluorophosphate salt **87** in 31% yield (**Scheme 40**).



Scheme 40. Synthesis of diazonium alkyne linker.

5.1.2 Tyrosine selective modification followed by CuAAC reaction with model peptide

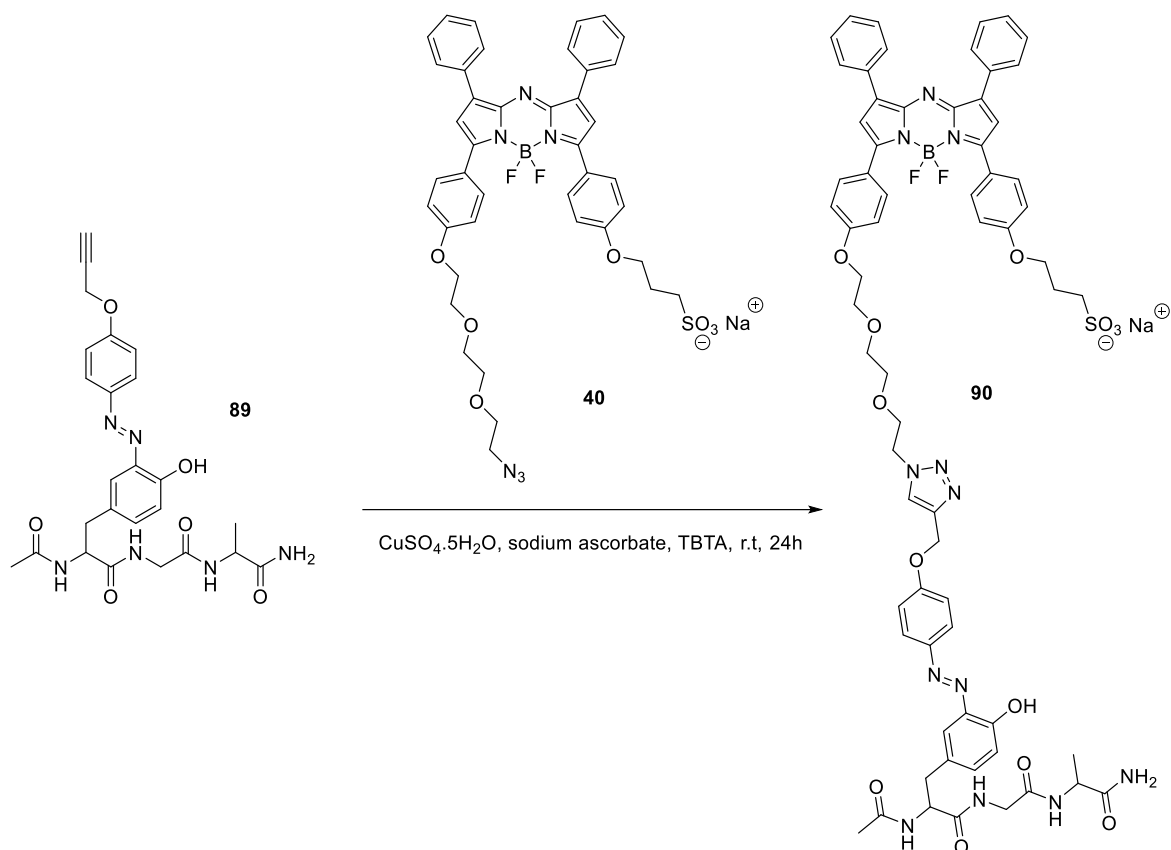
To examine the viability of tyrosine bioconjugation, the prepared 4-(prop-2-yn-1-yloxy) benzenediazonium hexafluorophosphate(V) **87** was conjugated with a simple three-unit peptide. Tyr-Gly-Ala (YGA) **88** synthesised by Dr. Michael Reithofer and contained only one active tyrosine residue for bioconjugation. The bioconjugation was carried out modifying a previously reported azo-coupling method.¹⁶⁷ A stoichiometric quantity of 1.1 equivalent of **87** was reacted with the YGA peptide **88** in a 2:1 ratio of 0.1M $\text{NaH}_2\text{PO}_4/\text{Na}_2\text{HPO}_4$ buffer: DMSO solution for 45 minutes at room temperature. The azo bond generated resulted in a yellow solid, which was purified by water and ethyl acetate washing to afford an alkyne functionalised peptide **89** in 51% yield. This was then characterised by ^1H , ^{13}C -NMR, MS and UV-visible spectroscopy. The UV-visible spectrum showed a peak at 360 nm suggesting the success in conjugating to the tyrosine residue *via* an azo linkage. (**Scheme 41**)



Scheme 41. Peptide modification on the tyrosine residue.

Encouraged by the success of tyrosine conjugation with **87**, the alkyne modified peptide was subsequently reacted with anionic azido aza-BODIPY **40**. The alkyne modified peptide was treated with 1.1 equivalent of aza-BODIPY and catalytic reagents including, $\text{CuSO}_4 \cdot 5\text{H}_2\text{O}$, sodium ascorbate and TBTA were added, the reaction was then stirred for 24 hours at room temperature. Initially, an aliquot of the crude was purified using a sephadex G-10 size exclusion column, with an exclusion limit of 700 Da, since the desired conjugate has a molecular mass of 1316 Da.

However, upon HPLC analysis, a mixture of aza-BODIPY and the conjugate was detected at 7.98 minutes and 6.52 minutes, with the mixture composed of 55% aza-BODIPY and 45% conjugate respectively. Therefore, the counterion exchange method previously developed was used to generate a peptide aza-BODIPY conjugate **90** in 23% yield (**Scheme 42**).



Scheme 42. CuAAC of anionic azido aza-BODIPY and tyrosine modified peptide.

The success of the CuAAC click reaction was confirmed by HPLC with a single retention time of 6.68 minutes. Further characterisation of this conjugate was also obtained through MS to give 1315 m/z for the $[\text{M}]^-$ ion.

The resulting conjugate **90** was analysed by UV-visible spectroscopy. **Figure 98** shows a comparison between spectra of **89** and **90**. The azo bond from **89** was observed with a wavelength at 360 nm. After CuAAC conjugation and purification, peaks at 360 nm and 680 nm were observed for **90** indicating the azo bond and the coupled aza-BODIPY respectively.

UV-vis spectra of tyrosine modified peptide and aza-BODIPY conjugate

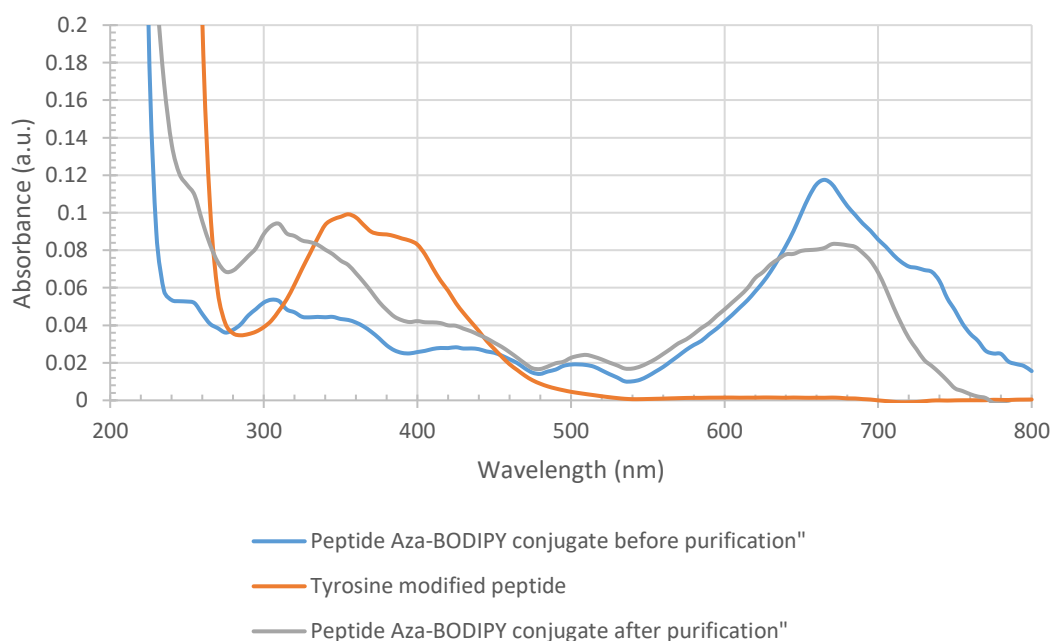


Figure 98. UV-visible spectrum showing the tyrosine modified peptide (orange) in DMSO, peptide aza-BODIPY conjugate before purification (blue) and after purification (grey) in methanol.

In order to determine the number of modified tyrosine residues, the Beer-Lambert Law was used to calculate the stoichiometric molar ratio between the two representative absorption bands and the equations were used as followed:

Equation 1. Beer-Lambert law, A = absorption, ϵ = molar absorption coefficient, c = concentration, l = length of pathway.

$$A = \epsilon cl$$

Equation 2. Rearrangement of the Beer-Lambert law to calculate the concentration.

$$c = \frac{A}{\epsilon l}$$

It was observed from the stoichiometric ratio calculation that before purification by counter ion exchange a two-time excess of dye was present. This was also confirmed by HPLC as represented by two peaks at 6.52 and 7.98 min, as well as MS ion fragments of 830 m/z in concurrence with 1315 m/z. Upon purification, a stoichiometric ratio of

1:1 of aza-BODIPY and peptide for the conjugate was observed with both HPLC and MS indicated the absence of starting material (**Table 7**).

Table 7. UV-visible spectroscopic stoichiometric calculation before and after purification of peptide aza-BODIPY conjugate **90**.

Before purification			
Peptide azo bond 360 nm		Aza BODIPY 660 nm	
Abs	0.042	Abs	0.115
Conc (mol dm^{-3})	3.10E-07	Conc (mol dm^{-3})	5.64E-07
Moles (mol)	3.10E-11	Moles (mol)	5.64E-11
Stoichiometric ratio	1	Stoichiometric ratio	2
ϵ (L mol $^{-1}$ cm $^{-1}$)	134011	ϵ (L mol $^{-1}$ cm $^{-1}$)	204173

After purification			
Peptide azo bond 360 nm		Aza BODIPY 680 nm	
Abs	0.068	Abs	0.080
Conc (mol dm^{-3})	5.06E-07	Conc (mol dm^{-3})	3.94E-07
Moles (mol)	5.06E-11	Moles (mol)	3.94E-11
Stoichiometric ratio	1	Stoichiometric ratio	1
ϵ (L mol $^{-1}$ cm $^{-1}$)	134011	ϵ (L mol $^{-1}$ cm $^{-1}$)	204173

5.1.3 Photophysical studies of multiwavelength BODIPYs and aza-BODIPY

Photostability is a major concern in fluorescence imaging, as small molecule fluorophores often experience irreversible photobleaching upon continuous illumination with light, therefore limiting their use.³¹⁰ The photostability of the aza-BODIPY **40** was investigated along with two NIR fluorescent dyes, ICG and MB. The photostability experiment was carried out in PBS solution p.H 7.4, with the dyes illuminated continuously with a strong red/NIR light source (685-733 nm) for 60 minutes. As shown in **Figure 99**, after 60 minutes, a slight decrease of 11 % absorption for aza-BODIPY **40** was observed. In contrast, a decrease of 38 % and 90% for MB and ICG respectively, was observed under the same conditions. This demonstrates the excellent photostability of aza-BODIPY **40** in comparison to two commercial fluorophores and highlights its potential use as an NIR emitter for fluorescence imaging.

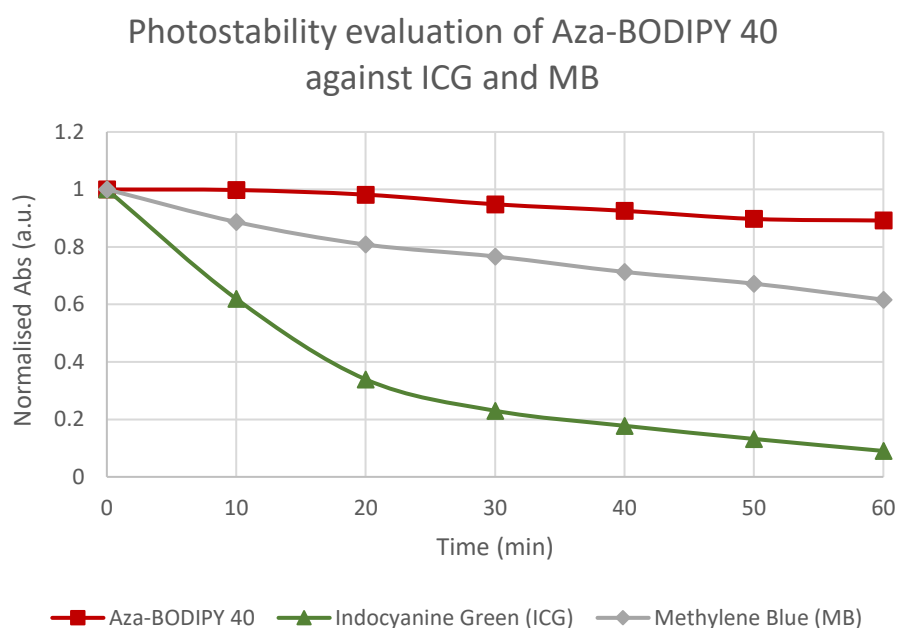


Figure 99. Normalised absorbance changes of 10 μ M PBS p.H 7.4 solution of aza-BODIPY **40**, ICG and methylene blue under continuous irradiation with NIR light band pass filter 685-733 nm for 60 minutes.

As an important optical property for imaging, fluorescence quantum yields of the azido BODIPYs **8**, **25**, **40** were also recorded. The results showed good agreement to similar structures previously reported^{219,253} and excellent fluorescence quantum yield for BODIPY **8** and BODIPY **25**. Despite the slightly lower fluorescence quantum yield of

$\Phi_f = 0.22$ for aza-BODIPY **40**, the result was still within the range required for imaging at red/NIR regions (**Table 8**).

Table 8. Fluorescence quantum yields of BODIPYs in methanol. Quantum yields were determined using two standards: fluorescein ($\Phi_f = 0.96$ in 0.1 M NaOH)³¹¹ and rhodamine B ($\Phi_f = 0.31$ in water).³¹²

Compound	Solvent	$\lambda_{ex}(nm)$	$\lambda_{ems}(nm)$	ϕ_f
8	MeOH	470	510	0.49
25	MeOH	570	635	0.57
40	MeOH	640	711	0.22

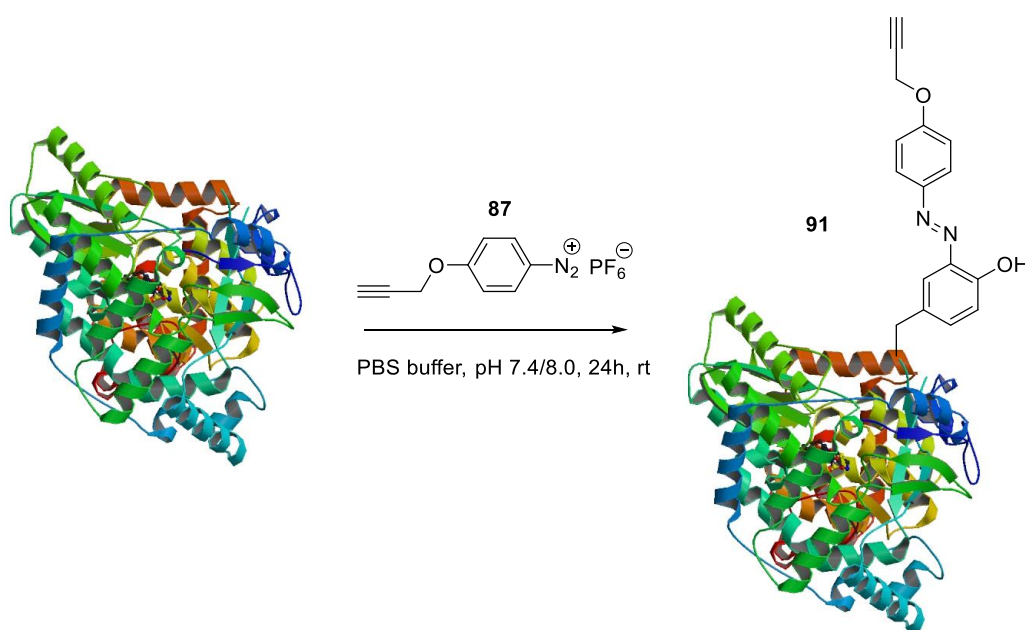
5.1.4 Tyrosine selective modification followed by CuAAC reaction on BSA

To demonstrate the potential of click bioconjugation between an alkyne modified protein and the azido BODIPYs, *bovine serum albumin* (BSA) was selected as a readily available model of a globular protein. BSA has often been used to selectively bind to receptors of particular cell lines, subsequently leading to receptor mediated endocytosis and cellular internalization, and as a result, offers potential as a targeting moiety for fluorescence imaging *in vitro*.^{110,313} The protein has a total of 21 tyrosine residues and these has been highlighted in **Figure 100**.³¹⁴

MKWVTFISLLLLFSSA**Y**SRGVFRRDTHKSEIAHRFKDLGEEHFKGLVLIAFSQ**Y**
 LQQCPFDEHVKLVNELTEFAKTCVADESHAGCEKSLHTLFGDELCKVASLRET
YGDMADCCEKQEPERNECFLSHKDDSPDLPKLPDPNTLCDEFKADEKKFW
 GK**Y**LYE**I**ARRHP**Y**F**Y**AP**ELLY**YANK**Y**NGVFQECCQAEDKGACLLPKIETMRE
 KVLASSARQRLRCASIQKFGERALKAWSVARLSQKFPKAEFVEVTKLVTDLTK
 VHKECCHGDLLECADDRADLAK**Y**ICDNQDTISSKLKECCDKPLLEKSHCIAE
 VEKDAIPENLPPLTADFAEDKDVCK**Y**QEAKDAFLGSFL**Y**E**Y**SRRHPE**Y**AVSV
 LLRLAKE**Y**EATLEECCA**KDD**PHAC**Y**STVFDK**LKHL**VDEPQNLIKQNC**DQ**FEK
 LGE**Y**GFQNALIV**Y**TRKVPQVSTPTLVEVSRSLGKVGTRCCTKPESERMPCTE
 D**Y**LSLILNRLC**VL**HEKTPVSEK**VTK**CCTESLVNRRPCFSALTPDET**Y**VPKAFDE
 KLFTFHADICTLPDTEKQIKKQTALVELLKHKPKATEEQLK**TV**MENFVAFV**DK**
 CCAADDKEACFAVEGPKLVVSTQTALA

Figure 100. Highlighted tyrosine residues in the amino acid sequence for BSA protein.³¹⁴

Tyrosine modification was first attempted in the reaction between BSA and an appropriate diazonium salt in PBS buffer pH 7.0. The mixture was co-incubated overnight at room temperature and then purified using a cut off filter (30kDa). The product was then characterised by UV-visible spectroscopy. The reaction rate was suggested to be very slow and the formation of an azo linkage was not observed from analysis of the UV-visible spectrum. Therefore, the pH of PBS buffer solution was adjusted to pH 8.0 by addition of NaOH solution. (**Scheme 43**)



Scheme 43. Tyrosine modification of BSA with an alkyne diazonium linker.

The UV-visible spectrum suggested successful conjugation at higher pH. It was postulated that this was due to deprotonation of the tyrosyl moiety allowing more exposure of the tyrosine residues on the protein surface and thereby increasing availability. Furthermore, the deprotonated oxygen anion would increase the reactivity towards electrophilic aromatic substitution at the adjacent *ortho*-position by stabilising the cationic intermediate (**Figure 101**).

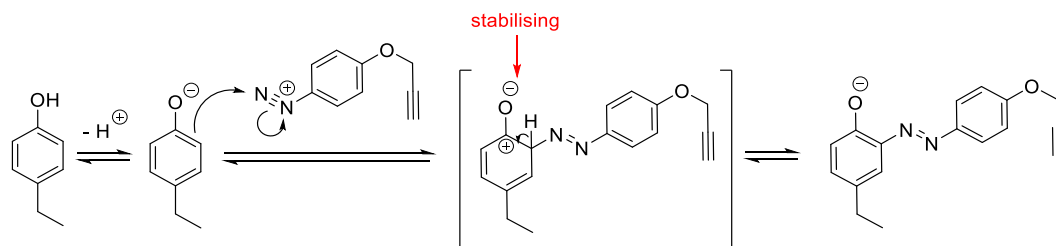


Figure 101. Proposed electrophilic aromatic substitution of tyrosyl moiety with diazonium linker.

Tyrosine modification using the diazonium linker **87** was therefore carried out in PBS solution (pH 8.0) at room temperature.^{14,166,172} The resulting compound was purified using a MW 30 kDa cut off filter and characterised by UV-visible analysis, to show a linker-loading ratio of *ca.* 1.7:1. (**Figure 102**)

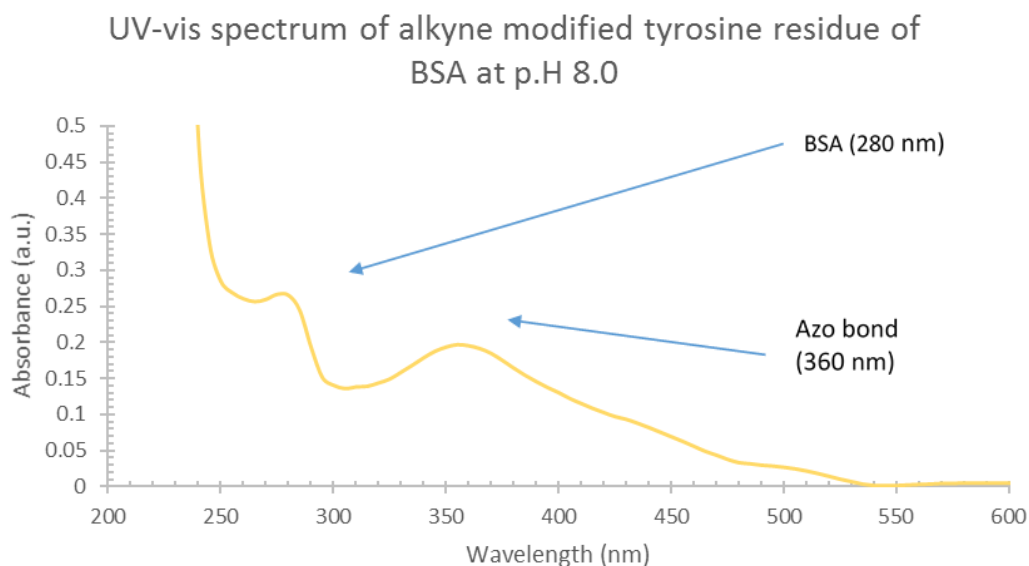
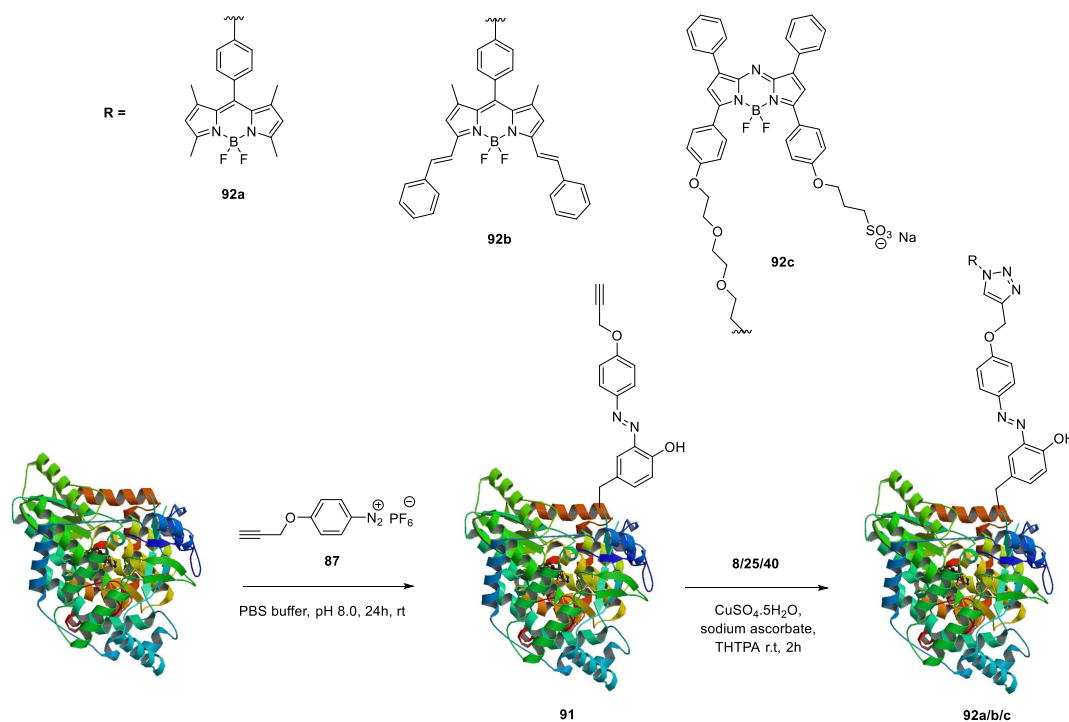


Figure 102. UV-visible spectrum of conjugate **91** after purification in PBS pH 7.4 solution, showing BSA (280 nm) and the azo linkage (360 nm).

Alkyne functionalised BSA **91** was then conjugated to BODIPYs **8**, **25** and aza-BODIPY **40** via CuAAC chemistry. Incubation of conjugate **91** with 20 equivalents of the BODIPY, and a premixed solution of $\text{CuSO}_4 \cdot 5\text{H}_2\text{O}$, THPTA and sodium ascorbate for 2 hours at room temperature, effected complete conversion to conjugates **92a-c** in relatively high yield and purity (**Scheme 44**).



Scheme 44. Tyrosine modification with alkyne diazonium linker followed by CuAAC with varying wavelength BODIPYs.



Figure 103. Optical colour difference for diazonium linker tyrosine modified BSA conjugate **91** and three BODIPY-BSA conjugates **92a/b/c**.

In order to determine the fluorophore/protein (F/P) ratio, the Beer-Lambert Law was used to calculate the stoichiometric molar ratio between the two representative absorption bands (one for the protein and one for the fluorophore) and the following equation¹⁹¹ was used:

$$r = \frac{A_{\lambda} / \epsilon_{\lambda}}{(A_{280} - \sum CF_{\lambda} \times A_{\lambda}) / \epsilon_{280}}$$

Calculation of fluorophore to protein ratios, r , follow the formula above with $\epsilon_{280} = 43824 \text{ M}^{-1} \text{ cm}^{-1}$ for BSA³¹⁵, ϵ for each modification (360, 509, 626, 740 nm) were used from **Table 9**. CF_{λ} is the correction factor for each modification with diazonium linker or BODIPYs dye and was calculated respectively for the protein absorbance at 280 nm. With A_{λ} the absorbance at the wavelength λ , and ϵ_{λ} for the extinction coefficient of the relevant molecule.

Table 9. Stoichiometric calculation of molecule to protein ratio.

	Diazonium modification		BODIPY		Red BODIPY		Aza-BODIPY	
Wavelength (nm)	280	360	280	509	280	626	280	740
Absorbance (a.u.)	0.624	0.448	0.783	0.939	0.533	0.448	0.355	1.42
ϵ ($\text{Lmol}^{-1}\text{cm}^{-1}$)	43824	27619	43824	58346	43824	61492	43824	204193
Conc (mol dm^{-3})	7.41E-04	1.28E-03	5.51E-04	8.21E-04	2.14E-04	2.50E-04	4.78E-04	7.02E-04
Correction factor	0.36		0.33		0.671		0.104	
Stoichiometric ratio.ca. (r)	1.73		1.49		1.37		1.47	

UV-visible and fluorescence spectra were obtained with the absorption wavelengths (λ_{max} of longest wavelength absorbing band) shown to be at 510 nm (BODIPY), 590, 640 nm (Red BODIPY) and 740 nm (Aza-BODIPY) respectively. The excitation and emission wavelength ($\lambda_{\text{ex}}/\lambda_{\text{em}}$) were shown to be at 480/515 nm (BODIPY), 570/645, 710 nm (Red BODIPY) and 730/755 nm (Aza-BODIPY) respectively (**Figure 104**).

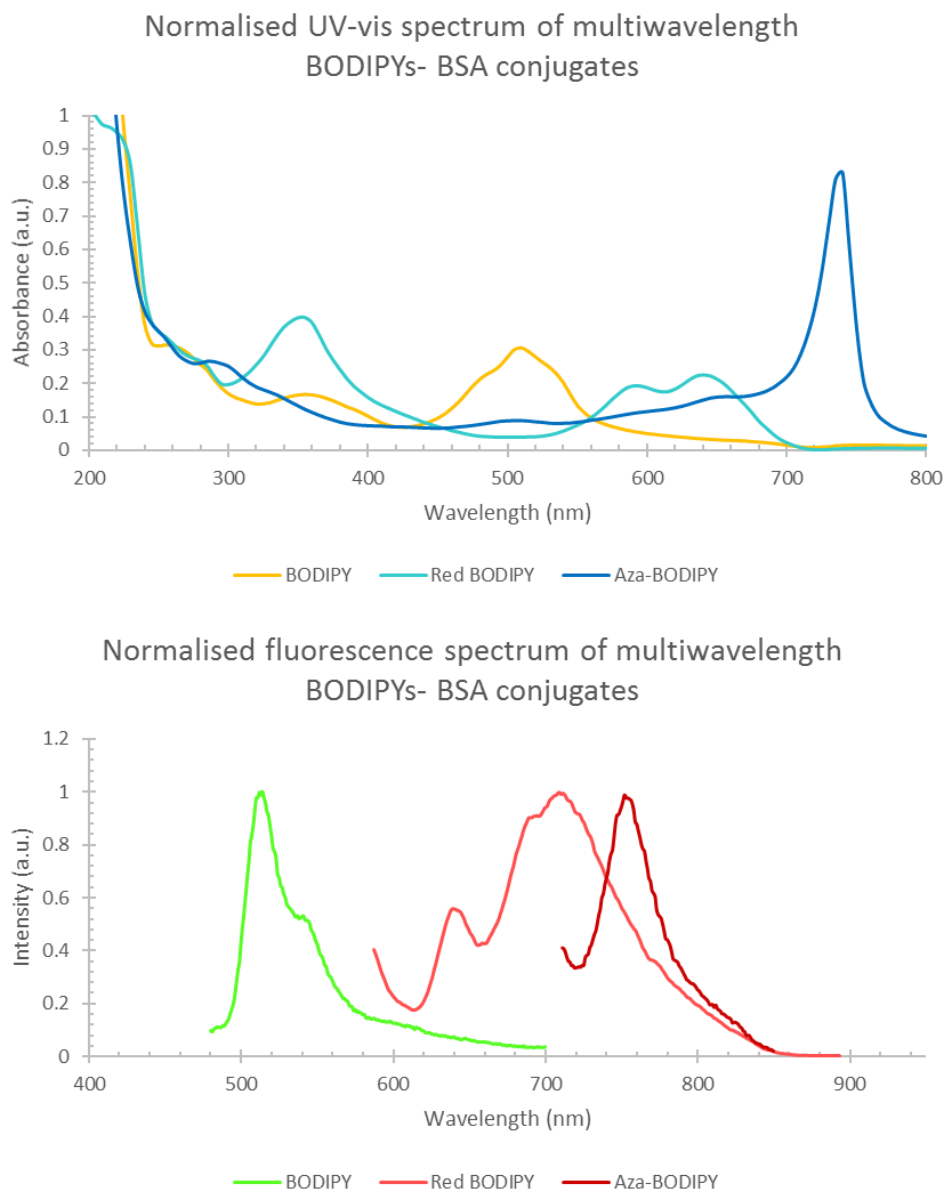
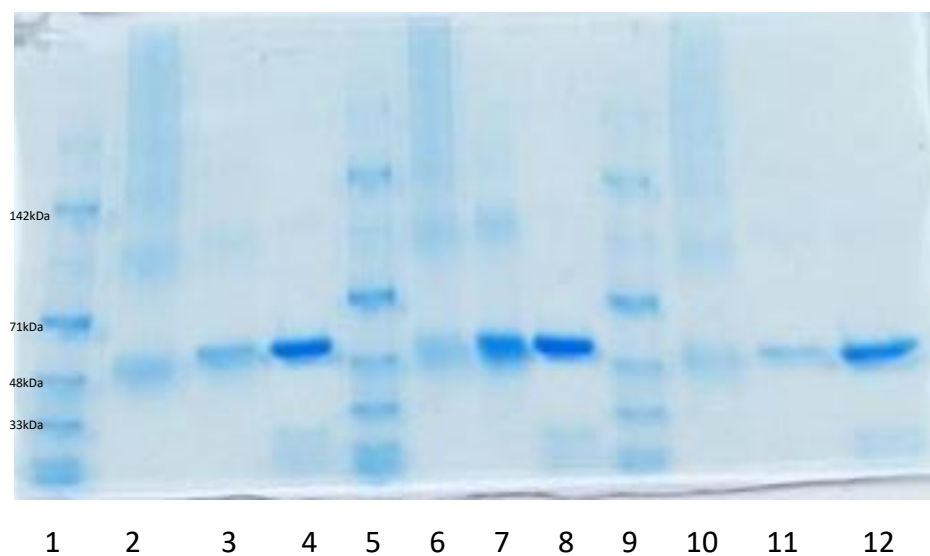


Figure 104. Normalised UV-visible and fluorescence spectra of **92a**, **92b** and **92c** in PBS solution pH 7.4.

BODIPY loadings were calculated by UV-visible spectroscopy and the stoichiometric ratios were found to be *ca.* $1.4 \pm 0.1:1$ (*F/P*) for all three BODIPYs. Purity of the conjugates was confirmed by SDS-PAGE (**Figure 105**). MS analysis was also obtained for conjugates **92a/b** showing good agreement with the UV-visible spectroscopy results (**Figure 106** and **Figure 107**). However, MALDI-TOF of conjugate **92c** could not be obtained, possibly due to the charged nature of the aza-BODIPY used to form this conjugate.



Lane 1/5/9: Protein ladder

Lane 2/6/10: Tyrosine modified with alkyne linker – 20 μ M

Lane 4/8/12: BSA - 20 μ M

Lane 3: BODIPY BSA conjugate **92a** – 20 μ M

Lane 7: Red BODIPY BSA conjugate **92b** – 20 μ M

Lane 11: NIR Aza-BODIPY BSA conjugate **92c** – 20 μ M

Figure 105. SDS-PAGE of conjugates **92a-c**.

Calibration of the BSA¹⁺ mass measurement was found by MALDI-TOF to be 66409.

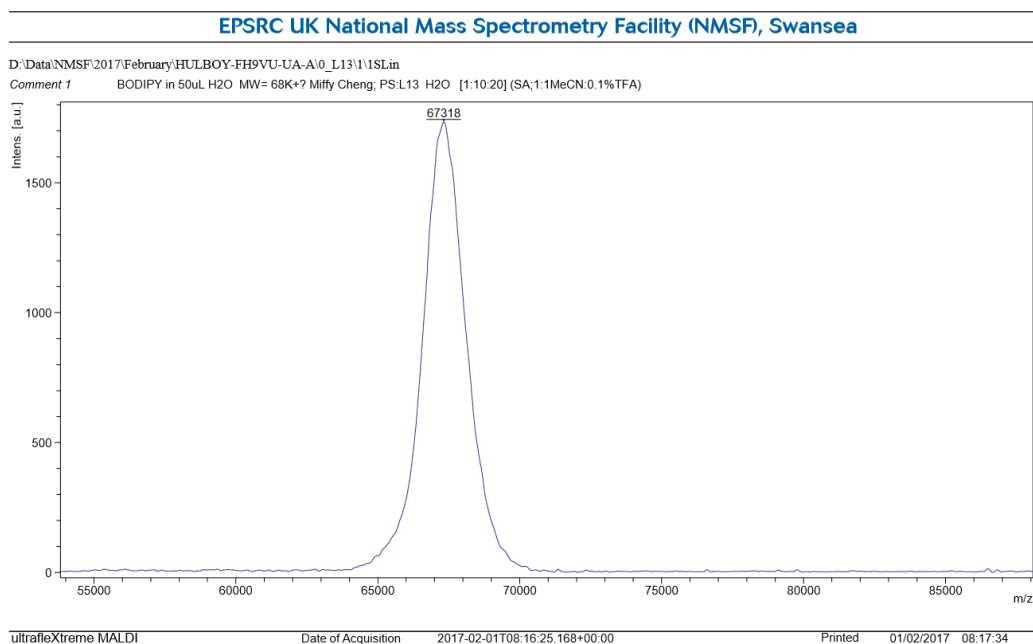


Figure 106. MALDI-TOF of conjugate **92a** - molecular weight increase 909 and *ca.* 1.73:1 (BODIPY/BSA).

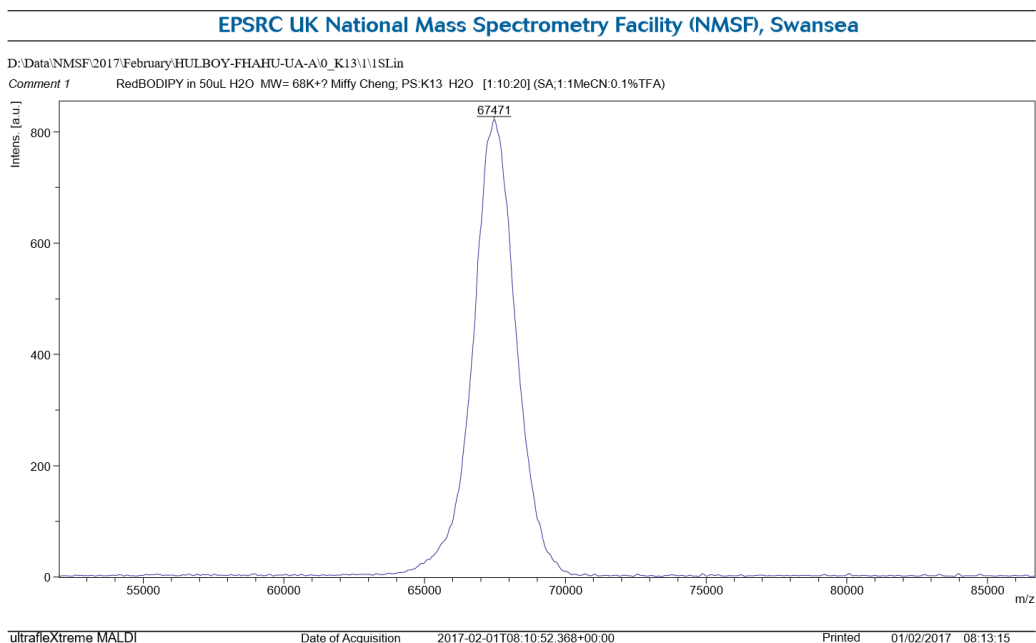


Figure 107. MALDI-TOF of conjugate **92b** - molecular weight increase 1062 and *ca.* 1.51:1 (RedBODIPY/BSA).

Overall, this approach offers a significant advantage in comparison to FITC labelling

of BSA previously reported³⁰⁸, allowing improved accuracy in quantification. It also offers an advantage over maleimide modification on BSA, with a higher loading ratio than offered by the single free thiol available for conjugation on BSA.³¹⁶

5.1.5 Cell imaging to produce fluorescence image

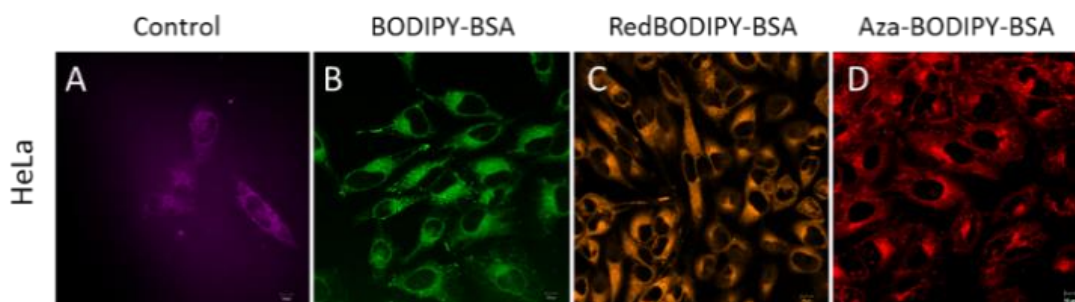


Figure 108. CLSM images of HeLa cells incubated with (A) control – BSA autofluorescence ($\lambda_{\text{ex}} = 405$ nm), (B) BODIPY-BSA **92a** conjugate ($\lambda_{\text{ex}} = 488$ nm), (C) RedBODIPY – BSA **92b** conjugate ($\lambda_{\text{ex}} = 513$ nm) and (D) Aza-BODIPY – BSA **92c** conjugate ($\lambda_{\text{ex}} = 633$ nm).

Fluorescence imaging was carried out to demonstrate the potential of the bioconjugates **92a-c** as fluorescent probes using HeLa cells. Prior to confocal laser scanning microscopy (CLSM) imaging, 5 μM of the bioconjugates **92a** and **92b** and 10 μM of **92c** were incubated with HeLa cells overnight, with unconjugated probe removed by PBS washing. **Figure 108** showed all BSA conjugates were internalized in the cells and showed fluorescence when excited at three different excitation wavelengths.

Autofluorescence is a widely-known limitation for fluorescence imaging, especially when using exogenous fluorophores, and can interfere with detection of the fluorescent signal of interest, making discrimination between different fluorescent signals challenging. To demonstrate the superiority of the BODIPYs as potential fluorophores in fluorescence imaging, a control autofluorescence study was performed. The three excitation wavelengths used (488 nm, 513 nm, 633 nm) were investigated without application of BODIPY conjugates, and these were compared to autofluorescence in HeLa cells when excited at 405 nm. In all cases, the autofluorescence observed was found to be negligible in comparison to that obtained when exciting at 405 nm.

In conclusion, we have synthesised, and developed methods for the bioconjugation of, multi-wavelength BODIPYs to generate new bioconjugates. A novel and versatile

synthesis of alkyne diazonium linker was introduced, and through conjugation with BSA a traceable azo linkage was formed, allowing confirmation of the average conjugation ratios of both the alkyne modified tyrosine and BODIPY dyes.

5.2 Lysine residue bioconjugation from CXCR4 receptor targeting peptide

Recently, peptides have become an increasingly attractive targeting species for FGS as many peptides have favourable biodistribution compared with larger molecules, resulting in higher uptake in targeted tissue as well as rapid clearance in the blood stream.⁹⁵ Peptide synthesis also utilises well established synthetic techniques, therefore structural manipulation can be easily achieved to conjugate to a variety of fluorophores or to enhance affinity and specificity toward the target.

Pentixafor is an excellent example of a peptide for targeted imaging of cancers, recently reported by Wester *et al.*^{317,318} Pentixafor is a high affinity chemokine receptor 4 (CXCR4) antagonist consisting of a small cyclic pentapeptide (FC131) labelled with gallium-68 for PET imaging. Since its discovery, Pentixafor has become of major interest in imaging and was applied in various clinical trials.³¹⁷⁻³¹⁹ There are several disadvantages to nuclear techniques however, such as lack of spatial resolution which can prevent identification of small metastatic tumours.^{25,26} Whereas, FGS is not hindered by the same restrictions in resolution. This technique is also beneficial to patients as fluorescence imaging does not require the use of ionising radiation and is readily available at a low cost.

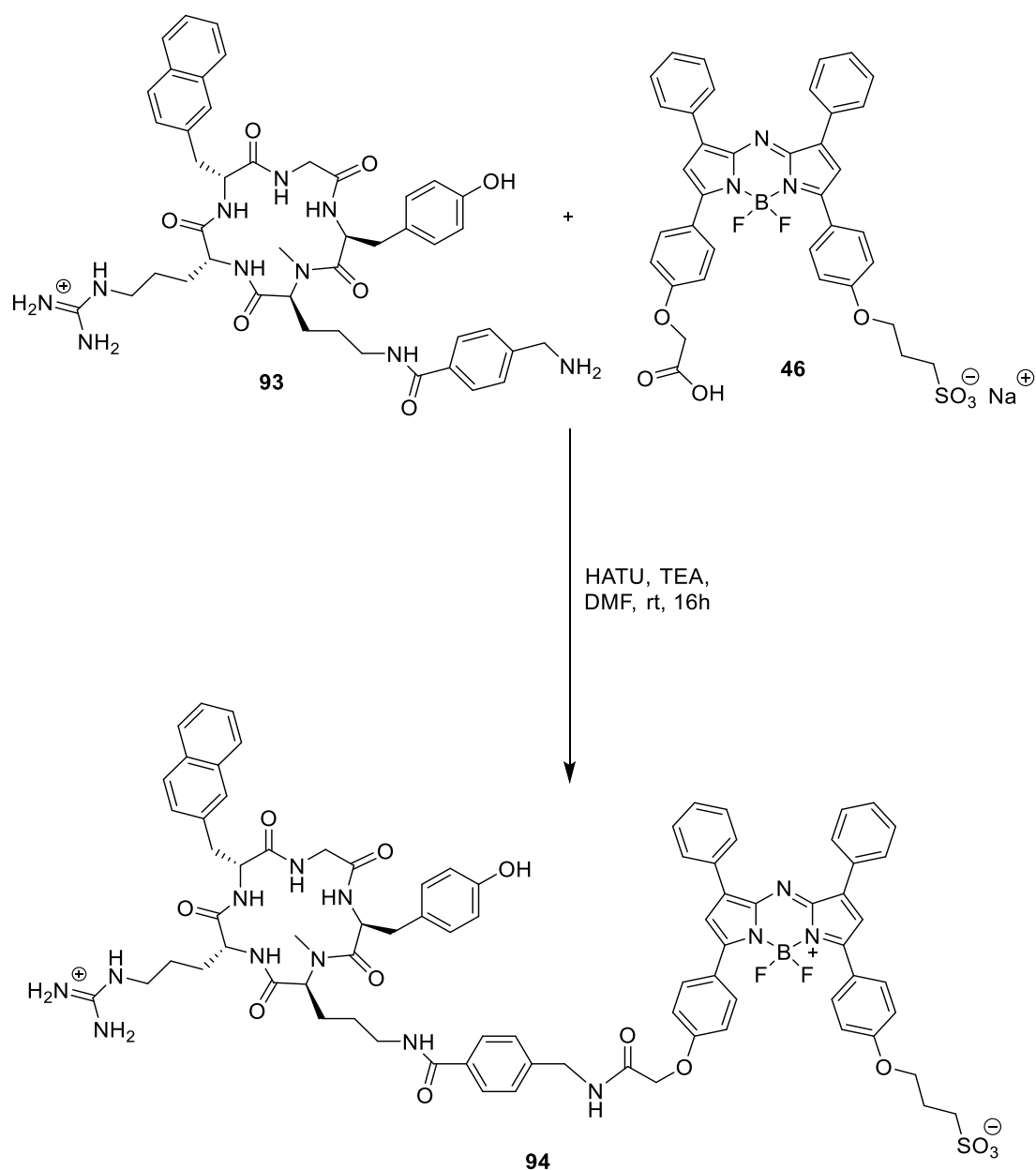
Brain tumours have been a major focus for FGS research due to the indistinct surgical margin and precision required for tissue preservation.²⁴ Since CXCR4 receptors have been shown to be overexpressed in brain cancers,³²⁰ it has become an attractive target to increase the selectivity of FGS. Furthermore, CXCR4 has been shown to play a crucial role in the metastatic process.³²¹ Identification of these metastatic tumours are extremely difficult and their removal by surgical interventions can often be the key to patient longevity.

Despite many efforts to produce a CXCR4 receptor targeting NIR fluorescence probe, drawbacks such as high non-specific uptake into cells^{322,323} and decreased binding affinity have limited their application in fluorescence imaging.³²⁴

Herein, the synthesis of a novel NIR aza-BODIPY conjugated CXCR4 targeting FC131 AMBA peptide and its ability in selectively targeting CXCR4 receptors in U87.CXCR4 glioblastoma cells is reported in collaboration with Archibald *et al.*

5.2.1 Synthesis of water soluble aza-BODIPY cyclic FC131. AMBA peptide conjugate

A versatile peptide coupling between **46** and FC131. AMBA peptide **93** synthesised by Rhiannon Lee was carried out with 1.2 equivalent of HBTU and 6 equivalent of TEA in amine free DMF for 16 hours at room temperature. The crude product was purified using a preconditioned Sep-pak C18 cartridge and the resulting conjugate **94** was characterised by UV-visible spectroscopy, HPLC and MS analysis. (Scheme 45)



Scheme 45. Synthesis of conjugate **94** from PCR4.2 AMBA peptide **93** and **46**.

5.2.2 Photophysical studies of peptide conjugate

The photophysical properties of the conjugate were confirmed by UV-visible and fluorescence spectroscopy to ensure the optical properties were not affected upon conjugation to the peptide **94**. Conjugate **94** showed slightly blue shifted absorption and emission maxima wavelength at 655 nm and 681 nm in MeCN as shown in **Figure 109**.

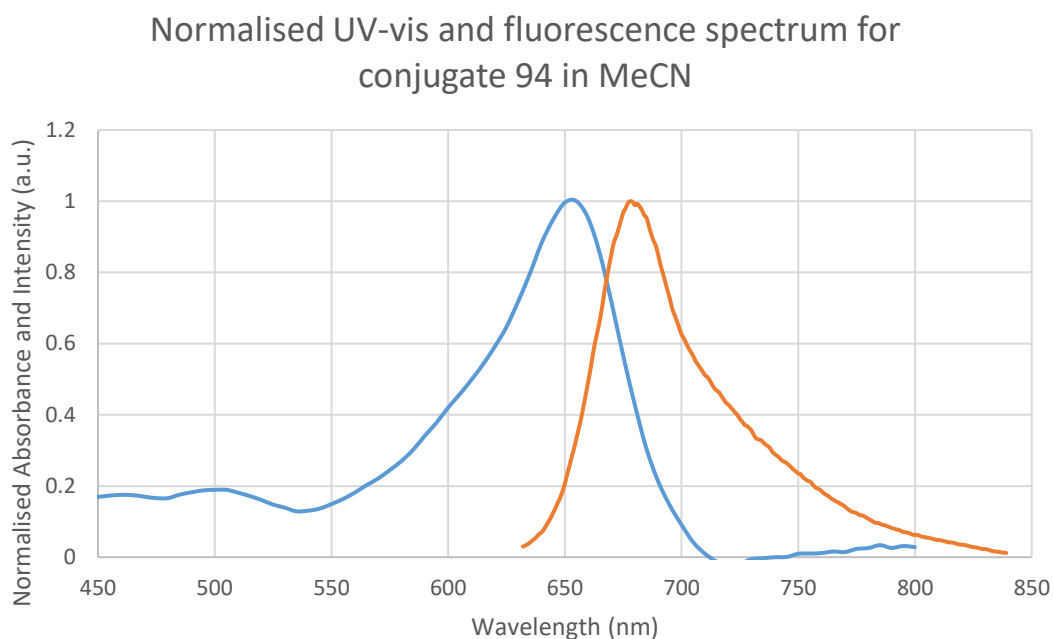


Figure 109. Normalised UV-visible (blue) and fluorescence (orange) spectra of **94** in MeCN.

Conjugate **94** exhibits excellent photostability upon continuous illumination with a strong red/NIR light source for 60 minutes in 10 μ M of PBS p.H 7.4 solution, with a slight decrease of 8% of absorption observed, a similar result can also be observed for aza-BODIPY **46** with only 10% decrease overall. This was compared to commonly used NIR commercial fluorophore ICG, which showed over 90% decrease under the same conditions. (**Figure 110**)

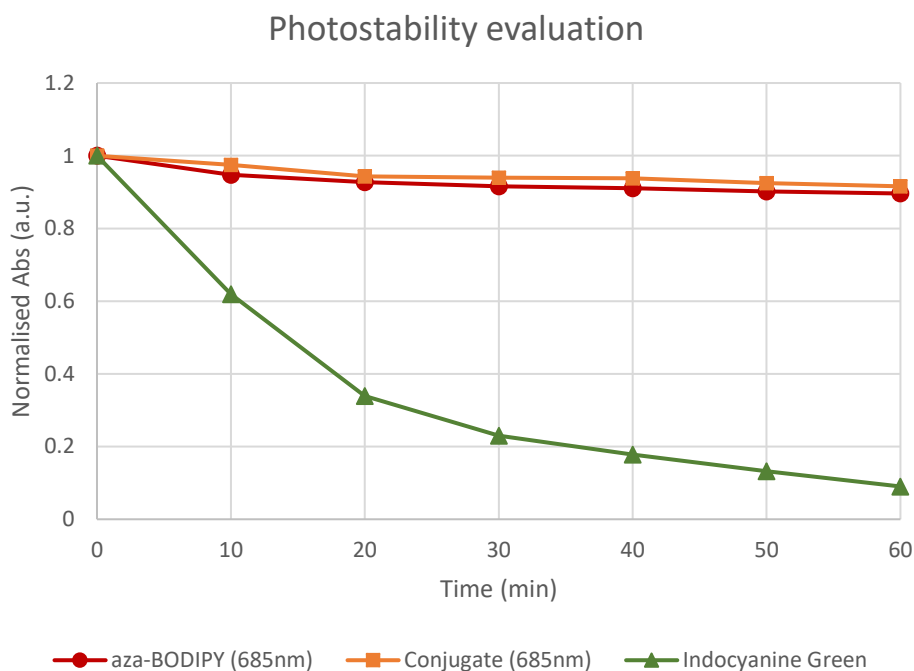


Figure 110. Photostability evaluation with NIR light illumination for 1 hour.

In addition, the fluorescence quantum yields of aza-BODIPY **46** and conjugate **94** were recorded and are shown in **Table 10**. Aza-BODIPY **46** has a fluorescence quantum yield of $\Phi_f = 0.23$, while a significant increase in fluorescence quantum yield of $\Phi_f = 0.60$ was observed upon conjugation with the peptide. The phenomenon of both hypochromic shift and a significant increase in fluorescence quantum yield was suspected to be either due to the conjugation to a hydrophilic sterically hindered group, reducing the aggregation of the dye in polar solvent³²⁵, or enhanced intramolecular π - π interaction.³²⁶

Table 10. Photophysical properties of aza-BODIPY **46** and conjugate **94** in acetonitrile at 298 K. The two reference systems used were cross-calibrated to fluorescein ($\Phi_f = 0.98$ in 0.1 M NaOH)³¹¹ and rhodamine B ($\Phi_f = 0.30$ in water).³¹²

Compound	Solvent	$\lambda_{\text{abs}}(\text{nm})$	$\lambda_{\text{em}}(\text{nm})$	ϵ (L mol ⁻¹ cm ⁻¹)	Φ_f
46	MeCN	660	710	37102	0.23
94	MeCN	655	681	35380	0.60

5.2.3 Molecular modelling

Molecular modelling and relevant calculations were carried out as a preliminary study to validate this concept of enhanced intramolecular π - π interaction. Initially, both the conjugate **94** and aza-BODIPY precursor **46** underwent MM2 energy minimisation to achieve a stable molecular conformation. Followed by Extended Hückel calculation to obtain the molecular orbital (MO) energy for the highest occupied molecular orbitals (HOMOs) and the lowest occupied molecular orbitals (LUMOs).

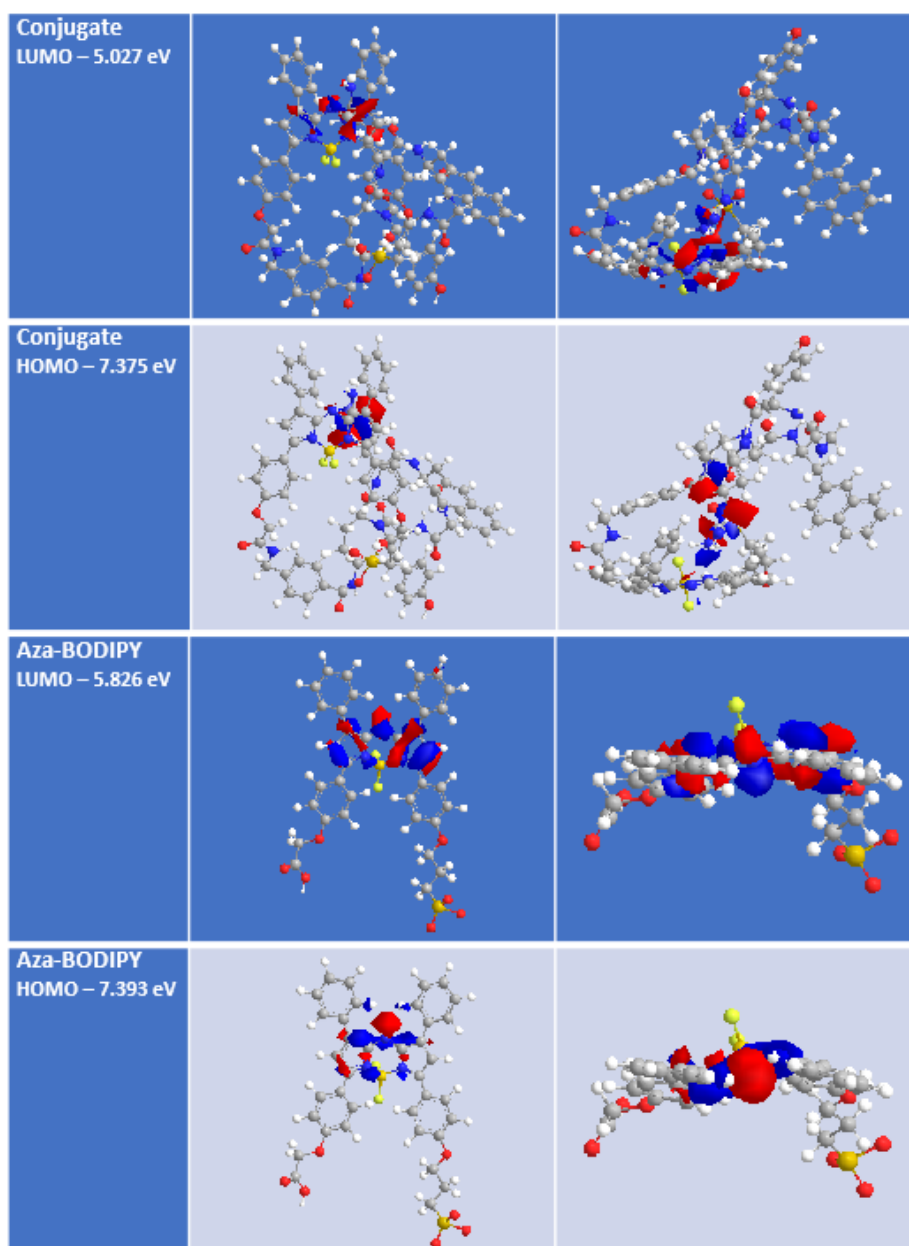


Figure 111. MO diagrams to show the HOMOs and LUMO of conjugate **94** and aza-BODIPY **46**.

The HOMO and LUMO in **Figure 111** were displayed as MO coefficients to show the electron density. Conjugate **94** in the HOMO state showed a high electron density at the arginine (Arg) side chain directed toward the lower electron density aza-BODIPY core, while the opposite was observed in the LUMO state. The electron density for aza-BODIPY **46** can clearly be seen fully distributed at the aza-BODIPY core in both HOMO and LUMO states. Therefore, these results indicated the introduction of the guanidinium from the Arg side chain induced a mesomeric effect at the aza-BODIPY core because of *p*-orbital overlap. This demonstration of an intramolecular molecular π -electron system gave a possible explanation for the significant increase in fluorescence quantum yield observed for conjugate **94**. (**Figure 112**)

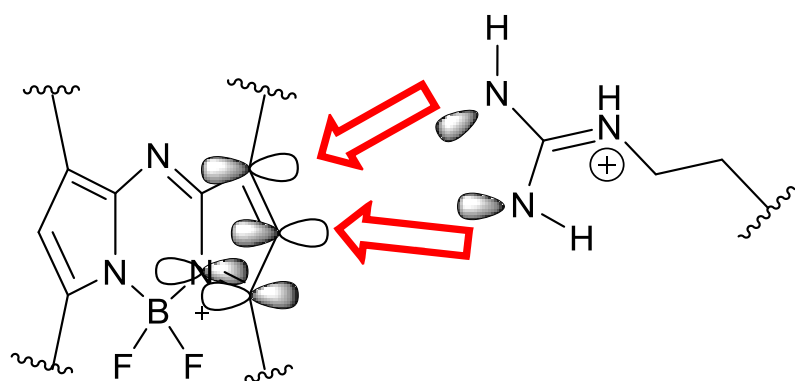


Figure 112. Projection of frontier orbitals for guanidinium and its mesomeric effect on the aza-BODIPY core.

The HOMO–LUMO energy gap for the conjugate **94** (2.35 eV) was calculated to be significantly higher than the aza-BODIPY **46** (1.57 eV). So the bathochromic shift caused by aza-BODIPY is due a reduction in the band gap. This increase in band gap was also consistent with the large blue-shifts observed in the spectroscopic studies. (**Figure 113**)

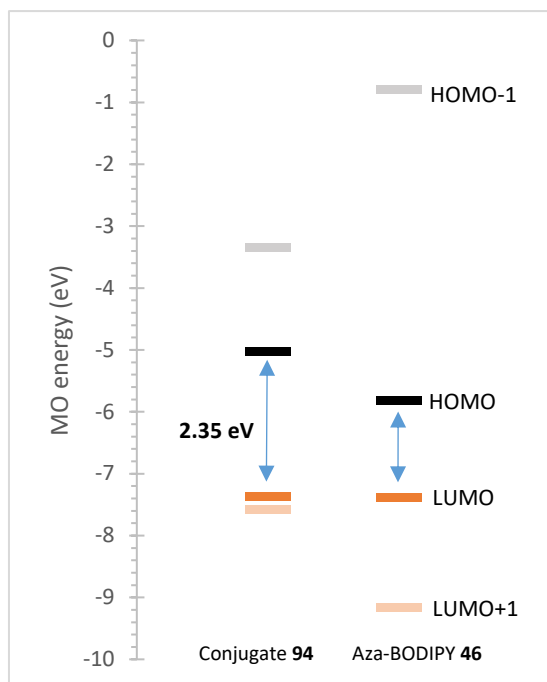


Figure 113. HOMO and LUMO gaps of conjugate **94** and aza-BODIPY **46**.

Overall, the photophysical properties of conjugate **94** have not been compromised and generally shown an excellent red/NIR fluorescence profile, suggesting the effect upon conjugation was not significant enough to affect its potential as a NIR targeting fluorophore.

5.2.4 FACS for binding affinity

The ability of **94** to bind to CXCR4 receptors was evaluated by flow cytometry on cancer cell lines with different levels of CXCR4 receptor expression: U87 (low), Jurkat (high) and transfected CXCR4 U87 cells (high). A fluorescence-activated cell sorting (FACS) displacement assay was conducted by Rhiannon Lee with peptide **94** at varying concentrations against the Phycoerythrin (PE)-antibody 12G5 in Jurkat.CXCR4 cells (**Figure 114A**). Using this technique an IC_{50} value of 82.7 nM was determined; which is 3.5 times larger than the IC_{50} value determined for Pentixafor using the same technique and was an acceptable value indicating selective binding. Inhibition of CXCL12 binding assay also showed that conjugate **94** had a high binding affinity toward Jurkat.CXCR4 cells with an IC_{50} value of 26 nM.

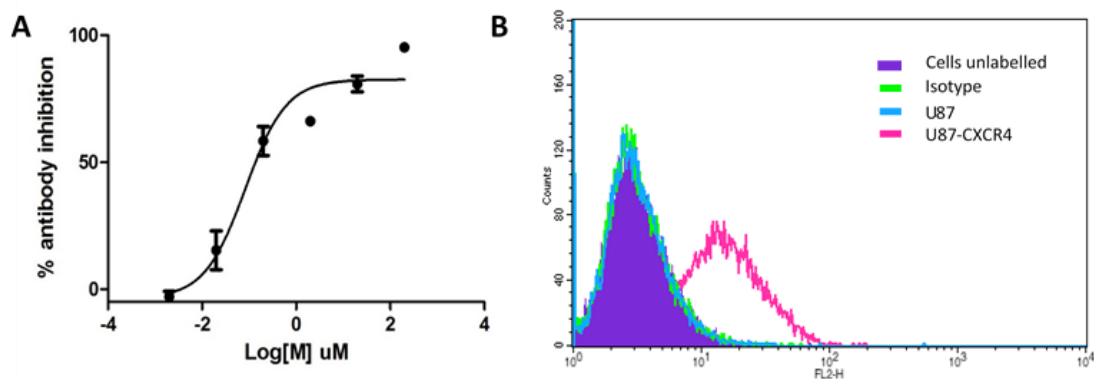


Figure 114. A) Antibody (IgG2A) displacement concentration curve obtained for **94** in Jurkat.CXCR4 cells, ($n = 3$). B) CXCR4 expression in U87-CXCR4 (pink curve) vs U87 (blue curve) cells as determined by flow cytometry.

The expression levels of CXCR4 receptors in U87 and U87-CXCR4 cell lines were validated via flow cytometry. The histogram showed that the U87 cells had no expression of CXCR4 receptor, whereas the transfected cell line, U87-CXCR4 shows significant overexpression of the CXCR4 receptor (**Figure 114B**).

5.2.5 *In vitro studies of fluorescence imaging*

Initially, the conjugate **94** were investigated for fluorescence imaging in both U87.CXCR4 and U87 cells. Prior to CLSM imaging, concentrations of 5, 10 and 20 μM of the conjugate **94** were incubated with U87.CXCR4 cells at 4 °C for 30 minutes and the excess was removed by PBS washing.

All concentrations showed localisation at the membrane when excited at 633 nm, which was confirmed by investigation of the corresponding Z stack, the results indicated successful binding to CXCR4 receptors in the U87-CXCR4 cells. With the higher concentration providing the greatest contrast and the quantitative data was shown through the total corrected cellular fluorescence (TCCT) in **Figure 115**.

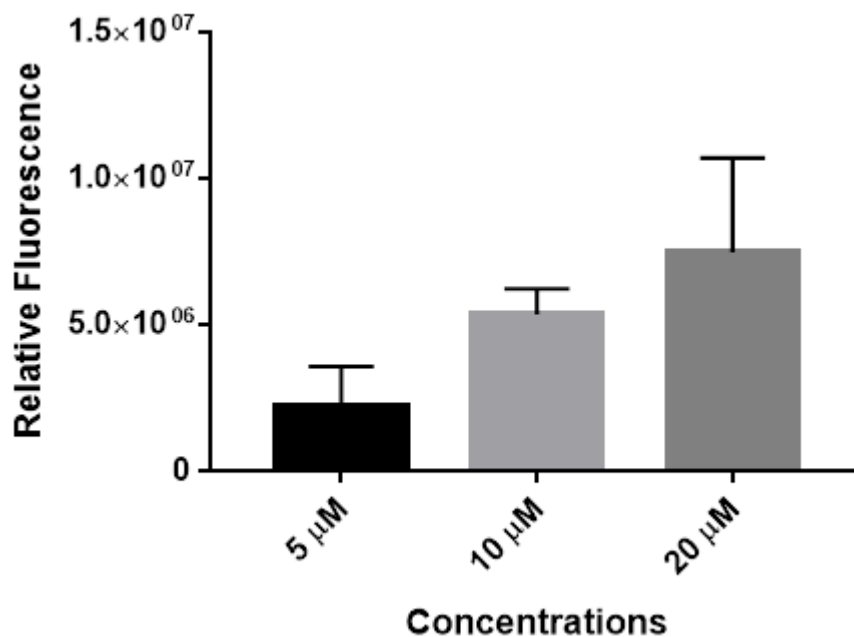


Figure 115. Calculated total corrected cellular fluorescence (TCCF) from confocal images of three different concentrations incubated with U87.CXCR4.

A CXCR4 negative cell line; U87 was used to validate the specificity of the conjugate **94** toward CXCR4 receptors. With the same conditions described above, U87 was incubated with 5 μM of the conjugate **94**. From the images, no fluorescence signals were detected in the U87 cell line (CXCR4-) and importantly no non-specific uptake was observed in the cytoplasm of the cells. The results showed conjugate **94** was selective toward receptor binding. (**Figure 116**)

Autofluorescence which is one of the major concern for FGS was also investigated by irradiating at 633 nm with no fluorophore applied. The resulting image showed no autofluorescence was detected at this excitation wavelength.

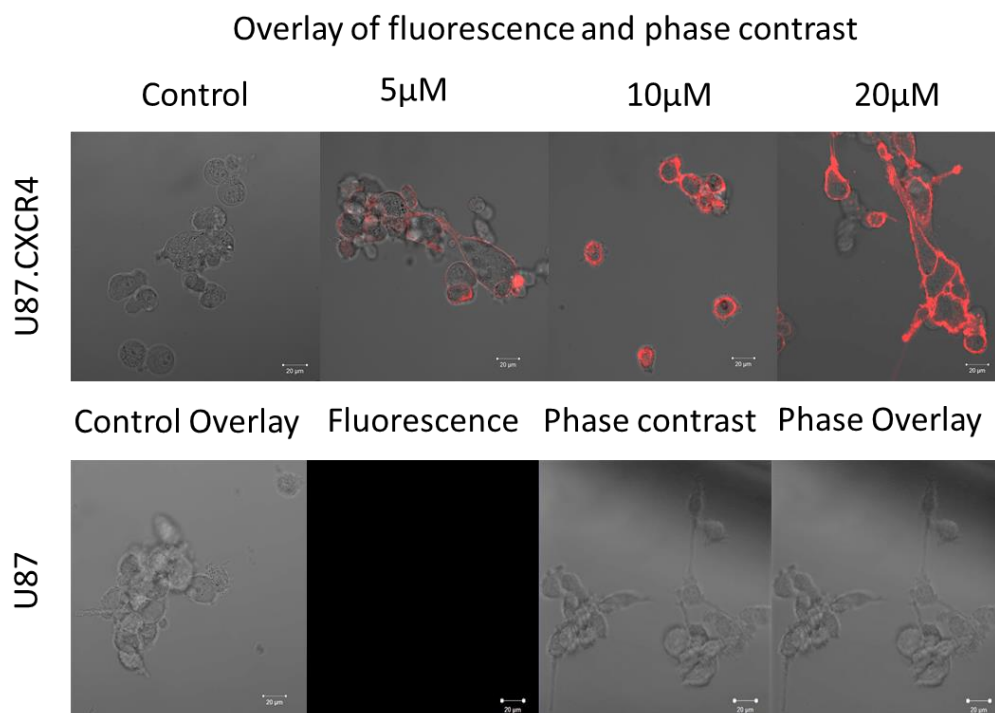


Figure 116. CLSM images of U87.CXCR4 (CXCR4+) cells incubated with three concentrations of conjugate **94** and U87 (CXCR4-) cells incubated with 5 μ M (λ_{ex} = 633 nm).

5.2.5.1 Co-localisation studies with hCXCR4 FITC-antibody

Co-localisation was observed with commercial human CXCR4 fluorescein-conjugated antibody and conjugate **94**. A concentration of 32 μ M of the FITC-antibody was first incubated with U87.CXCR4 cells at 4 °C for 30 min, the excess was removed by PBS washing. Followed by the incubation of 5 μ M of **94** under the same conditions for another 30 min. Subsequently, CLMS with dual excitation channels at ex. 488 nm and ex. 633 nm was used in live cell imaging shown in **Figure 117**. Internalisation of the FITC antibody into the cytoplasm was observed in the ex. 488 nm channel in the U87.CXCR4 (CXCR4+) cells, which was expected due to a high concentration of the antibody. The NIR fluorescence of conjugate **94** in the ex. 633 nm channel was also observed at the membrane specified for receptor binding. This was confirmed by the Z-stack shown in **Figure 118**.

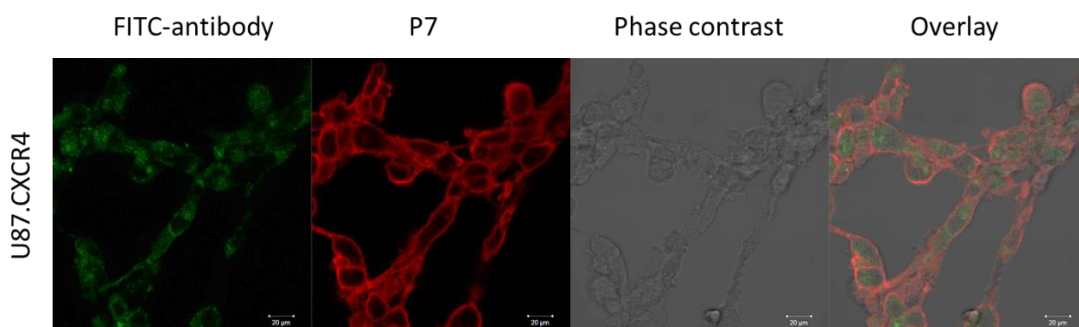


Figure 117. CLSM images of the co-localisation of FITC antibody ($\lambda_{\text{ex}} = 488 \text{ nm}$) and conjugate ($\lambda_{\text{ex}} = 633 \text{ nm}$) in a duel channel system.

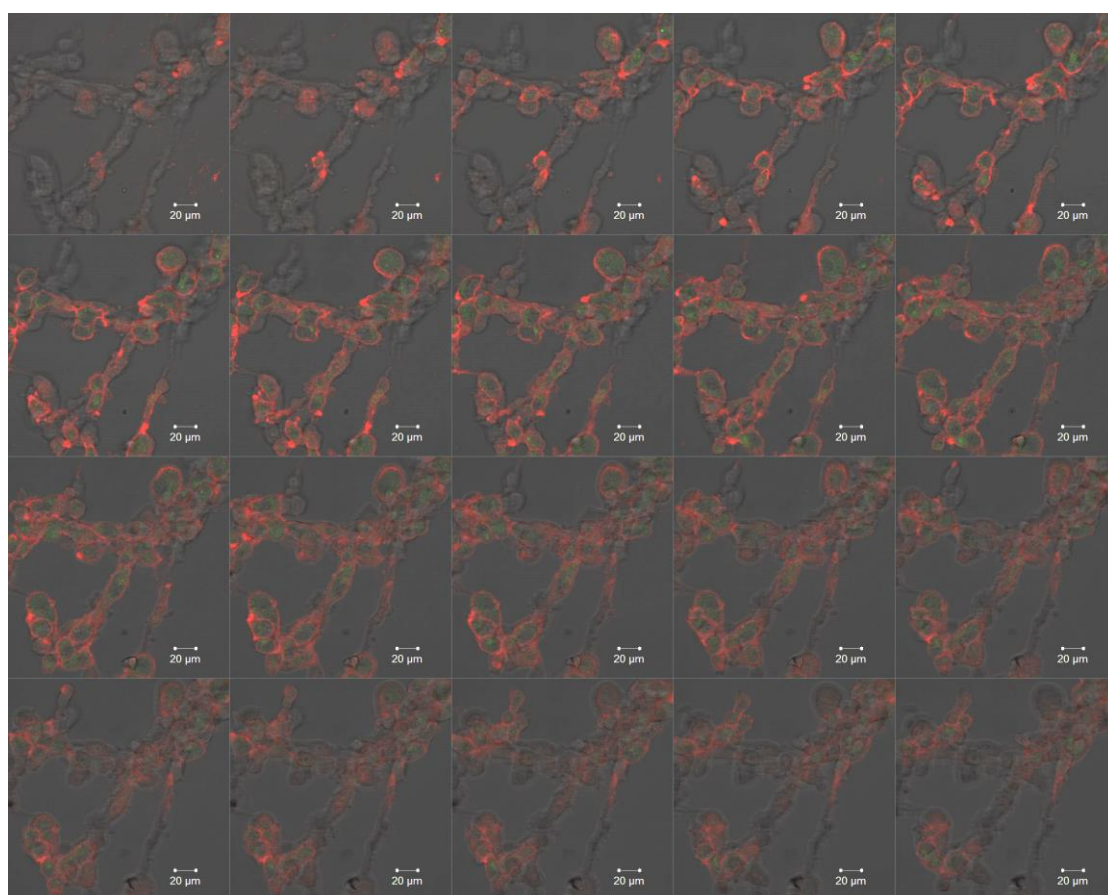


Figure 118. Z-stack of the co-localisation experiment of FITC antibody ($\lambda_{\text{ex}} = 488 \text{ nm}$) and conjugate ($\lambda_{\text{ex}} = 633 \text{ nm}$) in a duel channel system.

This result suggested that peptide conjugate **94** had a higher binding affinity toward the CXCR4 receptors. As it was likely that the FITC antibody which previously occupied the receptors was displaced by the conjugate peptide, subsequently the large globular proteins were internalised. This could possibly be the result of better binding kinetics of the conjugate in comparison to the FITC antibody.

In addition, the relative fluorescence observed between the FITC-antibody and conjugate **94** was calculated. The TCCF showed a 6-fold higher fluorescence intensity for aza-BODIPY, in comparison to fluorescein (**Figure 119**).

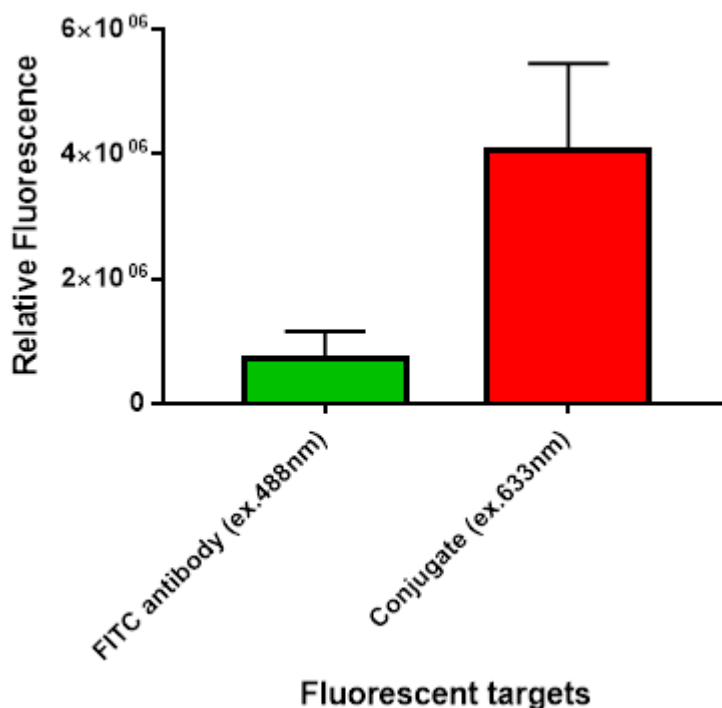
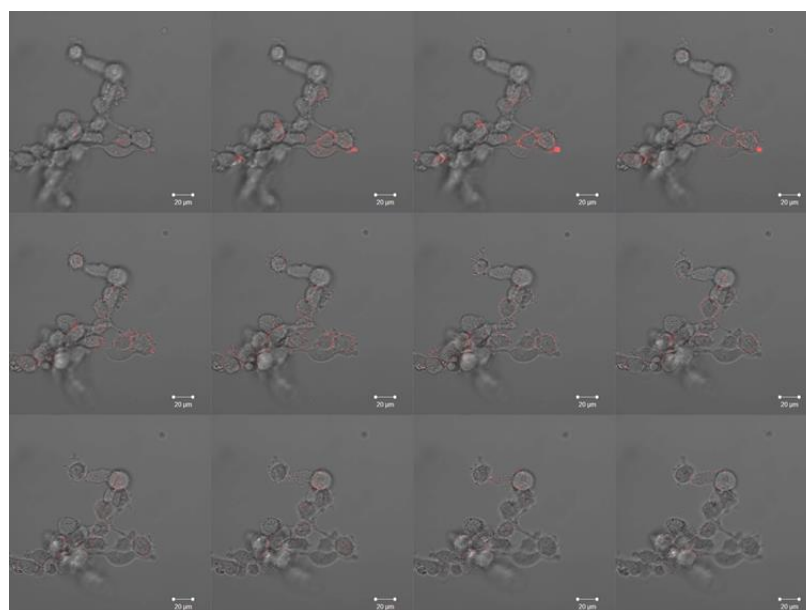


Figure 119. Calculated total corrected cellular fluorescence (TCCF) from the confocal images of co-localisation of FITC antibody and conjugate.

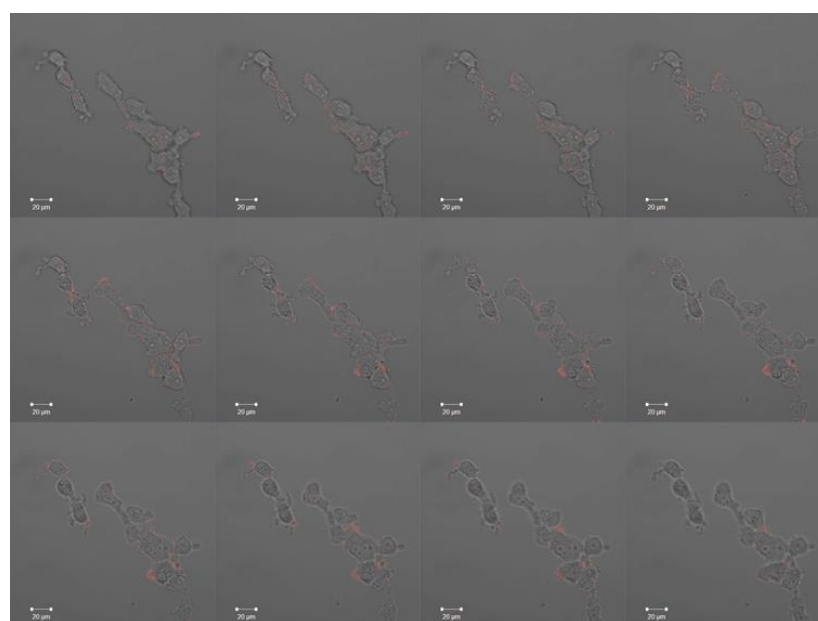
It was also observed during live cell imaging that FITC excited at 488 nm can undergo photobleaching rapidly when excited for a longer time during the z-stacking experiment, as the fluorescence became visibly weaker. In contrast, the aza-BODIPY conjugate **94** did not experience equivalent photobleaching activity. Overall, it was concluded that the conjugate **94** was superior to the FITC labelled antibody, as it is more photostable and results in a higher fluorescence intensity in target cells.

5.2.5.2 Non-specific binding experiment with starting material.

Non-specific binding / uptake was investigated for non-conjugated aza-BODIPY **46** in both CXCR4⁺ and CXCR4⁻ cell lines, in order to further determine the role of the peptide in the results shown above. Only a minimal fluorescence signal was seen when both cell lines were incubated with 5 μ M of the aza-BODIPY starting material **46** under the same conditions confirming the peptide is responsible for cell selective labelling with aza-BODIPY (**Figure 120**).



U87.CXCR4 (CXCR4+)



U87 (CXCR4-)

Figure 120. Z-stack of CXCR4+ and CXCR4- cells incubated with aza-BODIPY

In conclusion, a novel aza-BODIPY – Pentixafor based targeting probe was developed for CXCR4 imaging. For the first time, a NIR fluorescent probe showed superior photophysical properties and specificity for the CXCR4 receptor. This work validated the conjugation of aza-BODIPY to a targeting peptide as a possible strategy for accessing a red/NIR for use in FGS.

5.3 Cysteine residue bioconjugation with Herceptin antibody

In many biological and clinical studies, monoclonal antibodies have been used as targeting moieties to enhance the affinity of drugs and imaging agents towards cancerous tissues.^{112,113} They can be covalently bound to fluorescent probes to generate fluorescent antibody conjugates (FAC) for imaging purposes. Several FACs are in preclinical development featuring both FDA-approved antibodies and commercially available fluorophores.^{119,123,124,327} However, FACs are most commonly generated through multiple lysine labelling and this methodology results in heterogeneous mixtures of products that suffer from variability between batches.¹¹⁶ This could affect selectivity and specificity for targeting cancerous tissue, resulting in poor imaging in FGS. Breast conserving surgery is an example that can benefit from selective FGS, as it requires precise identification of the tumours, for both tissue preservation and preventing incomplete resection.¹⁵

To alleviate these issues, site selective bioconjugation methods to targeting moieties have been developed. Cysteine residues are a popular substitute for lysine residues, due to their low abundance and site-specific nature. A promising approach was recently introduced by Chudasama and co-workers^{159,191} with the use of dibromopyridazinediones (PDs) to regioselectively modify cysteine residues through disulfide re-bridging, and this technique has been demonstrated for formation of a variety of antibody conjugates.^{191,328–331}

Herein, regioselective conjugation to trastuzumab[®] with two different water-soluble aza-BODIPY, *via* a SPAAC reaction has been investigated as part of an ongoing collaboration with Chudasama *et al.* Biological evaluation of the resulting conjugates were carried out using *in vitro* fluorescence imaging with breast cancer cell lines expressing different levels of Human Epidermal Growth factor Receptor 2 (HER2) receptor.

5.3.1 Bioconjugation with anionic azido aza-BODIPY

Following on from the successful synthesis and promising properties of aza-BODIPY **40**, the synthesis of a “clickable” antibody was conducted to enable the controlled and site-selective attachment of this imaging moiety. Initially, the disulfide bridges of the

antibody were reduced through incubation with TCEP at 4 °C overnight. The functional rebridging of trastuzumab[®] disulfide bonds was then carried out by Dr. Antoine Maruani using PD derivative **95** (**Figure 121**) to prepare functionalised antibody **97** with a highly reactive strained alkyne for further SPAAC reaction with aza-BODIPY **40** (**Scheme 46**).

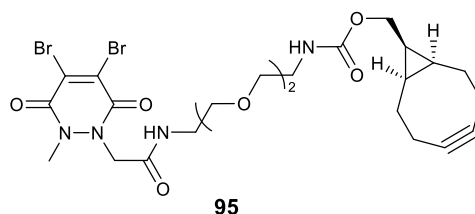
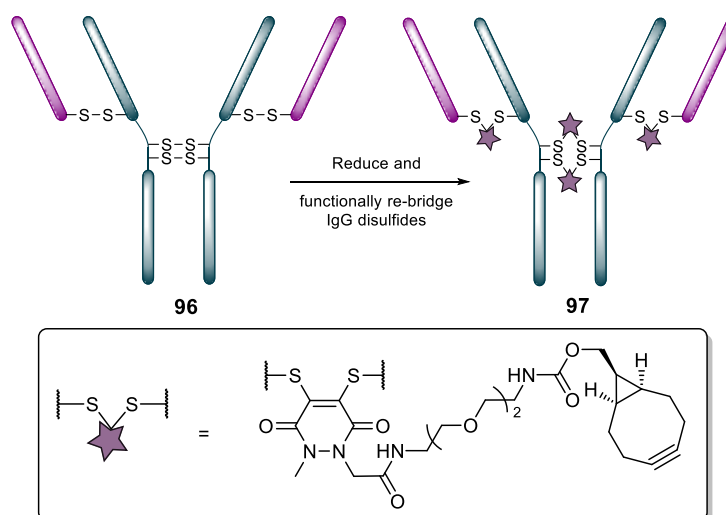
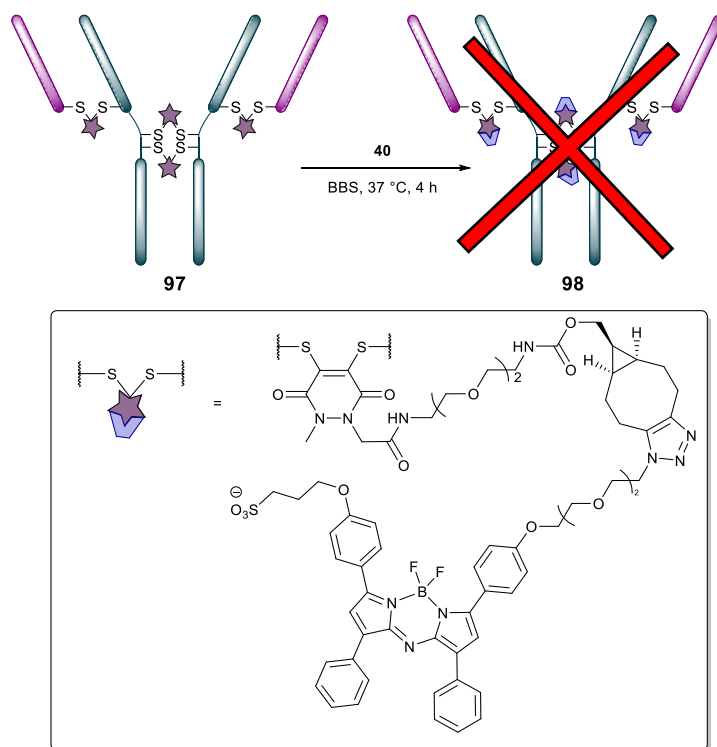


Figure 121. Structure of PD-based re-bridging reagent.



Scheme 46. Preparation of “clickable” trastuzumab **97**.

Subsequently, 20 equivalents (*i.e.* 5 eq per strained alkyne) of aza-BODIPY **40** were added and the reaction mixture was incubated at 37 °C for 4 hours. (**Scheme 47**) However, the reaction did not result in complete conversion with only low loading ratios and a large amount of aggregate observed.



Scheme 47. Attempted preparation of aza-BODIPY–trastuzumab conjugate **98**.

The purity of **98** was confirmed by SDS-PAGE. Unfortunately, the resulting gel showed several protein bands corresponding to 145, 71, 35 and 28 kDa. Through observation of those bands under both fluorescence and coomassie blue staining (separately), the unwanted bands were confirmed to be aggregates of the aza-BODIPY antibody conjugate (**Figure 122**).

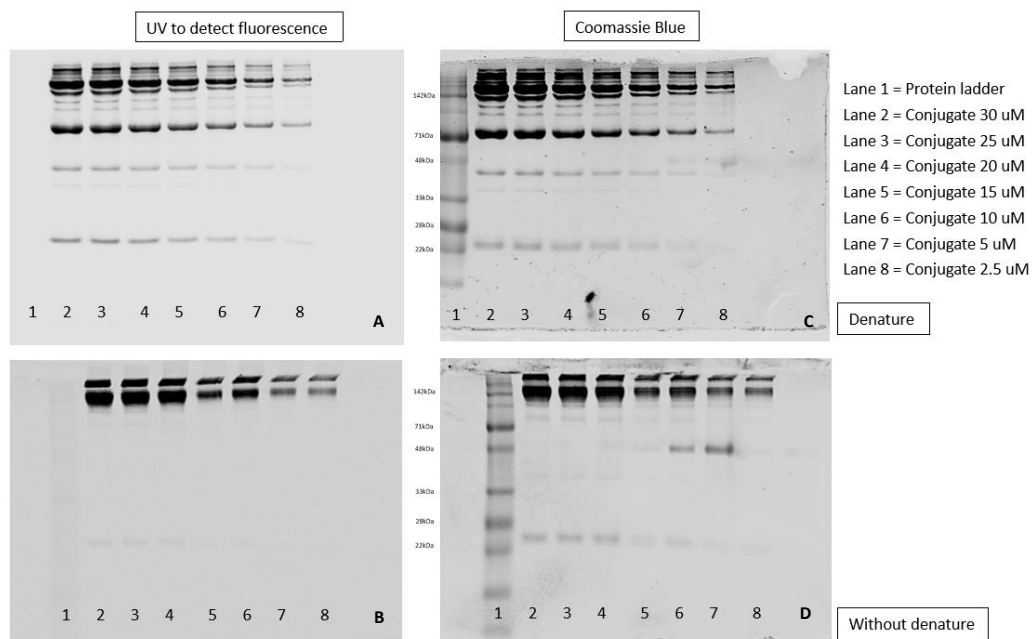


Figure 122. SDS-PAGE of the conjugate with denaturing at 90 °C for 3 minutes (A &C) and without denaturing (B &D).

5.3.1.1 In vitro imaging of NIR fluorescent conjugate

Live cell confocal imaging to validate selectivity was carried out by Huguette Savoie using BT-474 (HER2+) and MDA-MB-468 (HER2-) cell lines.

The two cell lines were individually incubated with 4 μ M of **98** for 30 minutes at 4 °C. Excess conjugate was removed by washing with PBS prior to CLSM imaging. The Z-stack images showed the conjugate had successfully bound to the membrane of the HER2+ cells (**Figure 123**). However, this was also observed for the HER2- cell lines and there were no significant differences in the levels of fluorescence detected. Hence, the selectivity was poor and could not discriminate between cell lines (**Figure 124**), both cell lines showed membrane bound fluorescence and this was likely caused by non-specific binding.

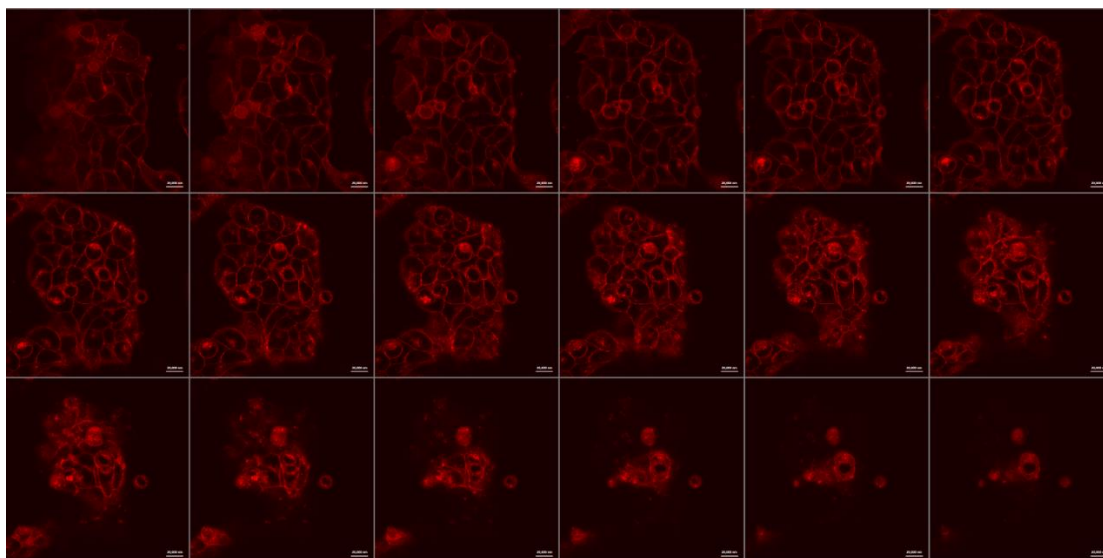


Figure 123. Z-stack of BT-474 (HER2+) cells incubated with FAC **98**.

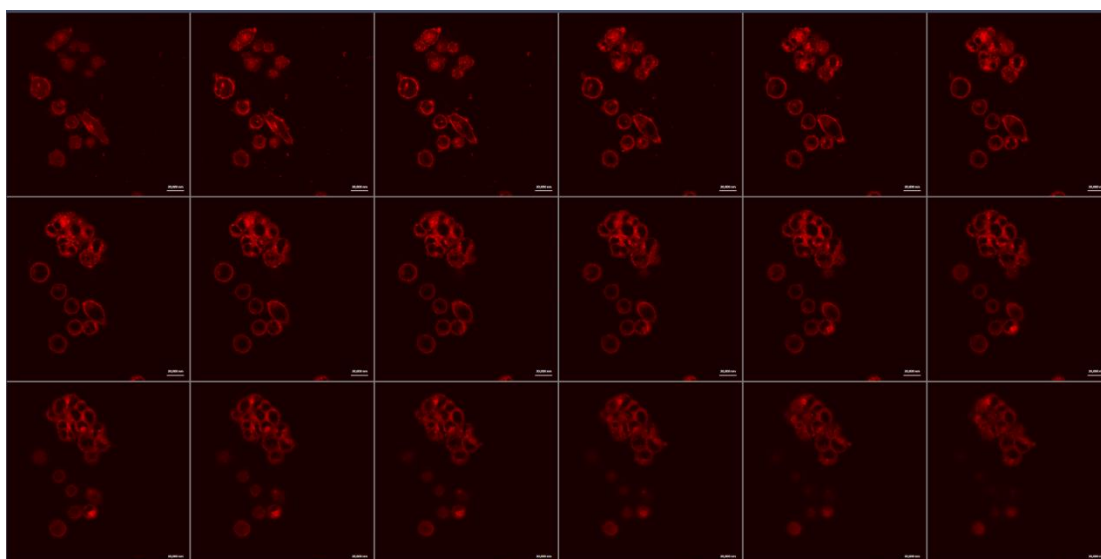


Figure 124. Z-stack of MDA-MB-468 (HER2-) cells incubated with FAC 98.

It was speculated that non-specific binding resulted from aggregation of the aza-BODIPY conjugate. The aggregation could be a result of interaction between the hydrophobic aza-BODIPYs forming H-dimer clusters that could not be removed. Therefore, these aggregates could either be redistributed to other proteins or interacted with binding sites of the antibody through non-covalent binding, inhibiting selective binding to HER2 receptors (**Figure 125**). Previous spectroscopic data for **40** suggested low aqueous solubility is a major limiting factor that contributes to non-specific binding, especially when labelling antibodies at a higher loading ratio.

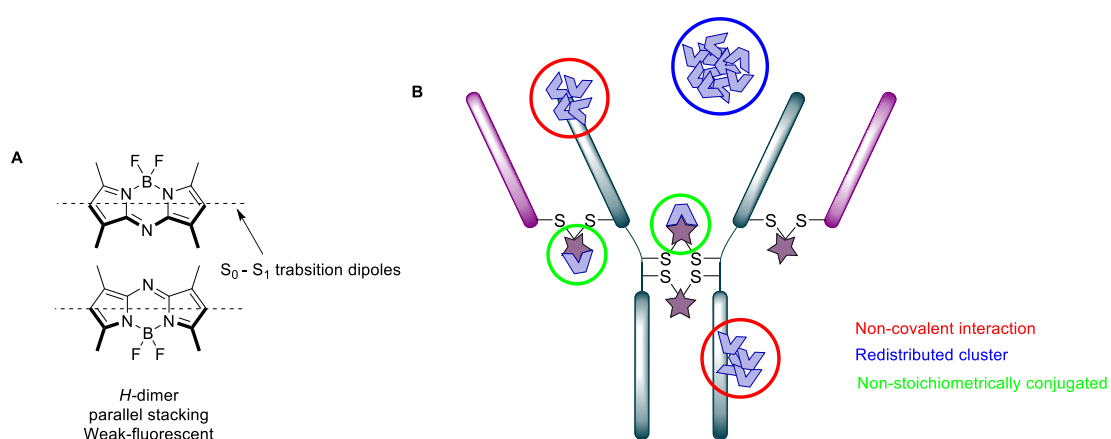


Figure 125. Proposed mechanism for observed aggregation of conjugate: a) Formation of *H*-dimer, b) Non-covalent interaction, redistribution and non-stoichiometric.

In conclusion, a more water-soluble azido aza-BODIPY was required to optimise the SPAAC reaction and to perform relevant biological evaluations.

5.3.2 Photophysical studies and bioconjugation of an enhanced water-soluble azido aza-BODIPY

Following the successful synthesis of water-soluble aza-BODIPY **68**, photophysical evaluation in aqueous media was carried out. The UV-visible and fluorescence spectra showed absorption and emission maxima in water at 635 nm and 713 nm respectively. The compound was shown to exhibit excellent photostability in a photobleaching study. After the continuous illumination (>600 nm) for 60 minutes at 10 μ M in PBS solution pH 7.4, a decrease of 13 % in absorbance was observed. This compared favourably with ICG, which showed a 90% decrease under the same conditions. (**Figure 126**).

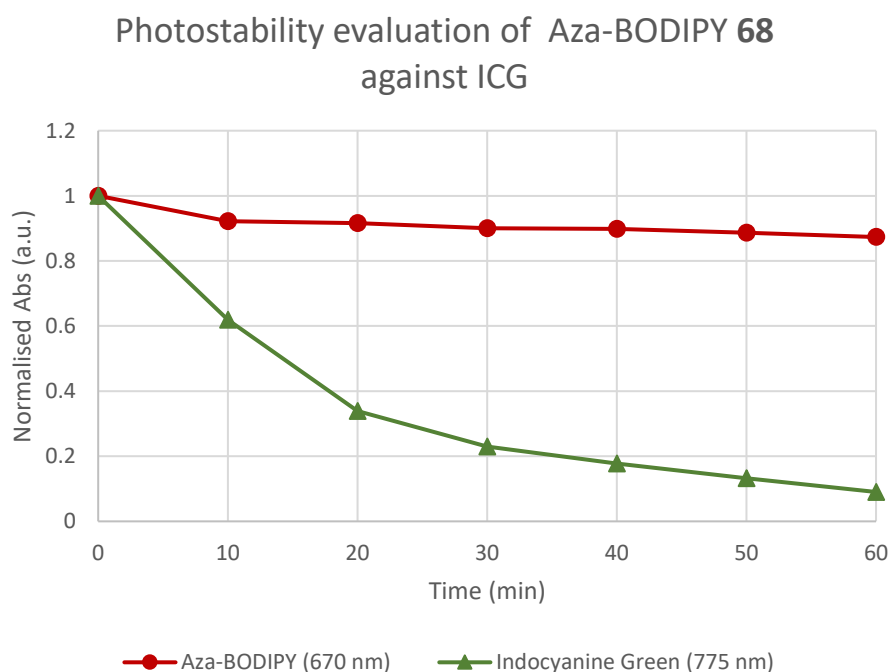


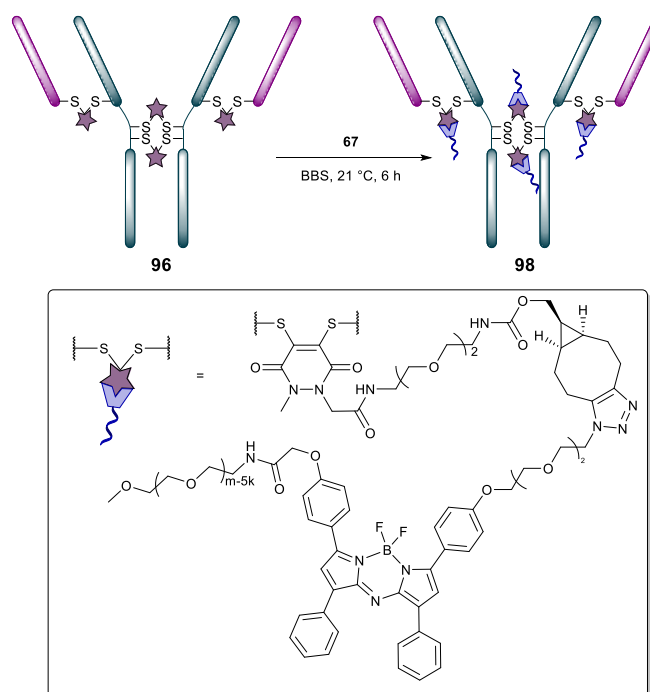
Figure 126. Photostability study for aza-BODIPY **68** and ICG in PBS (pH 7.4).

In addition, the fluorescence quantum yield of aza-BODIPY **68** was measured and was found to be $\Phi_f = 0.19$, this showed a slightly lower fluorescence quantum yield in comparison to literature values, but was still acceptable as a NIR fluorescence probe for imaging applications (**Table 11**).

Table 11. Photophysical properties of aza-BODIPY **68** at 298 K.

Compound	Solvent	$\lambda_{\text{abs}}(\text{nm})$	$\lambda_{\text{em}}(\text{nm})$	$\epsilon (\text{L mol}^{-1} \text{cm}^{-1})$	Φ_{f}
68	Water	645	713	23442	0.19

Thereafter, aza-BODIPY **68** was reacted with conjugate **97** using SPAAC chemistry (Scheme 48). After optimisation of conditions, it was found that incubation of conjugate **97** with 6 equivalents (*i.e.* 1.5 eq per strained alkyne) of aza-BODIPY **68** for 6 hours at 21 °C, was sufficient to effect complete conversion to aza-BODIPY–trastuzumab[®] conjugate **99** in near quantitative yield and in high purity.



Scheme 48. Preparation of aza-BODIPY–trastuzumab conjugate **99**.

The stoichiometric ratio was calculated using the formula below with $\epsilon_{280} = 215380 \text{ M}^{-1} \text{ cm}^{-1}$ for trastuzumab, $\epsilon_{345} = 9100 \text{ M}^{-1} \text{ cm}^{-1}$ for Mestra-PD, $\epsilon_{635} = 23442 \text{ M}^{-1} \text{ cm}^{-1}$ for the aza-BODIPY, 0.11 as a correction factor (CF) for Mestra-PD for the absorbance at 280 nm and 0.29 for aza-BODIPY at 635 nm:

$$r = \frac{A_{\lambda}/\epsilon_{\lambda}}{(A_{280} - \sum CF_{\lambda} \times A_{\lambda})/\epsilon_{280}}$$

With A_λ as the absorbance at the wavelength λ , and ϵ_λ being the extinction coefficient of the relevant molecule. The stoichiometric ratio of the conjugate **99** was found to be *ca.* 4:1 (F/A), with the resulting conjugates characterised by UV-visible and fluorescence spectroscopy, and SDS-PAGE. (**Figure 127** and **Figure 128**)

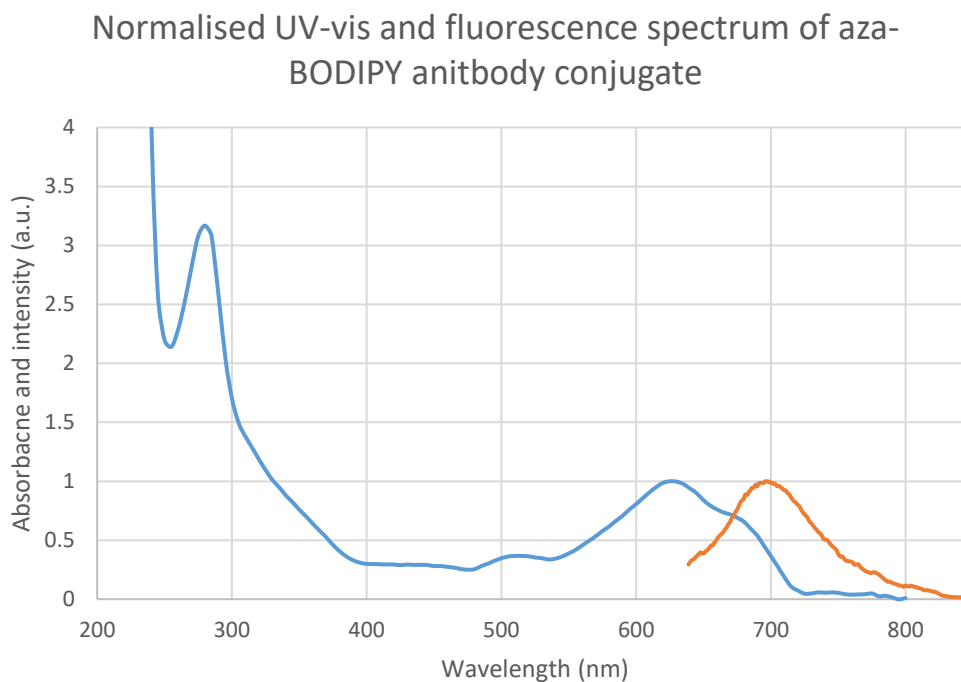


Figure 127. UV-visible (blue) and fluorescence (orange) spectra of conjugate **99** in PBS solution pH 7.4.

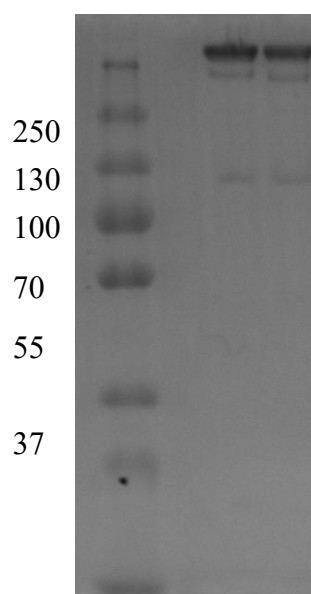


Figure 128. SDS-PAGE of (from left to right): ladder / functionalised trastuzumab **97** / conjugate **99**.

5.3.2.1 Cell preparation and confocal Imaging

With aza-BODIPY–trastuzumab[®] conjugate **99** in hand, we next appraised its potential as a tool for NIR FGS. To demonstrate the NIR fluorescence imaging properties of conjugate **99**, *in vitro* validation was carried out using cells which overexpress the HER2 cell surface receptor (BT-474), and another cell line which expresses native levels of the same receptor (MDA-MB-468) through fluorescence microscopy.

The seeding of both cell lines was performed under the same conditions as previously described. The two cell lines were individually incubated with 5 μ M of **99** for 30 minutes at 4 °C. The excess conjugate was again removed by washing with PBS prior to CLSM imaging. **Figure 129** shows intense fluorescence, predominately localised at the membrane of the BT-474 cells, and this was confirmed by Z-stacking (**Figure 130**).

Fluorescence was confined to the membrane suggesting receptor binding with no non-specific internalisation observed. A low, but detectable, intensity of fluorescence was observed for MDA-MB-468 cells (**Figure 129**) and was again confirmed by Z-stack as shown in **Figure 131**.

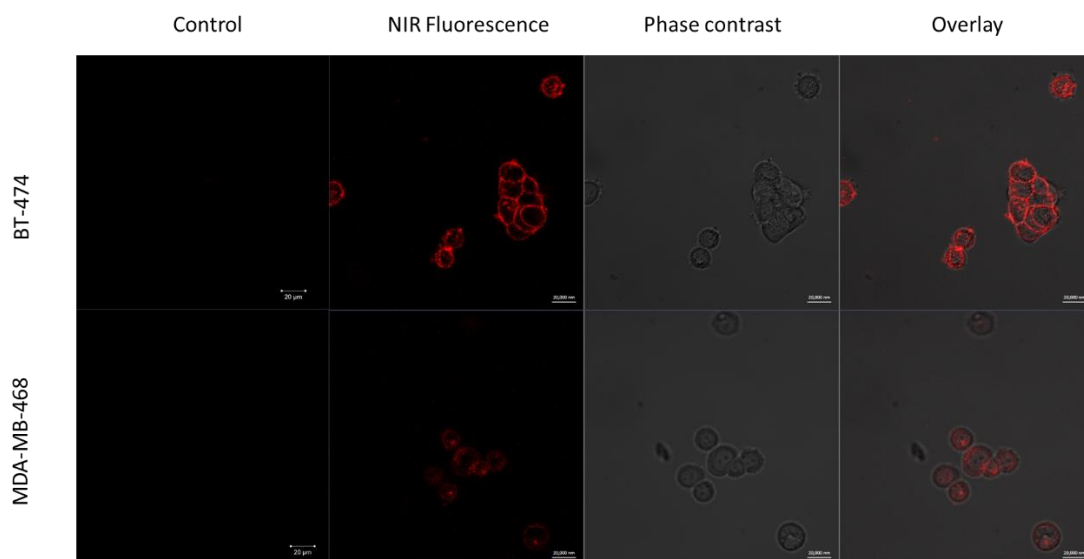


Figure 129. CLSM images of BT-474 (HER2+) and MDA-MB-468 (HER2-) incubated with 5 μ M conjugate **99** and control.

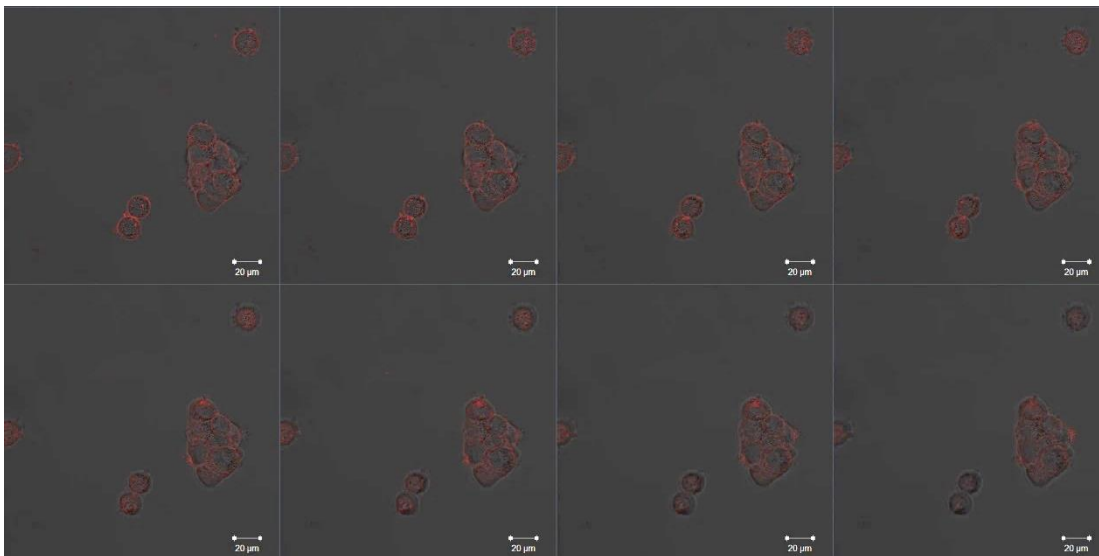


Figure 130. Z-stack images following 30 minutes incubation at 4 °C of **99** with BT-474 (HER2+) cells. Excitation at 633 nm by HeNe laser.

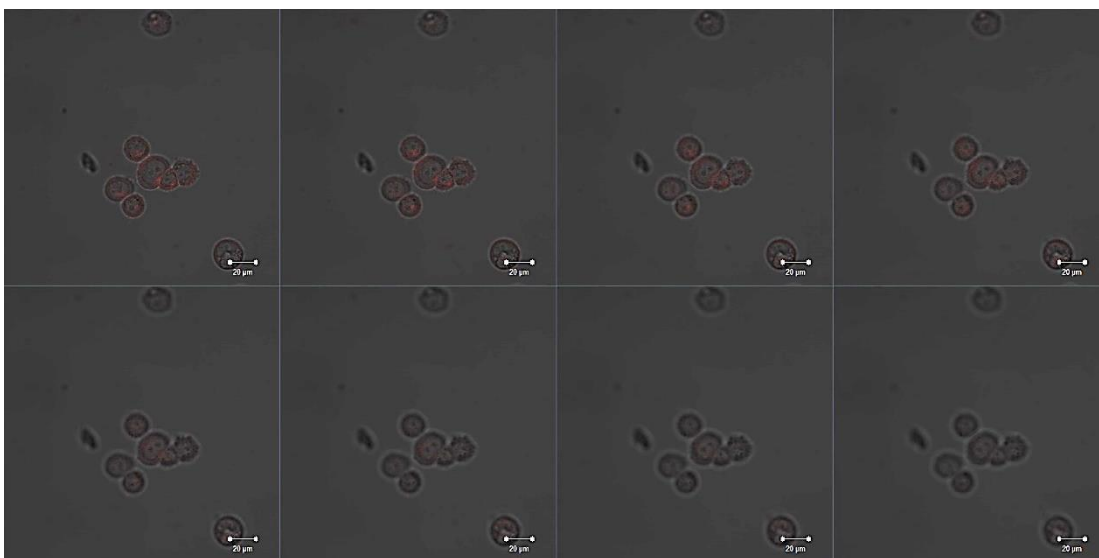


Figure 131. Z-stack images following 30 minutes incubation at 4 °C of **99** with MDA-MB-468 (HER2-) cells. Excitation at 633 nm with HeNe laser.

The detection of low intensity fluorescence was due to native expression levels of HER2 receptors, rather than overexpression. This was confirmed by the calculating the total corrected cellular fluorescence (TCCF) to show the significantly higher relative fluorescence observed in BT-474 cells, which was 2.6 times higher than the MDA-MB-468 cells as shown in **Figure 132**.

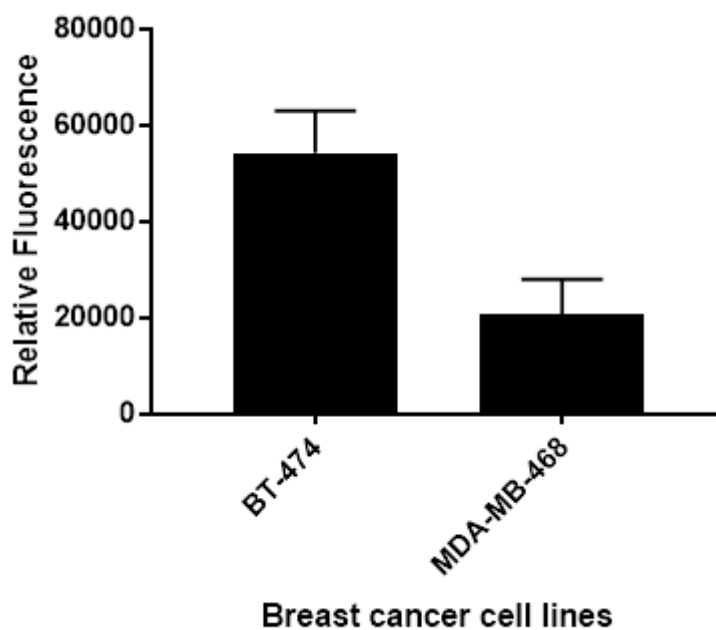


Figure 132. Calculated total corrected cellular fluorescence (TCCF) from the confocal images of BT-474 (HER2+) and MDA-MB-468 (HER2-) cells incubated with **99**.

In conclusion, an aza-BODIPY with enhanced water solubility was synthesised. This underwent regioselective and stoichiometrically-controlled bioconjugation to a clinical relevant antibody (trastuzumab[®]), resulting in a targeted aza-BODIPY–antibody conjugate. *In vitro* imaging validated the selectivity toward HER2 receptors in breast cancer cell lines. Overall, these preliminary results demonstrate excellent photophysical and biological properties of an aza-BODIPY based FAC, with further studies for *in vivo* imaging to follow.

6. Concluding remarks and future work

To date, the demand for optimised fluorescence probes remains high. This is due to the many limitations of the current FDA approved fluorophores such as PPIX, MB, ICG and other commercially available NIR dyes. These limitations typically include, lack of selectivity for target tissue and the absence of NIR absorptions / emissions, limiting light penetration for deeper seated tumours, thus, limiting discrimination between healthy and cancerous tissues, and hindering applications in FGS.

Throughout this project, we have investigated three classes of potential organic fluorophores with far red / NIR properties: BODIPYs, aza-BODIPYs and bacteriochlorins. All three classes of compounds were successfully synthesised and characterized and their far red / NIR properties were compared and analysed. A library of BODIPYs and aza BODIPYs with different conjugatable substituents and water-solubilising groups was successfully synthesized. BODIPYs were synthesised and modified with ease from a one pot reaction, and their wavelengths could also be finely tuned to induced bathochromic shifts through halogenations and extending conjugation. However, the overall induced bathochromic shifts were unfortunately insufficient, and fluorescence was only achieved in the red region. Therefore, further investigations into aza-BODIPYs and bacteriochlorins were pursued.

The synthesis of aza-BODIPY can be deemed as challenging, due to the physicochemical properties making purification difficult. Investigations into synthetic strategies to introduce bioconjugatable moieties was carried out, successful synthesis of functionalised aza-BODIPYs were then extended to incorporate water-solubilising groups. Despite the challenges of complex purifications, several different approaches such as the novel counterion exchange method and substitution methods were developed in order to allow more facile and larger scale synthesis of water-soluble aza-BODIPYs. Aza-BODIPYs have overall provided the most desired properties as a scalable, conjugatable and biocompatible NIR fluorescence probe, making it an attractive class of compound for further investigations.

Several different methods for bacteriochlorin synthesis were investigated and these included Whitlock's diimide reduction, 1,3-dipolar cycloaddition and Lindsey's *de novo* synthesis. This investigation found that the most efficient way to synthesise a

stable and multi-functional bacteriochlorin was through the *de novo* synthesis. However, due to synthetic complications involved in the synthesis of bacteriochlorins, the production of bacteriochlorin can often be compromised by factors such as low yield and high cost. Therefore, after extensive investigations of all three classes of compounds, BODIPYs and bacteriochlorins as far red / NIR fluorophores were found to be unsuitable for applications in FGS. On the other hand, aza-BODIPYs demonstrated excellent photophysical properties and biocompatibility as an optimised NIR fluorescence probe. Thus, highlighting their potential in biological applications and recommending them for further investigation toward applications in FGS.

Due to the need for a targeted NIR fluorescence probe, we investigated the bioconjugation of water-soluble aza-BODIPYs to several different amino acid residues and targeting moieties. Initially, tyrosine residues on a model protein (BSA) was investigated, and this demonstrated the versatility of tyrosine bioconjugation with BODIPYs and aza-BODIPYs. A novel alkyne functionalised diazonium linker was synthesised, which was then used to perform diazonium coupling with peptides and proteins. Followed by CuAAC with an azido water-soluble aza-BODIPY and *in vitro* fluorescence imaging with HeLa cells to show receptor mediated internalisation. This bioconjugation strategy for BODIPYs and aza-BODIPYs improved loading ratios and provided a more accurate and persistent labelling of BSA.

Targeting moieties, including peptides and antibodies, were also investigated to enhance the selectivity toward specific receptors. A water-soluble and carboxylic acid functionalised aza-BODIPY was conjugated to a CXCR4 receptor targeting peptide *via* lysine residue coupling. This resulted in some interesting changes in photophysical properties, as upon conjugation a significant increase in fluorescence quantum yield and hypsochromic shift resulted, this finding was explained, through preliminary computational modelling, to be due to intramolecular π interaction. This far red / NIR fluorescence probe was subjected to biological evaluation, including flow cytometry and fluorescence imaging, to show high selectivity toward CXCR4 receptors through a comparative study of CXCR4⁺ and CXCR4⁻ glioblastoma cells.

Lastly, a novel fluorescent antibody conjugate (FAC) targeting HER2 receptors was generated. The monoclonal antibody was first modified with a strained alkyne through cysteine rebridging, followed by bioconjugation with an enhanced water soluble aza-

BODIPY using SPACC. This FAC underwent fluorescence imaging, demonstrating significant binding toward HER2+ breast cancer cells and showed enhanced selectivity in comparison to HER2- breast cancer cells.

In conclusion, this project demonstrated the facile labeling of peptides, proteins and antibodies by aza-BODIPYs under different bioconjugation approaches and has successfully produced a novel targeted aza-BODIPY conjugate for selective receptor binding. In addition, these aza-BODIPY conjugates were shown to be translational toward biological applications as demonstrated through *in vitro* imaging, with further *ex vivo* and *in vivo* studies to follow, and will hopefully now migrate toward clinical applications in NIR FGS.

For future work, further *in vivo* studies will be carried out to access information about the biodistribution of the peptide and antibody conjugates in an *in vivo* model, and to further validate the selectivity and specificity toward cancerous tissues under an *in vivo* environment. Studies into the applications toward FGS can also be carry out through the excision of fluorescent tumours from the *in vivo* studies.

Such research will continue with further development of the aza-BODIPY scaffold as NIR fluorophores and its applications in FGS. There is great hope for further explorations of this class of compound in different areas of medical research, such as development into multimodal imaging agents, theranostics and their incorporation into nano-delivery technology, ultimately leading to more cutting-edge applications.

7. Experimental section

7.1 Materials

A Jeol JNMLA NMR spectrometer was used to measure ^1H -NMR at 400.18 MHz, ^{13}C -NMR at 100.62 MHz, ^{11}B -NMR at 128.39 MHz and ^{19}F -NMR at 376.54 MHz, the measurement was referenced against standard internal tetramethylsilane (TMS). Splitting patterns were written as s (singlet), d (doublet), t (triplet), q (quartet), quin (quintet), sex (sextet) and m (multiplet). The chemical shifts (δ) for ^1H , ^{19}F , ^{11}B and ^{13}C are were measured in ppm.

Mass spectral data was obtained from the National Mass Spectrometry Service EPSRC, Swansea using a LTQ Orbitrap XL mass spectrometer. Melting points were obtained with a Stuart SMP10 melting point apparatus. A Varian Cary 50 Bio UV-visible spectrometer was used for measuring absorptions from 250 nm to 800 nm. A Varian Cary Eclipse Fluorescence spectrometer was used for measuring excitations and emissions from 400 nm to 800 nm.

For the anionic aza-BODIPYs HPLC analyses were carried out with a Jasco HPLC system comprising Jasco PU-1580 pumps, separations were carried out on a Luna 5u C18 column (100Å, 150 × 4.6 mm). The flow rate of the mobile phase was 1 mLmin⁻¹ and was detected with a Jasco MD-1515 multiwavelength detector at 205, 660, 745 nm. The method used for anionic aza-BODIPYs used EtOH (0.05M TEA) (solvent B) and water (0.05M TEA) (solvent A) as mobile phases. For peptide conjugate **94** analytical RP-HPLC was used and separation was carried out on a ACE 5 C18 column (100Å, 4.6 × 250 mm) with (CH₃CN/0.1 % TFA) and (H₂O/0.1 % TFA) as eluents. UV-Visible detection used an Agilent Technologies 1200 series diode array detector at 214, 254, 280, 300 nm.

Gel electrophoresis was carried out with a Bio-rad mini-PROTEAN Tetra Cell System with RunBlue precast SDS gels 4-12% 12 wells, SDS running buffer TEO-Tricine 10x, LDS sample buffer and prestained dual colour markers purchased from Expedeon. The gel was imaged by a ChemiDoc™ MP System and LI-COR Odyssey® CLx for UV-visible and NIR fluorescence respectively.

Reagents were purchased from Alfa Aesar, ACROS Organic, Fluorochem and Sigma

Aldrich, and used as received. Microwave reactions were conducted using a CEM Benchmate microwave reactor and were carried out in 10 mL sealed reaction vessels. The specific programming is stated in the synthetic method. Dry solvents were obtained through drying over molecular sieves applying the method of Williams *et al.*³³² Rotary evaporation under reduced pressure and a vacuum oven were used to remove solvent.

All reactions were monitored by thin-layer chromatography (TLC) on Fluorochem 60 Å 40-63 micron UV indicator (F-254) silica gel plates. Purification was carried out using normal phase silica (Fluorochem LC60A 35-70µm) column chromatography and aluminium oxide (Sigma Aldrich neutral Brockmann I, 58 Å). Size exclusion column chromatography was carried out using Amicon® Ultra – 0.5 mL MWCO 30 kDa centrifugal filters and PD-10 desalting column MWCO < 5000 Da for the proteins and PD MiniTrap G-10 column MWCO < 700 Da for the peptide.

Tripeptide of Tyr-Gly-Ala **88** was synthesised and kindly provided by Dr. Michael Reithofer and was characterised using ¹H, ¹³C and COSY NMR and MS.

Cyclic peptide (FC131) **93** was synthesised and kindly provided by Rhiannon Lee and was characterised by HPLC, MS and HRMS.

PD derivatives **95**, antibody **96** and antibody platforms **97** were synthesised and prepared by Dr. Antoine Maruani and characterised by ¹H, ¹³C-NMR, HRMS (PDs) and UV-visible spectroscopy, SDS-PAGE and MS (antibody platforms).

Intermediate **35** and **77** was not separated from the reactions.

7.2 Methods

7.2.1 SDS-PAGE procedure

Bioconjugates were characterized by sodium dodecyl sulfate-polyacrylamide gel electrophoresis (SDS-PAGE). The samples (7 µL) were first prepared with a concentration between 20-50 µg/L and under non-reducing conditions with the addition of LDS samples loading buffer (3 µL), the loading buffer contained 40% (w/v) glycerol, 4% (w/v) LDS, 4% Ficoll 400, 0.8M triEtOHamine-Cl pH 7.6, 0.025% phenol red and 0.025% coomassie G250 and 2 mM EDTA disodium. The samples were then denatured

in a heated water bath at around 90-100°C. The casted 4% stacking, 12 % separating gel with 12 wells was placed in the Bio-rad mini-PROTEAN Tetra Cell caster and chamber. The running buffer used was 0.1% (w/v) SDS in 125 mM Tris-glycine buffer (pH 8.9) and was prepared by 10× dilution from the purchased concentrated buffer. Each sample was loaded into the corresponding cell and the chamber was filled with running buffer submerging the gel. A constant voltage of 180 V was applied with variable current and power. The electrophoresis proceeded for 30 mins. The gel was then imaged by ChemiDoc™ MP System and LI-COR Odyssey® CLx to observe fluorescence. Followed by staining with coomassie blue solution and reimaged to visualise protein using the same imaging systems.

7.2.2 Purification of protein via size exclusion chromatography and diafiltration

The sample (500 µL) was added to the Amicon® Ultra – 0.5 device that was inserted into a microcentrifuge unit. This was placed into a microcentrifuge and was spun at 14000 rpm for 25 mins, then diafiltrated with aqueous media. The resulting solution was spin upside down at 5000 rpm for 2 mins to recover the concentrated solutes and the collected solutes were diluted into 100 µL for further UV-visible spectroscopic analysis.

7.2.3 Photostability experiment

Photostability experiments were conducted in a 46 mm×12.5 mm×12.5 mm quartz cuvette in PBS p.H 7.4 solution at 298 K under continuous illumination from above the cuvette for 60 mins. The far red NIR light source was a 600 mW Paterson Xenon short arc lamp and equipped with a band pass filter (685-733 nm). The intensity of the light from the same distance was measured with a Macam R203 Radiometer to be 1709.8 Wm⁻². Measurements were taken every 10 min with a Varian Cary 50 Bio UV-visible spectrometer.

7.2.4 Fluorescence quantum yield measurement

Five normalised absorbance solutions for each compound were used for this experiment, and calculated using the equation below³³³:

$$\phi_x = \phi_{ST} \left(\frac{F_x \{1 - \exp(-A_{ST} \ln 10)\}}{F_{ST} \{1 - \exp(-A_x \ln 10)\}} \right) \left(\frac{\eta_x^2}{\eta_{ST}^2} \right)$$

Φ_x is the experimental fluorescence quantum yield of the analyte, Φ_{ST} is the literature fluorescence quantum yield of the standard, F is the integrated fluorescence intensity, A is the absorbance at the excitation wavelength, and n is the refractive index of the solvent. The two reference systems used were cross-calibrated to obtain fluorescein ($\Phi_f = 0.96$ in 0.1 M NaOH)³¹¹ and rhodamine B ($\Phi_f = 0.31$ in water).³¹²

7.2.5 Cell preparation and confocal imaging

7.2.5.1 HeLa cells seeding and incubation conditions

HeLa cells (human cervical adenocarcinoma, 5×10^4 cells/mL) and DMEM were seeded into 35 mm glass base dishes and left to attach overnight. The media was then removed and 5 μ M of conjugate **92a/b/c** was added. The dishes were then returned to the incubator overnight. On day 3, the media was removed, cells were washed with PBS, and fresh complete medium was added before conducting live cell imaging by laser scanning confocal microscope. The laser used was adapted to the absorption maximum of each conjugate:

Control (Ar 405 nm laser),

BODIPY-BSA **92a** (Ar 488 nm laser),

RedBODIPY-BSA **92b** (Ar 514 nm laser),

Aza-BODIPY-BSA **92c** (HeNe 633 nm laser).

7.2.5.2 U87.CXCR4 and U87 cells seeding and incubation conditions

U87 transfected CXCR4 and U87 cells (4×10^4 cells/mL) and DMEM were seeded into 35mm glass base dishes and left to attach overnight. The media was then removed and four different conditions were used:

- 5 μ M / 10 μ M / 20 μ M of the conjugate **94** was added to the U87 transfected CXCR4 cells
- 5 μ M of the conjugate **94** was added to the U87 cells.
- 32 μ M of the FITC-antibody was first incubated with U87.CXCR4 cells at 4 °C for 30 min. Followed by the incubation of 5 μ M of **94** under the same conditions for

another 30 min.

- 5 μ M of the non-conjugated aza-BODIPY **46** to both U87 transfected CXCR4 and U87 cells.

The dishes were incubated at 4°C for 30 min. The diluted conjugate was removed, the cells were washed with PBS and fresh complete medium added before live cell imaging on the confocal microscope. The laser used was adapted to the absorption maximum of conjugate:

Conjugate **94** - Single red channel (HeNe 633 nm laser),

FITC-antibody and Conjugate **94** - Dual green and red channels (Ar 488 nm laser), (HeNe 633 nm laser).

7.2.5.3 BT-474 and MDA-MB-468 cells seeding and incubation conditions

MDA-MB-468 (1×10^4 cells/mL) in DMEM-HG and BT-474 cells (2×10^4 cells/mL) and DMEM-F12 were seeded into 35mm glass base dishes and left to attach overnight. The media [DMEM-HG and DMEM-F12] was then removed and conjugate **99** was added and the dishes was incubated at 4°C for 30 min.

The diluted conjugate was removed, the cells were washed with PBS and fresh complete medium added before live cell imaging on the confocal microscope.

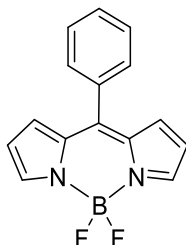
The laser used was adapted to the absorption maximum of conjugate:

Fluorescent antibody conjugate **99** (HeNe 633 nm laser)

7.3 Synthesis

7.3.1 BODIPY

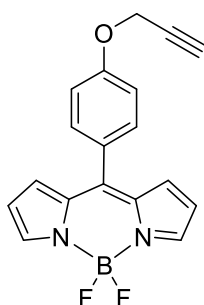
5,5-Difluoro-10-phenyl-5H,10H-514-dipyrrolo[1,2-c:2',1'-f][1,3,2]diazaborinine (1)



To a stirred solution of 5-phenyldipyrromethane (0.90 g, 4.06 mmol) in 80 mL DCM, a solution of DDQ (0.92 g, 4.06 mmol, 1 eq.) in dry DCM (10 mL) was added *via* syringe at 0°C. After stirring for 20 min at rt, TEA (4 mL, 28.7 mmol, 7 eq.) was added dropwise over a period of 5 min and the reaction mixture was stirred for another 30 min at rt. Further, BF₃·Et₂O (5.6 mL, 45.4 mmol, 11 eq.) was added dropwise at 0°C over a period of 10 min and the mixture was stirred for 10 h at rt. Once TLC indicated reaction completion, the reaction mixture was passed through a short pad of silica gel to get rid of the oxidized dipyrromethene derivatives and starting materials. The solvent was removed under reduced pressure and the residue was taken up in DCM (30 mL) and kept for overnight stirring at rt to decompose any unreacted BF₃·Et₂O. The subsequent reaction mixture was extracted with 0.1M HCl (2 × 30mL) to remove excess DDQ, brine (30 mL) and dried over Na₂SO₄ and the solvent was removed under reduced pressure. The crude product was purified by column chromatography on silica (50% DCM:hexane) and precipitated from hexane over DCM to yield a red solid (270 mg, 25%).

$R_f = 0.64$ (silica, 50 % hexane: DCM). UV-vis (DCM): λ_{max} , nm (log ϵ) 498 (4.66). Fluorescence (DCM): λ_{max} , (exc/em) nm 345/522. ¹H-NMR (CDCl₃): δ 6.54 (d, 2H, $J = 3.9$ Hz, Py), 6.94 (d, 2H, $J = 4.3$ Hz, Py), 7.37 – 7.67 (m, 5H, Ph), 7.94 (brs, 2H, Py). ¹³C-NMR (CDCl₃): δ 118.64, 128.54, 130.58, 130.85, 131.73, 133.88, 135.05, 144.22, 147.48. ¹⁹F-NMR (CDCl₃): δ -144.90 (q, 2F, $J = 57.9, 28.8$ Hz). MS: (APCI) m/z 268 (100[M + H]⁺), HRMS: 268.1092 calcd. for (C₁₅H₁₂N₂¹⁰B₁F₂) found 268.1098

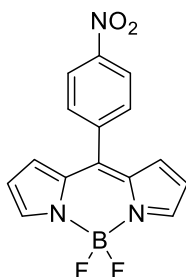
5,5-Difluoro-10-(4-(prop-2-yn-1-yloxy)phenyl)-5H-4[4,5]dipyrrolo[1,2-c:2',1'-f][1,3,2]diazaborinine (2)



4-(Prop-2-yn-1-yloxy)benzaldehyde (1.58 g, 9.89 mmol) was dissolved in freshly distilled pyrrole (17.2 mL, 0.25 mol) and the mixture was degassed with argon for 15 min; trifluoroacetic acid (0.1 mL) was added and the mixture was stirred at rt under argon for 15 min. The excess pyrrole was distilled off under reduced pressure. The oily residue was passed through a short pad of Celite (Hyflo supercell). The solvent was removed under reduced pressure and redissolved in dry DCM (50 mL) and chloranil (2.43 g, 9.89 mmol) was added and stirred for 15 h. DIPEA (18.95 mL, 0.11 mol) was added followed by $\text{BF}_3 \cdot \text{Et}_2\text{O}$ (18.79 mL, 0.15 mol). The solution was stirred at rt for 16 h. The solution was filtered through Celite (Hyflo supercell) and the filtrate was washed with water (4×75 mL) dried over with MgSO_4 , filtered and solvent was removed under reduced pressure. The crude product was purified by column chromatography on silica (30% hexane:DCM) to yield a brown solid (450 mg, 14%).

$R_f = 0.33$ (silica, DCM). Mp 157-158°C, UV-vis (DCM): λ_{max} , nm ($\log \epsilon$) 499 (4.47). Fluorescence (DCM): λ_{max} , (exc/em) nm 450/518. $^1\text{H-NMR}$ (CDCl_3): δ 2.61 (t, 2H, $J = 2.4$ Hz, CH_2), 4.78 (d, 1H, $J = 2.4$ Hz, CH), 6.53 (d, 2H, $J = 4.1$ Hz, Py), 6.95 (d, 2H, $J = 4.1$ Hz, Py), 7.12 (d, 2H, $J = 8.5$ Hz, Ar), 7.53 (d, 2H, $J = 8.5$ Hz, Ar), 7.91 (brs, 2H, Py). $^{13}\text{C-NMR}$ (CDCl_3): δ 56.03, 76.39 ($\text{C}\equiv\text{C}$), 77.92 ($\text{C}\equiv\text{C}$), 114.99, 118.47, 127.19, 131.51, 132.41, 134.91, 143.70, 147.19, 159.96. $^{19}\text{F-NMR}$ (CDCl_3): δ -144.60 (q, 2F, $J = 57.9, 29.2$ Hz). MS: (ESI) m/z 345 (100 [$M + \text{Na}$] $^+$), HRMS: 344.1018 calcd. for ($\text{C}_{18}\text{H}_{13}^{10}\text{BF}_2\text{N}_2\text{ONa}$) found 344.1021.

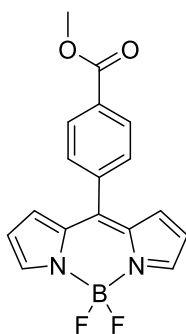
5,5-Difluoro-10-(4-nitrophenyl)-5H-4[1,4,5]dipyrrolo[1,2-c:2',1'-f][1,3,2]diazaborinine (3)²⁰²



4-Nitrobenzaldehyde (1.49 g, 9.89 mmol) was dissolved in freshly distilled pyrrole (17.2 mL, 0.25 mol) and the mixture was degassed with argon for 15 min. Trifluoroacetic acid (0.1 mL) was added and the mixture was stirred at rt under argon for 15 min, the excess pyrrole was distilled off under reduced pressure. The oily residue was passed through a short pad of Celite (Hyflo supercell). Solvent was removed under reduced pressure and redissolved in dry DCM (50 mL) and chloranil (2.43 g, 9.89 mmol) was added and stirred for 15 h. DIPEA (18.95 mL, 0.11 mol) was added followed by BF₃·Et₂O (18.79 mL, 0.15 mol). The solution was stirred at rt for 16 h. The solution was filtered through Celite (Hyflo supercell) and the filtrate was washed with water (4 × 75 mL), dried over with MgSO₄, filtered and the solvent was removed under reduced pressure. The crude product was purified by column chromatography on neutral alumina (20% hexane:DCM) to yield a red solid. (143 mg, 5%).

R_f = 0.49 (silica, DCM). *Mp* 247-248°C. *UV-vis* (DCM): λ_{max} , nm ($\log \epsilon$) 508 (4.27). *Fluorescence* (DCM): λ_{max} , (exc/em) nm 400/543. ¹H-NMR (CDCl₃): δ 6.58 (d, 2H, *J* = 4.2 Hz, Py), 6.84 (d, 2H, *J* = 4.4 Hz, Py), 7.75 (d, 2H, *J* = 8.5 Hz, Ar), 7.99 (brs, 2H, Py), 8.40 (d, 2H, *J* = 8.7 Hz, Ar). ¹³C-NMR (CDCl₃): δ 107.42, 119.49, 123.77, 131.32, 134.62, 139.88, 143.85, 145.66, 149.22. ¹⁹F-NMR (CDCl₃): δ -144.82 (q, 2F, *J* = 57.0, 28.4 Hz). *Mass spec data not obtained.*

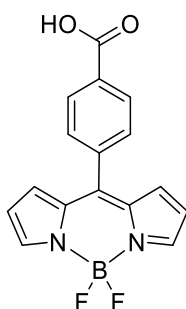
Methyl-4-(5,5-difluoro-5H-4H,5H-dipyrrolo[1,2-c:2',1'-f][1,3,2]diazaborinin-10-yl)benzoate (4)²⁰²



Methyl 4-formylbenzoate (1.62 g, 9.89 mmol) was dissolved in freshly distilled pyrrole (17.2 mL, 0.25 mol) and the mixture was degassed with argon for 15 min. Trifluoroacetic acid (0.1 mL) was added and the mixture was stirred at rt under argon for 15 min. The excess pyrrole was distilled off under reduced pressure. The oily residue was passed through a short pad of Celite (Hyflo supercell). Solvent was removed under reduced pressure and redissolved in dry DCM (50 mL) and chloranil (2.43 g, 9.89 mmol) was added and stirred for 15h. DIPEA (18.95 mL, 0.11 mol) was added followed by BF₃·Et₂O (18.79 mL, 0.15 mol). The solution was stirred at rt for 16 h. The solution was filtered through Celite (Hyflo supercell) and the filtrate was washed with water (4 × 75 mL) dried over with MgSO₄, filtered and reduced under reduced pressure. The crude product was purified by column chromatography on silica using DCM to yield a pink - red solid (1.65 g, 51%).

R_f = 0.53 (silica, DCM). *Mp* 207-209°C. *UV-vis* (DCM): λ_{max} , nm ($\log \epsilon$) 506 (4.77). *Fluorescence* (DCM): λ_{max} , (exc/em) nm 495/530. ¹H-NMR (CDCl₃): δ 3.98 (s, 3H, CH₃), 6.55 (d, 2H, *J* = 3.5 Hz, Py), 6.88 (d, 2H, *J* = 4.3 Hz, Py), 7.63 (d, 2H, *J* = 8.2 Hz, Ar), 7.96 (brs, 2H, Py), 8.19 (d, 2H, *J* = 8.4 Hz, Ar). ¹³C-NMR (CDCl₃): δ 52.65 (CH₃), 119.03, 129.68, 130.50, 131.52, 132.24, 134.81, 138.05, 144.91, 145.83, 166.31(C=O). ¹⁹F-NMR (CDCl₃): δ -144.88 (q, 2F, *J* = 57.4, 28.7 Hz). *MS*: (APCI) *m/z* 326 (100[M + H]⁺), *HRMS*: 326.1147 calcd. for (C₁₇H₁₄N₂O₂¹⁰B₁F₂) found 326.1148.

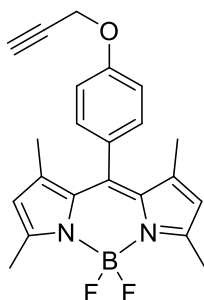
4-(5,5-Difluoro-5H-4l4,5l4-dipyrrolo[1,2-c:2',1'-f][1,3,2]diazaborinin-10-yl)benzoic acid (4a)



To a stirred solution of methyl 4-(5,5-difluoro-5H-4l4,5l4-dipyrrolo[1,2-c:2',1'-f][1,3,2]diazaborinin-10-yl)benzoate (400 mg, 1.28 mmol) in DMF (40 mL) was added a solution of potassium hydroxide (3.47 g, 61.9 mmol) in water (10 mL), and the mixture was stirred at rt overnight. The solvent was removed under reduced pressure, and the residue neutralised with 1M HCl and was removed by filtration and solvent was removed under reduced pressure.

The desired product was not isolated.

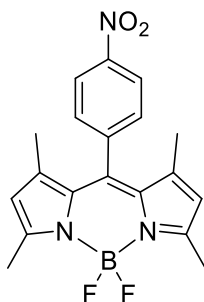
5,5-Difluoro-1,3,7,9-tetramethyl-10-(4-(prop-2-yn-1-yloxy)phenyl)-5H,10H-514-dipyrrolo[1,2-c:2',1'-f][1,3,2]diazaborinine (5)



2,4-Dimethylpyrrole (0.92 g, 8.12 mmol, 2 eq.) and 4-(prop-2-yn-1-yloxy)benzaldehyde (0.65 g, 4.06 mmol, 1 eq.) were dissolved in dry DCM (80 mL) under argon atmosphere. Three drops of trifluoroacetic acid were added and the reaction mixture was stirred overnight at rt. When the aldehyde was consumed (monitored by TLC), a solution of DDQ (0.92 g, 4.06 mmol, 1.2 eq.) in dry DCM (10 mL) was added *via* syringe at 0°C. After stirring for 20 min at rt, TEA (4 mL, 28.7 mmol, 7 eq.) was added dropwise over a period of 5 min and reaction mixture was stirred for another 30 min at rt. Further, BF₃.Et₂O (5.6 mL, 45.4 mmol, 11 eq.) was added dropwise at 0°C over a period of 10 min and the mixture was stirred for 10 h at rt. Once TLC indicated reaction completion, the reaction mixture was passed through a short pad of silica gel to get rid of the oxidized dipyrromethene derivatives and starting materials. The solvent was removed under reduced pressure and the residue was taken up in DCM (30 mL) and kept for overnight stirring at rt to decompose any unreacted BF₃.Et₂O. The subsequent reaction mixture was extracted with 0.1M HCl (2 × 30 mL) to remove excess DDQ, brine (30 mL) and dried over Na₂SO₄ and the solvent was removed under reduced pressure. The crude product was purified by column chromatography on silica (50% hexane: DCM) and precipitated from hexane over DCM to yield a pink solid (43 mg, 3%).

R_f = 0.61 (silica, 50% hexane: DCM). UV-vis (DCM): λ_{max} , nm (log ϵ) 501 (4.64). Fluorescence (DCM): λ_{max} , (exc/em) nm 480/510. ¹H-NMR (CDCl₃): δ 1.41 (s, 6H, CH₃), 2.16 (s, 1H, CH), 2.54 (s, 6H, CH₃), 4.74 (d, 2H, J = 2.4 Hz, CH₂), 5.96 (s, 2H, Py), 7.07 (d, 2H, J = 8.7 Hz, Ar), 7.18 (d, 2H, J = 8.6 Hz, Ar). ¹³C-NMR (CDCl₃): δ 14.66, 29.81, 56.09, 76.00 (C≡C), 78.11 (C≡C), 115.68, 121.26, 128.07, 129.31, 131.85, 141.57, 143.22, 155.44, 158.16. ¹⁹F-NMR (CDCl₃): δ -146.18 (q, 2F, J = 66.2, 32.9 Hz). MS: (ESI) *m/z* 379 (100[M + H]⁺), HRMS: *calcd.* for 378.1824 (C₂₂H₂₂N₂¹⁰BF₂O) *found* 378.1827.

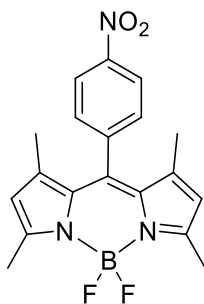
5,5-Difluoro-1,3,7,9-tetramethyl-10-(4-nitrophenyl)-5H-4l4,5l4-dipyrrolo[1,2-c:2',1'-f][1,3,2]diazaborinine (6)



2, 4-Dimethylpyrrole (0.92 g, 8.12 mmol, 2 eq.) and 4-nitrobenzaldehyde (0.61g, 4.06 mmol, 1 eq.) were dissolved in dry DCM (80 mL) under argon atmosphere. Three drops of trifluoroacetic acid were added and the reaction mixture was stirred overnight at rt. When the aldehyde was consumed (monitored by TLC), a solution of DDQ (0.92 g, 4.06 mmol, 1.2 eq.) in dry DCM (10 mL) was added *via* syringe at 0°C. After stirring for 20 min at rt, TEA (4.0 mL, 28.7 mmol, 7 eq.) was added dropwise over a period of 5 min and reaction mixture was stirred for another 30 min at rt. Further, BF₃·Et₂O (5.6 mL, 45.4 mmol, 11 eq.) was added dropwise at 0°C over a period of 10 min and the mixture was stirred for 10 h at rt. Once TLC indicated reaction completion, the reaction mixture was passed through a short pad of Celite (Hyflo supercell). The filtrate was washed with water (3 × 75 mL) and brine (75 mL) and dried over with MgSO₄, filtered and reduced under reduced pressure. The crude product was purified by column chromatography on silica (60% DCM:hexane) to yield a red solid (126 mg, 8%).

R_f = 0.28 (silica, 40% hexane: DCM). *Mp* 270-273°C. *UV-vis* (DCM): λ_{max} , nm (log ϵ) 505 (4.80). *Fluorescence* (DCM): λ_{max} , (exc/em) nm 450/514. ¹H-NMR (CDCl₃): δ 1.35 (s, 6H, CH₃), 2.56 (s, 6H, CH₃), 6.01 (s, 2H, Py), 7.53 (d, 2H, J = 8.5 Hz, Ar), 8.38 (d, 2H, J = 8.7 Hz, Ar). ¹³C-NMR (CDCl₃): δ 22.75, 31.68, 121.95, 124.46, 129.74, 130.72, 138.41, 142.06, 142.61, 148.42, 156.78. ¹⁹F-NMR (CDCl₃): δ -146.11 (q, 2F, J = 65.1, 32.5 Hz). *MS*: (ESI) *m/z* 370 (100[M + H]⁺), *HRMS*: *calcd.* for 369.1569 (C₁₉H₁₉N₃¹⁰BF₂O₂) *found* 369.1571

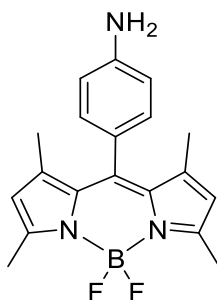
5,5-Difluoro-1,3,7,9-tetramethyl-10-(4-nitrophenyl)-5H-4[14,5]dipyrrolo[1,2-c:2',1'-f][1,3,2]diazaborinine (6a)



4-Nitrobenzaldehyde (302 mg, 2 mmol) and 2,4-dimethylpyrrole (380 mg, 4 mmol) were dissolved in DCM (300 mL). A catalytic amount of trifluoroacetic acid was added, and the solution was stirred overnight at ambient temperature. When TLC monitoring showed complete consumption of the aldehyde, a solution of DDQ (590 mg, 2.6 mmol) was added, and stirring was continued for 10 min. The reaction mixture was washed with water (3×100 mL). The combined organic layers were washed with brine (100 mL), dried over anhydrous Na_2SO_4 , filtered, and removed under reduced pressure. The crude product was purified by 10% MeOH:DCM neutral alumina column chromatography and dried under reduced pressure to constant weight to afford 6 as a crude red amorphous solid. The crude dipyrromethene and DIPEA (4.0 mL, 23.0 mmol) were dissolved in toluene (100 mL) and stirred at ambient temperature for 5 min. $\text{BF}_3 \cdot \text{Et}_2\text{O}$ (3.0 mL, 23.7 mmol) was added, and stirring was continued for 10 min. The reaction mixture was washed with water (3×80 mL), and brine (100 mL), dried over anhydrous Na_2SO_4 , filtered, and removed under reduced pressure. The crude compound was purified by silica gel column chromatography (50% hexane: DCM) to yield a red solid (56 mg, 8%).

UV-vis (DCM): λ_{max} , nm (log ϵ) 505 (4.80). Fluorescence (DCM): λ_{max} , (exc/em) nm 450/514. $^1\text{H-NMR}$ (CDCl_3): δ 2.25 (s, 6H, CH_3), 2.53 (s, 6H, CH_3), 6.05 (s, 2H, Py), 7.53 (d, 2H, $J = 9.0$ Hz, Ar), 7.70 (d, 2H, $J = 9.0$ Hz, Ar). $^{13}\text{C-NMR}$ (CDCl_3): δ 22.72, 29.77, 31.69, 53.47, 121.96, 124.43, 129.73, 142.06, 142.64, 148.42, 156.82. $^{11}\text{B-NMR}$ (CDCl_3): δ -3.16. $^{19}\text{F-NMR}$ (CDCl_3): δ -146.39 (d, $J = 33.3$ Hz), -146.56 (d, $J = 33.1$ Hz). MS: (ESI) m/z 370 (100[M+H] $^+$), HRMS: calcd. for 369.1569 ($\text{C}_{19}\text{H}_{19}\text{N}_3^{10}\text{BF}_2\text{O}_2$) found 369.1571.

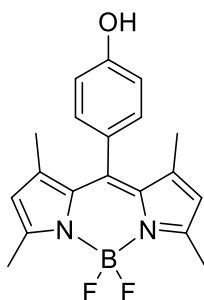
4-(5,5-Difluoro-1,3,7,9-tetramethyl-5H-414,514-dipyrrolo[1,2-c:2',1'-f][1,3,2]diazaborinin-10-yl)aniline (7)



5,5-Difluoro-1,3,7,9-tetramethyl-10-(4-aminophenyl)-5H-414,514-dipyrrolo[1,2-c:2',1'-f][1,3,2]diazaborinine (200.0 mg, 0.54 mmol) and hydrazine (0.40 mL, 12 mmol, 22.20 eq.) along with 10 % Pt/C (76.0 mg, 0.72 mmol, 1.33 eq.) were dissolved in EtOH (8 mL) and refluxed for 1h. The reaction mixture was cooled to 25 °C and filtered through Celite (Hyflo supercell) to remove Pt/C and any solid impurities. The filtrate obtained was then removed under reduced pressure under reduced pressure and purified by flash column chromatography using (50% EtOAc/hexanes) as eluent to yield a yellowish orange solid (111 mg, 60%).

$R_f = 0.63$ (silica, 50% EtOAc:hexane). UV-Vis (DCM): λ_{max} , 500 nm; $(\log \epsilon) = 4.66$. Fluorescence (DCM): λ_{max} (exc/em), 495/511 nm. $^1\text{H-NMR}$ (CDCl_3): δ 1.49 (s, 6H, CH_3), 1.57 (brs, 2H, NH_2), 2.54 (s, 6H, CH_3), 5.96 (s, 2H, Py), 6.78 (d, 2H, $J = 8.4$ Hz, Ar), 7.01 (d, 2H, $J = 8.4$ Hz, Ar). $^{13}\text{C-NMR}$ (CDCl_3): δ 14.65, 115.52, 121.02, 124.80, 129.05, 132.14, 142.74, 143.30, 147.12, 155.05. $^{19}\text{F-NMR}$ (CDCl_3): δ -146.19 (q, 2F, $J = 66.2, 33.0$ Hz). MS: (ESI) m/z 340 ($100[M + H]^+$), HRMS: calcd. for 339.1827 ($\text{C}_{19}\text{H}_{21}\text{N}_3^{11}\text{BF}_2$) found 339.1832.

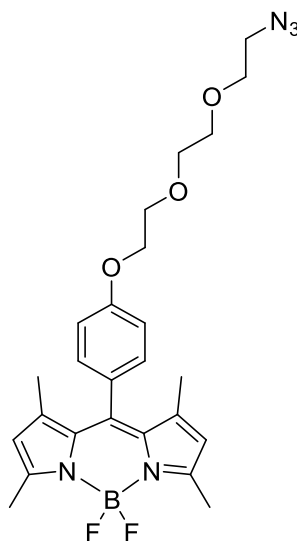
4-(5,5-Difluoro-1,3,7,9-tetramethyl-5H-4(14,5(14)-dipyrrolo[1,2-c:2',1'-f][1,3,2]diazaborinin-10-yl)phenol (9)



2, 4-Dimethylpyrrole (0.92, 8.12 mmol, 2 eq.) and 4-hydroxybenzaldehyde (0.50g, 4.06 mmol, 1 eq.) were dissolved in dry DCM (80 mL) under Ar. Three drops of trifluoroacetic acid were added and the reaction mixture was stirred overnight at rt. When the aldehyde was consumed (monitored by TLC), a solution of DDQ (0.92 g, 4.06 mmol, 1.2 eq.) in dry DCM (10 mL) was added at 0°C. After stirring for 20 min at rt, TEA (4 mL, 28.7 mmol, 7 eq.) was added dropwise over a period of 5 min and reaction mixture was stirred for another 30 min at rt. Further, BF₃·Et₂O (5.6 mL, 45.4 mmol, 11 eq.) was added dropwise at 0°C over a period of 10 min and the mixture was stirred for 10 h at rt. Once TLC indicated reaction completion, the reaction mixture was passed through a short pad of Celite (Hyflo supercell). The filtrate was washed with water (4 × 75 mL) and brine (75 mL) dried over with MgSO₄, filtered and reduced under reduced pressure. The crude product was purified by column chromatography on silica (DCM) to yield a red solid (110 mg, 8%).

R_f = 0.33 (silica, DCM). *Mp* 245-247°C. *UV-vis* (DCM): λ_{max} , nm (log ϵ) 500 (4.80). *Fluorescence* (DCM): λ_{max} , (exc/ems) nm 440/513. ¹H-NMR (CDCl₃): δ 1.44 (s, 6H, CH₃), 2.55 (s, 6H, CH₃), 5.97 (s, 2H, Py), 6.95 (d, 2H, *J* = 8.5 Hz, Ar), 7.13 (d, 2H, *J* = 8.5 Hz, Ar). ¹³C-NMR (CDCl₃): δ 14.66 (CH₃), 29.79 (CH₃), 116.20, 121.22, 127.39, 129.51, 131.89, 141.76, 143.22, 155.41, 156.27. ¹⁹F-NMR (CDCl₃): δ -146.17 (q, 2F, *J* = 66.0, 33.1 Hz). *MS*: (ESI) *m/z* 341(100[M +H]⁺), *HRMS*: *calcd.* for 340.1668 (C₁₉H₂₀N₂¹⁰BF₂O) *found* 340.1673

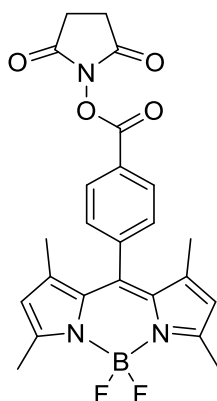
10-(4-(2-(2-(2-Azidoethoxy)ethoxy)ethoxy)phenyl)-5,5-difluoro-1,3,7,9-tetramethyl-5H-4l4,5l4-dipyrrolo[1,2-c:2',1'-f][1,3,2]diazaborinine (10)



To a solution of 4-(5,5-difluoro-1,3,7,9-tetramethyl-5H-4l4,5l4-dipyrrolo[1,2-c:2',1'-f][1,3,2]diazaborinin-10-yl)phenol (68 mg, 0.2 mmol) and anhydrous K_2CO_3 (42 mg, 0.3 mmol, 1.5 eq.) in acetone (10 mL) was added 1-azido-2-(2-(2-bromoethoxy)ethoxy)ethane (476 mg, 2 mmol, 10 eq.). The resulting mixture was heated under reflux overnight. The solvent was removed under reduced pressure and was purified by silica column chromatography (1% MeOH/DCM) to yield red solid (55 mg, 55%)

UV-vis (DCM): λ_{max} , nm (log ϵ) 499 (6.09). Fluorescence (DCM): λ_{max} , (exc/em) nm 480/512. 1H -NMR ($CDCl_3$): δ 1.41 (s, 6H, CH_3), 2.54 (s, 6H, CH_3), 3.40 (t, 2H, $J = 4.8$ Hz, PEG), 3.63-3.74 (m, 4H, PEG), 3.75-3.83 (m, 2H, PEG), 3.92 (t, 2H, $J = 4.6$ Hz, PEG), 4.18 (t, 2H, $J = 4.6$ Hz, PEG), 5.96 (s, 2H, Py), 7.02 (d, 2H, $J = 8.7$ Hz, Ar), 7.15 (d, 2H, $J = 8.7$ Hz, Ar). ^{13}C -NMR ($CDCl_3$): δ 13.90, 36.12, 102.90, 103.03, 103.75, 104.15, 115.34, 115.98, 130.54, 132.23, 136.45, 136.81, 139.15, 141.15, 143.72, 145.35, 147.89. ^{19}F -NMR ($CDCl_3$): δ -146.18 (q, 2F, $J = 66.3, 32.6$ Hz). MS: (ESI) m/z 498 [$M + H^+$], HRMS: calcd. for 497.2519 ($C_{25}H_{31}O_3N_5^{10}BF_2$) found 497.2510.

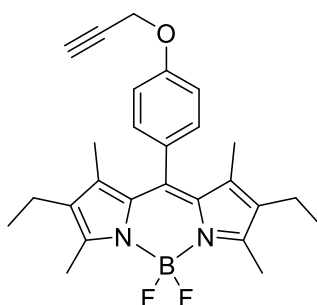
2,5-Dioxopyrrolidin-1-yl-4-(5,5-difluoro-1,3,7,9-tetramethyl-5H-4l4,5l4-dipyrrolo[1,2-c:2',1'-f][1,3,2]diazaborinin-10-yl)benzoate (11)



2, 4-Dimethylpyrrole (0.92 g, 8.12 mmol, 2 eq.) and 2,5-dioxopyrrolidin-1-yl 4-formylbenzoate (1.00g, 4.06 mmol) were dissolved in dry DCM (80 mL) under Ar. Three drops of trifluoroacetic acid were added and the reaction mixture was stirred overnight at rt. When the aldehyde was consumed (monitored by TLC), a solution of DDQ (0.92 g, 4.06 mmol, 1.2 eq.) in dry DCM (10 mL) was added *via* syringe at 0°C. After stirring for 20 min at rt, TEA (4.0 mL, 28.7 mmol, 7 eq.) was added dropwise over a period of 5 min and reaction mixture was stirred for another 30 min at rt. Further, BF₃. Et₂O (5.6 mL, 45.4 mmol, 11 eq.) was added dropwise at 0°C over a period of 10 min and the mixture was stirred for 10 h at rt. Once TLC indicated reaction completion, the reaction mixture was passed through a short pad of Celite (Hyflo supercell) to get rid of the polypyrrole. The filtrate was washed with water (3 × 75 mL) and brine (75 mL) and dried over MgSO₄, filtered and reduced under reduced pressure. The crude product was purified by column chromatography on silica (0-1% MeOH:DCM) to yield a red solid. (165 mg, 9%)

$R_f = 0.71$ (silica, 1% MeOH: DCM). UV-vis (DCM): λ_{max} , nm (log ϵ) 504 (6.09). Fluorescence (DCM): λ_{max} , (exc/ems) nm 490/521. ¹H-NMR (CDCl₃): δ 1.38 (s, 6H, CH₃), 2.56 (s, 6H, CH₃), 2.87 (t, 2H, J = 6.1 Hz, NHS), 3.32 (t, 2H, J = 6.3 Hz, NHS) 6.01(s, 2H, Py), 7.50 (d, 2H, J=8.2Hz, Ar), 8.28 (d, 2H, J=8.3 Hz, Ar). ¹³C-NMR (CDCl₃): δ 14.90, 25.80, 70.16 (NHS), 70.77 (NHS), 121.76, 125.86, 129.13, 130.79, 131.40, 139.30, 142.19, 142.92, 152.70, 156.45 (C=O), 161.37 (C=O), 169.25 (C=O). ¹⁹F-NMR (CDCl₃): δ -146.14 (q, 2F, J = 65.1, 33.0 Hz). MS: (APCI) m/z 465 [M⁺], HRMS: 464.1702 calcd. for (C₂₄H₂₂O₄ N₃¹¹BF₂) found 464.1697.

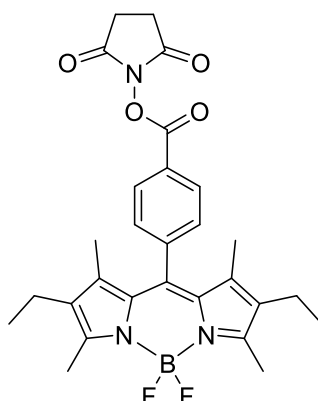
2,8-Diethyl-5,5-difluoro-1,3,7,9-tetramethyl-10-(4-(prop-2-yn-1-yloxy)phenyl)-5H-4l4,5l4-dipyrrolo[1,2-c:2',1'-f][1,3,2]diazaborinine (12)



Kryptopyrrole, (1.00 g, 8.12 mmol, 2 eq.) and 4-(prop-2-yn-1-yloxy) benzaldehyde (0.65 g, 4.06 mmol, 1 eq.) were dissolved in dry DCM (80 mL) under Ar. Three drops of trifluoroacetic acid were added and the reaction mixture was stirred overnight at rt. When the aldehyde was consumed a solution of DDQ (0.92 g, 4.06 mmol, 1.2 eq.) in dry DCM (10 mL) was added *via* syringe at 0°C. After stirring for 20 min at rt, TEA (4.0 mL, 28.7 mmol, 7 eq.) was added dropwise over a period of 5 min and reaction mixture was stirred for another 30 min at rt. Further, BF₃·Et₂O (5.6 mL, 45.4 mmol, 11 eq.) was added dropwise at 0°C over a period of 10 min and the mixture was stirred for 10 h at rt. Once TLC indicated reaction completion, the reaction mixture was passed through a short pad of Celite (Hyflo supercell). The solvent was removed under reduced pressure and the residue was taken up in DCM (30 mL) and kept for overnight stirring at rt to decompose any unreacted BF₃·Et₂O. The subsequent reaction mixture was extracted with 0.1M HCl (2 × 30 mL) to remove excess DDQ, brine (30 mL) and dried over Na₂SO₄ and the solvent was removed under reduced pressure. The crude product was purified by column chromatography on silica using (50% DCM:hexane) to yield a red solid (241 mg, 14%).

R_f = 0.94 (silica, DCM). UV-vis (DCM): λ_{max}, nm (log ε) 525 (4.80). Fluorescence (DCM): λ_{max}, (exc/ems) nm 480/539. ¹H-NMR (CDCl₃): δ 0.98 (t, 6H, J = 7.5 Hz, CH₂-CH₃), 1.32 (s, 6H, CH₃), 1.55 (s, 1H, CH), 2.30 (q, 4H, J = 7.5 Hz, CH₂-CH₃), 2.52 (s, 6H, CH₃), 4.76 (s, 2H, CH₂), 7.08 (d, 2H, J = 8.6 Hz, Ar), 7.19 (d, 2H, J = 8.6 Hz, Ar) ¹³C-NMR (CDCl₃) δ 11.92, 12.58, 14.72, 17.16, 56.12, 75.93 (C≡C), 78.19(C≡C), 115.61, 128.95, 129.59, 131.19, 132.79, 138.49, 139.99, 153.70, 158.03. ¹⁹F-NMR (CDCl₃): δ -145.69 (q, 2F, J = 66.9, 32.6 Hz). MS: (ESI) m/z 435 [M + H⁺], HRMS: calcd. for 434.2450 (C₂₆H₃₀ON₂¹⁰BF₂) found 434.2449.

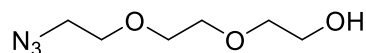
2,5-Dioxopyrrolidin-1-yl-4-(5,5-difluoro-1,3,7,9-tetramethyl-5H-4l4,5l4-dipyrrolo[1,2-c:2',1'-f][1,3,2]diazaborinin-10-yl)benzoate (13)



Kryptopyrrole (0.92 g, 7.48 mmol, 1.84 eq.) and 2,5-dioxopyrrolidin-1-yl 4-formylbenzoate (1.00 g, 4.06 mmol) were dissolved in dry DCM (80 mL) under argon. Three drops of trifluoroacetic acid were added and the reaction mixture was stirred overnight at rt. When the aldehyde was consumed (monitored by TLC), a solution of DDQ (0.92 g, 4.06 mmol, 1.2 eq.) in dry DCM (10 mL) was added at 0 °C. After stirring for 20 min at rt, TEA (4.0 mL, 28.7 mmol, 7 eq.) was added dropwise over a period of 5 min and the reaction mixture was stirred for another 30 min at rt. Further, BF₃·Et₂O (5.6 mL, 45.4 mmol, 11 eq.) was added dropwise at 0°C over a period of 10 min and the mixture was stirred for 10 h at rt. Once TLC indicated reaction completion, the reaction mixture was passed through a short pad of Celite (Hyflo supercell). The filtrate was washed with water (3 × 75 mL) and brine (75 mL) and dried over with MgSO₄, filtered and reduced under reduced pressure. The crude product was purified by column chromatography on silica (0-4% MeOH:DCM) to yield a green solid (355mg, 17%).

R_f = 0.42 (silica, DCM). UV-vis (DCM): λ_{max}, nm (log ε) 529 (6.09). Fluorescence (DCM): λ_{max}, (exc/em) nm 500/550. ¹H-NMR (CDCl₃): δ 0.98 (t, 6H, J= 7.5 Hz, CH₂-CH₃), 1.27 (s, 6H, CH₃), 2.31 (q, 4H, J= 7.5 Hz, CH₂-CH₃), 2.54 (s, 6H, CH₃), 2.96 (brs, 4H, NHS), 7.50 (d, 2H, J= 8.1 Hz, Ar), 8.26 (d, 2H, J= 8.1 Hz, Ar). ¹³C-NMR (CDCl₃): δ 12.21, 12.67, 14.68, 17.15, 25.81, 26.83, 114.44, 121.96, 125.62, 129.42, 131.31, 133.39, 134.03, 138.08, 143.09, 165.09 (C=O), 166.69 (C=O), 169.31 (C=O). ¹⁹F-NMR (CDCl₃): δ -145.66 (q, 2F, J = 65.7, 33.2 Hz). MS: (ESI) m/z 520 [M - H⁺], HRMS: 519.2250 calcd. for (C₂₈H₂₉O₄ N₃¹¹BF₂) found 519.2245.

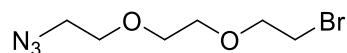
2-(2-(2-Azidoethoxy)ethoxy)ethanol (14)



A solution of 2-(2-(2-chloroethoxy)ethoxy)ethanol (4.22 g, 25 mmol) and sodium azide (2.47 g, 38 mmol, 1.5 eq.) in DMF (250 mL) was heated at 100 °C overnight. The reaction mixture was cooled on an ice bath, filtered and the organic solvent was removed under reduced pressure under reduced pressure. The residue was dissolved in DCM (200 mL), washed with water (75 mL), the water- phase was extracted with additional DCM (75 mL) and the combined organic phases were dried (MgSO₄), filtered and reduced under reduced pressure giving an oil which was used without further purification. (4.35 g, 99 %)

R_f = 0.10 (silica, DCM). ¹H-NMR (CDCl₃): δ 3.31-3.33 (m, 2H, CH₂-N₃), 3.51-3.54 (m, 2H, CH₂-CH₂N₃), 3.59-3.61 (m, 6H, PEG), 3.63-3.66 (m, 2H, CH₂-OH). ¹³C-NMR (CDCl₃): δ 50.67, 61.68, 70.01, 70.38, 70.63, 72.57. MS: (ESI) *m/z* 193 [M +NH₄⁺], HRMS: *calcd. for* 193.1295 (C₆H₁₇O₃N₄) *found* 193.1295

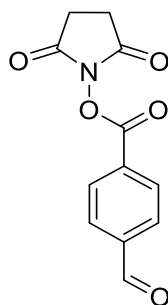
1-Azido-2-(2-(2-bromoethoxy)ethoxy)ethane (15)



2-(2-(2-Azidoethoxy)ethoxy)ethanol (3.0 g, 17.14 mmol) was dissolved in dry DCM (20 mL) and PBr₃ (1.9 mL, 20.57 mmol, 1.2 eq.) was added and heated under reflux for 36 h. It was cooled to 5 °C and the organic layer was washed with aqueous 4% NaHCO₃ solution. The mixture was taken on to the next reaction without further purification. (1.83 g, 45%)

R_f = 0.42 (silica, DCM). ¹H-NMR (CDCl₃): δ 3.31-3.33 (m, 2H, CH₂-N₃), 3.39-3.42 (m, 2H, CH₂), 3.60-3.63 (m, 6H, PEG), 3.73-3.76 (m, 2H, CH₂-Br). ¹³C-NMR (CDCl₃): δ 30.53, 50.69, 70.14, 70.58, 70.68, 71.27. MS: (ESI) *m/z* 255 (100 [M + NH₄]⁺), HRMS: *calcd. for* 255.0451 (C₆H₁₆O₂N₄Br) *found* 255.0455

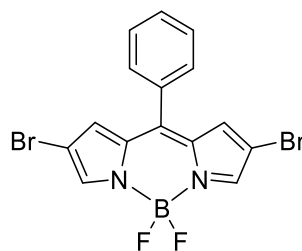
2,5-Dioxopyrrolidin-1-yl 4-formylbenzoate (17)



4-Formylbenzoic acid (3.0 g, 22.4 mmol) and NHS (2.3 g, 20.0 mmol) were dissolved in a mixture of DMF (10 mL) and DCM (27 mL) under an argon atmosphere. The solution was cooled to around 0 °C in an ice–salt bath, followed by gradually adding 4 mL of a DCM solution of DCC (4.1 g, 20.0 mmol) in an airtight reaction vessel. After removing the ice–salt bath, The precipitated *N,N'*-dicyclohexylurea (DCU) was removed by filtration. The solvent was removed under reduced pressure and the remaining solution was frozen in liquid nitrogen and lyophilized to remove the DMF solvent. The dry residue was dissolved in 2-propanol (135 mL) under reflux. The hot solution was immediately filtered and then cooled to rt. Subsequently, the precipitate was collected by filtration and dried under vacuum at 45°C for 24 h. A white product was obtained. (3.28g, 66%)

Mp 165-168 °C. ¹H-NMR (CDCl₃): δ 2.93 (brs, 4H, NHS), 8.01 (d, 2H, J= 8.4 Hz, Ar), 8.30 (d, 2H, J= 8.4 Hz, Ar), 10.13 (s, 1H, CHO). ¹³C-NMR (CDCl₃): δ 25.77 (CH₂), 129.82, 131.29, 134.05, 140.42, 159.41 (C=O), 161.15 (C=O), 169.01 (C=O), 191.24 (HC=O). MS: (APCI) *m/z* 248 (100[M +H]⁺), HRMS: *calcd. for* 248.0553 (C₁₂H₁₀O₅N₁) *found* 248.0550

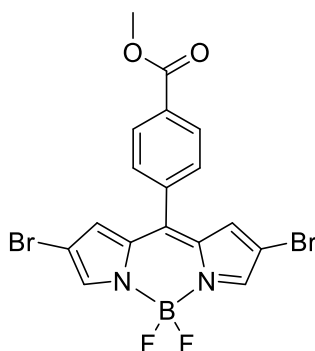
**2,8-Dibromo-5,5-difluoro-10-phenyl-5H-4(14,5)14-dipyrrolo[1,2-c:2',1'
f][1,3,2]diazaborinine (18)²¹³**



To a solution of 5,5-difluoro-10-phenyl-5H,10H-5(14,5)14-dipyrrolo[1,2-c:2',1'-f][1,3,2]diazaborinine (100 mg, 0.373 mmol) in DMF/DCM (25 mL/ 25 mL) was added dropwise to a solution of NBS (159 mg, 0.895 mmol) in DCM (15 mL) at rt. The mixture was stirred at rt for 2 h. The solvent was removed under reduced pressure, the mixture was purified by column chromatography on silica (50-100% DCM/hexane) to afford a gold-red solid (125 mg, 79%).

R_f = 0.39 (silica, DCM). *Mp.* 198-199°C. *UV-vis* (DCM): λ_{max} , nm ($\log \epsilon$) 540 (4.76). *Fluorescence* (DCM): λ_{max} , (exc/em) nm 500/562. ¹H-NMR (CDCl₃): δ 6.95 (s, 2H, Py), 7.54 (m, 5H, Ph), 7.84 (s, 2H, Py). ¹³C-NMR (CDCl₃): δ 107.32, 128.92, 130.49, 131.64, 131.86, 132.92, 134.74, 144.32, 147.12. ¹⁹F-NMR (CDCl₃): δ -145.68 (q, 2F, *J* = 66.9, 32.9 Hz). *MS*: (APCI) *m/z* 423 (100[M + H]⁺), *HRMS*: 423.9303 *calcd.* for (C₁₅H₁₀N₂¹⁰BBr₂F₂) *found* 423.9309.

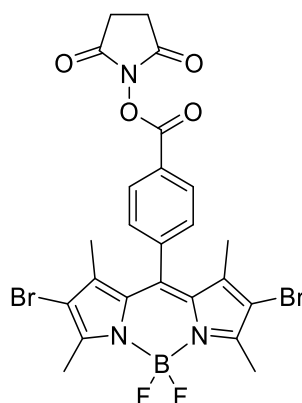
Methyl-4-(2,8-dibromo-5,5-difluoro-5H-4(4,5)14-dipyrrolo[1,2-c:2',1'-f][1,3,2]diazaborinin-10-yl)benzoate (19)



4-(5,5-Difluoro-5H-4(4,5)14-dipyrrolo[1,2-c:2',1'-f][1,3,2]diazaborinin-10-yl)benzoic acid (100 mg, 0.307 mmol) in DMF/DCM (25 ml/ 25 ml) was added dropwise a solution of NBS (159 mg, 0.895 mmol) in DCM (15 mL) at rt and stirred for 2 h. Purification by column chromatography with silica (50% DCM/hexane) yielded a red solid (90 mg, 60%).

R_f = 0.82 (silica, 50% DCM/hexane) UV-vis (water): λ_{max} , nm (log ϵ) 545 (4.76). Fluorescence (water): λ_{max} , (exc/em) nm 540/572. ¹H-NMR (CDCl₃): δ 4.00 (s, 3H, CH₃), 6.91 (s, 2H, Py), 7.62 (d, *J* = 8.1 Hz, 1H), 7.87 (s, 2H, Py), 8.22 (d, *J* = 8.3 Hz, 1H). ¹³C-NMR (CDCl₃) δ 52.75, 107.79, 129.99, 130.40, 131.62, 132.90, 134.55, 136.94, 145.04, 145.41, 166.01. MS: (APCI) *m/z* 480 (100[M]⁺), HRMS: 480.9285 calcd. for (C₁₇H₁₁N₂O₂¹⁰BBr₂F₂) found 480.9288. X-ray crystal structure: C₁₇H₁₁BBr₂F₂N₂O₂.

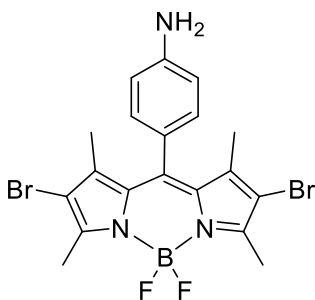
2,5-Dioxopyrrolidin-1-yl-4-(2,8-dibromo-5,5-difluoro-1,3,7,9-tetramethyl-5H-414,514-dipyrrolo[1,2-c:2',1'-f][1,3,2]diazaborinin-10-yl)benzoate (20)²¹²



2,5-Dioxopyrrolidin-1-yl-4-(5,5-difluoro-1,3,7,9-tetramethyl-5H-414,514-dipyrrolo[1,2-c:2',1'-f][1,3,2]diazaborinin-10-yl)benzoate (100 mg, 0.215 mmol), AIBN (70 mg, 0.430 mmol, 2 eq.) and NBS (77 mg, 0.430 mmol, 2 eq) were heated under reflux for 30 min in CCl₄ (10 mL). The solvent was removed under reduced pressure, and purified by silica column chromatography (75% Hexane: EtOAc) to yield a red solid.

The desired product was not isolated

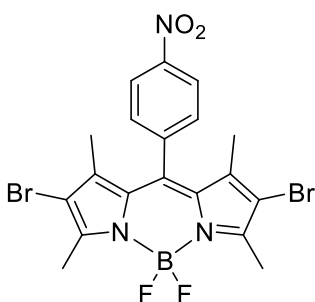
4-(2,8-Dibromo-5,5-difluoro-1,3,7,9-tetramethyl-5H-4,5,14-dipyrrolo[1,2-c:2',1'-f][1,3,2]diazaborinin-10-yl)aniline (21)



4-(5,5-Difluoro-1,3,7,9-tetramethyl-5H-4,5,14-dipyrrolo[1,2-c:2',1'-f][1,3,2]diazaborinin-10-yl)aniline (73 mg, 0.215 mmol), AIBN (70 mg, 0.430 mmol, 2 eq.) and NBS (77 mg, 0.430 mmol, 2 eq.) were heated under reflux for 30 min in CCl₄ (10 ml). The solvent was removed under reduced pressure, and purified by silica column chromatography (75% Hexane: EtOAc) to yield a red solid.

The desired product was not isolated

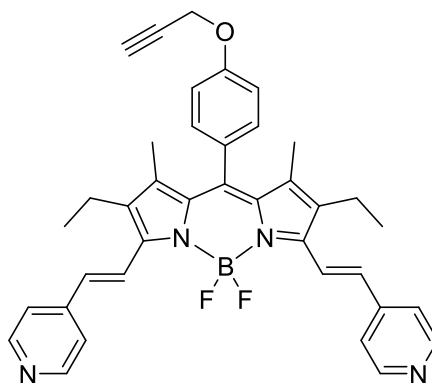
2,8-Dibromo-5,5-difluoro-1,3,7,9-tetramethyl-10-(4-nitrophenyl)-5H-414,514-dipyrrolo[1,2-c:2',1'-f][1,3,2]diazaborinine (22)



To a solution of 5,5-difluoro-1,3,7,9-tetramethyl-10-(4-nitrophenyl)-5H-414,514-dipyrrolo[1,2-c:2',1'-f][1,3,2]diazaborinine (80 mg, 0.217 mmol) in DMF/DCM (20 mL/20 mL) was added dropwise a solution of NBS (92 mg, 0.520 mmol, 2.4 eq.) in DCM (10 mL) at rt. The mixture was stirred at rt for 2 h. The solvent was removed under reduced pressure, the mixture was purified by silica-gel column chromatography (70% DCM/hexane) to provide a gold-red solid (70 mg, 61%).

$R_f = 0.69$ (silica, 70% DCM/hexane) UV-vis (DCM): λ_{max} , nm (log ϵ) 535 (4.90). Fluorescence (DCM): λ_{max} , (exc/ems) nm 580/656. $^1\text{H-NMR}$ (CD_3Cl): δ 1.35 (s, 6H, CH_3), 2.61 (s, 6H, CH_3), 7.52 (d, 2H, Ph, $J=8.4$ Hz), 8.42 (d, 2H, Ph, $J=8.6$ Hz). $^{13}\text{C-NMR}$ (CD_3Cl) δ 13.93, 14.15, 29.81, 112.59, 124.74, 129.63, 138.66, 140.07, 141.30, 148.73, 155.37. $^{19}\text{F-NMR}$ (CD_3Cl) δ -145.81 (q, 2F, $J = 63.1, 31.7$ Hz). MS: (ESI) m/z 526 [M^+], HRMS: calcd. for 504.9723 ($\text{C}_{19}\text{H}_{16}^{10}\text{BFN}_3\text{O}_2\text{Br}_2$) found 504.9723

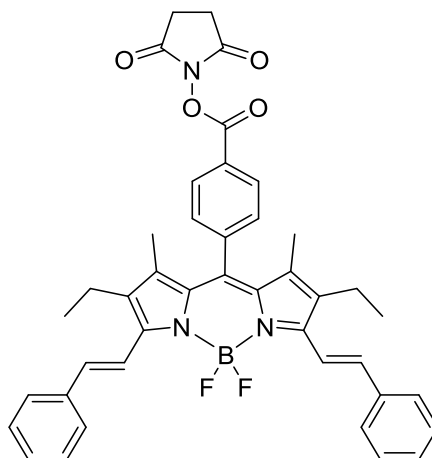
2,8-Diethyl-5,5-difluoro-1,9-dimethyl-10-(4-(prop-2-yn-1-yloxy)phenyl)-3,7-bis((E)-2-(pyridin-4-yl)vinyl)-5H-4l4,5l4-dipyrrolo[1,2-c:2',1'-f][1,3,2]diazaborinine²²⁸ (23)



2,8-Diethyl-5,5-difluoro-1,3,7,9-tetramethyl-10-(4-(prop-2-yn-1-yloxy)phenyl)-5H-4l4,5l4-dipyrrolo[1,2-c:2',1'-f][1,3,2]diazaborinine (65 mg, 0.15 mmol) was dissolved in dry EtOH (1 mL). 4-Pyridinecarboxaldehyde (64 mg, 0.6 mmol, 4 eq.) was added, followed by acetic acid (90 mg, 1.5 mmol, 10 eq.) and piperidine (127 mg, 1.5 mmol, 10 eq.). The mixture was put under an argon atmosphere before it was subjected to microwave irradiation (20 min, 130°C, 1 min pre-stirring). After removal of the solvent under reduced pressure the mixture was purified by silica column chromatography to yield blue solid.

The desired product was not isolated.

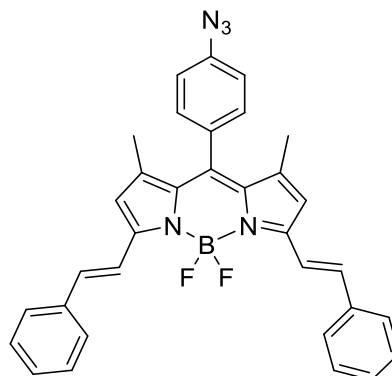
2,5-Dioxopyrrolidin-1-yl-4-(2,8-diethyl-5,5-difluoro-1,9-dimethyl-3,7-di((E)-styryl)-5H-4l4,5l4-dipyrrolo[1,2-c:2',1'-f][1,3,2]diazaborinin-10-yl)benzoate (24)



2,8-Diethyl-5,5-difluoro-1,3,7,9-tetramethyl-10-(4-(prop-2-yn-1-yloxy)phenyl)-5H-4l4,5l4-dipyrrolo[1,2-c:2',1'-f][1,3,2]diazaborinine (78 mg, 0.15 mmol) was dissolved in dry EtOH (1 mL). Benzaldehyde (63 mg, 0.6 mmol, 4 eq.) was added, followed by acetic acid (90 mg, 1.5 mmol, 10 eq.) and piperidine (127 mg, 1.5 mmol, 10 eq.). The mixture was put under an argon atmosphere before it was subjected to microwave irradiation (30 min, 130°C, 1 min pre-stirring). After removal of the solvent under reduced pressure the mixture was purified by silica column chromatography (4% MeOH) to yield a blue solid (28 mg, 27%).

$R_f = 0.83$ (silica, 4% MeOH:DCM). UV-vis (DCM): λ_{max} , nm (log ϵ) 640 (6.09). Fluorescence (DCM): λ_{max} , (exc/em) nm 580/656. $^1\text{H-NMR}$ (CDCl_3): δ 1.16 (t, 6H, $J = 7.5$ Hz, CH_2CH_3), 1.36 (s, 6H, CH_3), 1.72 (brs, 4H, NHS), 2.61 (q, 4H, $J = 7.5$ Hz, CH_2CH_3), 7.26 (d, 2H, $J = 16.8$ Hz, $\text{HC}=\text{CH}$), 7.33 (d, 2H, $J = 7.3$ Hz, *p*-Ph), 7.35 – 7.46 (m, 6H, *o*-Ph, Ar), 7.56 (d, 2H, $J = 8.1$ Hz, Ar), 7.63 (d, 4H, $J = 7.3$ Hz, *m*-Ph), 7.79 (d, 2H, $J = 16.8$ Hz, $\text{HC}=\text{CH}$). $^{13}\text{C-NMR}$ (CDCl_3): δ 11.88, 14.16, 18.45, 24.68, 120.10, 127.50, 127.90, 128.78, 128.85, 128.90, 132.97, 134.18, 136.24, 137.17, 137.38, 138.92, 150.74, 155.47, 162.54 (C=O), 169.63 (C=O). $^{19}\text{F-NMR}$ (CDCl_3): δ -138.87 (q, 2F, $J = 67.4, 33.1$ Hz).

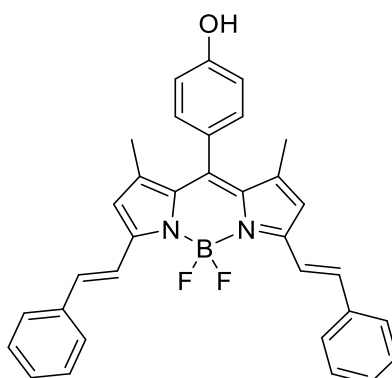
10-(4-Azidophenyl)-5,5-difluoro-1,9-dimethyl-3,7-di((E)-styryl)5H-414,514-dipyrrolo[1,2-c:2',1'-f][1,3,2]diazaborinine (25)



10-(4Azidophenyl)-5,5-difluoro-1,3,7,9-tetramethyl-5H-414,514-dipyrrolo[1,2-c:2',1'-f][1,3,2]diazaborinine (9 mg, 0.025 mmol) was dissolved in dry MeCN (4 mL), and benzaldehyde (11 mg, 0.10 mmol, 4 eq.) was added, followed by acetic acid (14 μ L, 0.25 mmol, 10 eq.) and pyrrolidine (20 μ L, 0.25 mmol, 10 eq.). The reaction mixture was heated under reflux at 80 °C and the colour turned from red to dark blue. The reaction was monitored by TLC until the formation of the product occurred. After 30 min, the reaction was complete, and the mixture was allowed to cool to rt and the solvent was removed under reduced pressure. The product was purified by column chromatography on silica (50% DCM/hexane) to yield a dark blue solid (10 mg, 74%).

$R_f = 0.75$ (silica, 50% DCM:hexanes). UV-vis (DCM): λ_{max} , nm (log ϵ) 625 (5.21). Fluorescence (DCM): λ_{max} , (exc/ems) nm 570/635. $^1\text{H-NMR}$ (CDCl_3): δ 1.50 (s, 6H, CH_3), 6.66 (s, 2H, Py), 7.18 (d, 2H, $J = 8.4$ Hz, Ar), 7.27 (d, 2H, $J = 16.2$ Hz, $\text{HC}=\text{CH}$), 7.32–7.34 (m, 4H, Ar, *p*-Ph), 7.41 (t, 4H, $J = 7.4$ Hz, *m*-Ph), 7.64 (d, 4H, $J = 7.4$ Hz, *o*-Ph), 7.74 (d, 2H, $J = 16.2$ Hz, $\text{HC}=\text{CH}$). $^{13}\text{C-NMR}$ (CDCl_3): δ 15.0, 29.8, 118.1, 119.3, 119.8, 127.7, 128.9, 129.1, 130.2, 131.8, 133.5, 136.6, 136.6, 138.0, 141.2, 142.0, 152.9. $^{19}\text{F-NMR}$ (CDCl_3): δ -138.02 (q, 2F, $J = 66.9, 32.7$ Hz). MS: (ESI) m/z 542 (100[$\text{M} + \text{H}$] $^+$), HRMS: calcd for 541.2358 ($\text{C}_{33}\text{H}_{27}\text{N}_5^{10}\text{BF}_2$) found 541.2348.

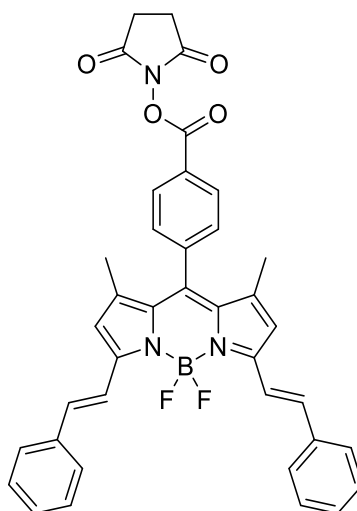
4-(5,5-Difluoro-1,9-dimethyl-3,7-di(E)styryl)-5H-4λ4,5λ4-dipyrrolo[1,2-c:2',1'-f][1,3,2]diazaborin-10-yl) phenol (26)



4-(5,5-Difluoro-1,3,7,9-tetramethyl-5H-4λ4,5λ4-dipyrrolo[1,2-c:2',1'-f][1,3,2]diazaborin-10-yl)phenol (8.5 mg, 0.025 mmol) was dissolved in dry EtOH (4 mL), and benzaldehyde (11 mg, 0.10 mmol, 4 eq.) was added, followed by acetic acid (14 μL, 0.25 mmol, 10 eq.) and pyrrolidine (20 μL, 0.25 mmol, 10 eq.). The reaction mixture was heated under reflux at 90 °C and the colour turned from red to dark blue. The reaction was monitored by TLC until the formation of the product occurred. After 30 min, the reaction was complete, and the mixture was allowed to cool to rt and the solvent was removed under reduced pressure. The product was purified by column chromatography on silica (70% DCM/hexane) to yield a dark blue solid (8.2 mg, 63%).

$R_f = 0.80$ (silica, 70% DCM:hexanes) UV-vis (DCM): λ_{max} , nm (log ϵ) 626 (4.90). Fluorescence (DCM): λ_{max} , (exc/em) nm 600/639. $^1\text{H-NMR}$ (CDCl_3): δ 1.48 (s, 6H, CH_3), 6.65 (s, 2H, Py), 7.23 (d, 2H, $J = 8.2$ Hz, Ar), 7.30 (d, 2H, $J = 15.3$ Hz, $\text{HC}=\text{CH}$), 7.34 (d, 2H, $J = 9.2$ Hz, *p*-Ph), 7.40 (d, 4H, $J = 7.5$ Hz, *m*-Ph), 7.63 (d, 4H, $J = 7.3$ Hz, *o*-Ph), 7.66 (d, 2H, $J = 8.3$ Hz, Ar), 7.72 (d, 2H, $J = 16.3$ Hz, $\text{HC}=\text{CH}$). $^{13}\text{C-NMR}$ (CDCl_3): δ 15.07, 118.11, 119.22, 122.65, 123.42, 127.69, 128.90, 129.14, 130.36, 130.36, 132.21, 132.51, 134.17, 134.58, 136.55, 136.66. $^{19}\text{F-NMR}$ (CDCl_3): δ -138.03 (q, 2F, $J = 66.8, 33.0$ Hz). MS: (APCI) m/z 515 (100[$M + H$] $^+$), HRMS: calcd for 515.2221 ($\text{C}_{33}\text{H}_{27}\text{N}_2\text{O}^{10}\text{BF}_2$) found 515.2216.

2,5-Dioxopyrrolidin-1-yl-4-(5,5-difluoro-1,9-dimethyl-5H-4 λ^4 ,5 λ^4 -dipyrrolo[1,2-c:2',1'-f][1,3,2]diazaborinin-10-yl)benzoate (27)

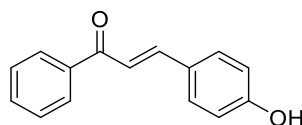


2,5-Dioxopyrrolidin-1-yl-4-(5,5-difluoro-1,3,7,9-tetramethyl-5H-4 λ^4 ,5 λ^4 -dipyrrolo[1,2-c:2',1'-f][1,3,2]diazaborinin-10-yl)benzoate (11.6 mg, 0.025 mmol) was dissolved in dry EtOH (4 mL), and benzaldehyde (11 mg, 0.10 mmol, 4 eq.) was added, followed by acetic acid (14 μ L, 0.25 mmol, 10 eq.) and pyrrolidine (20 μ L, 0.25 mmol, 10 eq.). The reaction mixture was heated under reflux at 90 °C and the colour turned from red to dark blue. The reaction was monitored by TLC until the formation of the product occurred. After 2 h, the reaction was complete, and the mixture was allowed to cool to rt and the solvent was removed under reduced pressure. The product was purified by column chromatography on silica (2% MeOH: DCM) to yield a dark blue solid (3 mg, 20 %).

$R_f = 0.41$ (silica, 2% MeOH: DCM) UV-vis (DCM): λ_{max} , nm (log ϵ) 625 (4.48). Fluorescence (DCM): λ_{max} , (exc/em) nm 600/643. $^1\text{H-NMR}$ (CDCl_3): δ 1.46 (s, 6H, CH_3), 3.43 (t, 2H, $J = 6.5$ Hz, NHS), 3.68 (t, 2H, $J = 6.8$ Hz, NHS), 6.65 (s, 2H, Py), 7.26 (d, 2H, $J = 14.9$ Hz, $\text{HC}=\text{CH}$), 7.32 (t, 4H, $J = 7.3$ Hz, *o*-Ph), 7.36-7.40 (m, 4H, *m*-Ph), 7.40-7.42 (m, 2H, Ar), 7.63 (d, 2H, $J = 7.3$ Hz, *p*-Ph), 7.68 (d, 2H, $J = 8.3$ Hz, Ar), 7.73 (d, 2H, $J = 16.3$ Hz, $\text{HC}=\text{CH}$). $^{13}\text{C-NMR}$ (CDCl_3): δ 14.98 (CH_3), 46.51, 49.84, 127.10, 127.69, 128.12, 128.60, 128.83, 128.90, 129.13, 130.06, 136.57, 136.61, 136.85, 138.01, 142.05, 150.55, 152.95, 168.94 (C=O). $^{19}\text{F-NMR}$ (CDCl_3): δ -138.01 (q, 2F, $J = 67.1, 32.9$ Hz).

7.3.2 Aza-BODIPY

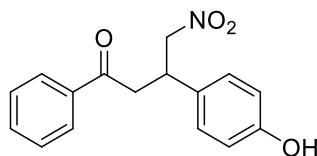
(*E*)-1-(4-Hydroxyphenyl)-3-phenylprop-2-en-1-one (**28**)²⁵⁴



4-Hydroxybenzaldehyde (9.23 g, 76 mmol, 1.2 eq.) and acetophenone (7.35 mL, 63 mmol) were dissolved in MeOH (70 mL) and conc. H₂SO₄ (0.34 mL) was added and the solution was heated under reflux for 16 h. The mixture was cooled and neutralised with NaOH_(aq) and precipitated out with water. The resulting product was filtered and recrystallized from EtOH to yield yellow flakes (9.08 g, 64%).

Mp 246-247°C. ¹H-NMR (CD₃OD): δ 6.85 (d, 2H, *J* = 8.6 Hz, *Ar*), 7.55 (m, 3H, *m,p*-*Ph*), 7.61 (m, 3H, *o-Ph*, HC=CH), 7.75 (d, 1H, *J* = 15.6 Hz, HC=CH), 8.04 (d, 2H, *J* = 8.6 Hz, *Ar*) ¹³C-NMR (CD₃OD): δ 115.66, 118.35, 126.37, 128.18, 128.43, 130.62, 132.63, 138.39, 145.71, 160.48 (C=O). *MS*: (ESI) *m/z* 225 (100[M + H]⁺), *HRMS*: *calcd.* for 225.0910 (C₁₅H₁₃O₂) *found* 225.0909

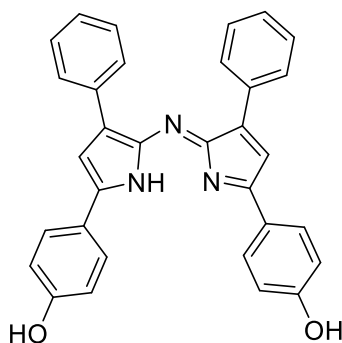
1-(4-Hydroxyphenyl)-4-nitro-3-phenylbutan-1-one (29)²⁵⁴



A solution of 1-(4-hydroxyphenyl)-3-phenylpropenone (6.08 g, 27 mmol) in EtOH (45 mL) was treated with DEA (13.8 mL, 45 mmol, 1.7 eq.) and nitromethane (14.4 mL, 270 mmol, 10 eq.) and heated under reflux for 16 h. The solution was cooled and acidified with 4 M HCl, partitioned between EtOAc (150 mL) and water (150 mL). The organic layer was separated, dried (Na₂SO₄) and solvent was removed under reduced pressure. The residue was stirred in cold Et₂O (90 mL) for 10 min and filtered to give the product as a colourless solid (6.4 g, 83%).

$R_f = 0.09$ (silica, DCM). M_p 91-93°C. 1H -NMR (CH_3OD): δ 3.41 (d, 1H, $J = 5.4$ Hz, CH_2), 3.42 (d, 2H, $J = 4.8$ Hz, CH_2), 4.16 (p, 1H, $J = 7.1$ Hz, CH), 4.64 (dd, 1H, $J = 12.3, 7.9$ Hz, C-H), 4.79 (dd, 1H, $J = 12.4, 6.8$ Hz, C-H), 6.76 (d, 2H, $J = 8.5$ Hz, Ar), 7.13 (d, 2H, $J = 8.5$ Hz, Ar), 7.46 (t, $J = 7.7$ Hz, 2H, *o*-Ph), 7.53 – 7.66 (m, 1H, *p*-Ph), 7.92 (dd, 2H, $J = 8.3, 1.1$ Hz, *m*-Ph). ^{13}C -NMR (CH_3OD): δ 38.78, 41.75, 65.99, 79.97, 116.02, 128.14, 128.86, 130.90, 133.71, 136.43, 155.43, 197.36. MS: (ESI) m/z 286 ($100[M + H]^+$), HRMS: calcd. for 286.1074(C₁₆H₁₆NO₄) found 286.1076.

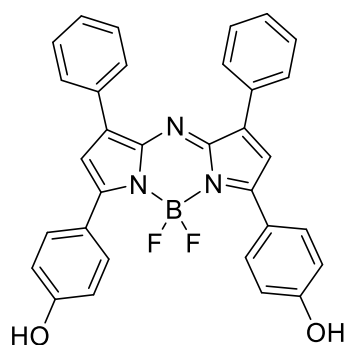
4-(2-((5-(4-Hydroxyphenyl)-3-phenyl-1H-pyrrol-2-yl)imino)-3-phenyl-2H-pyrrol-5-yl)phenol (30)²⁵⁴



1-(4-Hydroxyphenyl)-4-nitro-3-phenylbutan-1-one (6.4 g, 0.0224 mol) and ammonium acetate (56.9 g, 0.855 mol, 40 eq.) in EtOH (250 mL) were heated under reflux for 24 h. The reaction was cooled to rt, the precipitate filtered and the isolated solid washed with cold EtOH (20 mL) to yield the product as a blue-black solid (8.15 g, 75 %).

$R_f = 0.63$ (silica, 4:1 DCM;EtOAc). M_p 243-244 °C. 1H -NMR (DMSO- d_6): δ 6.85 (d, 4H, $J = 8.3$ Hz, *m*-Ph), 7.49 (s, 2H, Py), 7.70-7.83 (m, 6H, *m,p*-Ph), 7.96 (dt, 8H, $J = 24.5, 8.4$ Hz, *o*-PhOH, *o*-Ph), 9.82 (s, 1H, OH). ^{13}C -NMR (DMSO- d_6): δ 114.03, 116.08, 124.46, 127.03, 129.96, 130.79, 130.87, 132.14, 142.73, 149.22, 155.28, 159.39. MS: (ESI) m/z 483 (100[$M + H$]⁺), HRMS: calcd.482.1863 for ($C_{32}H_{24}N_3O_2$) found 482.1853.

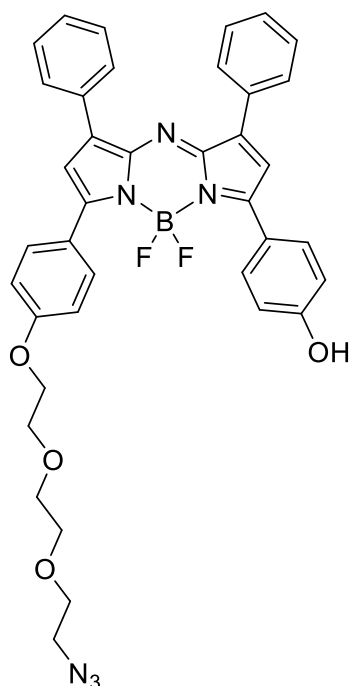
4,4'-(5,5-Difluoro-1,9-diphenyl-5H-4H,5H4-dipyrrolo[1,2-c:2',1'-f][1,3,5,2]triazaborinine-3,7-diyl)diphenol (31)²⁵⁴



4-(2-((5-(4-Hydroxyphenyl)-3-phenyl-1H-pyrrol-2-yl)imino)-3-phenyl-2H-pyrrol-5-yl)phenol (1.5 g, 3.1 mmol) was dissolved in dry DCM (15 mL), added with DIPEA (5.4 mL, 31.1 mmol, 10 eq.) and $\text{BF}_3 \cdot \text{Et}_2\text{O}$ (5.5 mL, 43.5 mmol, 14 eq.), and stirred under Ar for 24 h. The reaction mixture was diluted with EtOAc (300 mL), washed with water (300 mL) and the solvent was removed under reduced pressure. Purification by column chromatography on silica (75% DCM/EtOAc) yielded the product as a red metallic solid (1.18 g, 72 %).

$R_f = 0.76$ (silica, 75% DCM:EtOAc). Mp. 255-256 °C. UV-vis (DCM): λ_{max} , nm ($\log \epsilon$) 660 (6.09). Fluorescence (DCM): λ_{max} , (exc/em) nm 630/690. $^1\text{H-NMR}$ (CHCl_3): δ 6.88 (d, 4H, *m*-PhOH), 7.08 (s, 2H, Py), 7.46 (m, 6H, *m,p*-Ph), 8.04 (m, 8H, *o*-Ph-OH, *o*-Ph). OH was not observed. $^{13}\text{C-NMR}$ (CDCl_3): δ 115.98, 117.20, 124.96, 128.61, 129.55, 130.71, 131.23, 131.94, 145.17, 145.50, 158.01, 159.11. $^{19}\text{F-NMR}$ (CDCl_3): δ -131.34 (q, 2F, $J = 62.5, 30.6$ Hz). MS: (ESI) m/z 530 ($100[M+H]^+$), HRMS: 529.1882 calcd. for ($\text{C}_{32}\text{H}_{23}^{10}\text{BF}_2\text{N}_3\text{O}_2$) found 529.1876.

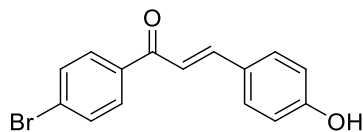
4-(7-(4-(2-(2-(2-Azidoethoxy)ethoxy)ethoxy)phenyl)-5,5-difluoro-1,9-diphenyl-5H-4l4,5l4-dipyrrolo[1,2-c:2',1'-f][1,3,5,2]triazaborinin-3-yl)phenol (32)



4,4'-(5,5-Difluoro-1,9-diphenyl-5H-4l4,5l4-dipyrrolo[1,2-c:2',1'-f][1,3,5,2] triazaborinine-3,7-diyl)diphenol (375 mg, 0.70 mmol) and NaH (60% oil dispersion, 60 mg, 2.60 mmol, 3.7 eq.) were stirred in dry THF (40 mL) and treated with 1-((2-(2-(2-azidoethoxy)ethoxy)ethyl)toluolsulfonate (60 mg, 1.8 mmol, 2.6 eq.) at 0 °C under Ar. The reaction was warmed to rt and then heated under reflux for 3 h. The reaction mixture was cooled, and the solution was extracted with EtOAc (50 mL) and washed with brine (100 mL). The organic layer was dried (Na₂SO₄) and the solvent removed under reduced pressure. Purification by column chromatography on silica (50% hexane/EtOAc) to yield product as a red blue metallic solid. (221 mg, 46%).

R_f = 0.61 (silica, 50% hexane: EtOAc). Mp 218-220 °C. UV-vis (DCM): λ_{max} , nm (log ϵ) 654 (6.09). Fluorescence (DCM): λ_{max} , (exc/em) nm 630/690. ¹H-NMR (CDCl₃): δ 3.42 (t, 2H, J = 10.0 Hz, PEG), 3.72-3.79 (m, 6H, PEG), 3.92 (t, 2H, J = 9.7 Hz, PEG), 4.24 (t, 2H, J = 9.7 Hz, PEG), 6.91-6.93 (m, 4H, 2,5-*o*-PhOH), 7.00 (s, 1H, Py), 7.02 (s, 1H, Py), 7.46-7.48 (m, 6H, *m,p*-Ph), 7.99-8.03 (m, 8H, 4,6-*m*-PhOH, *o*-Ph). OH were not observed. ¹³C-NMR (CDCl₃): δ 50.77, 67.62, 69.81, 70.28, 70.85, 71.05, 114.95, 115.79, 117.57, 125.45, 125.58, 128.62, 129.58, 130.75, 131.03, 131.24, 131.91, 157.32, 159.21, 160.22. ¹⁹F-NMR (CHCl₃): δ -130.82 (q, 2F, J = 62.5, 31.5 Hz). MS: (ESI) *m/z* 687 (100[M + H]⁺), HRMS: 687.2733 calcd. for (C₃₈H₃₄¹⁰BF₂N₆O₄) found 686.2735.

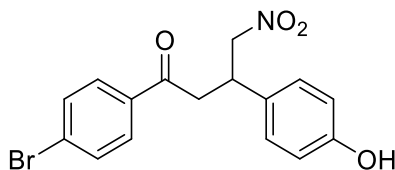
(E)-1-(4-Bromophenyl)-3-(4-hydroxyphenyl)prop-2-en-1-one (28a)



4-Hydroxybenzaldehyde (9.23 g, 76 mmol, 1.2 eq.) and 4-bromoacetophenone (12.53 g, 63 mmol) were dissolved in MeOH (70 mL) and conc. H₂SO₄ (0.34 mL) was added and the solution was heated under reflux for 16 h. The mixture was cooled and neutralised with NaOH_(aq) and precipitated out with water. The resulting product was filtered and washed with cold EtOH to yield a yellow solid (6.30 g, 33%).

¹H-NMR (CD₃OD): δ 6.84 (d, 2H, J = 8.7 Hz, Ar), 7.53 (d, 2H, J=15.4 Hz, HC=CH), 7.61 (d, 2H, J = 8.7 Hz, Ar), 7.68 (d, 2H, J = 8.7 Hz, Ar), 7.75 (d, 2H, J = 15.6 Hz, HC=CH), 7.94-7.96 (d, 2H, J = 8.5 Hz, Ar). ¹³C-NMR (CD₃OD): δ 115.67, 117.80, 126.26, 127.37, 129.95, 130.71, 131.72, 137.28, 146.07, 160.59, 189.98 (C=O). MS: (ESI) m/z 303 (100[M +H]⁺), HRMS: calcd. for 303.0015 (C₁₅H₁₂O₂Br) found 303.0020.

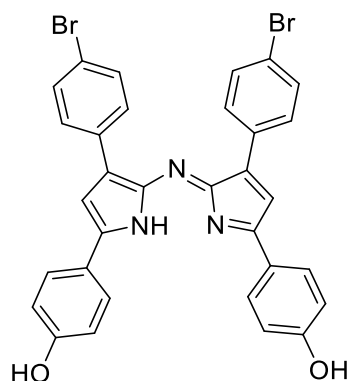
1-(4-Bromophenyl)-3-(4-hydroxyphenyl)-4-nitrobutan-1-one (29a)



A solution of 1-(4-bromophenyl)-3-(4-hydroxyphenyl)prop-2-en-1-one (2.7 g, 9 mmol) in EtOH (15 mL) was added with DEA (4.6 mL, 45 mmol, 5 eq.) and nitromethane (4.8 mL, 90 mmol, 10 eq.) and heated under reflux for 16 h. The solution was cooled and acidified with 4 M HCl, partitioned between EtOAc (50 mL) and water (50 mL). The organic layer was separated, dried (Na_2SO_4) and solvent was removed under reduced pressure. The residue was stirred in cold Et_2O (30 mL) for 10 min and filtered to give the product as a colourless solid (2.4 g, 73%).

$^1\text{H-NMR}$ (CD_3OD): δ 3.31 – 3.57 (m, 2H, CH_2NO_2), 4.04 (dq, 1H, $J = 9.1, 6.8$ Hz, CH), 4.68 (dd, , 1H, $J = 12.6, 9.0$ Hz, C-H), 4.83 (dd, 1H, $J = 12.5, 6.2$ Hz, C-H), 6.70 (d, 2H, $J = 8.5$ Hz, Ar), 7.12 (d, 2H, $J = 8.7$ Hz, Ar), 7.63 (d, 2H, $J = 8.7$ Hz, Ar), 7.82 (d, 2H, $J = 8.4$ Hz, Ar). $^{13}\text{C-NMR}$ (CD_3OD): δ 39.05, 41.48, 79.64, 115.20, 127.98, 128.55, 129.58, 130.28, 131.71, 135.70, 156.52, 197.32 (C=O). MS: (ESI) m/z 364 (100[M + H] $^+$), HRMS: calcd. for 364.0179 ($\text{C}_{16}\text{H}_{15}\text{O}_4\text{NBr}$) found 364.0181.

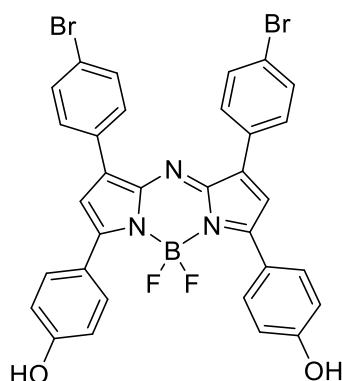
(Z)-4-(3-(4-Bromophenyl)-2-((3-(4-bromophenyl)-5-(4-hydroxyphenyl)-1H-pyrrol-2-yl)imino)-2H-pyrrol-5-yl)phenol(Z)-4-(3-(4-bromophenyl)-2-((3-(4-bromophenyl)-5-(4-hydroxyphenyl)-1H-pyrrol-2-yl)imino)-2H-pyrrol-5-yl)phenol (30a)



1-(4-Bromophenyl)-3-(4-hydroxyphenyl)-4-nitrobutan-1-one (1.93 g, 5.3 mmol) and ammonium acetate (13.5 g, 175 mmol, 33 eq.) in EtOH (50 mL) were heated under reflux for 24 h. The reaction was cooled to rt, the precipitate filtered and the isolated solid washed with cold EtOH (20 mL) to yield blue-black solid (340 mg, 10 %).

Due to the poor solubility no NMRs were obtained. MS: (ESI) m/z 640 (100[M + H]⁺), HRMS: calcd. for 638.0073 (C₃₂H₂₂O₂N₃Br₂) found 638.0061.

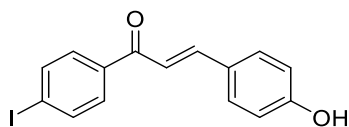
4,4'-(1,9-Bis(4-bromophenyl)-5,5-difluoro-5H-4,5,14-dipyrrolo[1,2-c:2',1'-f][1,3,5,2]triazaborinine-3,7-diyl)diphenol (31a)



(Z)-4-(3-(4-Bromophenyl)-2-((3-(4-bromophenyl)-5-(4-hydroxyphenyl)-1H-pyrrol-2-yl)imino)-2H-pyrrol-5-yl)phenol(Z)-4-(3-(4-bromophenyl)-2-((3-(4-bromophenyl)-5-(4-hydroxyphenyl)-1H-pyrrol-2-yl)imino)-2H-pyrrol-5-yl)phenol (198 mg, 0.31 mmol) was dissolved in dry DCM (15 mL), added with DIPEA (0.54 mL, 3.11 mmol, 10 eq.) and $\text{BF}_3 \cdot \text{Et}_2\text{O}$ (0.55 mL, 4.35 mmol, 14 eq.), and stirred under Ar for 24 h. The reaction mixture was diluted with EtOAc (30 mL), washed with water (30 mL) and the solvent was removed under reduced pressure. Purification by column chromatography on silica eluting with DCM/EtOAc (4:1) gave the product as a dark blue solid (37 mg, 17%).

The desired product was not isolated.

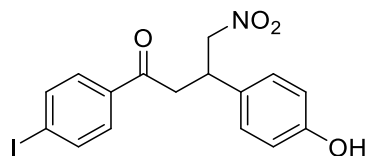
(E)-3-(4-Hydroxyphenyl)-1-(4-iodophenyl)prop-2-en-1-one (28b)



4-Hydroxybenzaldehyde (2.31 g, 19.0 mmol, 1.2 eq.) and 4-iodoacetophenone (3.88 g, 15.8 mmol) were dissolved in MeOH (40 ml) and conc. H₂SO₄ (0.12 ml) was added and the solution was heated under reflux for 16 h. The mixture was cooled and neutralised with NaOH_(aq) and precipitated out with water. The resulting product was filtered and washed with cold EtOH to yield a yellow solid (2.99 g, 54 %).

¹H-NMR (CD₃OD): δ 6.80 (d, 2H, J= 8.5 Hz, Ar), 7.51 (d, 2H, J=15.5 Hz, C=C), 7.60 (d, 2H, J= 8.4 Hz, Ar), 7.73 (d, 2H, J= 15.5 Hz, C=C), 7.78 (d, 2H, J=8.6 Hz, Ar), 7.89 (d, 2H, J=8.4 Hz, Ar). ¹³C-NMR (CD₃OD): δ 100.57, 115.72, 117.75, 129.61, 130.72, 136.37, 137.85, 146.09, 198.37 (C=O). MS: (ESI) m/z 350 (100[M +H]⁺), HRMS: calcd. for 350.9876 (C₁₅H₁₂O₂I) found 350.9878.

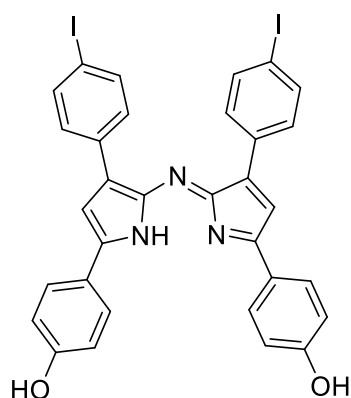
3-(4-Hydroxyphenyl)-1-(4-iodophenyl)-4-nitrobutan-1-one (29b)



A solution of 1-(4-iodophenyl)-3-(4-hydroxyphenyl)prop-2-en-1-one (2.7 g, 7.7 mmol) in EtOH (15 mL) was added with DEA (3.9 mL, 38.5 mmol, 5 eq.) and nitromethane (4.12 mL, 77 mmol, 10 eq.) and heated under reflux for 16 h. The solution was cooled and acidified with 4 M HCl, partitioned between EtOAc (50 mL) and water (50 mL). The organic layer was separated, dried (Na₂SO₄) and solvent was removed under reduced pressure. The residue was stirred in cold MeOH over water for 30 min and filtered to give the product as a colorless solid (2.5 g, 78%).

¹H-NMR (CD₃OD): δ 3.28 – 3.51 (m, 2H, CH₂NO₂), 4.01 (dq, 1H, J = 9.1, 6.8 Hz, CH), 4.64 (dd, , 1H, J = 12.6, 9.0 Hz, C-H), 4.80 (dd, 1H, J = 12.5, 6.2 Hz, C-H), 6.66 (d, 2H, J = 8.5 Hz, Ar), 7.09 (d, 2H, J = 8.7 Hz, Ar), 7.63 (d, 2H, J = 8.5 Hz, Ar), 7.82 (d, 2H, J = 8.4 Hz, Ar). ¹³C-NMR (CD₃OD): δ 18.47, 25.23, 100.54, 115.16, 128.53, 129.31, 129.61, 136.38, 137.85, 142.83, 148.14, 189.32 (C=O). MS: (ESI) m/z 429 (100[M + NH₄]⁺), HRMS: calcd. for 429.0306(C₁₆H₁₈O₄ArI) found 429.0302

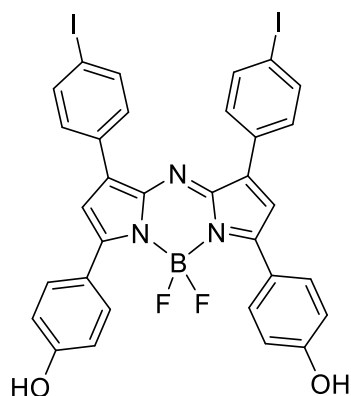
4-(2-((5-(4-Hydroxyphenyl)-3-iodophenyl-1H-pyrrol-2-yl)imino)-3-iodophenyl-2H-pyrrol-5-yl)phenol (30b)



1-(4-Hydroxyphenyl)-4-nitro-3-iodophenylbutan-1-one (2.17 g, 5.3 mmol) and ammonium acetate (13.5 g, 175 mmol, 33 eq.) in EtOH (50 mL) were heated under reflux for 24 h. The reaction was cooled to rt, the precipitate filtered and the isolated solid washed with cold EtOH (20 mL) to yield the product as a blue-black solid (290 mg, 7.5%).

$^1\text{H-NMR}$ (CD_3OD): δ 6.04 (m, 1H, Py), 6.20 (m, 1H, Py), 8.02 (d, 4H, $J = 8.6$ Hz, Ar), 8.48 (d, 4H, $J = 8.5$ Hz, Ar), 9.02 (d, 4H, $J = 8.6$ Hz, Ar), 9.18 (d, 4H, $J = 8.6$ Hz, Ar). $^{13}\text{C-NMR}$ (CD_3OD) δ 101.82, 116.65, 130.18, 130.97, 131.19, 131.89, 132.08, 139.22, 139.26, 158.00, 161.05, 172.60. MS: (API-APCI) m/z 733 ($100[M + H]^+$), HRMS: calcd. for 733.9801 ($\text{C}_{32}\text{H}_{22}\text{O}_2\text{N}_3\text{I}_2$) found 733.9806

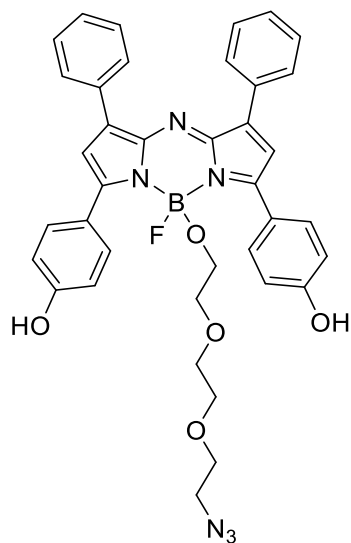
4,4'-(5,5-Difluoro-1,9-bis(4-iodophenyl)-5H-4l4,5l4-dipyrrolo[1,2-c:2',1'-f][1,3,5,2]triazaborinine-3,7-diyl)diphenol (31b)



4-(2-((5-(4-Hydroxyphenyl)-3-iodophenyl-1H-pyrrol-2-yl)imino)-3-iodophenyl-2H-pyrrol-5-yl)phenol (227 mg, 0.31 mmol) was dissolved in dry DCM (15 mL), added with DIPEA (0.54 mL, 3.11 mmol, 10 eq.) and $\text{BF}_3 \cdot \text{Et}_2\text{O}$ (0.55 mL, 4.35 mmol, 14 eq.), and stirred under Ar for 24 h. The reaction mixture was diluted with EtOAc (30 mL), washed with water (30 mL) and the solvent removed under reduced pressure. Purification by column chromatography on silica (75% DCM/EtOAc) to afford the product as a red metallic solid.

The desired product was not isolated.

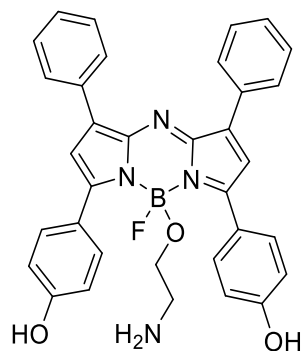
4,4'-(5-(2-(2-(2-Azidoethoxy)ethoxy)ethoxy)-5-fluoro-1,9-diphenyl-5H-4l4,5l4-dipyrrolo[1,2-c:2',1'-f][1,3,5,2]triazaborinine-3,7-diyl)diphenol (33)



2-(2-(2-Azidoethoxy)ethoxy)ethanol (53 mg, 0.3 mmol) were added to a vigorously stirred suspension of aluminium trichloride (41 mg, 0.3 mmol) and 4,4'-(5,5-Difluoro-1,9-diphenyl-5H-4l4,5l4-dipyrrolo[1,2-c:2',1'- f] [1,3,5,2]triazaborinine-3,7-diyl)diphenol (33 mg, 0.062 mmol) in dry DCM (15 mL) that has previously been heated under reflux for 20 min. The mixture was stirred at room temperature for 5 h. The crude product was purified by silica gel column chromatography (60% DCM: EtOAc) to obtain a blue solid.

The desired product was not isolated.

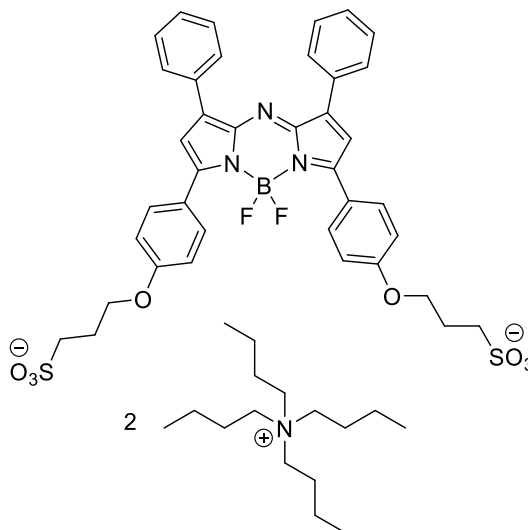
4,4'-(5-(2-Aminoethoxy)-5-fluoro-1,9-diphenyl-5H-4l4,5l4-dipyrrolo[1,2-c:2',1'-f][1,3,5,2]triazaborinine-3,7-diyl)diphenol (34)



4,4'-(5,5-Difluoro-1,9-diphenyl-5H-4l4,5l4-dipyrrolo[1,2-c:2',1'-f][1,3,5,2]triazaborinine-3,7-diyl)diphenol (50 mg, 0.095 mmol) was dissolved in DCM (50 mL). The solution was cooled at 0 °C on an ice–water bath and, under stirring, TMSOTf (0.086 mL, 0.475 mmol, 5 eq.) was added. The reaction was allowed to proceed for 2 min and 30 s. Then, a premixed solution of aminoethanol (0.58 mL, 9.5 mmol, 100 eq.) and DIPEA (0.165 mL, 0.95 mmol, 10 eq.) was rapidly injected into the reaction. The mixture was then extracted with DCM and washed with water. The organics were washed three times with brine, dried (Na₂SO₄) and solvents removed under reduced pressure. Purified on aluminum oxide column (50 % toluene:MeCN) to yield a blue solid.

The desired product was not obtained.

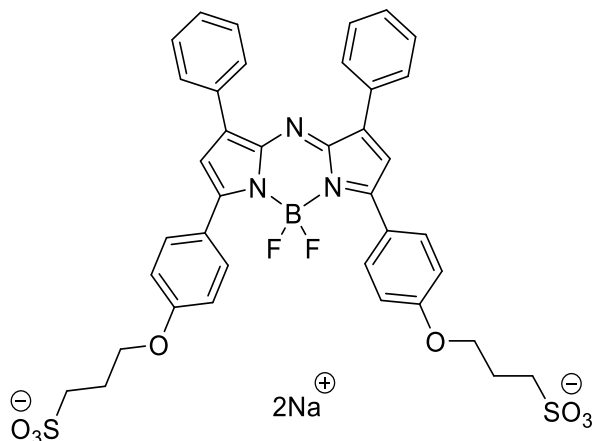
Di(tetrabutylammonium)(3,3'-(((5,5-difluoro-1,9-diphenyl-5H-414,514-dipyrrolo[1,2-c:2',1'-f][1,3,5,2]triazaborinine-3,7-diyl)bis(4,1-phenylene))bis(oxy))bis(propane-1-sulfonate)) (36) ²⁵¹



4,4'-(5,5-Difluoro-1,9-diphenyl-5H-414,514-dipyrrolo[1,2-c:2',1'-f][1,3,5,2]triazaborinine-3,7-diyl)diphenol (164 mg, 0.32 mmol), propane-1,3-sultone (97 mg, 0.80 mmol, 2.5 eq.) and K_2CO_3 (110 mg, 0.80 mmol, 2.5 eq.) were heated under reflux in acetone (60 mL) for 6 h, under Ar atmosphere. The resulting precipitate was filtered, washed with acetone. The compound was transformed into tetrabutylammonium salt by extraction of aqueous solution with DCM in presence of tetrabutylammonium chloride. The organic phase was washed with water (2×20 mL), dried and the solvent was removed under reduced pressure. Purification by column chromatography on silica (1-20% MeOH:DCM) to give the product as a red metallic solid (154 mg, 38%).

$R_f = 0.08$ (silica, DCM). UV-vis (DCM): λ_{max} , nm ($\log \epsilon$) 665 (6.09). Fluorescence (DCM): λ_{max} , (exc/ems) 600/713 nm. 1H -NMR ($CDCl_3$): δ 1.00 (t, 12H, $J = 7.3$ Hz, $NCH_2CH_2CH_2CH_3$), 1.36 (t, 16H, $J = 7.3$ Hz, $NCH_2CH_2CH_2CH_3$), 1.44 (q, 8H, $J = 7.3$ Hz, $NCH_2CH_2CH_2CH_3$), 1.64 (dt, 8H, $J = 15.7, 7.9$ Hz, $NCH_2CH_2CH_2CH_3$), 1.79 (s, 12H), 2.36 (p, 4H, $J = 6.3$ Hz, $CH_2CH_2CH_2$), 3.05 (t, 4H, $J = 6.3$ Hz, $CH_2CH_2CH_2$), 3.12 (q, 8H, $J = 7.3$ Hz, $NCH_2CH_2CH_2CH_3$), 3.23 – 3.32 (m, 8H, $NCH_2CH_2CH_2CH_3$), 4.23 (t, 4H, $J = 6.2$ Hz, $CH_2CH_2CH_2$), 6.91 (s, 2H, Py), 6.98 (d, 4H, $J = 8.8$ Hz, 3,5-*m*-Ar), 7.32 – 7.50 (m, 6H, 3,5-*m*,4-*p*-Ph), 7.78 – 8.12 (m, 8H, 2,6-*o*-Ar). ^{13}C -NMR ($CDCl_3$): δ 13.82, 19.84, 24.11, 25.58, 48.39, 58.87, 67.08, 114.91, 117.50, 125.18, 128.60, 129.56, 130.69, 130.90, 131.97, 143.90, 145.50, 159.06, 160.67. ^{19}F -NMR ($CDCl_3$): δ -130.75 (q, 2F, $J = 62.5, 30.5$ Hz). MS: (ESI) m/z 385 ($100[M-C_{32}H_{72}Ar]^2-$), HRMS: calcd. for 385.0870 ($C_{38}H_{32}^{10}BF_2O_8N_3S_2$) found 385.0870.

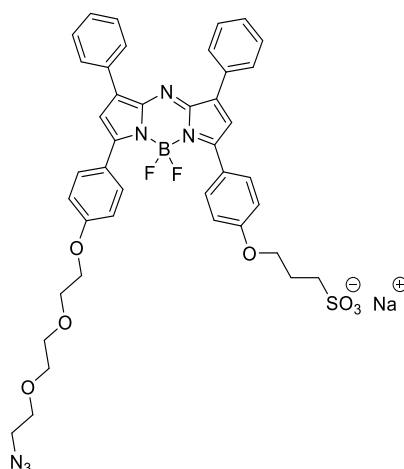
Di(sodium)(3,3'-(((5,5-difluoro-1,9-diphenyl-5H-414,514-dipyrrolo[1,2-c:2',1'-f][1,3,5,2]triazaborinine-3,7-diyl)bis(4,1-phenylene))bis(oxy))bis(propane-1-sulfonate)) (37)



Di(tetrabutylammonium)(3,3'-(((5,5-difluoro-1,9-diphenyl-5H-414,514-dipyrrolo[1,2-c:2',1'-f][1,3,5,2]triazaborinine-3,7-diyl)bis(4,1-phenylene))bis(oxy))bis(propane-1-sulfonate)) (41 mg, 0.033 mmol) was dissolved in MeCN and NaI was added. The mixture was filtered and washed with MeCN to yield product as a solid (26 mg, 98%).

R_f = 0.42 (silica, KNO₃: water:MeCN). HPLC: 5-95% B over 16 minutes. *R_f* = 13.35 minutes. UV-vis (H₂O): λ_{max}, nm (log ε) 735 (6.09). Fluorescence (H₂O): λ_{max}, (exc/em) nm 640/767&822. MS: (ESI) *m/z* 385 (100[M - 2Na]²⁻), HRMS: calcd. for 385.0870 (C₃₈H₃₂¹⁰BF₂O₈N₃S₂) found 385.0868

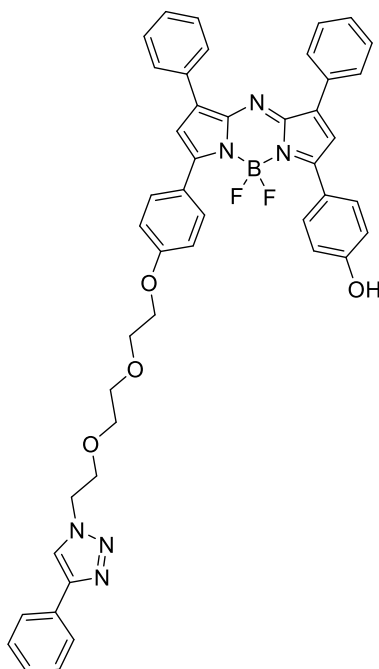
3-(4-(7-(4-(2-(2-(2-Azidoethoxy)ethoxy)ethoxy)phenyl)-5,5-difluoro-1,9-diphenyl-5H-4l4,5l4-dipyrrolo[1,2-c:2',1'-f][1,3,5,2]triazaborinin-3-yl)phenoxy)propane-1-sulfonate (40)



A solution of 4-(7-(4-(2-(2-(2-azidoethoxy)ethoxy)ethoxy)phenyl)-5,5-difluoro-1,9-diphenyl-5H-4l4,5l4-dipyrrolo[1,2-c:2',1'-f][1,3,5,2]triazaborinin-3-yl)phenol (48 mg, 0.07 mmol) in dry acetone (10 mL) was added with 1,3-propane sultone (21 mg, 0.18 mmol, 2.6 eq.) and potassium carbonate (9.6 mg, 0.07 mmol) and the mixture stirred at reflux for 6 h. The reaction mixture was cooled to rt, precipitate filtered and washed with dry acetone (3 × 25 mL). The compound was transformed into Bu₄N⁺ ion salt by extraction of aqueous solution with DCM in presence of TBAC. The organic phase was washed with water (2 × 20 mL), dried and solvent removed under reduced pressure. Purification was carried out by column chromatography on silica eluting with 1-10% MeOH: DCM. The product was dissolved in MeCN and NaI was added, stirred at 0°C until product precipitated. The precipitate was filtered and washed with MeCN to yield a red metallic solid (32 mg, 57%).

R_f = 0.66 (silica, KNO₃:water:MeCN). HPLC: 60-95% B over 9 minutes. *R_f* = 7.51 minutes. UV-vis (MeOH): λ_{max}, nm (log ε) 660 (4.86). Fluorescence (MeOH): λ_{max}, (exc/em) nm 600/710. ¹H-NMR (DMSO-*d*₆): δ 2.07 (q, 2H, *J* = 6.7 Hz, CH₂CH₂CH₂), 2.62 (t, 2H, *J* = 7.5 Hz, CH₂CH₂CH₂), 3.45 (2H, PEG, under *d*-DMSO peak), 3.62–3.64 (m, 6H, PEG), 3.83 (t, 2H, *J* = 4.4 Hz, PEG), 4.22 (t, 2H, *J* = 6.6 Hz, CH₂CH₂CH₂), 4.25–4.27 (m, 2H, PEG), 7.17 (t, 4H, *J* = 8.6 Hz, *m*-Ph), 7.46 (s, 2H, Py), 7.55–7.57 (m, 6H, *p*-Ph, Ar), 8.06–8.08 (m, 4H, *o*-Ph), 8.19 (d, 4H, *J* = 8.5 Hz, Ar). ¹³C-NMR (DMSO-*d*₆): δ 25.8, 48.4, 50.6, 67.6, 68.1, 69.5, 69.9, 70.3, 70.5, 115.6, 119.0, 124.8, 125.0, 129.2, 130.0, 131.4, 131.5, 131.6, 131.6, 131.8, 131.8, 143.6, 143.8, 145.2, 145.3, 149.3, 158.8, 159.1, 160.9, 161.1. ¹⁹F-NMR (DMSO-*d*₆): δ -128.66 (q, 2F, *J* = 63.6, 31.3 Hz). MS: (ESI) *m/z* 807 (100[M – Na]⁻), HRMS: calcd. for 806.2626 (C₄₁H₃₈O₇N₆¹⁰BF₂S) found 806.2611.

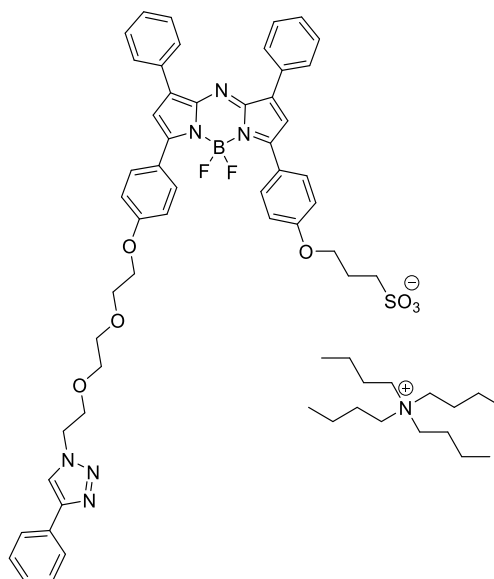
4-(5,5-Difluoro-1,9-diphenyl-7-(4-(2-(2-(2-(4-phenyl-1H-1,2,3-triazol-1-yl)ethoxy)ethoxy)ethoxy)phenyl)-5H-4l4,5l4-dipyrrolo[1,2-c:2',1'-f][1,3,5,2]triazaborinin-3-yl)phenol (41)



4-(7-(4-(2-(2-(2-Azidoethoxy)ethoxy)ethoxy)phenyl)-5,5-difluoro-1,9-diphenyl-5H-4l4,5l4-dipyrrolo[1,2-c:2',1'-f][1,3,5,2]triazaborinin-3-yl)phenol (10 mg, 0.0146 mmol), phenyl acetylene (1.5 mg, 0.015 mmol), sodium ascorbate (2 mg, 0.015 mmol), Cu(II)SO₄·5H₂O (2 mg, 0.008 mmol) and TBTA (2 mg, 0.004 mmol) in THF: water (7:1, 8 mL). The mixture heated to 80°C by MW (200 W, max pressure 17 bar, max stirring) for 40 min. The solvent was removed under reduced pressure and column chromatography in silica (EtOAc: DCM, 4:6) to yield a dark blue solid (10.7 mg, 93 %).

$R_f = 0.50$ (silica, EtOAc:DCM, 4:6). ¹H-NMR (CD₃Cl): δ 3.70 – 3.83 (m, 6H, PEG), 4.04-4.13 (m, 4H, PEG), 4.70 (t, 2H, J = 4.6 Hz, PEG), 6.81 (d, 2H, J = 8.9 Hz, m-Ar), 6.88 (s, 1H, Py), 6.92 (s, 1H, Py), 7.06 (d, 2H, J = 8.8 Hz, o-Ar), 7.33 (t, 2H, J = 7.4 Hz, o-Ph-triazole), 7.37 – 7.54 (m, 8H, o,m-PhOH, m,p-Ph), 7.89 (t, 3H, J = 7.2 Hz, m,p-Ph-triazole), 7.94 – 8.07 (m, 6H, o-Ph), 8.25 (s, 1H, CHN-triazole). ¹³C-NMR (CD₃Cl): δ 51.26, 67.20, 69.71, 70.14, 70.89, 71.57, 114.44, 115.80, 116.36, 117.04, 121.88, 124.03, 125.80, 125.93, 128.57, 128.68, 129.16, 129.50, 129.61, 129.87, 130.48, 130.79, 130.97, 131.29, 131.95, 132.11, 159.78, 160.00. ¹¹B NMR (CD₃Cl): δ -3.88. ¹⁹F-NMR (CD₃Cl): δ -130.64 (q, 2F, J = 62.9, 31.6 Hz). MS: (ESI) m/z 789 (100[M + H]⁺), HRMS: 788.3203 calcd. for (C₄₆H₄₀BF₂O₄N₆) found 788.3214.

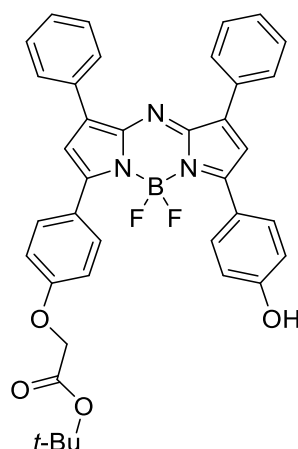
Tetrabutylammonium 3-(4-(5,5-difluoro-1,9-diphenyl-7-(4-(2-(2-(2-(4-phenyl-1H-1,2,3-triazol-1-yl)ethoxy)ethoxy)ethoxy)phenyl)-5H-4l4,5l4-dipyrrolo[1,2-c:2',1'-f][1,3,5,2]triazaborinin-3-yl)phenoxy)propane-1-sulfonate (42)



To a 10 mL microwave tube was added 3-(4-(7-(4-(2-(2-(2-azidoethoxy)ethoxy)ethoxy)ethoxy)phenyl)-5,5-difluoro-1,9-diphenyl-5H-4l4,5l4-dipyrrolo[1,2-c:2',1'-f][1,3,5,2]triazaborinin-3-yl)phenoxy)propane-1-sulfonate (9 mg, 0.0011mmol), phenyl acetylene (1.5 mg, 0.0146 mmol), sodium ascorbate (2 mg), Cu(II)SO₄·5H₂O (2 mg) and TBTA (2 mg) in t-BuOH : water (1:1, 8 mL). The mixture heated to 80 °C by MW (200 W, max pressure, 17 bars, max stirring) for 40 min. The solvent was removed under reduced pressure. The compound was transformed into Bu₄N⁺ ion salt by extraction of aqueous solution with DCM in presence of TBAC. The organic phase was washed with water (2 × 20 mL), dried and solvent removed under reduced pressure and was precipitated from DCM over hexane to yield a dark blue solid (8 mg, 67%).

$R_f = 0.50$ (silica, KNO₃: water:MeCN). ¹H-NMR (CD₃Cl): δ 0.62 – 0.90 (m, 8H, NCH₂CH₂CH₂CH₃), 0.98 (t, 12H, J = 7.2 Hz, NCH₂CH₂CH₂CH₃), 1.42 (sex, 8H, J = 7.2 Hz, NCH₂CH₂CH₂CH₃), 1.52 – 1.71 (m, 8H, NCH₂CH₂CH₂CH₃), 3.23-3.27 (m, 8H, CH₂CH₂CH₂SO₃), 3.71 (d, 4H, J = 20.5 Hz, PEG), 3.90 (d, 4H, J = 21.6 Hz, PEG), 4.20 (d, 4H, J = 8.4 Hz, PEG), 6.90 (s, 2H, Py), 6.97 (dd, 4H, J = 7.8, 5.2 Hz, o-PhO), 7.28 (s, 1H, CHN- triazole), 7.34-7.37 (t, 3H, J = 7.0 Hz, m,p-Ph - triazole), 7.45-7.47 (m, 6H, m,p-Ph), 7.82 (d, 2H, J = 6.5 Hz, m,p-Ph), 8.00-8.02 (m, 8H, 4,6-m-PhO, o-Ph). ¹³C-NMR (CD₃Cl): δ 13.78, 14.23, 19.82, 22.79, 24.11, 29.80, 32.02, 50.49, 53.55, 58.91, 67.69, 69.63, 70.74, 114.94, 117.50, 125.01, 125.53, 125.73, 128.09, 128.59, 128.90, 129.57, 130.66, 130.71, 130.93, 131.96, 141.32, 143.61, 144.11, 145.40, 145.60, 158.84, 159.26, 160.22, 160.80. ¹¹B NMR (CD₃Cl): δ -5.82. ¹⁹F-NMR (CD₃Cl): δ -130.73 (q, 2F, J = 62.4, 30.9 Hz).

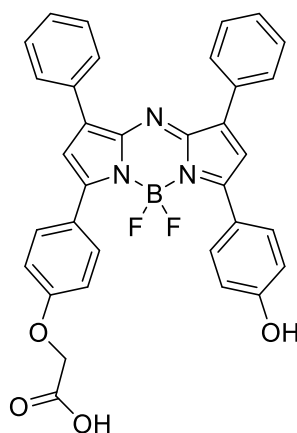
Tert-butyl 2-(4-(5,5-difluoro-7-(4-hydroxyphenyl)-1,9-diphenyl-5H-514,614-dipyrrolo[1,2-c:2',1'-f][1,3,5,2]triazaborinin-3-yl)phenoxy)acetate (43)²⁵²



A solution 4,4'-(5,5-difluoro-1,9-diphenyl-5H-414,514-dipyrrolo[1,2-c:2',1'- f][1,3,5,2]triazaborinine-3,7-diyl)diphenol (378 mg, 0.71 mmol) in dry DMSO (20 mL) was added with CsF (542 mg, 3.57 mmol, 5 eq.) and tert-butylbromoacetate (174 mg, 0.89 mmol, 1.3 eq.). The mixture was stirred at 40 °C for 20 min. The mixture was cooled to 0 °C, a saturated solution of NH₄Cl (30 mL) was added and the product extracted with EtOAc (2 × 30 mL). The combined organic layers were washed with brine, dried (Na₂SO₄) and the solvent was removed under reduced pressure. The residue was purified by column chromatography on silica gel (DCM to 90% DCM: EtOAc) to afford a blue solid (169 mg, 37%).

R_f = 0.90 (silica, 1:9, EtOAc:DCM). *Mp* 198-200 °C. *UV-vis* (DCM): λ_{max} , nm ($\log \epsilon$) 660 (4.96). *Fluorescence* (DCM): λ_{max} , (exc/em) nm 660/688. ¹H-NMR (CDCl₃): δ 1.52 (s, 9H, (CH₃)₃), 4.60 (s, 2H, CH₂), 6.92 (dd, 4H, *J* = 6.7 Hz, 2.0 Hz, *o*-Ar), 6.98 (s, 1H, *Py*), 7.00 (s, 1H, *Py*), 7.46-7.48 (m, 6H, *m,p*-Ph), 7.98-8.05 (m, 8H, *o*-Ph, *m*-Ar). ¹³C-NMR (CDCl₃): δ 28.17, 65.78, 82.83, 114.87, 115.82, 125.58, 126.23, 128.63, 129.60, 130.77, 130.81, 130.99, 131.24, 131.86, 131.88, 157.18, 159.22, 167.84 (C=O). ¹⁹F-NMR (CDCl₃): δ -130.91 (q, 2F, *J* = 62.2, 30.5 Hz). *MS*: (ESI) *m/z* 664 (100[M + H⁺]), *HRMS*: 643.2563 calcd. for (C₃₈H₃₃O₄N₃¹⁰BF₂) found 643.2554

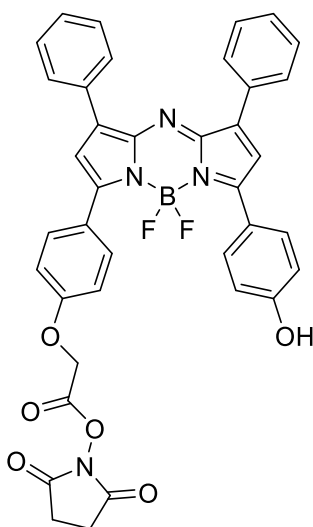
2-(4-(5,5-Difluoro-7-(4-hydroxyphenyl)-1,9-diphenyl-5H-514,614-dipyrrolo[1,2-c:2',1'-f][1,3,5,2]triazaborinin-3-yl)phenoxy)acetic acid (44)²⁵²



A solution of tert-butyl 2-(4-(5,5-difluoro-7-(4-hydroxyphenyl)-1,9-diphenyl-5H-514, 614-dipyrrolo[1,2-c:2',1'-f][1,3,5,2]triazaborinin-3-yl)phenoxy)acetate (169 mg, 0.26 mmol) in dry DCM (5 mL) was added with TFA (1 mL), the mixture stirred at rt for 2 h under Ar and the solvent removed under reduced pressure. The residue was added with DCM (5 mL), the suspension placed under sonication for 5 min, filtered and washed with DCM (40 mL) to yield the product as a dark red metallic solid (145 mg, 95%).

$R_f = 0.70$ (silica, KNO_3 : water:MeCN). Mp 234-235°C. UV-vis (MeOH): λ_{max} , nm (log ϵ) 660 (4.95). Fluorescence (MeOH): λ_{max} , (exc/em) nm 660/715. 1H -NMR (DMSO- d_6): δ 4.83 (s, 2H, CH_2), 6.96 (d, 2H, $J = 8.5$ Hz, *o*-PhOH), 7.11 (d, 2H, $J = 8.6$ Hz, *o*-Ar.), 7.42 (s, 1H, Py), 7.45 (s, 1H, Py), 7.54-7.57 (m, 6H, *m,p*-Ph), 8.06-8.16 (m, 8H, 4,6-*m*-PhO, *o*-Ph), 10.21 (brs, 1H, CO_2H). ^{13}C -NMR (DMSO- d_6): δ 65.15, 115.51, 116.59, 123.51, 125.60, 129.22, 129.90, 129.95, 130.00, 131.36, 131.74, 131.78, 131.84, 159.84, 160.45, 170.55 (C=O). ^{19}F -NMR (DMSO- d_6): δ -128.65 (q, 2F, $J = 63.7, 32.2$ Hz). MS: (ESI) m/z 586 (100[M -H]⁻), HRMS: 585.1791 calcd. for ($C_{34}H_{23}O_4N_3^{10}BF_2$) found 585.1793

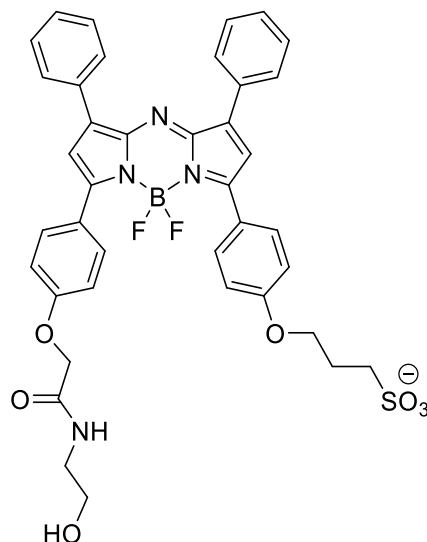
2,5-Dioxopyrrolidin-1-yl 2-(4-(5,5-difluoro-7-(4-hydroxyphenyl)-1,9-diphenyl-5H-514,614-dipyrrolo[1,2-c:2',1'-f][1,3,5,2]triazaborinin-3-yl)phenoxy)acetic acid (45)



To a stirred solution of 2-(4-(5,5-difluoro-7-(4-hydroxyphenyl)-1,9-diphenyl-5H-514,614-dipyrrolo[1,2-c:2',1'-f][1,3,5,2]triazaborinin-3-yl)phenoxy)acetic acid (80 mg, 0.136 mmol) in dry pyridine (10 mL) was slowly added thionyl chloride (0.18 mL, 2.44 mmol, 18 eq.). The reaction was stirred at 50 °C, protected from light and atmospheric moisture, for 30 min. After this period, *N*-hydroxysuccinimide (360 mg, 3.13 mmol, 23 eq.) was added and the mixture maintained under previous condition for 3 h. The solvent was removed under reduced pressure and redissolved in DCM. The organic layer was washed with sat. sodium hydrogen carbonate solution and water, dried (MgSO₄), and the solvent removed under reduced pressure. The crude was precipitated from hexane over DCM to yield product as a dark blue solid.

The desired product was not obtained.

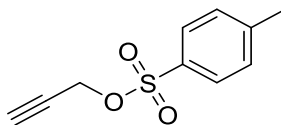
3-(4-(5,5-Difluoro-7-(4-(2-((2-hydroxyethyl)amino)-2-oxoethoxy)phenyl)-1,9-diphenyl-5H-4l4,5l4-dipyrrolo[1,2-c:2',1'-f][1,3,5,2]triazaborinin-3-yl)phenoxy)propane-1-sulfonate (47)



To a 10 mL microwave tube was added 3-(4-(7-(4-(carboxymethoxy)phenyl)-5,5-difluoro-1,9-diphenyl-5H-4l4,5l4-dipyrrolo[1,2-c:2',1'-f][1,3,5,2]triazaborinin-3-yl)phenoxy)propane-1-sulfonate (20 mg, 0.028 mmol), HOBt (20 mg, 0.148 mmol, 5.3 eq.), EDC (20 mg, 0.129 mmol, 4.6 eq.), aminoethanol (0.02 mL, 0.028 mmol) and DIPEA (0.05 mL, 0.287 mmol, 10 eq.) in a solution with DMF (5 mL). Microwave heating (max stirring, 80°C, 1 min pre-stirring) for 1 h. Purification was carried out by counterion exchange to Bu_4N^+ ion salt by extraction of aqueous solution with DCM in presence of TBAC. The organic phase was washed with water (2×20 mL), dried and solvent removed under reduced pressure and was precipitated from DCM over hexane to yield a dark blue solid (15 mg, 71%).

$^1\text{H-NMR}$ ($\text{DMSO-}d_6$): δ 2.33 (t, 2H, $J= 5.4$ Hz, $\text{CH}_2\text{CH}_2\text{CH}_2$), 2.57 (quin, 2H, $J= 5.5$ Hz, $\text{CH}_2\text{CH}_2\text{CH}_2$), 2.68 (t, 2H, $J= 5.3$ Hz, $\text{CH}_2\text{CH}_2\text{CH}_2$), 3.23-3.29 (m, 4H, CH_2CH_2), 4.58 (s, 2H, CH_2), 4.76 (brs, 1H, NH), 6.89 (d, 2H, $J= 6.8$ Hz, 2,5-*o-Ph* (CH_2) $_3\text{SO}_3$), 7.08 (d, 2H, $J= 6.9$ Hz, 2,5-*o-Ar*), 7.51-7.63 (m, 8H, *m,p-Ph*, Py), 7.93-8.10 (m, 8H, 4,6-*m-Ar*, *o-Ph*). $^{11}\text{B NMR}$ ($\text{DMSO-}d_6$): δ -3.55.

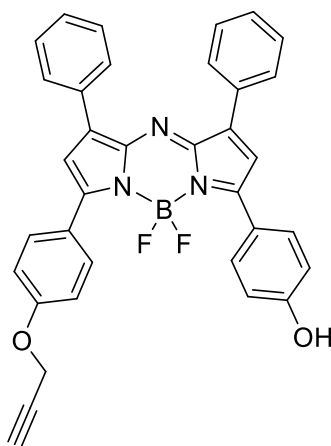
2-Propyn-1-ol-4-methylbenzene sulfonate (propargyl tosylate) (48)



Propargyl alcohol (0.56 g, 10 mmol) and p-toluenesulfonyl chloride (2.28 g, 12 mmol, 1.2 eq.) were dissolved in anhydrous diethyl ether (10 ml) and cooled to -5 °C. Powdered KOH (2.8 g, 50 mmol, 5 eq.) was added in 10 portions and stirred for an hour at -5 °C. The reaction was stirred further at room temperature for 4 h, after which the mixture was poured into cold water (5 mL). The layers were separated and the aqueous layer was extracted with ether (2 × 5 mL) and brine (5 mL). The combined ether extract was dried over anhydrous Na₂SO₄, filtered and dried under reduced pressure to afford a pure dark brownish syrupy liquid (1.79 g, 85%).

¹H-NMR (CDCl₃): δ 2.43 (s, 3H, Tol), 2.48 (t, 1H, J= 2.5 Hz, CH), 4.66 (d, 2H, J= 2.5 Hz, CH₂), 7.33 (d, 2H, J=8.5 Hz, Ar), 7.78 (d, 2H, J=8.4 Hz, Ar). ¹³C-NMR (CDCl₃): δ 21.77, 57.53, 75.42 (C≡C), 77.53 (C≡C), 128.18, 130.01, 132.83, 145.43. MS: (APCI) m/z 211 (100[M + H]⁺), HRMS: 211.0429 calcd. for (C₁₀H₁₁O₃S) found 211.0425

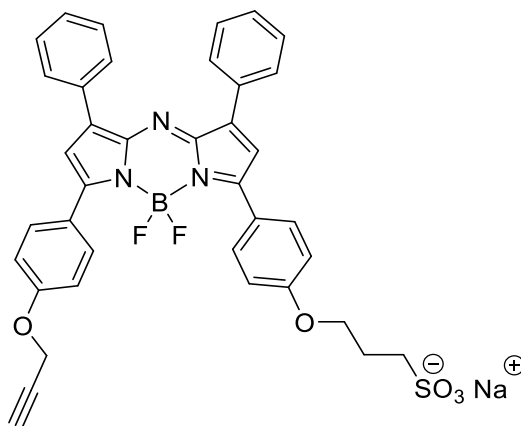
4-(5,5-Difluoro-1,9-diphenyl-7-(4-(prop-2-yn-1-yloxy)phenyl)-5H-4l4,5l4-dipyrrolo[1,2-c:2',1'-f][1,3,5,2]triazaborinin-3-yl)phenol (49)²⁵⁴



4,4'-(5,5-Difluoro-1,9-diphenyl-5H-4l4,5l4-dipyrrolo[1,2-c:2',1'-f][1,3,5,2]triazaborinine-3,7-diyl)diphenol (300 mg, 0.56 mmol) and NaH (60% oil dispersion, 68 mg, 2.08 mmol, 4.4 eq.) were stirred in dry THF (50 mL) at 0 °C under Ar for 5 min and treated with propargyltoluolsulfonate (68 mg, 1.24 mmol, 2.2 eq.). The reaction was stirred at 0 °C for 10 min and warmed to rt and then heated under reflux at 80 °C for 5 h. The reaction mixture was cooled and partitioned between EtOAc (50 mL) and brine (3 × 50 mL). The organic layer was separated, dried over Na₂SO₄ and the solvent removed under reduced pressure. Purification by column chromatography on silica (75% hexane/EtOAc) to yield a red metallic solid (100 mg, 32 %).

$R_f = 0.83$ (silica, 90% DCM: EtOAc). UV-vis (DCM): λ_{max} , nm (log ϵ) 660 (4.99). Fluorescence (DCM): λ_{max} , (exc/em) nm 620/690. ¹H-NMR (CDCl₃): δ 2.59 (s, 1H, CH), 4.78 (s, 2H, CH₂), 6.92 (d, 4H, $J = 7.0$ Hz, *o*-Ar, *o*-Ph), 7.06 (s, 1H, Py), 7.08 (s, 1H, Py), 7.53 – 7.38 (m, 6H, *m,p*-Ph), 8.12 – 7.90 (m, 8H, 4,6-*m*-Ar, *o*-Ph). ¹³C-NMR (CDCl₃): δ 55.93, 60.65, 76.10, 92.35, 115.15, 115.83, 117.74, 117.85, 118.12, 128.67, 129.61, 130.82, 130.98, 131.28, 131.86, 143.60, 143.92. ¹⁹F-NMR (CDCl₃): δ -130.89 (q, 2F, $J = 62.5, 31.1$ Hz). MS: (APCI) m/z 568 (100[M + H]⁺), HRMS: 567.2044 calcd. for (C₃₅H₂₄¹⁰BF₂N₃O₂) found 567.2040

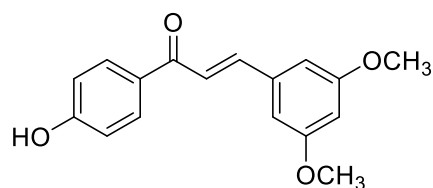
3-(4-(5,5-Difluoro-1,9-diphenyl-7-(4-(prop-2-yn-1-yloxy)phenyl)-5H-4l4,5l4-dipyrrolo[1,2-c:2',1'-f][1,3,5,2]triazaborinin-3-yl)phenoxy)propane-1-sulfonate (50)



A solution of 4-(5,5-difluoro-1,9-diphenyl-7-(4-(prop-2-yn-1-yloxy)phenyl)-5H-4l4, 5l4-dipyrrolo[1,2-c:2',1'-f][1,3,5,2]triazaborinin-3-yl)phenol (40 mg, 0.07 mmol) in dry acetone (10 mL) was treated with 1,3-propane sultone (20 mg, 0.17 mmol, 2.4 eq.) and cesium carbonate (45 mg, 0.14 mmol, 2 eq.) and the mixture heated at reflux for 1h. The reaction mixture was cooled to rt, precipitate filtered and washed with dry acetone (3 × 25 mL). The compound was transformed into Bu₄N⁺ ion salt by extraction of aqueous solution with DCM in presence of TBAC. The organic phase was washed with water (2 × 20 mL), dried and solvent removed under reduced pressure. The product was then dissolved in MeCN and NaI was added, stirred at 0 °C until product precipitated. The precipitate was filtered and washed with MeCN to yield a red metallic solid (45 mg, 90%).

$R_f = 0.62$ (silica, KNO_3 :water:MeCN). UV-vis (MeOH): λ_{max} , nm (log ϵ) 660 (4.54). Fluorescence (MeOH): λ_{max} , (exc/em) nm 640/695. ¹H-NMR (CD₃OD) δ 2.00 (s, 2H, CH₂), 2.24 (p, 2H, $J = 12.8, 6.1$ Hz, CH₂CH₂CH₂), 2.96 (t, 2H, $J = 6.1$ Hz, CH₂CH₂CH₂), 3.07 (s, 1H, HC), 4.15 (t, 2H, $J = 6.1$ Hz, CH₂CH₂CH₂), 7.01 (d, 2H, $J = 8.4$ Hz, 2,5-*o*-Ph(CH₂)₃SO₃), 7.09 (d, 2H, $J = 8.5$ Hz, 2,5-*o*-Ar), 7.15 (s, 2H, Py), 7.16 – 7.70 (m, 6H, 4,6-*m*-Ar, *o*-Ph), 7.70 – 8.19 (m, 8H, *m,p*-Ph). ¹³C-NMR (CD₃OD) δ 27.60, 57.99, 69.17, 69.31, 78.75, 81.01, 100.00, 117.21, 117.58, 120.18, 120.26, 128.24, 130.89, 132.10, 133.30, 133.47, 133.52, 134.34, 134.44, 141.17, 145.97, 147.98. ¹⁹F-NMR (CD₃OD) δ -128.33 (q, 2F, $J = 62.5, 31.1$ Hz). MS: (APCI) m/z 688 (100[M - Na]⁻), HRMS: 687.1931 calcd. for (C₃₈H₂₉¹⁰BF₂N₃O₅S) found 687.1923.

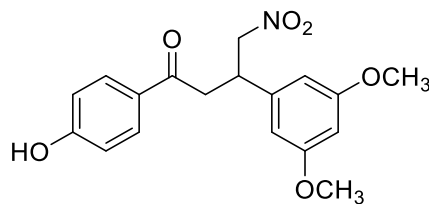
(E)-3-(3,5-Dimethoxyphenyl)-1-(4-hydroxyphenyl)prop-2-en-1-one (51)



To an aqueous alcoholic solution of sodium hydroxide (3 g in 100 mL water and 40 mL EtOH) was added the 4-hydroxyacetophenone (1.63 g, 0.012 mol) with stirring and the reaction mixture was cooled in an ice bath during addition. The mixture was later allowed to warm up to rt and the 2,4-dimethoxybenzaldehyde (1.99 g, 0.012 mol) was added, with vigorous stirring until the product precipitated. After maintaining the mixture at 0 °C for 12 h, the product was filtered, washed with water, dried, and recrystallized from EtOH to yield a white solid (1.55 g, 45%).

Mp 156-159°C. ¹H-NMR (CD₃OD): δ 3.31 (s, 6H, CH₃), 6.55 (t, 1H, J = 2.1 Hz, Ar), 6.90 (d, 2H, J = 8.8 Hz, Ar), 6.90 (d, 2H, J = 4.8 Hz, Ar), 7.65 (d, 1H, J = 15.6 Hz, HC=CH), 7.73 (d, 1H, J = 16.2 Hz, HC=CH) 8.03 (d, 2H, J = 8.6 Hz, Ar). ¹³C-NMR (CD₃OD): δ 54.64, 102.45, 106.08, 115.14, 122.08, 129.55, 131.15, 137.04, 143.93, 161.37, 162.71, 189.45. MS: (ESI) m/z 285 (100[M + H]⁺), HRMS: 285.1121 calcd. for (C₁₇H₁₇O₄) found 285.1124.

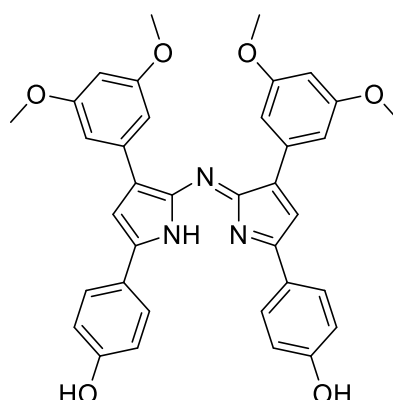
3-(3,5-Dimethoxyphenyl)-1-(4-hydroxyphenyl)-4-nitrobutan-1-one (52)



To a solution of (*E*)-3-(3,5-dimethoxyphenyl)-1-(4-hydroxyphenyl)prop-2-en-1-one (1.33 g, 4.68 mmol) was dissolved in EtOH (40 mL) and added DEA (3.6 mL) and nitromethane (4 mL, 7.47 mmol) and heated under reflux for 24 h. The mixture was neutralised with 4M HCl and extracted with DCM (2 × 20 mL) and dried (MgSO₄). The solvent was removed under reduced pressure. Redissolved in EtOAc and the impurity was removed by filtration when added with Et₂O, the filtrate was collected and TLC to confirm purity. The solvent was removed under reduced pressure to yield a brown oil (723 mg, 45%).

The crude was taken on to the next reaction without further purification.

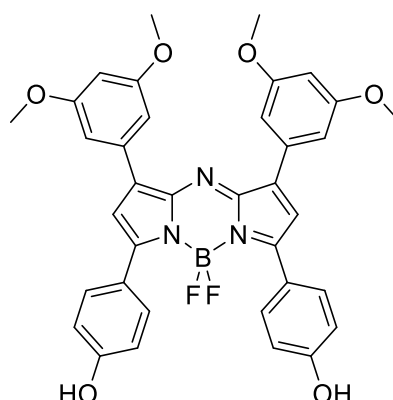
(Z)-4-(3-(3,5-Dimethoxyphenyl)-2-((3-(3,5-dimethoxyphenyl)-5-(4-hydroxyphenyl)-1H-pyrrol-2-yl)imino)-2H-pyrrol-5-yl)phenol (53)



3-(3,5-Dimethoxyphenyl)-1-(4-hydroxyphenyl)-4-nitrobutan-1-one (723 mg, 2.09 mmol) and ammonium acetate (7.6 g, 95 mmol, 46 eq.) were dissolved in EtOH (20 mL) and heated under reflux for 48 h. The precipitated product was filtered, washed with cold EtOH, dried and recrystallized from chloroform to give the product as a dark metallic compound (243 mg, 39%).

$R_f = 0.54$ (silica, 40% EtOAc:DCM). $^1\text{H-NMR}$ (CD_3OD): δ 3.68 (s, 12H, CH_3), 6.46 (d, 2H, $J = 1.6$ Hz, *o*-Ar), 6.81 (q, 2H, $J = 7.1$ Hz, *p*-Ar), 6.97 (d, 4H, $J = 8.4$ Hz, Ar), 7.12 (d, 2H, $J = 1.6$ Hz, *o*-Ar), 7.23 (s, 2H, Py), 7.89 (d, 2H, $J = 8.4$ Hz, Ar). $^{13}\text{C-NMR}$ (CD_3OD) δ 21.23, 100.24, 105.57, 106.54, 107.00, 114.96, 115.92, 128.14, 130.53, 135.71, 135.89, 151.80, 160.80. MS: (ESI) m/z 602 (100[M + H⁺]), HRMS: 602.2286 calcd. for ($\text{C}_{36}\text{H}_{32}\text{N}_3\text{O}_6$) found 602.2280.

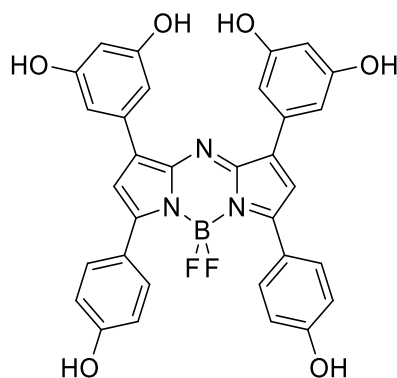
4,4'-(1,9-Bis(3,5-dimethoxyphenyl)-5,5-difluoro-5H-414,514-dipyrrolo[1,2-c:2',1'-f][1,3,5,2]triazaborinine-3,7-diyl)diphenol (54)



(*Z*)-4-(3-(3,5-Dimethoxyphenyl)-2-((3-(3,5-dimethoxyphenyl)-5-(4-hydroxyphenyl)-1H-pyrrol-2-yl)imino)-2H-pyrrol-5-yl)phenol (200 mg, 0.33 mmol) was dissolved in dry DCM (100 mL), was added with DIPEA (2.4 mL, 13.7 mmol, 42 eq.) and BF₃.OEt₂ (2.5 mL, 20.3 mmol, 62 eq.) and stirred under Ar at rt overnight. The reaction mixture was then washed with water and dried (MgSO₄). The solvent was removed under reduced pressure and purified by column chromatography on silica (90% DCM/EtOAc) and precipitated with DCM over hexane and washed with chloroform to give a red metallic solid (65 mg, 30%).

R_f = 0.53 (silica, 90% DCM:EtOAc). UV-vis (MeOH): λ_{max} , nm (log ϵ) 680 (4.94). Fluorescence (MeOH): λ_{max} , (exc/em) nm 640/715. ¹H-NMR (CD₃OD): δ 3.72 (s, 12H, CH₃), 6.51 (t, 2H, *J* = 2.2 Hz, *p*-Ar), 6.90 (d, 4H, *J* = 8.8 Hz, Ar), 7.18 (d, 4H, *J* = 2.2 Hz, *o*-Ar), 7.20 (s, 2H, Py), 8.07 (d, 2H, *J* = 8.9 Hz, Ar). ¹³C-NMR (CDCl₃) δ : 57.06, 104.05, 109.53, 110.29, 117.93, 121.74, 134.49, 136.91, 160.52, 161.82, 163.35, 163.61, 170.12. MS: (ESI) *m/z* 650 (100 [*M* + H⁺]), HRMS: 649.2305 calcd. for (C₃₆H₃₁¹⁰BF₂N₃O₆) found 649.2304.

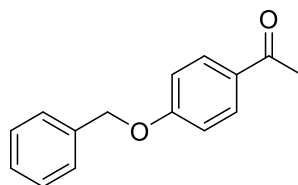
5,5'-(5,5-Difluoro-3,7-bis(4-hydroxyphenyl)-5H-4l4,5l4-dipyrrolo[1,2-c:2',1'-f][1,3,5,2]triazaborinine-1,9-diyl)bis(benzene-1,3-diol) (55)



4,4'-(1,9-Bis(3,5-dimethoxyphenyl)-5,5-difluoro-5H-4l4,5l4-dipyrrolo[1,2-c:2',1'-f][1,3,5,2]triazaborinine-3,7-diyl)diphenol (40 mg, 0.062 mmol) in chloroform (5 mL) was added boron tribromide in hexane (0.24 ml, 0.24 mmol, 4 eq.) dropwise at -78°C , and the mixture stirred under Ar for 24 h. Afterward, water (15 mL) was added and the mixture maintained under previous conditions for 1 h. The solvent was removed under reduced pressure, and the residue was dissolved in DCM/TEA (9:1, 50 mL) and stirred for 10 min at rt. The solution was removed under reduced pressure, and the crude purified by column chromatography on silica to yield product as red metallic solid.

The desired product was not isolated

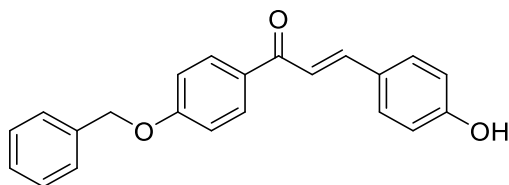
1-(4-(Benzyloxy)phenyl)ethan-1-one (56)



To a solution of 4-hydroxyacetophenone (13.6 g, 100 mmol) in DMF (100 mL) was added K_2CO_3 (20 g, 144 mmol, 1.4 eq.) and benzyl bromide (12 mL, 100 mmol). The reaction was stirred for 1.5 h at ambient temperature, and added water (300 mL) to give a white precipitate. This was filtered and washed with water (50 mL). The crude was redissolved in DCM, and washed with water. The organic layer was extracted with water (125 mL) and brine (125 mL), dried over $MgSO_4$, filtered, and concentrated to yield a white solid (19.9 g, 88%).

Mp 94-96°C. 1H -NMR ($CDCl_3$) δ 2.54 (s, 3H, CH_3), 5.11 (s, 2H, CH_2), 7.00 (d, 2H, $J = 9.0$ Hz, Ar), 7.97 – 7.28 (m, 5H, Ph), 7.93 (d, 2H, $J = 8.8$ Hz, Ar). ^{13}C -NMR ($CDCl_3$) δ 26.47, 70.21, 114.64, 127.58, 128.35, 128.80, 130.61, 130.71, 136.28, 162.71, 196.85 (C=O). MS: (ESI) m/z 227 (100 [$M + H^+$]), HRMS: 227.1067 calcd. for ($C_{15}H_{15}O_2$) found 227.1069.

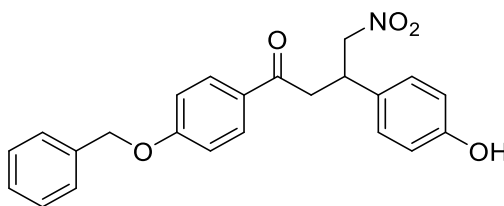
(E)-1-(4-(Benzyloxy)phenyl)-3-(4-hydroxyphenyl)prop-2-en-1-one (57)



4-Hydroxybenzaldehyde (7.32 g, 60 mmol) and 4-benzyloxyacetophenone (15.36 g, 60 mmol) were dissolved in MeOH (60 ml) and conc. H₂SO₄ was added and the solution was refluxed for 16 h. The mixture was cooled and neutralised with NaOH_(aq) and precipitated out with water. The resulting crude was filtered and washed with cold EtOH to yield a yellow solid. (6.36 g, 64%).

R_f = 0.46 (silica, 50% EtOAc:hexane). *Mp* 160-164°C. ¹H-NMR (CD₃OD): δ 5.19 (s, 2H, CH₂), 6.83 (d, 2H, *J* = 8.1 Hz, Ar), 7.12 (d, 2H, *J* = 8.6 Hz, Ar), 7.50 – 7.21 (m, 5H, Ph), 7.58 (d, 1H, *J* = 15.6 Hz, HC=CH), 7.61 (d, 2H, *J* = 8.6 Hz, Ar), 7.73 (d, 1H, *J* = 15.5 Hz, HC=CH), 8.08 (d, 2H, *J* = 8.4 Hz, Ar). ¹³C-NMR (CD₃OD) δ 72.45 (CH₂), 117.13, 118.17, 120.66, 129.07, 129.94, 130.38, 130.87, 133.05, 133.21, 139.33, 147.39, 161.37, 162.87, 165.55, 192.25 (C=O). *MS*: (ESI) *m/z* 331 (100 [M + H⁺]), *HRMS*: 331.1329 *calcd.* for (C₂₂H₁₉O₃) *found* 331.1332.

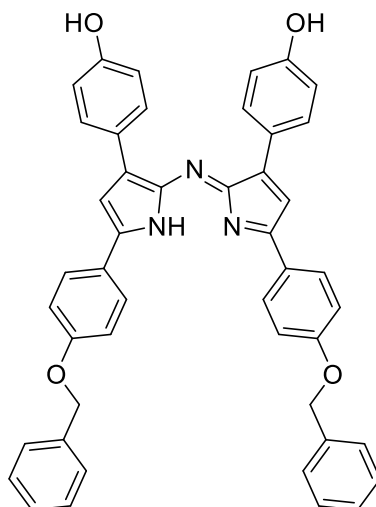
1-(4-(Benzyloxy)phenyl)-3-(4-hydroxyphenyl)-4-nitrobutan-1-one (58)



To a solution of (*E*)-1-(4-(benzyloxy)phenyl)-3-(4-hydroxyphenyl)prop-2-en-1-one (6.20 g, 18.72 mmol) in EtOH (160 mL) was added DEA (14.4 mL, 0.14 mol, 7.4 eq.) and nitromethane (16 mL, 0.30 mol, 16 eq.) and the solution was heated under reflux for 24 h. The mixture was neutralised with 4M HCl and extracted with DCM (2 × 20 mL) and dried (MgSO₄). The solvent was removed under reduced pressure and purified by column chromatography with silica (50 % EtOAc:hexane) to yield a light brown liquid (6.29 g, 86%).

$R_f = 0.42$ (silica, 50% EtOAc:hexane). $^1\text{H-NMR}$ (CD_3OD): δ 3.59 (d, 2H, $J = 16.0$ Hz, CH_2), 4.42 (brs, 1H, CH), 5.16 – 4.85 (m, 2H, CH_2NO_2), 5.31 (s, 2H, CH_2O), 7.13 (d, 2H, $J = 9.8$ Hz, Ar), 7.24 (d, 2H, $J = 8.3$ Hz, Ar), 7.47 (d, 2H, $J = 9.7$ Hz, Ar), 7.81 – 7.49 (m, 5H, Ph), 8.16 (d, 2H, $J = 8.9$ Hz, Ar). $^{13}\text{C-NMR}$ (CD_3OD) δ 42.18, 49.00, 70.88, 80.91, 115.55, 116.46, 128.54, 129.02, 129.49, 129.78, 130.75, 131.39, 131.62, 137.57, 157.58, 164.06, 197.76. MS: (ESI) m/z 392 (100 [$M + \text{H}^+$]), HRMS: 392.1498 calcd. for ($\text{C}_{23}\text{H}_{22}\text{NO}_5$) found 392.1504.

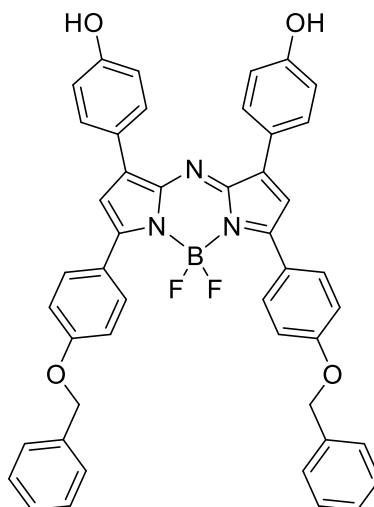
(Z)-4-(3-(4-(Benzyloxy)phenyl)-2-((3-(4-(benzyloxy)phenyl)-5-(4-hydroxyphenyl)-1H-pyrrol-2-yl)imino)-2H-pyrrol-5-yl)phenol (59)



1-(4-(Benzyloxy)phenyl)-3-(4-hydroxyphenyl)-4-nitrobutan-1-one (6.29 g, 16 mmol) and ammonium acetate (27.12 g, 352 mmol, 22 eq.) in EtOH (50 mL) were heated under reflux for 24 h. The reaction was allowed to cool to rt. The precipitated solid was filtered and wash with cold EtOH (3 × 20 mL) to yield a dark metallic solid (2.74 g, 49 %).

$R_f = 0.57$ (silica, 50% THF :hexane). $^1\text{H-NMR}$ (CDCl_3) δ 5.12 (s, 4H, CH_2), 6.77 (d, 4H, $J = 7.5$ Hz, Ar), 6.86 (s, 1H, Py), 6.87 (s, 1H, Py), 6.99-7.01 (m, 6H, Ph), 7.04 (d, 2H, $J = 7.7$ Hz, Ar), 7.13 (d, 4H, $J = 7.6$ Hz, Ar), 7.51 – 7.58 (m, 2H, Ph), 7.70 – 7.79 (m, 2H, Ph), 7.83 – 7.97 (m, 4H, o-Ar), 8.02 (d, 2H, $J = 7.1$ Hz, Ar). $^{13}\text{C-NMR}$ ($\text{DMSO-}d_6$) δ 56.52, 70.02, 115.89, 116.27, 124.94, 128.37, 128.54, 128.65, 129.04, 130.56, 130.60, 137.21, 142.06, 148.92, 154.31, 160.69, 174.83. MS: (ESI) m/z 694 (100 [$M + \text{H}^+$]), HRMS: 694.2700 calcd. for ($\text{C}_{46}\text{H}_{36}\text{N}_3\text{O}_4$) found 694.2697.

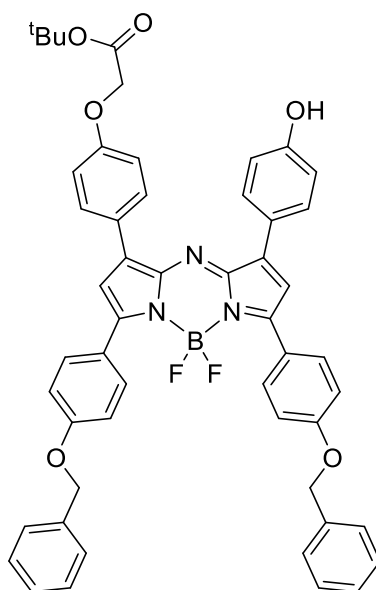
4,4'-(1,9-Bis(4-(benzyloxy)phenyl)-5,5-difluoro-5H-4,5,14,14-dipyrrolo[1,2-c:2',1'-f][1,3,5,2]triazaborinine-3,7-diyl)diphenol (60)



(*Z*)-4-(3-(4-(Benzyloxy)phenyl)-2-((3-(4-(benzyloxy)phenyl)-5-(4-hydroxyphenyl)-1H-pyrrol-2-yl)imino)-2H-pyrrol-5-yl)phenol (1.07 g, 1.55 mmol) was dissolved in dry CH_2Cl_2 (75 mL), treated with diisopropylethylamine (2.7 mL, 15.6 mmol, 10 eq.) and $\text{BF}_3 \cdot \text{OEt}_2$ (2.75 mL, 21.8 mmol, 14 eq.), and stirred under Ar for 24 h. The reaction mixture was diluted with EtOAc (150 mL), washed with water (300 mL) and the organic layer was separated and the solvent was removed under reduced pressure. Purification by column chromatography on silica (50% THF/hexane) gave the product as a red metallic solid (644 mg, 56%).

$R_f = 0.53$ (silica, 90% DCM:EtOAc) and 0.65 (silica, 50% THF :hexane). UV-vis (MeOH): λ_{max} , nm (log ϵ) 695 (5.03). Fluorescence (MeOH): λ_{max} , (exc/em) nm 670/722. $^1\text{H-NMR}$ (THF- d_8) δ 5.18 (s, 4H, CH_2), 6.86 (d, 4H, $J = 8.8$ Hz, PhOH), 7.10 (d, 4H, $J = 9.0$ Hz, Ar), 7.15 (s, 2H, Py), 7.33 (dt, 6H, $J = 28.0, 7.2$ Hz, *m,p*-Ph), 7.46 (d, 4H, $J = 7.5$ Hz, *o*-Ph), 8.06 (d, 4H, $J = 8.8$ Hz, PhOH), 8.16 (d, 4H, $J = 9.0$ Hz, Ar). $^{13}\text{C-NMR}$ (THF- d_8) δ 70.12, 114.85, 115.75, 116.85, 124.67, 125.01, 127.74, 128.01, 128.61, 131.17, 131.87, 137.52, 143.17, 145.33, 157.78, 159.62, 161.44. $^{19}\text{F-NMR}$ (THF- d_8) δ -131.14 (q, 2F, $J = 64.6, 32.7$ Hz). MS: (ESI) m/z 742 (100 [$M + \text{H}^+$]), HRMS: 741.2720 calcd. for ($\text{C}_{46}\text{H}_{35}^{10}\text{BF}_2\text{N}_3\text{O}_4$) found 741.2725.

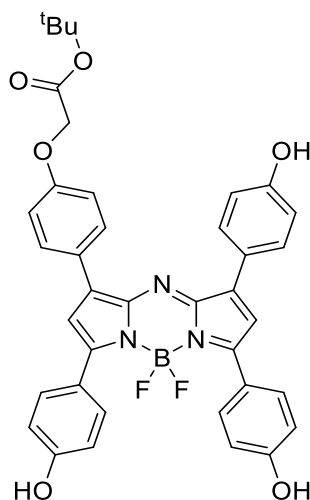
Tert-butyl 2-(4-(1,9-bis(4-(benzyloxy)phenyl)-5,5-difluoro-7-(4-hydroxyphenyl)-5H-5l4,6l4-dipyrrolo[1,2-c:2',1'-f][1,3,5,2]triazaborinin-3-yl)phenoxy)acetate (61)



A solution 4,4'-(1,9-bis(4-(benzyloxy)phenyl)-5,5-difluoro-5H-4l4,5l4-dipyrrolo[1,2-c:2',1'-f][1,3,5,2]triazaborinine-3,7-diyl)diphenol (132 mg, 0.178 mmol) in dry DMSO (5 mL) was treated with CsF (136 mg, 0.893 mmol, 5 eq.) and tert-butylbromoacetate (44 mg, 0.223 mmol, 1.3 eq.). The mixture stirred at 40 °C for 40 minutes. The mixture was cooled in an ice bath to 0 °C, a saturated solution of NH₄Cl (7.5 mL) was added and the product extracted with ethyl acetate (2 × 7.5 mL). The combined organic layers were washed with brine, dried over anhydrous Na₂SO₄, filtered and the filtrate concentrated under reduced pressure. The residue was purified by column chromatography on silica (40% EtOAc:hexane) using as eluent affording a red metallic solid (20 mg, 13%).

$R_f = 0.67$ (silica, 40% EtOAc: hexane). UV-vis (MeOH): λ_{max} , nm (log ϵ) 690 (4.78). Fluorescence (MeOH): λ_{max} , (exc/em) nm 660/722. ¹H-NMR (THF-*d*₈) δ 1.48 (s, 9H, (CH₃)₃), 4.62 (s, 2H, CH₂), 5.19 (s, 4H, CH₂), 6.87 (d, 2H, $J = 13.1$ Hz, Ar-*t*-Bu), 7.00 (d, 2H, $J = 13.3$ Hz, Ar-*t*-Bu), 7.10 (d, 4H, $J = 6.4$ Hz, *m*-Ar), 7.17 (s, 1H, Py), 7.20 (s, 1H, Py), 7.26 – 7.42 (m, 6H, *m,p*-Ph), 7.46 (d, 4H, $J = 7.1$ Hz, *o*-Ph), 7.99 – 8.10 (m, 2H, *m*-PhOH), 8.17 (d, 6H, $J = 6.3$ Hz, *o*-Ar, *o*-PhOH). ¹³C-NMR (THF-*d*₈) δ 27.04, 65.07, 69.53, 80.85, 104.97, 114.32, 115.27, 127.19, 127.46, 128.05, 128.17, 130.27, 130.31, 130.62, 130.68, 131.43, 131.51, 136.89, 136.93, 141.59, 159.16, 159.25, 166.22 (C=O). ¹⁹F-NMR (THF-*d*₈) δ -131.85 (q, 2F, $J = 65.3, 33.6$ Hz). MS: (ESI) m/z 856 (100 [M + H⁺]), HRMS: 855.3400 calcd. for (C₅₂H₄₅¹⁰BF₂N₃O₆) found 855.3409.

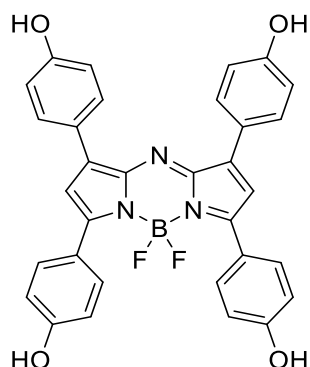
Tert-butyl 2-(4-(5,5-difluoro-1,7,9-tris(4-hydroxyphenyl)-5H-514,614-dipyrrolo [1,2-c:2',1'-f][1,3,5,2]triazaborinin-3-yl)phenoxy)acetate (62)



A mixture of tert-butyl 2-(4-(1,9-bis(4-(benzyloxy)phenyl)-5,5-difluoro-7-(4-hydroxy phenyl)-5H-514,614-dipyrrolo[1,2-c:2',1'-f][1,3,5,2]triazaborinin-3-yl)phenoxy)acetate (27 mg, 0.031 mmol) and 10% Pd/C (18 mg, 0.56 mol % Pd, 18 eq.) in THF/MeOH (5 mL, 2:3) was stirred under H₂ atmosphere (1 atm) at rt for 24 h. The mixture was filtered through Celite (Hyflo supercell), washed with MeOH. Purification by column chromatography on silica.

The desired product was not isolated

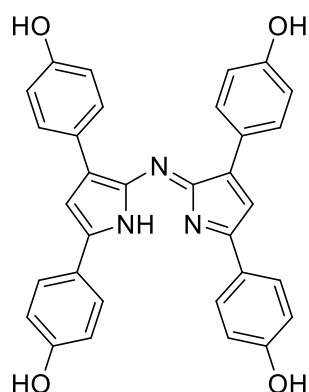
4,4',4'',4'''-(5,5-Difluoro-5H-4l4,5l4-dipyrrolo[1,2-c:2',1'-f][1,3,5,2]triazaborinine-1,3,7,9-tetrayl)tetraphenol (63)



A mixture of 4,4'-(1,9-bis(4-(benzyloxy)phenyl)-5,5-difluoro-5H-4l4,5l4-dipyrrolo [1,2-c:2',1'-f][1,3,5,2]triazaborinine-3,7-diyl)diphenol (230 mg, 0.32 mmol) and 10% Pd/C (180 mg, 5.6 mol % Pd, 18 eq.) in THF (50 mL) was stirred under H₂ atmosphere (1 atm) at rt for 24 h. The mixture was filtered through Celite (Hyflo supercell), washed with MeOH and EtOAc Purification by column chromatography on silica.

The desired product was not isolated

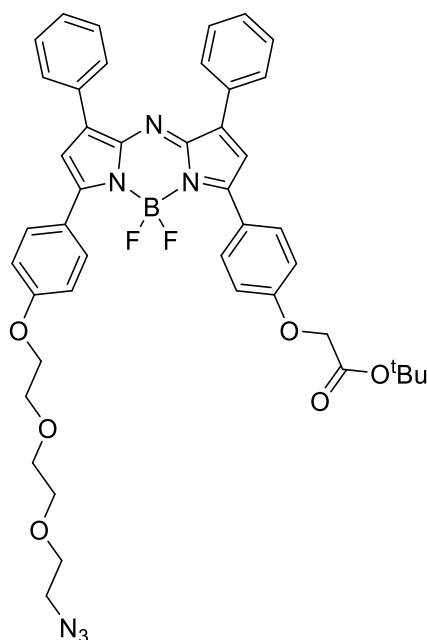
4,4',4'',4'''-(5,5-Difluoro-5H-4l4,5l4-dipyrrolo[1,2-c:2',1'-f][1,3,5,2]triazaborinine-1,3,7,9-tetrayl)tetraphenol (64)



A mixture of (Z)-4-(3-(4-(benzyloxy)phenyl)-2-((3-(4-(benzyloxy)phenyl)-5-(4-hydroxyphenyl)-1H-pyrrol-2-yl)imino)-2H-pyrrol-5-yl)phenol (224 mg, 0.31 mmol), and 10% Pd/C (183 mg, 5.6 mol % Pd, 18 eq.) in MeOH (15 mL) was stirred under H₂ atmosphere (1 atm) at rt for 24 h. The mixture was filtered through Celite (Hyflo supercell), washed with MeOH. Purification by column chromatography on silica (50% THF: hexance) to yield a metallic red solid (89 mg, 56%).

$R_f = 0.19$ (silica, 50% THF :hexane). ¹H-NMR (THF-d₈): δ 6.76 (d, 2H, $J=8.7$ Hz, Ar), 6.89 6.76 (d, 2H, $J=8.7$ Hz, Ar), 7.09 (s, 2H, Py), 7.84 (d, 2H, $J=8.6$ Hz, Ar), 7.95 (d, 2H, $J=8.7$ Hz, Ar) ¹³C-NMR (THF-d₈): δ 114.23, 116.81, 117.08, 118.13, 128.03, 130.22, 132.42, 133.54, 151.21, 156.39, 160.03, 161.94. MS: (ESI) m/z 514 (100[M +H]⁺), HRMS : 514.1761 calcd. for (C₃₂H₂₄O₄N₃) found 514.1754

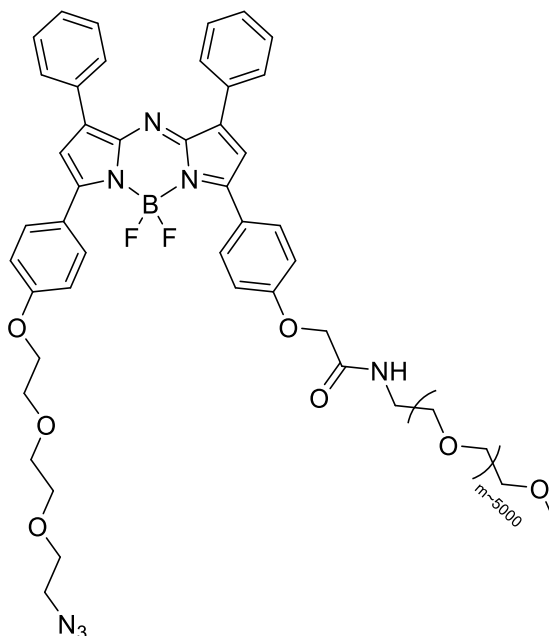
Tert-butyl 2-(4-(7-(4-(2-(2-(2-azidoethoxy)ethoxy)ethoxy)phenyl)-5,5-difluoro-1,9-diphenyl-5H-4H,5H-dipyrrolo[1,2-c:2',1'-f][1,3,5,2]triazaborinin-3-yl)phenoxy)acetate (65)



A solution 4-(7-(4-(2-(2-(2-azidoethoxy)ethoxy)ethoxy)phenyl)-5,5-difluoro-1,9-diphenyl-5H-4H,5H-dipyrrolo[1,2-c:2',1'-f][1,3,5,2]triazaborinin-3-yl)phenol (80 mg, 0.116 mmol) in dry DMSO (8 mL) was treated with CsF (88 mg, 580 mmol, 5 eq.) and tert-butylbromoacetate (280 mg, 0.144 mmol, 1.2 eq.). The mixture stirred at 40 °C for 3h. The mixture was cooled in an ice bath to 0 °C, a saturated solution of NH₄Cl (12 mL) was added and the product extracted with ethyl acetate (2 × 50 mL). The combined organic layers were washed with brine, dried over anhydrous Na₂SO₄, filtered and the filtrate concentrated under reduced pressure. The residue was purified by column chromatography on silica gel using 50 %EtOAc and hexane as eluent affording a blue solid (72 mg, 78%).

$R_f = 0.51$ (silica, 50% EtOAc:hexane). UV-vis (DCM): λ_{max} , nm (log ϵ) 660 (4.98). Fluorescence (DCM): λ_{max} , (exc/ems) nm 660/697. ¹H-NMR (CDCl₃): δ 1.53 (s, 9H, Boc), 3.40 (t, $J = 4.9$ Hz, 2H, CH₂N₃), 3.63-3.76 (m, 4H, PEG), 3.74-3.83 (m, 2H, PEG), 3.94 (t, $J = 4.8$ Hz, 2H, PEG) 4.24 (t, $J = 4.9$ Hz, 2H, PEG), 4.61 (s, 2H, CH₂), 6.93 (s, 2H, Py) 7.00 (dd, $J = 8.8, 6.1$ Hz, 4H, o-Ar), 7.46-7.48 (m, 6H, m,p-Ph), 8.01-8.06 (m, 8H, o-Ph, m-Ar). ¹³C-NMR (CDCl₃): δ 28.18 (Boc), 50.78, 65.73, 67.68, 69.87, 70.23, 70.87, 71.04, 82.75, 114.89, 114.94, 125.49, 126.26, 128.61, 129.57, 129.59, 129.64, 130.72, 130.79, 130.95, 131.87, 131.90, 159.18, 160.33, 167.77 (C=O). MS: (APCI) m/z 801 (100 [M + H⁺]), HRMS: 801.3383 calcd. for (C₄₄H₄₄O₆N₆¹⁰BF₂) found 801.3381.

2-(4-(7-(4-(2-(2-(2-Azidoethoxy)ethoxy)ethoxy)phenyl)-5,5-difluoro-1,9-diphenyl-5H-4l4,5l4-dipyrrolo[1,2-c:2',1'-f][1,3,5,2]triazaborinin-3-yl)phenoxy)-N-(2-(2-methoxyethoxy)ethyl)acetamide (68)

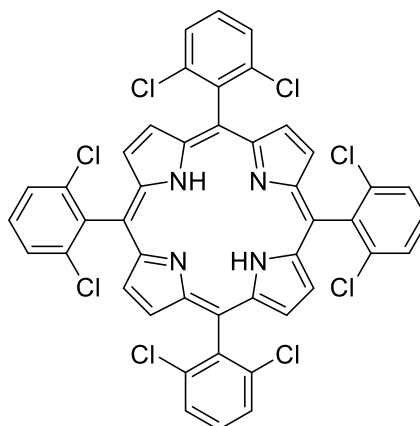


2-(4-(7-(4-(2-(2-(2-Azidoethoxy)ethoxy)ethoxy)phenyl)-5,5-difluoro-1,9-diphenyl-5H-4l4,5l4-dipyrrolo[1,2-c:2',1'-f][1,3,5,2]triazaborinin-3-yl)phenoxy)acetic acid (11 mg, 0.015 mmol), HOBT (11 mg, 0.079 mmol, 5.3 eq.) EDC (11 mg, 0.138 mmol, 9.2 eq.), methoxypolyethylene glycol amine, M.W. 5,000 (115 mg, 0.023 mmol, 1.53 eq.) and DIPEA (27 μ L, 0.308 mmol, 20.5 eq.) in a solution with dry DMF (2.2 mL) was stirred overnight at 40 °C. The solvent was removed under reduced pressure and further purified by Sep Pak C18 reverse phase cartridge eluting with water to give the product as a yield a blue solid (84 mg, 98%).

$R_f = 0.64$ (silica, KNO_3 :water:MeCN). UV-vis (water): λ_{max} , nm (log ϵ) 635 (4.37). Fluorescence (water): λ_{max} , (exc/em) nm 635/713. 1H -NMR ($CDCl_3$): δ 3.36–3.93 (m, PEG 5k), 4.23 (s, 2H, CH_2), 6.91 (s, 1H, Py), 6.93 (s, 1H, Py), 6.96-7.05 (m, 4H, *o*-Ar), 7.40-7.52 (m, 6H, *m,p*-Ph), 7.91-8.16 (m, 8H, *o*-Ph, *m*-Ar). ^{19}F -NMR ($CDCl_3$) δ -130.80 (q, 2F, $J = 61.4, 30.6$ Hz), -130.91 (q, 2F, $J = 62.3, 31.1$ Hz). MS: (MALDI) normal distribution with m/z 5649.1.

7.3.3 Bacteriochlorins

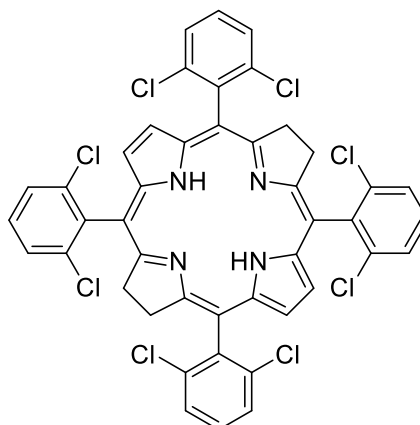
5,10,15,20-Tetrakis(2,6-dichlorophenyl)porphyrin (69)³³⁵



2,6-Dichlorobenzaldehyde (0.88 g, 5 mmol), and pyrrole (0.35 ml, 5 mmol) was dissolved in chloroform (500 mL). After the solution was purged with Ar for 5 min, $\text{BF}_3 \cdot \text{OEt}_2$ (0.66 mL, 1.65 mmol) was added and stirred for 1 h. *p*-Chloranil (0.94 g, 3.75 mmol) was added and the reaction mixture was gently heated under reflux at 61 °C for 1 h. The reaction mixture then was cooled to room temperature, TEA (0.23 mL, 1.65 mmol) was added, and the solvent was removed under pressure. The product precipitated from DCM over MeOH and filtered to yield a purple solid (227 mg, 5%).

$R_f = 0.87$ (silica, DCM). UV-vis (DCM): λ_{max} , nm ($\log \epsilon$) 420 (5.65), 509, 590. Fluorescence (DCM): λ_{max} , (exc/em) nm 420/655, 717. $^1\text{H-NMR}$ (CDCl_3): δ 7.67-7.71 (dd, 4H, $J = 9.0, 7.2$ Hz, *p*-Ar), 7.77-7.80 (m, 8H, *m*-Ar), 8.66 (s, 8H, βH). $^{13}\text{C-NMR}$ (CDCl_3): δ 114.40, 127.90 ($\beta\text{-C}$), 130.64, 138.84, 139.52, 140.66. MS: (MALDI) m/z 885 (100[M]⁺), HRMS: 885.9347 calcd. for ($\text{C}_{44}\text{H}_{22}\text{N}_4\text{Cl}_8$) found 885.9369.

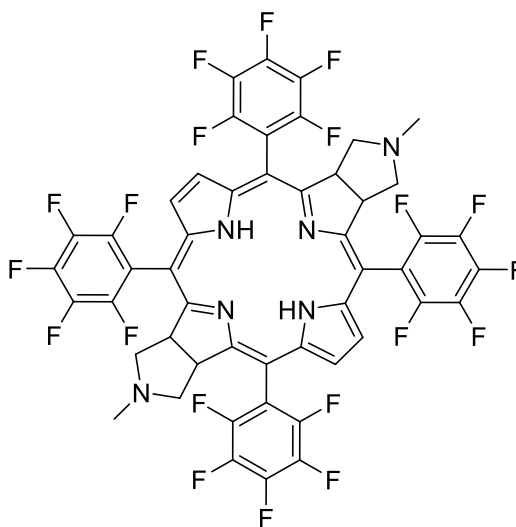
5,10,15,20-Tetrakis(2,6-dichlorophenyl)-7H,8H,17H,18H-bacteriochlorin (70)



5,10,15,20-Tetrakis(2,6-dichlorophenyl)porphyrin (30 mg, 0.037 mmol) and *p*-toluenesulfonylhydrazine (50 mg, 0.28 mmol, 7.5 eq.) was dissolved in dry pyridine (10 mL) was heated with stirring at 105 °C under Ar. After each 0.5 h a solution of *p*-toluenesulfonylhydrazine (50 mg, 0.28 mmol, 7.5 eq) and dry pyridine (1.0 mL) was added. This was repeated at the end of 4 h. A solution of *p*-toluenesulfonylhydrazine (100 mg, 0.56 mmol, 15 eq.) and dry pyridine (1.5 mL) was then added for every hour until 6.5 h, in which the reaction was left to reflux for 15 h and repeat the addition of *p*-toluenesulfonylhydrazine (200 mg, 1.11 mmol, 20 eq.) After heating for a total of 6.5 h the pyridine was removed under reduced pressure and washed with NaHCO₃. The mixture was then extracted from DCM and washed with 4M HCl and water (5 × 50 mL), dried (Na₂SO₄) and the solvent was removed under reduced pressure. The crude was purified by column chromatography (50% hexane:DCM) and precipitated with MeOH over DCM to yield a dark purple solid.

The desired product was not isolated

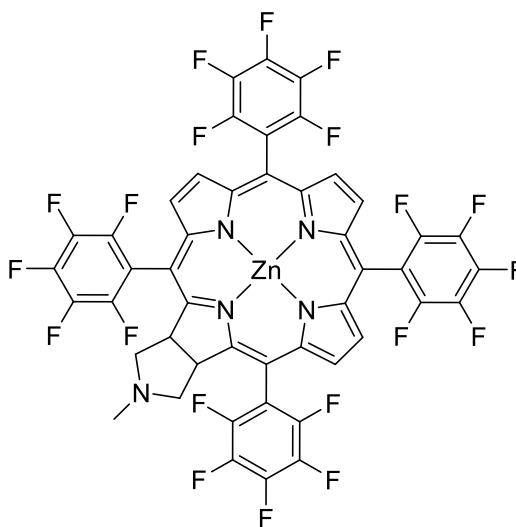
(2Z,6Z,9R,13S,14Z,22R,26S)-11,24-Dimethyl-2,7,15,20-tetrakis(pentafluorophenyl)-11,24,27,28,29,30-hexaazaheptacyclo[19.5.1.13,6.18,14.116,19.09,13.022,26]triaconta-1(27),2,4,6,8(29),14,16,18,20-nonaene (71)



To a 50 mL microwave tube, a solution of 5,10,15,20-tetrakis(perfluorophenyl) porphyrin (110 mg, 0.11 mmol), *N*-methylglycine (20 mg, 0.23 mmol, 2 eq.) and paraformaldehyde (17 mg, 0.53 mmol, 5 eq.) in toluene (25 mL) was heated under microwave irradiation (2 h, 130°C, 1 min pre-stirring). TLC of the reaction mixture showed that about half of the starting porphyrin was converted into two new products. Further portions of *N*-methylglycine (200 mg, 2.3 mmol, 20 eq.) and paraformaldehyde (170 mg, 5.3 mmol, 50 eq.) were then added and the resulting mixture was heated under microwave irradiation (16 h, 130 °C, 1 min pre-stirring).

The desired product was not obtained

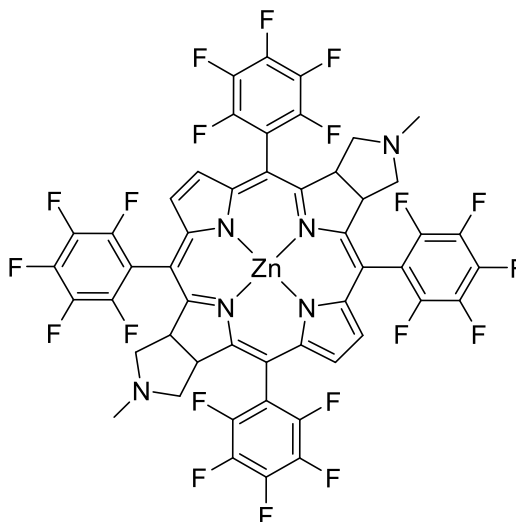
Zinc (2Z,6Z,11Z,17Z)-21-methyl-2,7,12,17-tetrakis(pentafluorophenyl)-21,24,25,26,27-pentaazahexacyclo[16.5.1.13,6.18,11.113,16.019,23]heptacosa-1(24),2,4,6,8(26),9,11,13,15,17-decaene (72)²⁸⁷



A solution of zinc 5,10,15,20-tetrakis(perfluorophenyl) porphyrin (110 mg, 0.11 mmol), *N*-methylglycine (20 mg, 0.23 mmol, 2 eq.) and paraformaldehyde (17 mg, 0.53 mmol, 5 eq.) in toluene (25 mL) was heated at reflux for 5 h under Ar. TLC of the reaction mixture showed that about half of the starting porphyrin was converted into two new products. Further portions of *N*-methylglycine (200 mg, 2.3 mmol, 20 eq.) and paraformaldehyde (170 mg, 5.3 mmol, 50 eq.) were then added and the resulting mixture was refluxed for overnight. The solvent was removed under reduced pressure and the compounds were separated by column chromatography (50%-100% DCM and hexane) to yield chlorin adduct as a blue solid (27 mg, 23%).

$R_f = 0.79$ (silica, 10% MeOH: DCM). UV-vis (MeOH): λ_{max} , nm (log ϵ) 415 (5.39), 620. Fluorescence (MeOH): λ_{max} , (exc/em) nm 410/624, 620/673. ¹H-NMR (*d*₆-DMSO) δ 0.71-0.96 (m, 1H, CH), 2.12 (s, 3H, CH₃), 2.60-2.78 (m, 1H, CH), 3.17 (brs, 2H, CH₂), 5.12 (brs, 2H, CH₂), 8.36 (d, 2H, *J* = 4.5 Hz, Py), 8.55 (s, 2H, 7,8-Py), 8.73 (d, 2H, *J* = 4.6 Hz, Py). ¹³C-NMR (*d*₆-DMSO) δ 29.64, 53.33, 69.97, 95.62, 107.14, 117.38, 128.36, 129.34, 140.56, 146.93, 153.96, 191.11. ¹⁹F-NMR (DMSO-*d*₆) δ -137.36 (dd, 2F, *J* = 26.2, 7.6 Hz, 5-*o*-Ar), -139.48 (dd, 2F, *J* = 26.1, 7.7 Hz, 10-*o*-Ar), -139.75 (dt, 4F, *J* = 26.3, 8.7 Hz, 15, 20-*o*-Ar), -153.92 (t, 2F, *J* = 22.8 Hz, 5, 10-*p*-Ar), -154.78 (t, 2F, *J* = 22.5 Hz, 15, 20-*p*-Ar), -161.84 (ddt, 4F, *J* = 31.4, 24.4, 6.9 Hz, 5, 10-*m*-Ar), -163.09 (dddd, 4F, *J* = 35.0, 26.3, 22.7, 7.8 Hz, 15, 20-*m*-Ar).

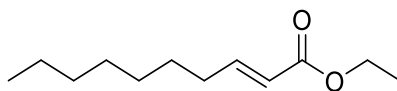
Zinc (2Z,6Z,9R,13S,14Z,22R,26S)-11,24-dimethyl-2,7,15,20-tetrakis(pentafluorophenyl)-11,24,27,28,29,30-hexaazaheptacyclo[19.5.1.13,6.18,14.116,19.09,13.022,26]triaconta-1(27),2,4,6,8(29),14,16,18,20-nonaene (73)



A solution of zinc (2Z,6Z,11Z,17Z)-21-methyl-2,7,12,17-tetrakis(pentafluorophenyl)-21,24,25,26,27-pentaazahexacyclo[16.5.1.13,6.18,11.113,16.019,23]heptacos-1(24),2,4,6,8(26),9,11,13,15,17-decaene (11 mg, 0.011 mmol), *N*-methylglycine (2.0 mg, 0.023 mmol, 2 eq.) and paraformaldehyde (1.7 mg, 0.053 mmol, 5 eq.) in toluene (25 mL) was heated at reflux for 5 h under Ar. TLC of the reaction mixture showed that about half of the starting porphyrin was converted into two new products. Further portions of *N*-methylglycine (20 mg, 0.23 mmol, 20 eq.) and paraformaldehyde (17 mg, 0.53 mmol, 50 eq.) were then added and the resulting mixture was refluxed for overnight.

The desired product was not isolated.

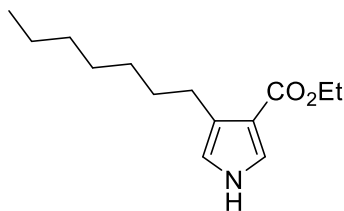
Dec-2-enoic acid ethyl ester (74)³³⁶



Triethyl phosphonoacetate (26 g, 116 mmol, 1.16 eq.) was added dropwise to a suspension of NaH (60% in oil dispersion, 5.58 g, 116 mmol) in Et₂O (500 mL) at 0 °C. After hydrogen evolution was complete in 5 min, octanal (12.82 g, 100 mmol) was added dropwise with vigorous stirring. After 15 min, the reaction was quenched by the addition of saturated ammonium chloride solution_(aq) (200 mL). The organic layer was separated and washed twice with water, once with brine, dried (MgSO₄) and the solvent was removed under reduced pressure to yield a colourless oil, which was purified by flash chromatography on silica (5% EtOAc in hexane), to yield a colourless oil (19.57 g, 98%).

MS: (ESI) m/z 199 (100[M + H]⁺), HRMS: 199.1693 calcd. for (C₁₂H₂₃ O₂) found 199.1693.

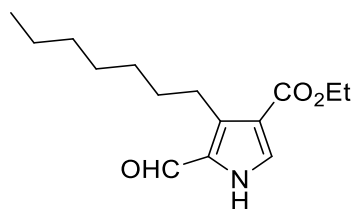
3-(Ethoxycarbonyl)-4-heptylpyrrole (75) ²⁹⁸



A solution of dec-2-enoic acid ethyl ester (12.3 g, 58.0 mmol) and toluenesulfonylmethyl isocyanide (12.6 g, 64.5 mmol) in Et₂O/ DMSO (300 mL, 2:1) was slowly added to a suspension of NaH (60% in oil dispersion, 5.0 g, 0.12 mol) in Et₂O (100 mL). The resulting exotherm caused the mixture to reflux. The reaction mixture was stirred at rt for 16 h. Water was added carefully, and the mixture was extracted with Et₂O. The solvent was removed under reduced pressure and dried (Na₂SO₄). Column chromatography (silica, DCM) afforded a light-yellow solid (7.2 g, 52%).

$R_f = 0.47$ (silica, DCM). ¹H-NMR (CDCl₃): δ 0.87 (t, 3H, $J = 6.8$ Hz, CH₃-C7chain), 1.10 – 1.42 (m, 11H, C7 chain & CH₃CH₂), 1.57 (quin, 2H, $J = 7.5$ Hz, C7 chain), 2.70 (t, 2H, $J = 7.6$ Hz, C7 chain), 4.25 (q, 2H, $J = 7.3$ Hz, CH₃CH₂), 6.51 (s, 1H, Py), 7.36 (s, 1H, Py), 8.75 (brs, 1H, NH). ¹³C-NMR (CDCl₃): δ 14.08, 14.67, 22.67, 26.23, 29.35, 29.73, 30.60, 32.02, 59.48, 114.19, 116.78, 124.70, 126.46, 165.85 (C=O). MS: (ESI) m/z 238 (100[M + H]⁺), HRMS: 238.1802 calcd. for (C₁₄H₂₄ O₂N) found 238.1802.

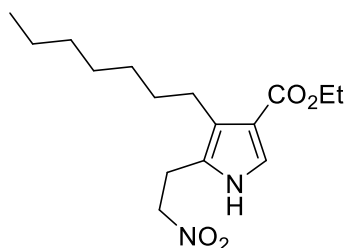
4-(Ethoxycarbonyl)-2-formyl-3-heptylpyrrole (76)²⁹⁸



The Vilsmeier reagent was prepared by treatment of dry DMF (30 mL) with POCl₃ (4.6 mL, 49 mmol, 1.6 eq.) at 0 °C and stirring of the resulting mixture for 10 min. A solution of 3-(ethoxycarbonyl)-4-heptylpyrrole (7.2 g, 30.35 mmol) in DMF (150 mL) was reacted with the freshly prepared Vilsmeier reagent at 0 °C. The resulting mixture was stirred at 0 °C for 1 h and then 2 h at rt. The reaction mixture was reacted with a mixture of saturated aqueous sodium acetate: DCM (400 mL, 1:1 (v/v)) and stirred for 1 h. The water layer was separated and extracted with DCM. The combined organic layer was washed with brine, dried (Na₂SO₄), and the solvent was removed under reduced pressure to yield a brown solid (4.4 g, 54 %).

R_f = 0.51 (silica, DCM). *M.p* 44-46 °C. ¹H-NMR (CDCl₃): δ 0.83 (t, 3H, *J* = 6.8 Hz, CH₃-C7chain), 1.10-1.44 (m, 11H, C7 chain & CH₃CH₂), 1.59 (quin, 2H, *J* = 7.6 Hz, C7 chain), 3.01 (t, 2H, *J* = 7.6 Hz, C7 chain), 4.26 (q, 2H, *J* = 7.0 Hz, CH₃CH₂), 7.67 (s, 1H, Py), 9.63 (s, 1H, CHO), 10.90 (brs, 1H, NH). ¹³C-NMR (CDCl₃): δ 14.08, 22.67, 24.45, 29.21, 29.60, 31.80, 32.20, 60.00, 116.45, 130.40, 131.50, 140.07, 164.09 (C=O), 178.78 (CHO). MS: (ESI) *m/z* 266 (100[M + H]⁺), HRMS: 266.1751 calcd. for (C₁₅H₂₄O₃N) found 266.1754. CHN: C (67.98%), H (8.92%), N (5.23%) – literature value: C (67.90%), H (8.74%), N (5.28%).

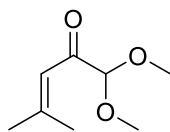
4-(Ethoxycarbonyl)-3-heptyl-2-(2-nitroethyl)pyrrole (78) ²⁹⁸



A stirred mixture of 4-(ethoxycarbonyl)-2-formyl-3-heptylpyrrole (4.2 g, 15.8 mmol), potassium acetate (1.7 g, 12.9 mmol), and methylamine hydrochloride (1.2 g, 12.9 mmol) in EtOH (8 mL) was added with nitromethane (3.0 mL, 25.3 mmol, 1.6 eq.). The mixture was stirred for 2 h, whereupon water was added. The reaction mixture was filtered, and was washed with water and a small amount of cold EtOH. The filtered material was dried under high vacuum to afford a yellow solid, which was used directly in the next step. The crude solid material was dissolved in CHCl₃/2-propanol (3:1, 250 mL). Silica (24 g) and NaBH₄ (1.32 g, 40 mmol, 2.5 eq.) were added and the mixture was stirred at rt under Ar for 2 h. The reaction mixture was filtered, and the filtrate was concentrated. The resulting crude solid was dissolved in DCM. The organic solution was washed (water, brine), dried (Na₂SO₄), and the solvent was removed under reduced pressure to afford a pale brown solid (1.92 g, 39%).

$R_f = 0.66$ (silica, 10% MeOH: DCM). ¹H-NMR (CDCl₃): δ 0.86 (t, 3H, $J = 7.1$ Hz, CH₃-C7chain), 1.22 – 1.37 (m, 11H, C7 chain & CH₃CH₂), 1.49 (quin, 2H, $J = 7.2$ Hz, C7 chain), 2.62 (t, 2H, $J = 7.7$ Hz, C7 chain), 3.24 (t, 2H, $J = 6.5$ Hz, CH₂), 4.25 (q, 2H, $J = 7.1$ Hz, CH₃CH₂), 4.53 (t, 2H, $J = 6.5$ Hz, CH₂), 7.31 (d, 1H, $J = 3.2$ Hz, Py), 8.43 (brs, 1H, NH). ¹³C-NMR (CDCl₃): δ 14.20, 14.54, 22.78, 23.27, 24.98, 29.35, 29.99, 31.88, 32.02, 59.52, 75.45, 114.89, 123.53, 123.65, 124.02, 165.13 (C=O). MS: (ESI) m/z 311[M + H⁺], HRMS: 311.1965 calcd. for (C₁₆H₂₇O₄Ar) found 311.1961.

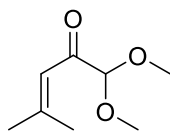
1,1-Dimethoxy-4-methylpent-3-en-2-one (79) ³⁰¹



2,2-Dimethoxyacetonitrile (0.42 g, 4.2 mmol) was added under Ar with 2-methyl-1-propenylmagnesium bromide solution (10 mL, 5 mmol, 0.5 M in THF, 1.2 eq.) over 5 min at 0 °C, followed by stirring for 2 h at rt. The bright yellow-orange solution was added with saturated aqueous NH₄Cl (10 mL), and the reaction mixture was vigorously stirred for 2 h. The aqueous phase was extracted with Et₂O (3 × 35 mL), and each organic extract was washed with brine. The combined organic extract was dried (Na₂SO₄) and the solvent was removed under reduced pressure. Purification by column chromatography on silica (DCM) yielded a yellow liquid (215 mg, 32%).

$R_f = 0.40$ (silica, DCM). ¹H-NMR (CDCl₃): δ 1.95 (s, 3H, CH₃C=C), 2.20 (s, 3H, CH₃C=C), 3.41 (s, 6H, CH₃O), 4.48 (s, 1H, C=CH), 6.36 (s, 1H, CH). ¹³C-NMR (CDCl₃): δ 21.37, 28.29, 54.63, 104.59, 119.11, 160.35, 194.29 (C=O). MS: (ESI) m/z 159 (100[M + H]⁺), HRMS: 159.1016 calcd. for (C₈H₁₅O₃) found 159.1013

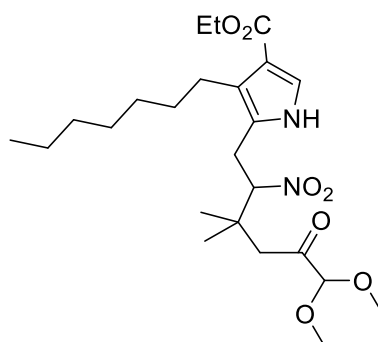
1,1-Dimethoxy-4-methylpent-3-en-2-one (79)³⁰¹



2,2-Dimethoxyacetonitrile (3.78 g, 37.8mmol) was added under Ar with 2-methyl-1-propenylmagnesium bromide solution (90 mL, 45 mmol, 0.5 M in THF, 1.2 eq.) over 20 min at 0 °C, followed by stirring for 2 h at rt. The bright yellow-orange solution was added with saturated aqueous NH₄Cl (120 mL), and the reaction mixture was vigorously stirred for 2 h. The aqueous phase was extracted with Et₂O (3 ×100 mL), and each organic extract and was washed with brine. The combined organic extract was dried (Na₂SO₄) and the solvent was removed under reduced pressure to afford an orange liquid (5.18 g, 90% purity).

The product was taken on to the next reaction without further purification.

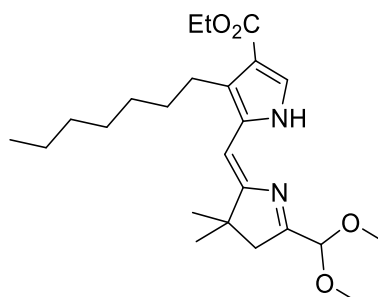
6-(4-(Ethoxycarbonyl)-3-heptylpyrrol-2-yl)-1,1-dimethoxy-4,4-dimethyl-5-nitrohexan-2-one. (80)²⁹⁸



A mixture of 4-(ethoxycarbonyl)-3-heptyl-2-(2-nitroethyl)pyrrole (1.9 g, 6.1 mmol) and 1,1-dimethoxy-4-methylpent-3-en-2-one (3.2 g, 18.4 mmol, 3 eq. 90% pure) was added with DBU (2.75 mL, 18.4 mmol, 3 eq.). The reaction mixture was stirred under Ar at rt for 16 h. A saturated solution of cold aqueous NH_4Cl was added. The mixture was extracted with EtOAc, and the organic layer was washed with brine, dried (Na_2SO_4), and the solvent was removed under reduced pressure. Column chromatography on silica (90% DCM/EtOAc) afforded a pale brown solid (1.08 g, 38%).

$R_f = 0.71$ (silica, 90% DCM: EtOAc). $^1\text{H-NMR}$ (CDCl_3): δ 0.78 – 0.97 (m, 4H), 1.11 – 1.50 (m, 17H), 1.37 – 1.58 (m, 3H), 1.62 (s, 1H), 2.47 – 2.67 (m, 3H), 3.24 (t, 2H, $J = 6.4$ Hz, 6- CH_2), 3.33 – 3.53 (m, 2H), 4.25 (q, 3H, $J = 7.1$ Hz), 4.53 (t, 2H, $J = 6.5$ Hz, 9- CH_2), 7.31 (d, 1H, $J = 3.2$ Hz, CH), 8.43 (brs, 1H, NH). $^{13}\text{C-NMR}$ (CDCl_3): δ 14.21, 14.53, 22.76, 23.28, 24.98, 29.38, 29.98, 30.05, 31.74, 31.89, 32.03, 32.07, 45.05, 55.36, 59.41, 59.49, 75.43, 114.93, 123.53, 123.66, 124.03, 165.11(C=O), 203.71(C=O). MS: (ESI) m/z 469 (100[M + H]⁺), HRMS: 469.2908 calcd. for ($\text{C}_{24}\text{H}_{41}\text{O}_7\text{N}_2$) found 469.2904

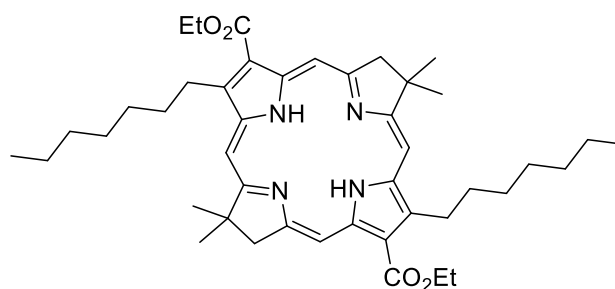
8-(Ethoxycarbonyl)-2,3-dihydro-1-(1,1-dimethoxymethyl)-7-heptyl-3,3-dimethylpyrrolin (81)



To a solution of 6-(4-(ethoxycarbonyl)-3-heptylpyrrol-2-yl)-1,1-dimethoxy-4,4-dimethyl-5-nitrohexan-2-one (1.08 g, 2.3 mmol) in freshly distilled THF (13 mL) at 0°C was added with NaOMe (3.8 g, 12 mmol, 5.2 eq.). The mixture was stirred and degassed the solution with Ar for 45 min. In a second flask purged with Ar, a mixture of TiCl₃ (16.65 mL, 12% in HCl solution, 17 mmol, 7.4 eq.), THF (40 mL), and NH₄OAc (10 g, 130.5 mmol) were combined under Ar, and the mixture was degassed with Ar for 45 min. Then, the first flask mixture was transferred via cannula to the buffered TiCl₃ mixture. The resulting mixture was stirred under Ar at rt for 16 h. The mixture was extracted with EtOAc. The organic extract was washed with saturated NaHCO_{3(aq)}, dried (Na₂SO₄) and the solvent was removed under reduced pressure. Column chromatography (silica, DCM) afforded a yellow oil (270 mg, 28%).

R_f = 0.15 (silica, DCM). ¹H-NMR (CDCl₃) δ 0.64 – 1.04 (m, 3H), 1.12 – 1.45 (m, 20H), 1.39 – 1.61 (m, 3H), 1.71 (s, 1H), 2.50 – 2.77 (m, 1H), 3.25 (t, 3H, *J* = 6.6 Hz), 4.08 – 4.36 (m, 3H), 4.54 (t, 2H, *J* = 6.6 Hz), 7.32 (d, 1H, *J* = 3.3 Hz), 8.58 (brs, 1H). ¹³C-NMR (CDCl₃) δ 14.21, 14.53, 22.76, 23.32, 24.98, 29.37, 29.65, 29.97, 31.89, 32.03, 40.33, 48.30, 54.69, 59.49, 76.80, 102.71, 114.34, 124.72, 125.30, 128.70, 159.98, 165.70 (C=O), 174.69. MS: (ESI) *m/z* 419 (100[M + H]⁺), HRMS: 419.2904 calcd. for (C₂₄H₃₉N₂O₄) found 419.2904

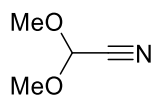
3,13-Bis(ethoxycarbonyl)-2,12-diheptyl-8,8,18,18-tetramethylbacteriochlorin (82)



A solution of 8-(ethoxycarbonyl)-2,3-dihydro-1-(1,1-dimethoxymethyl)-7-heptyl-3,3-dimethyldipyrrin (250 mg, 0.597 mmol) in anhydrous MeCN (45 mL) was added with $\text{BF}_3 \cdot \text{OEt}_2$ (0.59 mL, 4.78 mmol). The reaction mixture was stirred at rt for 16 h. Excess TEA (0.89 mL, 6.39 mmol) was added to the reaction mixture. The solvent was removed under reduced pressure. Purification of column chromatography (silica, DCM) to afford a purple solid (10 mg, 2%).

$R_f = 0.93$ (silica, DCM). UV-vis (DCM): λ_{max} , nm ($\log \epsilon$) 355, 384, 519, 759 (4.80). Fluorescence (DCM): λ_{max} , (exc/em) nm 730/767. $^1\text{H-NMR}$ (CDCl_3): δ -1.43 (brs, 2H, NH), 0.93 – 1.07 (m, 6H), 1.33 – 1.81 (m, 22H), 1.94 (s, 12H, 8,17- CH_3), 2.12 (p, 4H, $J = 7.7$ Hz), 4.11 (t, 4H, $J = 7.7$ Hz), 4.41 (s, 4H, 7,18- CH_2), 4.77 (q, 4H, $J = 7.1$ Hz), 8.63 (s, 2H, meso), 9.65 (s, 2H, meso). $^{13}\text{C-NMR}$ (CDCl_3): δ 14.21, 14.74, 22.75, 27.39, 29.79, 30.28, 31.03, 31.99, 33.30, 45.91, 51.91, 60.86, 94.75, 98.60, 119.27, 133.86, 134.95, 140.43, 160.51, 166.63, 170.98. MS: (ESI) m/z 711 ($100[M + H]^+$), HRMS: 711.4844 calcd. for ($\text{C}_{44}\text{H}_{63}\text{N}_4\text{O}_4$) found 711.4843.

2,2-Dimethoxyacetonitrile (83) ³⁰¹

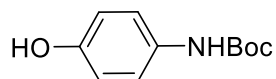


Trimethyl orthoformate (10.6 mL, 100 mmol) and trimethylsilylcyanide (10.2 mL, 103 mmol) were added dropwise of $\text{BF}_3 \cdot \text{OEt}_2$ (1.3 mL, 10 mmol) under Ar at rt. The reaction mixture was stirred for 3 h at rt whereupon saturated aqueous NaHCO_3 (200 mL) was added. The aqueous phase was extracted with ether (3×75 mL). The combined organic extract was dried (Na_2SO_4) and the solvent was removed under reduced pressure. The crude product was distilled (150 °C) to afford a transparent liquid (4.65 g, 46%).

$^1\text{H-NMR}$ (CDCl_3): δ 3.45 (s, 6H, CH_3O), 5.21 (s, 1H, CH). $^{13}\text{C-NMR}$ (CDCl_3): δ 53.83 (CH_3), 91.42, 114.21. MS: (ESI) m/z 102 ($100[\text{M} + \text{H}]^+$), HRMS: 102.0550 calcd. for ($\text{C}_4\text{H}_8\text{O}_2\text{N}$) found 102.0549.

7.3.4 Bioconjugation linker and conjugates

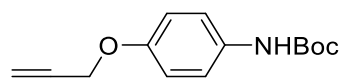
Tert-butyl (4-hydroxyphenyl)carbamate (84)



To a solution of 4-aminophenol (2.20 g, 20.1 mmol) in MeOH (40 mL) was added TEA (6 mL) and di-tert-butyl dicarbonate (4.81 g, 22.06 mmol, 1.1 eq.) and the mixture stirred at rt overnight. The solvent was removed under reduced pressure and the product redissolved in DCM washed with water. The organic layer was dried, and the solvent was removed under reduced pressure to obtain the product as a white solid (4.12 g, 98%).

$R_f = 0.26$ (silica, DCM). M_p 144-145°C. 1H -NMR (CD_3Cl): δ 1.50 (s, 9H, Boc), 6.63 (brs, 1H, OH), 6.74 (d, 2H, $J = 8.9$ Hz, Ph), 7.17 (d, 2H, $J = 8.3$ Hz, Ph). ^{13}C -NMR (CD_3Cl): δ 27.79, 28.46, 115.79 (C=O), 121.32, 121.79, 131.21. MS: (ESI) m/z 232 ($100[M + Na]^+$), HRMS: 232.0944 calcd. for ($C_{11}H_{15}O_3NNa$) found 232.0945

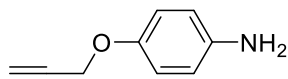
Tert-butyl (4-(prop-2-yn-1-yloxy)phenyl)carbamate (85)



To a solution of tert-butyl (4-hydroxyphenyl)carbamate (2.0 g, 10 mmol) and K_2CO_3 (2.0 g, 15 mmol, 1.5 eq.) in DMF (30 mL) was added propargyl bromide (2.3 g, 15 mmol, 1.5 eq.) and the mixture stirred at rt for 24 h. The crude product was extracted with DCM, washed with water, dried (Na_2SO_4) and the solvent was removed under reduced pressure. Purified by column chromatography with DCM to afford a pale-yellow solid (2.21, 89%).

$R_f = 0.74$ (silica, DCM). Mp 92-93°C. ^1H-NMR (CD_3Cl): δ 1.50 (s, 9H, Boc), 2.49 (s, 1H, CH), 4.64 (s, 2H, CH_2), 6.43 (brs, 1H, $NHBoc$), 6.80 (d, 2H, $J = 8.9$ Hz, Ph), 7.26 (d, 2H, $J = 8.6$ Hz, Ph). $^{13}C-NMR$ (CD_3Cl): δ 56.29, 57.48, 75.56 ($C\equiv C$), 78.72 ($C\equiv C$), 101.56, 115.53 ($C=O$), 120.44, 132.41, 153.59. MS : (ESI) m/z 265 ($100[M + NH_4]^+$), $HRMS$: 265.1547 calcd. for ($C_{14}H_{21}O_3N$) found 265.1550

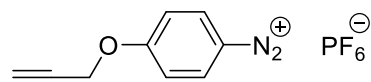
4-(Prop-2-yn-1-yloxy)aniline (86)



Tert-butyl (4-(prop-2-yn-1-yloxy)phenyl)carbamate (1 g, 4.044 mmol) was dissolved in TFA (10 mL) and stirred at rt for overnight. The solvent was removed under reduced pressure and the product precipitated from Et₂O to obtain a white powder (590 mg, 99%).

Mp 141-142°C. ¹H-NMR (CD₃OD): δ 2.98 (s, 1H, CH), 4.78 (s, 2H, CH₂), 4.96 (brs, 2H, NH₂), 7.12 (d, 2H, J= 9.1 Hz, Ph), 7.31(d, 2H, J= 8.8 Hz, Ph). ¹³C-NMR (CD₃OD): δ 55.63, 75.92 (C≡C), 77.88 (C≡C), 116.10, 123.67, 124.24, 157.81. MS: (ESI) m/z 148 (100[M +H]⁺), HRMS: 148.0757 calcd. for (C₉H₁₀ON) found 148.0753.

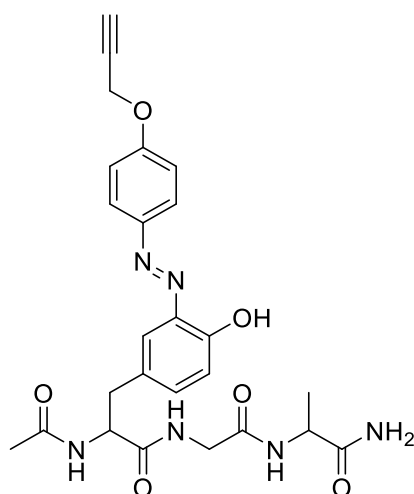
4-(Prop-2-yn-1-yloxy)benzene diazonium hexafluorophosphate (87)



To a solution of 4-(prop-2-yn-1-yloxy)aniline (100 mg, 0.68 mmol) in TFA (4 mL) at -10 °C was added dropwise NaNO₂ (176 mg, 2.55 mmol, 3.8 eq.) in water and the mixture stirred at -10 °C for 1.5 h. HPF₆ (60% w/w aq, 0.25 mL, 2.83 mmol, 4.2 eq.) was added dropwise. Followed by the addition of water (6 mL) and the reaction was maintained at -10 °C for 1 h then 30 min at rt. The mixture was filtered to collect the product as a white solid (65 mg, 31%).

Mp 149-150 °C. ¹H-NMR (DMSO-*d*₆): δ 3.83 (s, 1H, CH), 5.16 (d, 2H, *J* = 2.4 Hz, CH₂), 7.53 (d, 2H, *J* = 9.4 Hz, Ph), 8.65 (d, 2H, *J* = 9.4 Hz, Ph). ¹³C-NMR (DMSO-*d*₆): δ 58.12, 77.80 (C≡C), 80.75 (C≡C), 105.23, 118.44, 136.62, 167.02. MS: (ESI) *m/z* 159 (100[M - PF₆]⁺), HRMS: 159.0553 calcd. for (C₉H₇ON₂) found 159.0549.

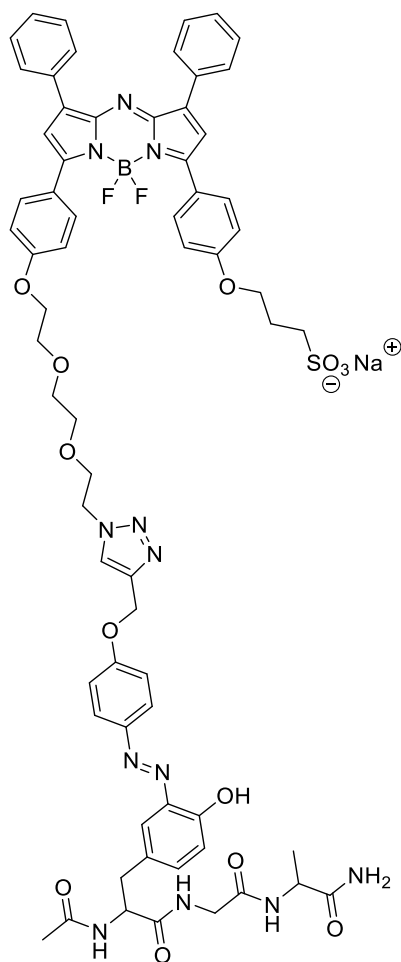
(E)-2-Acetamido-N-(2-((1-amino-1-oxopropan-2-yl)amino)-2-oxoethyl)-3-(4-hydroxy-3-((4-(prop-2-yn-1-yloxy)phenyl)diazenyl)phenyl)propanamide (89)



To a solution of 2-acetamido-*N*-(2-((1-amino-1-oxopropan-2-yl)amino)-2-oxoethyl)-3-(4-hydroxyphenyl)propanamide (30 mg, 0.085 mmol) in 100 mM pH 7.0 NaH₂PO₄/Na₂HPO₄ buffer (2.83 mL) and DMSO (1.41 mL) was added 4-(prop-2-yn-1-yloxy)benzene diazonium hexafluorophosphate (28 mg, 0.093 mmol, 1.1 eq.) at rt. The resulting solution was stirred at rt for 45 min. After the reaction was complete, water (2.82 mL) was added. The generated solid was filtered then washed with water and EtOAc to give a yellow solid (22 mg, 51%).

UV-vis (DMSO): λ_{max} , nm (log ϵ) 360 (5.13). *Fluorescence* (DMSO): λ_{max} , (exc/ems) nm 360/410. *¹H-NMR* (DMSO-*d*₆): δ 1.10 (t, 1H, *J* = 7.0 Hz, C \equiv C), 1.21 (d, 3H, *J* = 7.1 Hz, CH₃(Ala)), 1.77 (s, 3H, CH₃), 2.64 (dd, 1H, *J* = 14.0, 9.8 Hz, CH(Gly)), 2.89 (dd, 1H, *J* = 13.9, 4.7 Hz, CH(Gly)), 3.39 (q, 1H, *J* = 7.0 Hz, CH-Ala), 3.63 (dd, 2H, *J* = 16.6, 5.5 Hz, CH₂(Tyr)), 3.76 (dd, 1H, *J* = 16.6, 6.0 Hz, CH-Tyr), 4.18 (p, 1H, *J* = 7.1 Hz, CH₂), 4.34 (ddd, 1H, *J* = 9.7, 7.7, 4.6 Hz, CH₂), 6.64 (d, 2H, *J* = 8.4 Hz, Ar), 7.03 (d, 2H, *J* = 8.5 Hz, Ar), 7.29 (s, 1H), 7.86 (d, 1H, *J* = 7.6 Hz), 8.14 (d, 1H, *J* = 7.8 Hz), 8.26 (t, 1H, *J* = 5.8 Hz), 9.18 (brs, 1H, OH). *¹³C-NMR* (DMSO-*d*₆): δ 18.78, 23.05, 37.05, 42.65, 48.55, 55.02, 56.41, 65.49, 71.74, 75.20, 100.14, 115.43, 116.88, 127.87, 128.63, 129.59, 130.56, 155.74, 156.28, 168.83 (C=O), 170.07 (C=O), 172.54 (C=O), 174.70 (C=O). *MS*: (ESI) *m/z* 509 (100[M + H]⁺), *HRMS*: 509.2132 calcd. for (C₂₅H₂₉O₆N₆) found 509.2143.

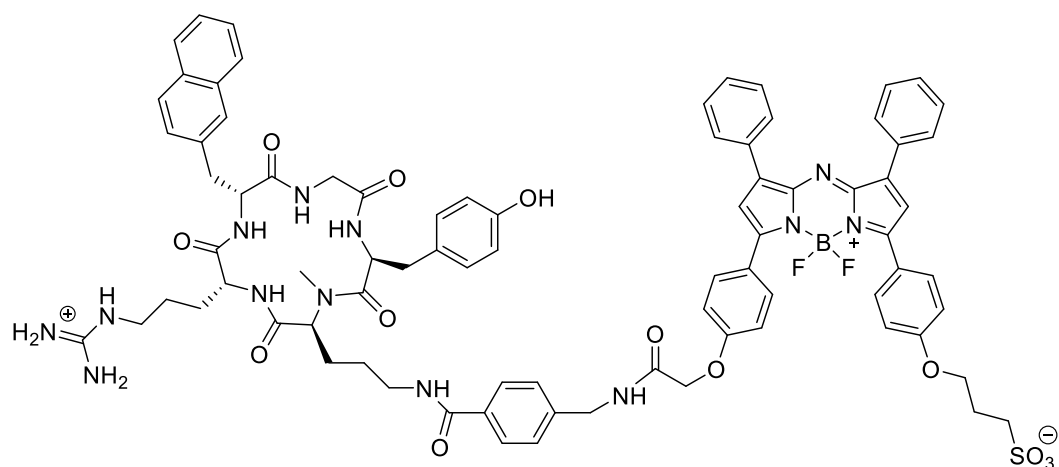
Tyrosine modified peptide aza-BODIPY conjugate (90)



Tyrosine modified peptide chain (1.1 mg, 22 μmol) in 100 mM pH 7.0 $\text{NaH}_2\text{PO}_4/\text{Na}_2\text{HPO}_4$ buffer (2.83 mL) and DMSO (1.41 mL) was added $\text{CuSO}_4 \cdot 5\text{H}_2\text{O}$, sodium ascorbate, 3-(4-(7-(4-(2-(2-(2-azidoethoxy)ethoxy)ethoxy)ethoxy)phenyl)-5,5-difluoro-1,9-dipyrrolo[1,2-c:2',1'-f][1,3,5,2]triazaborin-3-yl)phenoxy)propane-1-sulfonate (2 mg, 2.4 μmol , 1.1 eq.) at rt. The resulting solution was stirred at rt for 24 h. The compound was transformed into Bu_4N^+ ion salt by extraction of aqueous solution with DCM in presence of TBAC. The organic phase was washed with water (2×20 mL), dried (MgSO_4) and solvent removed under reduced pressure. Purification by column chromatography on silica eluting with 1-20% MeOH: DCM. The product was then dissolved in MeCN and NaI was added, stirred at 0 $^\circ\text{C}$ until product precipitated. The precipitate was filtered and washed with MeCN to yield a green-blue solid.

HPLC: 60-95% B over 9 minutes. $R_f = 6.68$ minutes. *UV-vis* (DMSO- d_6): λ_{max} , nm 360 and 660. *MS*: (ESI) m/z 1315 [M].

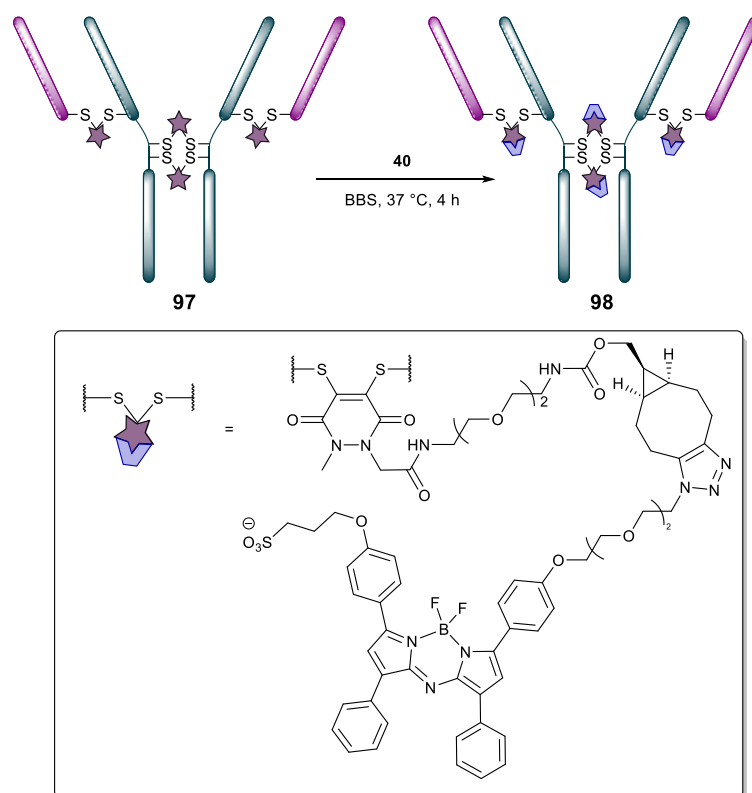
Fluorescent peptide conjugate (94)



FC131-AMBA peptide (5.58 mg, 5.2 μmol) and 3-(4-(7-(4-(carboxymethoxy)phenyl)-5,5-difluoro-1,9-diphenyl-5H-4l4,5l4-dipyrrolo[1,2-c:2',1'-f][1,3,5,2]triazaborinin-3-yl)phenoxy)propane-1-sulfonate (4.16mg, 5.8 μmol , 1.1 eq.) where combined with HBTU (2.39 mg, 6.3 μmol , 1.2 eq.) and TEA (4.39 μL , 31.5 μmol , 6 eq.) in amine-free DMF (0.5 mL) resulting in a dark blue solution. The reaction was shaken (550 RPM) at room temperature for 16 h. The reaction was diluted with water (20 mL). The obtained aqueous solution containing the product was flushed through a preconditioned C18 cartridge. A fraction was eluted off the cartridge using 10 mL solution of 80 % acetonitrile: 20% water. A second fraction was collected using 10 mL of acetonitrile. TLC and analytical HPLC was used to identify the correct fractions which were combined and lyophilised to yield FC131-AMBA aza-BODIPY conjugate (6.3 mg, 77.5%).

$R_f = 0.61$ (silica, KNO_3 :water:MeCN). HPLC: 20 to 95 % (20 min) of ($\text{CH}_3\text{CN}/0.1\%$ TFA) over 9 minutes. $R_f = 8.35$ minutes. UV-vis (MeCN): λ_{max} , nm ($\log \epsilon$) 655 (4.67). Fluorescence (MeCN): λ_{max} , (exc/ems) nm 620/680. ES-MS: m/z 1566.6 [$M+H$] $^+$ calcd for $\text{C}_{81}\text{H}_{83}\text{BF}_2\text{KN}_{13}\text{O}_{13}\text{S}^+$.

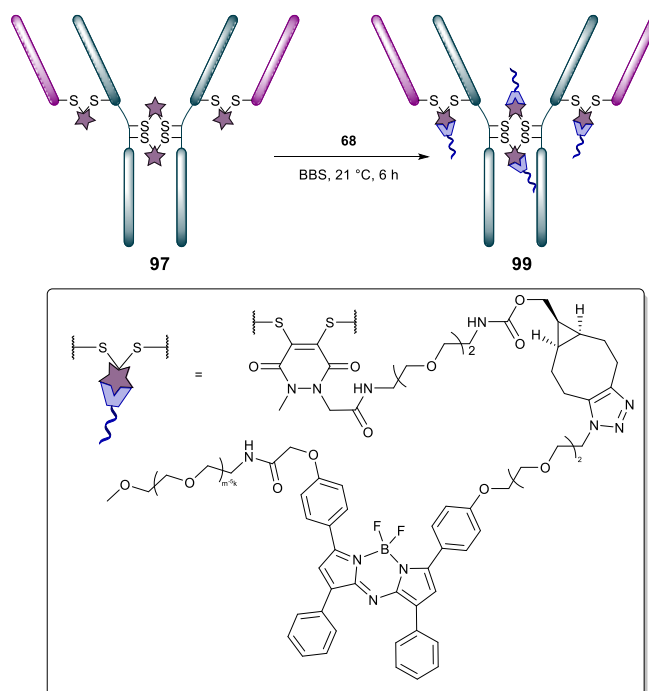
Fluorescent Antibody Conjugate (98)



To a solution of trastuzumab (100 μ L, 50 μ M, 1 eq.) in borate buffer (25 mM sodium borate, 25 mM NaCl, 0.5 mM EDTA, pH 8.0) was added TCEP (final concentration 500 μ M, 10 eq.) and **95** in DMSO (final concentration 1.0 mM, 25 eq.) and the reaction mixture incubated at 4 °C for 16 h. The excess reagents were then removed by repeated diafiltration into fresh buffer using VivaSpin sample concentrators (GE Healthcare, 10 000 MWCO). Following this, analysis by 10% SDS-PAGE gel and UV-Vis revealed conversion to the desired Her-Mestra conjugate with a PD-to-antibody ratio of *ca.* 4. Then, aza-BODIPY **40** (8 eq. from a 20 mM solution in DMSO) was added and the reaction mixture incubated at 37 °C for 4 h. The resulting mixture was then incubated for 10 min with protein A immobilised on beads and washed following manufacturer's protocol. Following this, analysis by SDS-PAGE gel and UV-Vis revealed conversion.

The desired product was not isolated.

Fluorescent Antibody Conjugate (99)



To a solution of trastuzumab (100 μ L, 50 μ M, 1 eq.) in borate buffer (25 mM sodium borate, 25 mM NaCl, 0.5 mM EDTA, pH 8.0) was added TCEP (final concentration 500 μ M, 10 eq.) and **95** in DMSO (final concentration 1.0 mM, 25 eq.) and the reaction mixture incubated at 4 $^{\circ}$ C for 16 h. The excess reagents were then removed by repeated diafiltration into fresh buffer using VivaSpin sample concentrators (GE Healthcare, 10 000 MWCO). Following this, analysis by 10% SDS-PAGE gel and UV-Vis revealed conversion to the desired Her-Mestra conjugate with a PD-to-antibody ratio of *ca.* 4. Then, aza-BODIPY **68** (8 eq. from a 20 mM solution in DMSO) was added and the reaction mixture incubated at 21 $^{\circ}$ C for 6 h. The resulting mixture was then incubated for 10 min with protein A immobilised on beads and washed following manufacturer's protocol. Following this, analysis by SDS-PAGE gel and UV-Vis revealed conversion to the desired Her-Mestra-aza-BODIPY conjugate **99** with a porphyrin-to-antibody ratio of *ca.* 4.

8. References

- 1 Q. T. Nguyen and R. Y. Tsien, *Nat. Rev. Cancer*, 2013, **13**, 653–62.
- 2 R. Haque, R. Contreras, M. P. McNicoll, E. C. Eckberg and D. B. Petitti, *BMC Ear. Nose. Throat Disord.*, 2006, **6**, 1–6.
- 3 P. J. Guillou, P. Quirke, H. Thorpe, J. Walker, D. G. Jayne, A. M. H. Smith, R. M. Heath and J. M. Brown, *Lancet*, 2005, **365**, 1718–1726.
- 4 C. Chiappa, F. Rovera, A. D. Corben, A. Fachinetti, V. De Berardinis, V. Marchionini, S. Rausei, L. Boni, G. Dionigi and R. Dionigi, *Int. J. Surg. Oncol.*, 2013, **11 Suppl 1**, S69–72.
- 5 F. Meric, N. Q. Mirza, G. Vlastos, T. a. Buchholz, H. M. Kuerer, G. V. Babiera, S. E. Singletary, M. I. Ross, F. C. Ames, B. W. Feig, S. Krishnamurthy, G. H. Perkins, M. D. McNeese, E. a. Strom, V. Valero and K. K. Hunt, *Cancer*, 2003, **97**, 926–933.
- 6 A. H. Feifer, J. M. Taylor, T. V. Tarin and H. W. Herr, *Eur. Urol.*, 2011, **59**, 978–984.
- 7 R. Weissleder and M. J. Pittet, *Nature*, 2008, **452**, 580–589.
- 8 I. Y. Eyüpoglu, N. Hore, N. E. Savaskan, P. Grummich, K. Roessler, M. Buchfelder and O. Ganslandt, *PLoS One*, 2012, **7**, 1–10.
- 9 J. Mislow, A. Golby and P. Black, *Neurosurg Clin N Am.*, 2009, **2**, 137–146.
- 10 G. M. Van Dam, G. Themelis, M. A. Lucia, N. J. Harlaar, R. G. Pleijhuis, W. Kelder, A. Sarantopoulos, J. S. De Jong, P. S. Low and V. Ntziachristos, *Nat. Med.*, 2011, **1315-1319**, 1–15.
- 11 A. L. Vahrmeijer, M. Hutteman, J. R. van der Vorst, C. J. H. van de Velde and J. V Frangioni, *Nat. Rev. Clin. Oncol.*, 2013, **10**, 507–18.
- 12 S. B. Mondal, S. Gao, N. Zhu, R. Liang, V. Gruev and S. Achilefu, *Adv Cancer Res.*, 2014, **124**, 171–211.
- 13 S. J. Yang, K. C. Tsai, C. L. Peng, F. H. Lin and M. J. Shieh, *NSTI-Nanotech*, 2007, **4**, 242–245.
- 14 W. Stummer, U. Pichlmeier, T. Meinel, O. D. Wiestler, F. Zanella and H. J. Reulen, *Lancet Oncol.*, 2006, **7**, 392–401.
- 15 A. Van Cleef, S. Altintas, M. Huizing, K. Papadimitriou, P. Van Dam and W. Tjalma, *Facts Views Vis Obgyn*, 2014, **6**, 210–218.
- 16 R. R. Zhang, A. B. Schroeder, J. J. Grudzinski and E. L. Rosenthal, *Nat. Rev.*

- Clin. Oncol.*, 2017, **14**, 347–364.
- 17 D. M. Parkin, P. Pisani and J. Ferlay, *CA Cancer J Clin*, 1999, **49**, 1,33–64.
- 18 R. L. Siegel, K. D. Miller and A. Jemal, *CA Cancer J Clin*, 2015, **65**, 5–29.
- 19 A. M. De Grand and J. V. Frangioni, *Technol. Cancer Res. Treat.*, 2003, **2**, 553–562.
- 20 H. Nelson, D. J. Sargent, H. S. Wieand, J. Fleshman, M. Anvari, S. J. Stryker, R. W. Beart, M. Hellinger, R. Flanagan, W. Peters and D. Ota, *N. Engl. J. Med.*, 2004, **350**, 2050–2059.
- 21 R. Veldkamp, *Lancet Oncol.*, 2009, **10**, 44–52.
- 22 S. Singhal, S. Nie and M. D. Wang, *Annu Rev Med.*, 2010, **61**, 359–373.
- 23 A. Moiyadi, P. Syed and S. Srivastava, *Nat. Rev. Cancer*, 2014, **14**, 146.
- 24 J. M. K. Mislaw, A. J. Golby and P. M. Black, *Neurosurg. Clin. NA*, 2009, **20**, 137–146.
- 25 S. Hao, D. Li, G. Ma, J. Yang and G. Wang, *J. Clin. Neurosci.*, 2013, **20**, 1269–1275.
- 26 M. Hojo, Y. Arakawa, T. Funaki, K. Yoshida, T. Kikuchi, Y. Takagi and Y. Araki, *World Neurosurg.*, 2014, **82**, e495–e501.
- 27 S. A. Mclaughlin, *Surg. Clin. NA*, 2013, **93**, 411–428.
- 28 M. Rizzo, R. Iyengar, S. G. A. Gabram, J. Park, G. Birdsong, K. L. Chandler and M. B. Mosunjac, *Ann. Surg. Oncol*, 2010, **17**, 228–234.
- 29 B. E. Schaafsma, J. R. Van Der Vorst, K. N. Gaarenstroom, A. A. W. Peters, F. P. R. Verbeek, C. D. De Kroon, J. B. M. Z. Trimbos, M. I. E. Van Poelgeest, J. V Frangioni, C. J. H. Van De Velde and A. L. Vahrmeijer, *Gynecol. Oncol.*, 2012, **127**, 126–130.
- 30 S. L. Troyan, V. Kianzad, S. L. Gibbs-strauss, S. Gioux, A. Matsui, R. Oketokoun, L. Ngo, A. Khamene and F. Azar, *Ann. Surg. Oncol*, 2009, **16**, 2943–2952.
- 31 J. F. Tamburrino and K. A. Swartz, *J Reconstr Microsurg*, 2010, **26**, 487–492.
- 32 A. M. Cohen, D. Kelsen, L. Saltz, B. D. Minsky, H. Nelson, R. Farouk, L. L. Gunderson, F. Michelassi, R. B. Arenas, R. L. Schilsky and C. G. Willet, in *Current Problems in Surgery*, 1997, vol. 34, pp. 601–676.
- 33 S. Scabini, *World J. Gastrointest. Surg.*, 2010, **2**, 6–8.
- 34 K. Harada, Y. Harada, M. Beika, N. Koizumi, K. Inoue, Y. Murayama, Y.

- Kuriu, M. Nakanishi, T. Minamikawa, Y. Yamaoka, P. Dai, A. Yanagisawa, E. Otsuji and T. Takamatsu, *Int. J. Mol. Sci.*, 2013, **14**, 23140–23152.
- 35 A. Kumar, R. Puri, P. V. Gadgil and I. Jatoi, *World J. Surg.*, 2012, **36**, 1453–1459.
- 36 S. L. Wong, C. M. Balch, P. Hurley, S. S. Agarwala, T. J. Akhurst, A. Cochran, J. N. Cormier, M. Gorman, T. Y. Kim, K. M. McMasters, R. D. Noyes, L. M. Schuchter, M. E. Valsecchi, D. L. Weaver and G. H. Lyman, *J. Clin. Oncol.*, 2012, **30**, 2912–2918.
- 37 D. G. Nicastrì, J. T. Doucette, T. E. Godfrey and S. J. Hughes, *J. Mol. Diagn.*, 2007, **9**, 563–571.
- 38 P. I. Haigh and A. E. Giuliano, *Ann. Surg.*, 1994, **220**, 391–401.
- 39 M. Yashiro and T. Matsuoka, *World J Gastrointest Surg*, 2015, **7**, 1–9.
- 40 M. Ankersmit, M. H. G. M. van der Pas, D. a. van Dam and W. J. H. J. Meijerink, *Color. Dis*, 2011, **13**, 70–73.
- 41 M. Hutteman, H. S. Choi, J. S. D. Mieog, J. R. van der Vorst, Y. Ashitate, P. J. K. Kuppen, M. C. van Groningen, C. W. G. M. Löwik, V. T. H. B. M. Smit, C. J. H. van de Velde, J. V Frangioni and A. L. Vahrmeijer, *Ann. Surg. Oncol.*, 2011, **18**, 1006–1014.
- 42 D. Jocham, H. Stepp and R. Waidelich, *Eur. Urol.*, 2008, **53**, 1138–1150.
- 43 K. T. Moesta, B. Ebert, T. Handke, D. Nolte, C. Nowak, W. E. Haensch, R. K. Pandey, T. J. Dougherty, H. Rinneberg and P. M. Schlag, *Cancer Res*, 2001, **61**, 991–999.
- 44 S. L. Gibbs, B. Chen, J. a O’Hara, P. J. Hoopes, T. Hasan and B. W. Pogue, *Photochem. Photobiol.*, 2006, **82**, 1334–1341.
- 45 J. Moan, G. Streckyte, S. Bagdonas, Ø. Bech and K. Berg, *Int. J. Cancer*, 1997, **70**, 90–97.
- 46 N. E. Dudley, *Br. Med. J.*, 1971, **3**, 680–681.
- 47 J. H. Winer, H. S. Choi, S. L. Gibbs-Strauss, Y. Ashitate, Y. L. Colson and J. V Frangioni, *Ann. Surg. Oncol.*, 2010, **17**, 1094–1100.
- 48 J. R. van der Vorst, *World J. Gastrointest. Surg.*, 2012, **4**, 180–184.
- 49 A. Matsui, E. Tanaka, H. S. Choi, V. Kianzad, S. Gioux, S. J. Lomnes and J. V Frangioni, *Surgery*, 2010, **148**, 78–86.
- 50 Y. Ashitate, C. S. Vooght, M. Hutteman, R. Oketokoun, H. S. Choi and J. V. Frangioni, *Mol. Imaging*, 2012, **11**, 301–308.

- 51 T. Ishizawa, N. Fukushima, J. Shibahara, K. Masuda, S. Tamura, T. Aoki, K. Hasegawa, Y. Beck, M. Fukayama and N. Kokudo, *Cancer*, 2009, **115**, 2491–2504.
- 52 M. Ishizuka, K. Kubota, J. Kita, M. Shimoda, M. Kato and T. Sawada, *Hepato-gastroenterol*, 2012, **59**, 90–92.
- 53 Ó. G. Björnsson, R. Murphy and V. S. Chadwick, *Experientia*, 1982, **38**, 1441–1442.
- 54 S. Obniski, S. J. Lomnes, R. G. Laurence, A. Gogbasian, G. Mariani and J. V. Frangioni, *Mol. Imaging*, 2005, **4**, 172–181.
- 55 S. Folli, G. Wagnieres, A. Pelegrin, J. M. Calmes, D. Braichotte, F. Buchegger, Y. Chalandon, N. Hardman, C. Heusser, J. C. Givel, G. Chapuis, A. Chatelain, H. Vandenberg and J. P. Mach, *Proc. Natl. Acad. Sci. U. S. A.*, 1992, **89**, 7973–7977.
- 56 R. Sjöback, J. Nygren and M. Kubista, *Spectrochim. Acta A*, 1995, **51**, L7–L21.
- 57 T. Fujii, M. Kamiya and Y. Urano, *Bioconjugate Chem.*, 2014, **25**, 1838–1846.
- 58 E. Kim, K. S. Yang, R. J. Giedt and R. Weissleder, *Chem. Commun.*, 2014, **50**, 4504–7.
- 59 E. Kim, K. S. Yang, R. H. Kohler, J. M. Dubach, H. Mikula and R. Weissleder, *Bioconjugate Chem.*, 2015, **26**, 1513–1518.
- 60 C. Zenz, *Occupational Medicine-Principles and Practical Applications. 2nd ed*, 1988.
- 61 T. Kaji, T. Kawashima, C. Yamamoto and S. M, *Toxicol. Lett*, 1992, **61**, p. 81–87.
- 62 S. Thaler, C. Haritoglou, T. J. Choragiewicz, A. Messias, A. Baryluk, C. A. May, R. Rejdak, M. Fiedorowicz, E. Zrenner and F. Schuettauf, *Investig. Ophthalmol. Vis. Sci.*, 2008, **49**, 2120–2126.
- 63 D. A. Hindtley and P. G. Seybold, *J. Chem. Educ*, 1987, **64**, 362–364.
- 64 Y. Ha and H. K. Choi, *Chem. Biol. Interact.*, 2016, **248**, 36–51.
- 65 H. Li, Y. Li, L. Cui, B. Wang, W. Cui, M. Li and Y. Cheng, *PLoS One*, 2014, **9**, 1–12.
- 66 X. Lin, H. Zhu, Z. Luo, Y. Hong, H. Zhang, X. Liu, H. Ding, H. Tian and Z. Yang, *Mol. Imaging Biol.*, 2014, **16**, 877–887.
- 67 A. P. Gorka, R. R. Nani and M. J. Schnermann, *Org. Biomol. Chem.*, 2015, **13**, 7584–7598.

- 68 J. J. McEwen and K. J. Wallace, *Chem. Commun.*, 2009, **0**, 6339–6351.
- 69 U. Mayerhöffer, B. Fimmel and F. Würthner, *Angew. Chem. Int. Ed.*, 2012, **51**, 164–167.
- 70 A. J. McKerrow, E. Buncel and P. M. Kazmaier, *Can. J. Chem.*, 1995, **73**, 1605–1615.
- 71 J. V Ros-Lis, R. Martínez-mañez and J. Soto, *Chem. Commun.*, 2002, **0**, 2248–2249.
- 72 R. Dyes, T. Weil, T. Weil, T. Vosch, J. Hofkens, K. Peneva and K. Müllen, *Angew. Chem. Int. Ed.*, 2010, **49**, 9068–9093.
- 73 C. Huang, S. Barlow and S. R. Marder, *J. Org. Chem.*, 2011, **76**, 2386–2407.
- 74 A. Margineanu, J. Hofkens, M. Cotlet, S. Habuchi, A. Stefan, J. Qu, C. Kohl, K. Mu, J. Vercammen, Y. Engelborghs, T. Gensch and F. C. De Schryver, *J. Phys. Chem. B*, 2004, **108**, 12242–12251.
- 75 T. Weil, M. A. Abdalla, C. Jatzke, J. Hengstler and K. Mu, *Biomacromolecules*, 2005, **6**, 68–79.
- 76 K. Koynov, A. Vonderheit, K. Mu and K. Peneva, *J. Am. Chem. Soc.*, 2016, **138**, 2881–2884.
- 77 N. Boens, V. Leen and W. Dehaen, *Chem. Soc. Rev.*, 2012, **41**, 1130–1172.
- 78 Y. Ni and J. Wu, *Org. Biomol. Chem.*, 2014, **12**, 3774–91.
- 79 L. B. Josefsen and R. W. Boyle, *Theranostics*, 2012, **2**, 916–966.
- 80 D. A. Heuveling, G. W. M. Visser, M. De Groot, J. F. De Boer, M. Baclayon, W. H. Roos, G. J. L. Wuite, C. R. Leemans, R. De Bree and G. A. M. S. Van Dongen, *Eur. J. Nucl. Med. Mol. Imaging*, 2012, **39**, 1161–1168.
- 81 R. Krabbendam, M. Pool, L. G. de Vries, H. L. Offerhaus, J. L. Herek and C. Otto, *J. Biomed. Opt.*, 2015, **20**, 086006.1–086006.9.
- 82 Y. Wang, K. Zhou, G. Huang, C. Hensley, X. Huang, T. Zhao, B. D. Sumer, R. J. Deberardinis and J. Gao, *Nat Mater.*, 2014, **13**, 204–212.
- 83 C. J. Tynan, D. T. Clarke, B. C. Coles, D. J. Rolfe, M. L. Martin-Fernandez and S. E. D. Webb, *PLoS One*, 2012, **7**, e36265.1–e36265.7.
- 84 R. Huang, J. Vider, J. L. Kovar, D. M. Olive, I. K. Mellinghoff, P. Mayer-Kuckuk, M. F. Kircher and R. G. Blasberg, *Clin. Cancer Res.*, 2012, **18**, 5731–5740.
- 85 V. Pansare, S. Hejazi, W. Faenza and R. K. Prud'homme, *Chem Mater.*, 2012, **24**, 812–827.

- 86 S. Tiash and E. H. Chowdhury, *J. Cancer Metastasis Treat.*, 2015, **1**, 190–200.
- 87 M. V. Marshall, D. Draney, E. M. Sevick-Muraca and D. M. Olive, *Mol. Imaging Biol.*, 2010, **12**, 583–594.
- 88 W. B. Nagengast, E. G. de Vries, G. a Hospers, N. H. Mulder, J. R. de Jong, H. Hollema, A. H. Brouwers, G. a van Dongen, L. R. Perk and M. N. Lub-de Hooge, *J. Nucl. Med.*, 2007, **48**, 1313–1319.
- 89 M. Srinivasarao, C. V Galliford and P. S. Low, *Nat. Rev. Drug Discov.*, 2015, **14**, 203–219.
- 90 E. De Jesus, J. J. Keating, S. A. Kularatne, J. Jiang, R. Judy, J. Predina, S. Nie, P. Low and S. Singhal, *Int. J. Mol. Imaging*, 2015, **2015**, 1–10.
- 91 J. P. Weichert, P. A. Clark, I. K. Kandela, A. M. Vaccaro, W. Clarke, M. A. Longino, A. N. Pinchuk, M. Farhoud, K. I. Swanson, J. M. Floberg, J. Grudzinski, B. Titz, A. M. Traynor, H. Chen, L. T. Hall, C. J. Pazoles, P. J. Pickhardt and J. S. Kuo, *Sci Transl Med*, 2014, **6**, 240ra75.
- 92 K. I. Swanson, P. A. Clark and R. R. Zhang, *Neurosurgery*, 2015, **76**, 115–124.
- 93 M. L. Korb, J. M. Warram, J. Grudzinski, J. Weichert, J. Jeffery and E. L. Rosenthal, *Mol. Imaging*, 2014, **13**, 1–9.
- 94 D. A. Deming, M. E. Maher, A. A. Leystra, J. P. Grudzinski, L. Clipson, D. M. Albrecht, M. K. Washington, K. A. Matkowskyj, L. T. Hall, S. J. Lubner, J. P. Weichert and R. B. Halberg, *PLoS One*, 2014, **9**, e109668–e109673.
- 95 S. Lee, J. Xie and X. Chen, *Biochemistry*, 2010, **49**, 1364–1376.
- 96 R. Schneider, L. Tirand, C. Frochot, R. Vandresse, N. Thomas, J. Gravier, F. Guillemain and M. Barberi-heyob, *Anticancer. Agents Med. Chem.*, 2006, **6**, 469–488.
- 97 M. Sibrian-vazquez, T. J. Jensen, F. R. Fronczek, R. P. Hammer and M. G. H. Vicente, *Bioconjugate Chem.*, 2005, **3**, 852–863.
- 98 N. Zhao, T. M. Williams, Z. Zhou, F. R. Fronczek, M. Sibrian-Vazquez, S. D. Jois and M. G. H. Vicente, *Bioconjugate Chem.*, 2017, **28**, 1566–1579.
- 99 J. Burggraaf, I. M. C. Kamerling, P. B. Gordon, L. Schrier, M. L. de Kam, A. J. Kales, R. Bendiksen, B. Indrevoll, R. M. Bjerke, S. A. Moestue, S. Yazdanfar, A. M. J. Langers, M. Swaerd-Nordmo, G. Torheim, M. V Warren, H. Morreau, P. W. Voorneveld, T. Buckle, F. W. B. van Leeuwen, L.-I. Ødegårdstuen, G. T. Dalsgaard, A. Healey and J. C. H. Hardwick, *Nat. Med.*, 2015, **21**, 955–961.
- 100 C. Eggeling, J. Widengren, L. Brand, J. Schaffer, S. Felekyan and C. A. M. Seidel, *J. Phys. Chem. A*, 2006, **110**, 2979–2995.

- 101 P. V. Butte, A. Mamelak, J. Parrish-Novak, D. Drazin, F. Shweikeh, P. R. Gangalum., A. Chesnokova, J. Y. Ljubimova and K. Black, *Neurosurg. Focus*, 2014, **36**, 1–8.
- 102 C. Xu, J. M. Olson, J. Parrish-novak and E. Méndez, *JAMA Otolaryngol. Head Neck Surg.*, 2016, **142**, 330–338.
- 103 J. Fidel, K. C. Kennedy, W. S. Dernell, S. Hansen, V. Wiss, M. R. Stroud, J. I. Molho, S. E. Knoblauch, J. Meganck, J. M. Olson, B. Rice and J. Parrish-novak, *Cancer Res*, 2015, **75**, 4283–4292.
- 104 E. Frei, *Diabetol Metab Syndr*, 2011, **3**, 2–5.
- 105 A. M. Merlot, D. S. Kalinowski and D. R. Richardson, *Front Physiol.*, 2014, **5**, 1–7.
- 106 G. Zheng, J. Chen, H. Li and J. D. Glickson, *PNAS*, 2005, **102**, 17757–17762.
- 107 J. W. Hawkins and A. Dugaiczky, *Gene.*, 1982, **19**, 55–58.
- 108 H. Lodish, A. Berk, S. L. Zipursky, P. Matsudaira, D. Baltimore and J. Darnell, in *Molecular Cell Biology. 4th edition.*, W. H. Freeman, New York, 4th edn., 2000, p. Sec. 17.9.
- 109 L. B. Josefsen and R. W. Boyle, *Br. J. Pharmacol.*, 2008, **154**, 1–3.
- 110 J. M. Sutton, O. J. Clarke, N. Fernandez and R. W. Boyle, *Bioconjugate Chem.*, 2002, **13**, 249–263.
- 111 K. G and M. C, *Nature*, 1975, **256**, 495–497.
- 112 G. J. Weiner, *Nat. Rev. Cancer*, 2015, **15**, 361–370.
- 113 X. Zhang, G. Soori, T. J. Dobleman and G. G. Xiao, *Expert Rev. Mol. Diagn.*, 2014, **14**, 97–106.
- 114 P. Winnard and V. Raman, *J. Cell Biochem.*, 2003, **90**, 454–463.
- 115 A. M. Wu and P. D. Senter, *Nat. Biotechnol.*, 2005, **23**, 1137–1146.
- 116 T. Barrett, Y. Koyama, Y. Hama, G. Ravizzini, I. S. Shin, B. Jang, C. H. Paik, Y. Urano, P. L. Choyke and H. Kobayashi, *Clin. Cancer Res.*, 2007, **13**, 6639–6649.
- 117 S. Muyldermans, *Annu. Rev. Biochem.*, 2013, **82**, 775–797.
- 118 A. L. Nelson, *MAbs*, 2010, **2**, 77–83.
- 119 J. McMahan, C. J. O. Brien, I. Pathak, R. Hamill, E. Mcneil and N. Hammersley, *Br J Oral Maxillofac Surg.*, 2003, **41**, 224–231.
- 120 J. P. Spano, C. Lagorce, D. Atlan, G. Milano, J. Domont, R. Benamouzig, A.

- Attar, J. Benichou, A. Martin, J. F. Morere, M. Raphael, F. Penault-Llorca, J. L. Breau, R. Fagard, D. Khayat and P. Wind, *Ann. Oncol.*, 2005, **16**, 102–108.
- 121 A. Bardelli and P. A. Jänne, *Nat. Med.*, 2012, **18**, 199–200.
- 122 A. Witt, N. Macdonald and P. Kirkpatrick, *Nat. Rev. Drug Discov.*, 2004, **3**, 109–110.
- 123 J. M. Warram, E. De Boer, G. M. Van Dam, L. S. Moore, S. L. Bevans, E. M. Walsh, E. S. Young, W. R. Carroll, T. M. Stevens and E. L. Rosenthal, *J. Pathol. Clin. Res*, 2016, **2**, 104–112.
- 124 J. M. Warram, E. de Boer, M. Korb, Y. Hartman, J. Kovar, J. M. Markert, G. Y. Gillespie and E. L. Rosenthal, *Br. J. Neurosurg.*, 2015, **8697**, 1–9.
- 125 P. Conaghan, S. Ashraf, M. Tytherleigh, J. Wilding, E. Tchilian, D. Bicknell, N. J. Mortensen and W. Bodmer, *Br. J. Cancer*, 2008, **98**, 1217–1225.
- 126 J. P. Tiernan, S. L. Perry, E. T. Verghese, N. P. West, S. Yeluri, D. G. Jayne and T. a Hughes, *Br. J. Cancer*, 2013, **108**, 662–667.
- 127 J. F. Lovell, C. S. Jin, E. Huynh, H. Jin, C. Kim, J. L. Rubinstein, W. C. W. Chan, W. Cao, L. V Wang and G. Zheng, *Nat. Mater.*, 2011, **10**, 324–332.
- 128 M. Grossi, M. Morgunova, S. Cheung, D. Scholz, E. Conroy, M. Terrile, A. Panarella, J. C. Simpson, W. M. Gallagher and D. F. O’Shea, *Nat. Commun.*, 2016, **7**, 10855–10868.
- 129 N. Stephanopoulos and M. B. Francis, *Nat. Chem. Biol.*, 2011, **7**, 876–884.
- 130 A. . Coons and K. Melvin, *J. Immunol.*, 1942, **45**, 159–170.
- 131 R. Norman, J. Creech and R. Norman, *J. Am. Chem. Soc*, 1940, **3396**, 1670–1673.
- 132 L. Goodfriend and A. H. Schon, *Can. J. Biochem.*, 1958, **36**, 1177–1184.
- 133 A. Todrick and E. Walker, *Biochem.J.*, 1937, **31**, 297–298.
- 134 D. Podhradsk, L. Drobica and P. Kristian, *Experientia*, 1979, **35**, 154–155.
- 135 J. L. Riggs, R. J. Seiwald, J. H. Burckhalter, C. M. Downs and T. G. Metcalf, *Am J Pathol.*, 1958, **34**, 1081–1097.
- 136 J. Tuls, L. Geren and F. Millett, *J. Biol. Chem.*, 1989, **264**, 16421–16425.
- 137 L. D. Burtnick, *Biochim. Biophys. Acta*, 1984, **791**, 57–62.
- 138 G. W. Anderson, J. E. Zimmerman and F. M. Callahan, *J. Am. Chem. Soc*, 1964, **86**, 1839–1842.
- 139 M. D. Leavell, P. Novak, C. R. Behrens, J. S. Schoeniger and G. H. Kruppa, *J.*

- Am. Soc. Mass Spectrom.*, 2004, **15**, 1604–1611.
- 140 P. Cuatrecasas and I. Parikh, *Biochemistry*, 1972, **11**, 2291–2299.
- 141 J. V. Staros, R. W. Wright and D. M. Swingle, *Anal. Biochem.*, 1986, **156**, 220–222.
- 142 S. J. Sirk, T. Olafsen, B. Barat, K. B. Bauer and A. M. Wu, *Bioconjugate Chem.*, 2008, **19**, 2527–2534.
- 143 F. Brotzel and H. Mayr, *Org. Biomol. Chem.*, 2007, **5**, 3814–3820.
- 144 R. E. Hansen and J. R. Winther, *Anal. Biochem.*, 2009, **394**, 147–158.
- 145 F. R. N. Gurd, *Methods Enzymol.*, 1972, **25**, 424–438.
- 146 E. T. Kaiser and D. S. Lawrence, *Science (80-.)*, 1984, **226**, 505–511.
- 147 E. Friedmann and D. H. Marrian, *Brit. J. Pharmacol.*, 1949, **4**, 105–108.
- 148 Y. Ishii and S. S. Lehrer, *Biophys. J.*, 1986, **50**, 75–80.
- 149 X. Chen, Y. Zhou, X. Peng and J. Yoon, *Chem Soc Rev*, 2010, **39**, 2120–2135.
- 150 J. Porath and A. Rolf, *Methods Enzym.*, 1976, **44**, 19–45.
- 151 A. Massi and D. Nanni, *Org. Biomol. Chem.*, 2012, **10**, 3791–3807.
- 152 M. Lo Conte, S. Pacifico, A. Chambery, A. Marra and A. Dondoni, *J. Org. Chem*, 2010, **75**, 4644–4647.
- 153 M. Lo Conte, S. Staderini, A. Marra, M. Sanchez-Navarro, B. G. Davis and A. Dondoni, *Chem. Commun.*, 2011, **47**, 11086–11088.
- 154 J. Rademann, *Angew. Chem. Int. Ed. Engl.*, 2004, **43**, 4554–4556.
- 155 M. E. B. Smith, F. F. Schumacher, C. P. Ryan, L. M. Tedaldi, D. Papaioannou, G. Waksman, S. Caddick and J. R. Baker, *J. Am. Chem. Soc.*, 2010, **132**, 1960–1965.
- 156 M. W. Jones, R. A. Strickland, F. F. Schumacher, S. Caddick, J. R. Baker, M. I. Gibson and D. M. Haddleton, *J. Am. Chem. Soc.*, 2012, **134**, 1847–1852.
- 157 D. Richards, S. Fletcher, M. Nobles, H. Kossen, L. Tedaldi, V. Chudasama, A. Tinker and J. R. Baker, *Org. Biomol. Chem.*, 2015, **14**, 455–459.
- 158 P. Moody, M. E. B. Smith, C. P. Ryan, V. Chudasama, J. R. Baker, J. Molloy and S. Caddick, *ChemBioChem*, 2012, **13**, 39–41.
- 159 A. Maruani, M. E. B. Smith, E. Miranda, K. A. Chester, V. Chudasama and S. Caddick, *Nat. Commun.*, 2015, **6**, 6645–6654.
- 160 R. L. Lundblad, in *Chemical Reagents for Protein Modification*, CRC Press, 3rd edn, 2010, pp. 435–488.

- 161 M. Kai, J. Ishida and Y. Ohkura, *J. Chromatogr. B, Biomed. Appl.*, 1988, **430**, 271–278.
- 162 M. K. and Y. O. J. Ishida, *J. Chromatogr. A*, 1986, **356**, 171–177.
- 163 S. D. Tilley and M. B. Francis, *J. Am. Chem. Soc.*, 2006, **128**, 1080–1081.
- 164 O. Koniev and A. Wagner, *Chem. Soc. Rev.*, 2015, **44**, 5495–551.
- 165 H. G. Higgins and K. J. Harrington, *Arch. Biochem. Biophys.*, 1959, **85**, 409–425.
- 166 T. L. Schlick, Z. Ding, E. W. Kovacs and M. B. Francis, *J. Am. Chem. Soc.*, 2005, **127**, 3718–3723.
- 167 J. Gavriilyuk, H. Ban, M. Nagano, W. Hakamata and C. F. Barbas, *Bioconjug. Chem.*, 2012, **23**, 2321–2328.
- 168 H. Fraenkel-Conrat and H. S. Olcott, *J. Biol. Chem.*, 1948, **174**, 827–843.
- 169 D. W. Romanini and M. B. Francis, *Bioconjugate Chem.*, 2008, **19**, 153–157.
- 170 H. M. Guo, M. Minakawa and F. Tanaka, *J. Org. Chem.*, 2008, **73**, 3964–3966.
- 171 G. Desimoni, G. Faita, S. Guidetti and P. P. Righetti, *Tetrahedron*, 1994, **50**, 1821–1832.
- 172 H. Ban, M. Nagano, J. Gavriilyuk, W. Hakamata, T. Inokuma and C. F. Barbas, *Bioconjugate Chem.*, 2013, **24**, 520–532.
- 173 E. M. Sletten and C. R. Bertozzi, *Angew. Chem. Int. Ed.*, 2009, **48**, 6974–6998.
- 174 E. M. Sletten and C. R. Bertozzi, *Acc. Chem. Res.*, 2011, **44**, 666–676.
- 175 K. Lang and J. W. Chin, *ACS Chem. Biol.*, 2014, **9**, 16–20.
- 176 H. C. Kolb, M. G. Finn and K. B. Sharpless, *Angew. Chem. Int. Ed.*, 2001, **40**, 2004–2021.
- 177 K. Nwe and M. W. Brechbiel, *Cancer Biother. Radiopharm.*, 2009, **24**, 289–302.
- 178 V. V. Rostovtsev, L. G. Green, V. V. Fokin and K. B. Sharpless, *Angew. Chem. Int. Ed.*, 2002, **41**, 2596–2599.
- 179 L. Jin, D. R. Tolentino, M. Melaimi and G. Bertrand, *Sci. Adv.*, 2015, **1**, 1–5.
- 180 S. L. Presolski, V. P. Hong and M. G. Finn, *Curr. Protoc. Chem. Biol.*, 2011, **3**, 153–162.
- 181 D. C. Kennedy, C. S. McKay, M. C. B. Legault, D. C. Danielson, J. A. Blake, A. F. Pegoraro, A. Stolow, Z. Mester and J. P. Pezacki, *J. Am. Chem. Soc.*, 2011, **133**, 17993–18001.

- 182 R. Schönauer, A. Kaiser, C. Holze, S. Babilon, J. Köbberling and A. G. Beck-sickinger, *J. Pept. Sci.*, 2015, **21**, 905–912.
- 183 Q. Xie, X. Weng, L. Lu, Z. Lin, X. Xu and C. Fu, *Biosens. Bioelectron.*, 2016, **77**, 46–50.
- 184 V. M. Farzan, I. O. Aparin, O. A. Veselova, A. T. Podkolzin, G. A. Shipulin, A. Korshun and T. S. Zatsepin, *Anal. Methods*, 2016, **8**, 5826–5831.
- 185 D. Eglo, I. A. Oleinich, M. Zhao, S. L. B. Ko, R. K. O. Sigel and E. Freisinger, *ACS Chem. Biol.*, 2016, **11**, 2558–2567.
- 186 J. Melorose, R. Perroy and S. Careas, *ACS Chem. Biol.*, 2006, **1**, 644–648.
- 187 J. A. Codelli, J. M. Baskin, N. J. Agard and C. R. Bertozzi, *J. Am. Chem. Soc.*, 2008, **130**, 11486–11493.
- 188 C. G. Gordon, J. L. MacKey, J. C. Jewett, E. M. Sletten, K. N. Houk and C. R. Bertozzi, *J. Am. Chem. Soc.*, 2012, **134**, 9199–9208.
- 189 C. S. McKay and M. G. Finn, *Chem. Biol.*, 2014, **21**, 1075–1101.
- 190 J. Tummatorn, P. Batsomboon, R. J. Clark, I. V Alabugin and G. B. Dudley, *J. Org. Chem.*, 2012, **77**, 2093–2097.
- 191 A. Maruani, H. Savoie, F. Bryden, S. Caddick, R. Boyle and V. Chudasama, *Chem. Commun.*, 2015, **51**, 15304–15307.
- 192 K. Lang, L. Davis, S. Wallace, M. Mahesh, D. J. Cox, M. L. Blackman, J. M. Fox and J. W. Chin, *J. Am. Chem. Soc.*, 2012, **134**, 10317–10320.
- 193 O. Boutureira and J. L. Bernardes, *Chem. Rev.*, 2015, **115**, 2174–2195.
- 194 A. Treibs and F. H. Kreuzer, *Justus Liebigs Ann. Chem.*, 1968, **718**, 208–223.
- 195 G. Ulrich, R. Ziessel and A. Harriman, *Angew. Chem., Int. Ed.*, 2008, **47**, 1184–1201.
- 196 A. Loudet and K. Burgess, *Chem. Rev.*, 2007, **107**, 4891–4932.
- 197 J. L. E.V. Wael, J.A. Pardoën, J.A Koeverving, *Recl. Trav. Chim.Pays-Bas*, 1977, **96**, 306–309.
- 198 I. Mikhalyov, N. Gretskaya, F. Bergstrom and L. B.-Å. Johansson, *Phys. Chem. Chem. Phys.*, 2002, **4**, 5663–5670.
- 199 D. Marushchak, S. Kalinin, I. Mikhalyov, N. Gretskaya and L. B.-Å. Johansson, *Spectrochim Acta A*, 2006, **65**, 113–122.
- 200 F. Bergstro, I. Mikhalyov, P. Ha, T. Ny and L. B.-Å. Johansson, *J. Am. Chem.*

- Soc.*, 2002, **124**, 397–405.
- 201 G. Clavier, S. Badre, A. I. Mikhaleva, C. Laprent, R. Pansu, P. Audebert and B. A. Trofimov, *Russ. J. Gen. Chem.*, 2008, **78**, 2247–2256.
- 202 T. E. Wood and A. Thompson, *Chem. Rev*, 2007, **107**, 1831–1861.
- 203 T. Rohand, *Arkivoc*, 2007, **2007**, 307–324.
- 204 M. Shah, K. Thangaraj, M.-L. Soong, L. T. Wolford, J. H. Boyer, I. R. Politzer and T. G. Pavlopoulos, *Heteroat. Chem*, 1990, **1**, 389–399.
- 205 J. H. Boyer, A. M. Haag, G. Sathyamoorthi, M.-L. Soong, K. Thangaraj and T. G. Pavlopoulos, *Heteroat. Chem.*, 1993, **4**, 39–49.
- 206 Z. Li, E. Mintzer and R. Bittman, *J. Org. Chem*, 2006, **71**, 1718–1721.
- 207 V. P. Yakubovskiy, M. P. Shandura and Y. P. Kovtun, *Eur. J. Org. Chem*, 2009, 3237–3243.
- 208 L. Wu and K. Burgess, *Chem. Commun.*, 2008, 4933–4935.
- 209 R. Weissleder, *Nat. Biotechnol.*, 2001, **19**, 316–317.
- 210 J. V. Frangioni, *Curr. Opin. Chem. Biol.*, 2003, **7**, 626–634.
- 211 E. Kim and S. B. Park, in *Advanced Fluorescence Reporters in Chemistry and Biology I*, 2010, pp. 161–167.
- 212 E. Deniz, G. C. Isbasar, O. A. Bozdemir, L. T. Yildirim, A. Siemiarczuk and E. U. Akkaya, *Org. Lett.*, 2008, **10**, 3401–3.
- 213 Y. Hayashi, S. Yamaguchi, W. Y. Cha, D. Kim and H. Shinokubo, *Org. Lett.*, 2011, **13**, 2992–2995.
- 214 S. Atilgan, Z. Ekmekci, A. L. Dogan, D. Guç and E. U. Akkaya, *Chem. Commun.*, 2006, **0**, 4398–4400.
- 215 S. Kim, T. Y. Ohulchansky, A. Baev and P. N. Prasad, *J. Mater. Chem.*, 2009, **19**, 3181.
- 216 S. Rihn, P. Retailleau, N. Bugsaliewicz, A. De Nicola and R. Ziessel, *Tetrahedron Lett.*, 2009, **50**, 7008–7013.
- 217 N. Zhao, S. Xuan, B. Byrd, F. R. Fronczek, K. M. Smith and M. G. H. Vicente, *Org. Biomol. Chem.*, 2016, **14**, 6184–6188.
- 218 T. Rohand, W. Qin, N. Boens and W. Dehaen, *Eur. J. Org. Chem.*, 2006, **2006**, 4658–4663.
- 219 H. Lu, J. Mack, Y. Yang and Z. Shen, *Chem. Soc. Rev.*, 2014, **43**, 4778–823.
- 220 J. Killoran, L. Allen, J. F. Gallagher, W. M. Gallagher and D. F. O’Shea,

- Chem. Commun.*, 2002, **317**, 1862–1863.
- 221 A. Gorman, J. Killoran, C. O'Shea, T. Kenna, W. M. Gallagher and D. F. O'Shea, *J. Am. Chem. Soc.*, 2004, **126**, 10619–10631.
- 222 M. Tasior and D. F. O'Shea, *Bioconjugate Chem.*, 2010, **21**, 1130–1133.
- 223 Y. Chen, L. Wan, D. Zhang, Y. Bian and J. Jiang, *Photochem. Photobiol. Sci.*, 2011, **10**, 1030–1038.
- 224 Z. Dost, S. Atilgan and E. U. Akkaya, *Tetrahedron*, 2006, **62**, 8484–8488.
- 225 O. Buyukcakir, O. A. Bozdemir, S. Kolemen, S. Erbas and E. U. Akkaya, *Org. Lett.*, 2009, **11**, 4644–4647.
- 226 S. Erbas, A. Gorgulu, M. Kocakusakogullari and E. U. Akkaya, *Chem. Commun.*, 2009, **0**, 4956–4958.
- 227 P. Didier, G. Ulrich, Y. Mely and R. Ziessel, *Org. Biomol. Chem.*, 2009, **7**, 3639–3642.
- 228 S. Hoogendoorn, A. E. M. Blom, L. I. Willems, G. a van der Marel and H. S. Overkleeft, *Org. Lett.*, 2011, **13**, 5656–5659.
- 229 M. Di Donato, A. Iagatti, A. Lapini, P. Foggi, S. Cicchi, L. Lascialfari, S. Fedeli, S. Caprasecca and B. Mennucci, *J. Phys. Chem. C*, 2014, **118**, 23476–23486.
- 230 M. A. T. Rogers, *J. Chem. Soc.*, 1943, 590–596.
- 231 H. Liu, J. Mack, Q. Guo, H. Lu, N. Kobayashi and Z. Shen, *Chem. Commun.*, 2011, **47**, 12092–12094.
- 232 H. C. Daly, G. Sampedro, C. Bon, D. Wu, G. Ismail, R. A. Cahill and D. F. O. Shea, *Eur. J. Med. Chem.*, 2017, **135**, 392–400.
- 233 T. Li, T. Meyer, R. Meerheim, H. Marco and K. Christian, *J. Mater. Chem. A.*, 2017, **31**, 10696–10703.
- 234 J. Joshi, T. Kumari and Y. Duchaniya, *IJETMAS*, 2015, **3**, 200–211.
- 235 W. Zhao and E. M. Carreira, *Angew. Chem., Int. Ed.*, 2005, **44**, 1677–1679.
- 236 T. Jokic, S. M. Borisov, R. Saf, D. A. Nielsen, M. Kühl and I. Klimant, *Anal. Chem.*, 2012, **84**, 6723–6730.
- 237 S. Schutting, T. Jokic, M. Strobl, S. M. Borisov, D. de Beer and I. Klimant, *J. Mater. Chem. C*, 2015, **3**, 5474–5483.
- 238 M. A. T. Rogers, *Nature*, 1943, **151**, 504.
- 239 D. Wu and D. F. O'Shea, *Org. Lett.*, 2013, **15**, 3392–3395.

- 240 M. J. Hall, S. O. McDonnell, J. Killoran and D. F. O'Shea, *J. Org. Chem.*, 2005, **70**, 5571–5578.
- 241 X. Zhang, H. Yu and Y. Xiao, *J. Org. Chem.*, 2012, **77**, 669–673.
- 242 W. Senevirathna, C. M. Daddario and G. Sauvé, *J. Phys. Chem. Lett.*, 2014, **5**, 935–941.
- 243 A. Palma, J. F. Gallagher, H. Müller-Bunz, J. Wolowska, E. J. L. McInnes and D. F. O'Shea, *Dalt. Trans.*, 2009, 273–279.
- 244 T. S. Teets, D. V. Partyka, A. J. Esswein, J. B. Updegraff, M. Zeller, A. D. Hunter and T. G. Gray, *Inorg. Chem.*, 2007, **46**, 6218–6220.
- 245 T. S. Teets, J. B. Updegraff, A. J. Esswein and T. G. Gray, *Inorg. Chem.*, 2009, **48**, 8134–8144.
- 246 Y. Ge and D. F. O'Shea, *Chem. Soc. Rev.*, 2016, **45**, 3846–3864.
- 247 A. Palma, M. Tasiar, D. O. Frimannsson, T. T. Vu, R. Méallet-Renault and D. F. O'Shea, *Org. Lett.*, 2009, **11**, 3638–3641.
- 248 V. Bandi, H. B. Gobeze and F. D'Souza, *Chemistry*, 2015, **21**, 11483–11494.
- 249 A. Loudet, R. Bandichhor, K. Burgess, A. Palma, S. O. McDonnell, M. J. Hall and D. F. O'Shea, *Org. Lett.*, 2008, **10**, 12–15.
- 250 A. Kamkaew and K. Burgess, *Chem. Commun.*, 2015, **51**, 10664–10667.
- 251 M. Tasiar, J. Murtagh, D. O. Frimannsson, S. O. McDonnell and D. F. O'Shea, *Org. Biomol. Chem.*, 2010, **8**, 522–525.
- 252 D. Wu, S. Cheung, R. Daly, H. Burke, E. M. Scanlan and D. F. O'Shea, *Eur. J. Org. Chem.*, 2014, **2014**, 6841–6845.
- 253 D. Wu, S. Cheung, M. Devocelle, L.-J. Zhang, Z.-L. Chen and D. F. O'Shea, *Chem. Commun.*, 2015, **51**, 16667–16670.
- 254 J. Murtagh, D. O. Frimannsson and D. F. O'Shea, *Org. Lett.*, 2009, **11**, 5386–5389.
- 255 B. Brizet, C. Bernhard, Y. Volkova, Y. Rousselin, P. D. Harvey, C. Goze and F. Denat, *Org. Biomol. Chem.*, 2013, **11**, 7729–7737.
- 256 C. Tahtaoui, C. Thomas, F. Rohmer, P. Klotz, G. Duportail, Y. Mély, D. Bonnet and M. Hibert, *J. Org. Chem.*, 2007, **72**, 269–272.
- 257 A. M. Courtis, S. A. Santos, Y. Guan, J. A. Hendricks, B. Ghosh, D. M. Szantai-Kis, S. A. Reis, J. V. Shah and R. Mazitschek, *Bioconjugate Chem.*, 2014, **25**, 1043–1051.

- 258 C. Reichardt and T. Welton, *Solvents and solvent effects in organic chemistry*, 2003.
- 259 T. Kim, J. Park, S. Park, Y. Choi and Y. Kim, *Chem. Commun.*, 2011, **47**, 12640–12642.
- 260 T.A. Eisner, *Bull. Mus. Comp. Zool*, 1957, **116**, 439–490.
- 261 T. Omata and N. Murata, *Plant Cell Physiol.*, 1983, **24**, 1093–1100.
- 262 M. R. Prinsep and R. A. Thomson, *J. Nat. Prod.*, 1996, **59**, 786–788.
- 263 Eva M. Beems, T. M. A. R. Dubbelman, J. Lugtenburg, J. A. Van Best, M. F. M. A. Smeets and J. P. J. Boegheim, *Photochem Photobiol*, 1987, **46**, 639–643.
- 264 H. Ryeng and A. Ghosh, *J. Am. Chem. Soc.*, 2002, **124**, 8099–8103.
- 265 H. W. Whitlock, R. Hanauer, M. Y. Oester and B. K. Bower, *J. Am. Chem. Soc.*, 1969, **91**, 7485–7489.
- 266 J. S. Lindsey, O. Mass and C.-Y. Chen, *New J. Chem.*, 2011, **35**, 511–516.
- 267 M. Luciano and C. Brückner, *Molecules*, 2017, **22**, 980–1027.
- 268 B. W. Henderson and T. J. Dougherty, *J. Photochem. Photobiol. BBiol.*, 1991, **10**, 303–313.
- 269 M. Taniguchi, D. L. Cramer, A. D. Bhise, H. L. Kee, D. F. Bocian, D. Holten and J. S. Lindsey, *New J. Chem.*, 2008, **32**, 947–958.
- 270 S. Sasaki and H. Tamiaki, *J. Org. Chem*, 2006, **71**, 2648–2654.
- 271 C. Liu, M. P. Dobhal, M. Ethirajan, J. R. Missert, R. K. Pandey, S. Balasubramanian, D. K. Sukumaran, M. Zhang, K. M. Kadish and K. Ohkubo, *J. Am. Chem. Soc.*, 2008, **13**, 14311–14323.
- 272 Y. Chen, A. Graham, W. Potter, J. Morgan, L. Vaughan, D. A. Bellnier, B. W. Henderson, A. Oseroff, T. J. Dougherty and R. K. Pandey, *J. Med. Chem.*, 2002, **45**, 255–258.
- 273 S. K. Sharma, M. Krayerb, F. F. Sperandio, L. Huang, Y.-Y. Huang, D. Holten, J. S. Lindsey and M. R. Hamblina, *J. Porphyr. Phthalocyanines*, 2013, **17**, 73–85.
- 274 G. D. Dorough and J. R. Miller, *J. Am. Chem. Soc.*, 1952, **74**, 6106–6108.
- 275 C. Brückner and D. Dolphin, *Tetrahedron Lett.*, 1995, **36**, 3295–3298.
- 276 J. M. Sutton, O. J. Clarke, N. Fernandez and R. W. Boyle, *Bioconjugate Chem.*, 2002, **13**, 249–263.
- 277 H. Fischer and H. Eckoldt, *Liebigs Ann. Chem.*, 1940, **544**, 138–162.

- 278 R. K. Pandey, F. Shiau, A. B. Sumlin, T. J. Dougherty and M. Kevin, *Bioorg. Med. Chem.*, 1994, **4**, 1263–1267.
- 279 R. K. Pandey, S. Constantine, T. Tsuchida, G. Zheng, C. J. Medforth, M. Aoudia, A. N. Kozyrev, M. A. J. Rodgers, H. Kato, K. M. Smith and T. J. Dougherty, *J. Med. Chem.*, 1997, **2623**, 2770–2779.
- 280 G. Zheng, T. J. Dougherty and R. K. Pandey, *J. Org. Chem.*, 1999, **64**, 3751–3754.
- 281 C. Brückner, S. J. Rettig and D. Dolphin, *J. Org. Chem.*, 1998, **3263**, 2094–2098.
- 282 L. P. Samankumara, M. Zeller, A. Krause and C. Brückner, *Org. Biomol. Chem.*, 2010, **8**, 1951–1965.
- 283 C. Brückner and D. Dolphin, *Tetrahedron Lett.*, 1995, **36**, 3295–3298.
- 284 C. Brückner and D. Dolphin, *Tetrahedron Lett.*, 1995, **36**, 9425–9428.
- 285 J. M. Sutton, N. Fernandez and R. W. Boyle, *J. Porphyrins Phthalocyanines*, 2000, **4**, 655–658.
- 286 A. M. G. Silva, A. C. Tomé, M. G. P. M. S. Neves, A. M. S. Silva and J. A. S. Cavaleiro, *Chem. Commun.*, 1999, **1999**, 1767–1768.
- 287 A. M. G. Silva, A. C. Tome, M. G. P. M. S. Neves, A. M. S. Silva and A. S. Cavaleiro, *J. Org. Chem.*, 2005, **70**, 2306–2314.
- 288 A. M. G. Silva, P. S. S. Lacerda, A. C. Tome, M. G. P. M. S. Neves, A. M. S. Silva, A. S. Cavaleiro, E. A. Makarova, E. A. Lukyanets and R. V June, *J. Org. Chem.*, 2006, **71**, 8352–8356.
- 289 Y. Feng, X. Chen, F. Li and X. Li, *Synlett*, 2005, **6**, 1030–1032.
- 290 X. Li, J. Zhuang, Y. Li, H. Liu, S. Wang and D. Zhu, *Tetrahedron Lett.*, 2005, **46**, 1555–1559.
- 291 A. M. G. Silva, A. C. Tome, M. G. P. M. S. Neves, A. M. S. Silva, A. S. Cavaleiro, D. Perrone and A. Dondoni, *Tetrahedron Lett.*, 2002, **43**, 603–605.
- 292 L. Xingang, F. Yaqing, H. Xiaofen and L. Xianggao, *Synthesis (Stuttg.)*, 2005, **2005**, 3632–3638.
- 293 N. A. M. Pereira, A. C. Serra and T. M. V. D. Pinho, *Eur. J. Org. Chem.*, 2010, **2010**, 6539–6543.
- 294 T. G. Minehan and Y. Kishi, *Angew. Chem., Int. Ed.*, 1999, **7**, 923–925.
- 295 W. Wang and Y. Kishi, *Org. Lett.*, 1999, **1**, 1129–1132.

- 296 J. Jiang, M. Taniguchi and J. S. Lindsey, *New J. Chem.*, 2015, **39**, 4534–4550.
- 297 M. Krayer, E. Yang, J. R. Diers, D. F. Bocian, D. Holten and J. S. Lindsey, *New J. Chem.*, 2011, **35**, 587.
- 298 C.-Y. Chen, E. Sun, D. Fan, M. Taniguchi, B. E. McDowell, E. Yang, J. R. Diers, D. F. Bocian, D. Holten and J. S. Lindsey, *Inorg. Chem.*, 2012, **51**, 9443–9464.
- 299 H.-J. Kim and J. S. Lindsey, *J. Org. Chem.*, 2005, **70**, 5475–86.
- 300 D. Fan, M. Taniguchi and J. S. Lindsey, *J. Org. Chem.*, 2007, **72**, 5350–5357.
- 301 O. Mass and J. S. Lindsey, *J. Org. Chem.*, 2011, **76**, 9478–9487.
- 302 T. Harada, K. Sano, K. Sato, R. Watanabe, Z. Yu, H. Hanaoka, T. Nakajima, P. L. Choyke, M. Ptaszek and H. Kobayashi, *Bioconjugate Chem.*, 2014, **25**, 362–369.
- 303 C. Muthiah, H. L. Kee, J. R. Diers, D. Fan, M. Ptaszek, D. F. Bocian, D. Holten and J. S. Lindsey, *Photochem Photobiol.*, 2008, 786–801.
- 304 H. L. Kee, R. Nothdurft, C. Muthiah, J. R. Diers, D. Fan, M. Ptaszek, D. F. Bocian, J. S. Lindsey, J. P. Culver and D. Holten, *Photochem Photobiol.*, 2008, **84**, 1061–1072.
- 305 M. Ptaszek, H. Ling, C. Muthiah, R. Nothdurft, W. Akers, S. Achilefu, J. P. Culver and D. Holten, *Proc. SPIE*, 2010, **7576**, 1–9.
- 306 W. Cao, K. K. Ng, I. Corbin, Z. Zhang, L. Ding, J. Chen and G. Zheng, *Bioconjugate Chem.*, 2009, **20**, 2023–2031.
- 307 M. M. Pereira, C. J. P. Monteiro, A. V. C. Simões, S. M. A. Pinto, A. R. Abreu, G. F. F. Sa, E. F. F. Silva, L. B. Rocha, J. M. Dbrowski, S. J. Formosinho, S. Simoes and L. G. Arnaut, *Tetrahedron*, 2010, **66**, 9545–9551.
- 308 C. Wischke and H. Borchert, *Pharmazie*, 2006, **61**, 770–774.
- 309 J. Zhang, D. Ma, D. Du, Z. Xi and L. Yi, *Org. Biomol. Chem.*, 2014, **12**, 9528–9531.
- 310 S. L. Gibbs, *Quant Imaging Med Surg*, 2012, **2**, 177–187.
- 311 J. R. Lakowicz, *Principles of Fluorescence Spectroscopy*, Kluwer Academic/Plenum Publishers, 2nd Ed., 1999.
- 312 D. Magde, G. E. Rojas and P. G. Seybold, *Photochem. Photobiol.*, 1999, **70**, 737–744.
- 313 S. L. Niu, C. Massif, G. Ulrich, R. Ziessel, P. Y. Renard and A. Romieu, *Org. Biomol. Chem.*, 2011, **9**, 66–69.

- 314 K. A. Majorek, P. J. Porebski, A. Dayal, M. D. Zimmerman, K. Jablonska, A. J. Stewart, M. Chruszcz and W. Minor, *Mol. Immunol.*, 2012, **52**, 174–182.
- 315 S. C. Gill and P. H. von Hippel, *Anal. Biochem.*, 1989, **182**, 319–326.
- 316 M. E. B. Smith, M. B. Caspersen, E. Robinson, M. Morais, A. Maruani, J. P. M. Nunes, K. Nicholls, M. J. Saxton, S. Caddick, R. Baker and V. Chudasama, *Org. Biomol. Chem.*, 2015, **13**, 7946–7949.
- 317 K. Philipp-abbrederis, K. Herrmann, S. Knop, M. Schottelius, M. Eiber, K. Lückerath, E. Pietschmann, S. Habringer, C. Gerngroß, K. Franke, M. Rudelius, A. Schirbel, C. Lapa, K. Schwamborn, S. Steidle, E. Hartmann, A. Rosenwald, S. Kropf, A. J. Beer, C. Peschel, H. Einsele, A. K. Buck, M. Schwaiger, K. Götze, H. Wester and U. Keller, *EMBO Mol. Med.*, 2015, **7**, 477–487.
- 318 P. Herhaus, S. Habringer, T. Vag, K. Steiger, J. Slotta-huspenina, C. Gerngroß, B. Wiestler, H. Wester, M. Schwaiger and U. Keller, *EJNMMI Res.*, 2017, **7**, 51–54.
- 319 T. L. Ross, A. Schäfer, J. Tillmanns, H. J. Wester, K. C. Wollert, J. Bauersachs and F. M. Bengel, *JACC Cardiovasc. IMAGING*, 2015, **8**, 1417–1426.
- 320 X. Sun, G. Cheng and M. Hao, *Cancer Metastasis Rev*, 2010, **29**, 709–722.
- 321 B. Homey, H. Soto, N. Ge, D. Catron, M. E. Buchanan, T. Mcclanahan, A. Mu, A. Zlotnik, E. Murphy, W. Yuan, S. N. Wagner, J. Luis, A. Mohar and E. Vera, *Nature*, 2001, **410**, 50–56.
- 322 G. Guan, Y. Lu, X. Zhu, L. Liu, J. Chen and Q. Ma, *Sci. Rep.*, 2015, **5**, 15244.
- 323 O. Tietz, N. Kamaly, G. Smith, E. Shamsaei, K. K. Bhakoo and N. J. Long, *Am J Nucl Med Mol Imaging*, 2013, **3**, 372–383.
- 324 T. Tanaka, W. Nomura, T. Narumi, A. Masuda and H. Tamamura, *J. Am. Chem. Soc.*, 2010, **132**, 15899–15901.
- 325 G. Fan, L. Yang and Z. Chen, *Front. Chem. Sci. Eng.*, 2014, **8**, 405–417.
- 326 N. Zhao, S. Xuan, F. R. Fronczek, K. M. Smith, M. Grac and H. Vicente, *J. Org. Chem.*, 2017, **82**, 3880–3885.
- 327 K. E. Day, L. N. Beck, C. H. Heath, C. C. Huang, K. R. Zinn and E. L. Rosenthal, *Cancer Biol. Ther.*, 2013, **14**, 271–277.
- 328 M. T. W. Lee, A. Maruani, J. R. Baker, S. Caddick and V. Chudasama, *Chem. Sci.*, 2016, **7**, 799–802.
- 329 V. Chudasama, A. Maruani and S. Caddick, *Nat. Chem.*, 2016, **8**, 114–119.

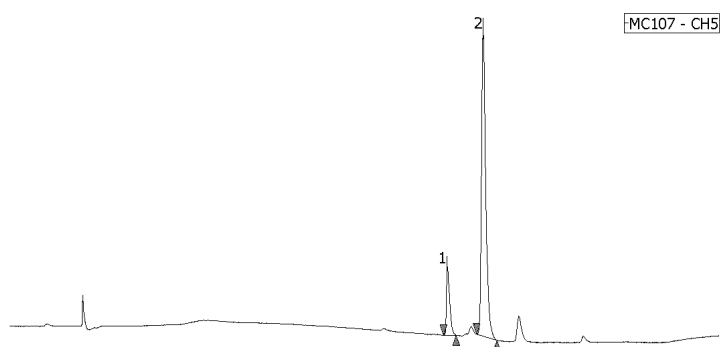
- 330 M. T. W. Lee, A. Maruani, D. A. Richards, J. R. Baker, S. Caddick and V. Chudasama, *Chem. Sci.*, 2017, **8**, 2056–2060.
- 331 E. Robinson, J. P. M. Nunes, V. Vassileva, A. Maruani, J. C. F. Nogueira, M. E. B. Smith, R. B. Pedley, S. Caddick, J. R. Baker and V. Chudasama, *RSC Adv.*, 2017, **7**, 9073–9077.
- 332 D. B. G. Williams and M. Lawton, *J. Org. Chem.*, 2010, **75**, 8351–8354.
- 333 A. M. Brouwer, *Pure Appl. Chem.*, 2011, **83**, 2213–2228.
- 334 J. Jose, Y. Ueno, J. C. Castro, L. Li and K. Burgess, *Tetrahedron Lett.*, 2009, **50**, 6442–6445.
- 335 J. S. Lindsey and R. W. Wagner, *J. Org. Chem.*, 1989, **54**, 828–836.
- 336 N. J. Matovic, P. Y. Hayes, K. Penman, R. P. Lehmann and J. J. De Voss, *J. Org. Chem.*, 2011, **76**, 4467–4481.

9. Appendix

9.1 HPLC traces

Compound 37

Chromatogram



Chromatogram Information

User Name Administrator
Date Modified 29/03/2016 17:08:59
Description
HPLC System Name hplc1
Injection Date 29/03/2016 16:48:55
Volume 10.00 [μL]
Sample Number 1
Project Name 2012-11-08
Acquisition Time 20.0 [min]
Acquisition Sequence Anionic Aza BODIPY MC155 0.05%TEA MeOH HPG
Control Method Anionic Aza-BODIPY MC107 0.05%TEA MeOH HPG
Peak ID Table
Calibration Method
Additional Information

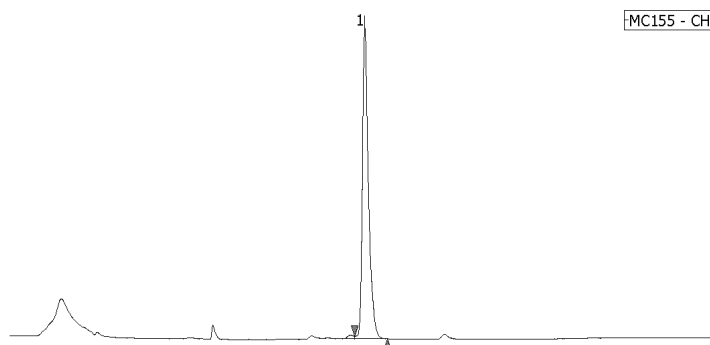
Channel & Peak Information Table

Chromatogram Name MC107-CH5
Sample Name
Channel Name 660.0nm
Sampling Interval 800 [msec]
Peak Method Peak method for tiny peaks
Formula
Decision

#	Peak Name	CH	tr [min]	Area [μV·sec]	Height [μV]	Area%	Height%	Quantity	NTP	Resolution	Symmetry Factor	Warning
1	Unknown	5	12.333	32047	5007	14.620	18.256	N/A	90531	5.481	2.103	
2	Unknown	5	13.347	187160	22419	85.380	81.744	N/A	66671	N/A	1.491	

Compound 40

Chromatogram



Chromatogram Information

User Name Administrator
 Date Modified 29/03/2016 19:10:40
 Description
 HPLC System Name hplc1
 Injection Date 29/03/2016 18:55:37
 Volume 10.00 [μL]
 Sample Number 1
 Project Name 2012-11-08
 Acquisition Time 15.0 [min]
 Acquisition Sequence Anionic Aza BODIPY MC155 0.05%TEA MeOH HPG3
 Control Method Anionic Aza-BODIPY MC155 0.05%TEA MeOH HPG2
 Peak ID Table
 Calibration Method
 Additional Information

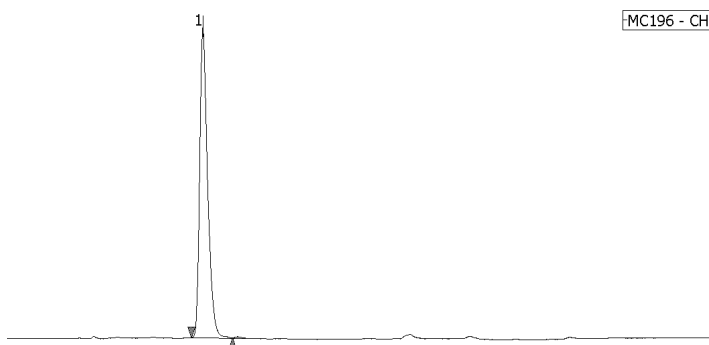
Channel & Peak Information Table

Chromatogram Name MC155-CH5
 Sample Name
 Channel Name 660.0nm
 Sampling Interval 800 [msec]
 Peak Method Fran1
 Formula
 Decision

#	Peak Name	CH	tR [min]	Area [μV·sec]	Height [μV]	Area%	Height%	Quantity	NTP	Resolution	Symmetry Factor
1	Unknown	5	7.507	791443	89112	100.000	100.000	N/A	19247	N/A	1.530
#	Warning										
1											

Compound 46

Chromatogram



Chromatogram Information

User Name Administrator
 Date Modified 28/06/2016 17:17:58
 Description
 HPLC System Name hplc1
 Injection Date 28/06/2016 17:02:55
 Volume 10.00 [µL]
 Sample Number 1
 Project Name 2012-11-08
 Acquisition Time 15.0 [min]
 Acquisition Sequence Anionic Aza BODIPY MC196 0.05%TEA MeOH HPG3 purified
 Control Method Anionic Aza-BODIPY MC196 0.05%TEA MeOH HPG3
 Peak ID Table
 Calibration Method
 Additional Information

Channel & Peak Information Table

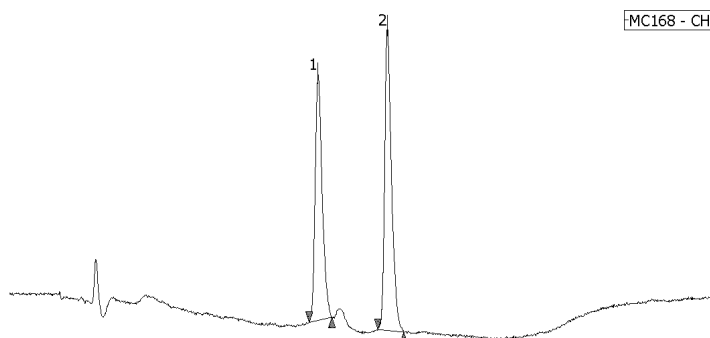
Chromatogram Name MC196-CH5
 Sample Name
 Channel Name 660.0nm
 Sampling Interval 800 [msec]
 Peak Method Anionic Azide Aza-BODIPY
 Formula
 Decision

#	Peak Name	CH	tR [min]	Area [µV·sec]	Height [µV]	Area%	Height%	Quantity	NTP	Resolution	Symmetry Factor
1	Unknown	5	4.133	764309	65931	100.000	100.000	N/A	3215	N/A	1.421

#	Warning
1	

Mixture of conjugate 90

Chromatogram



MC168 - CH5

Chromatogram Information

User Name Administrator
 Date Modified 26/04/2016 14:46:38
 Description
 HPLC System Name hplc1
 Injection Date 26/04/2016 14:31:36
 Volume 10.00 [μL]
 Sample Number 1
 Project Name 2012-11-08
 Acquisition Time 15.0 [min]
 Acquisition Sequence Anionic Aza BODIPY MC168 0.05%TEA MeOH HPG3
 Control Method Anionic Aza-BODIPY MC168 0.05%TEA MeOH HPG3
 Peak ID Table
 Calibration Method
 Additional Information

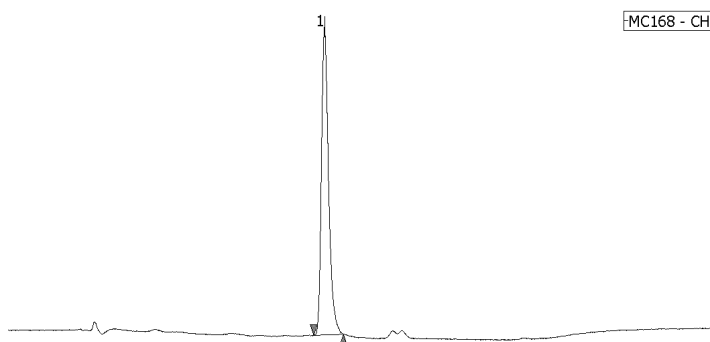
Channel & Peak Information Table

Chromatogram Name MC168-CH5
 Sample Name
 Channel Name 660.0nm
 Sampling Interval 800 [msec]
 Peak Method Anionic Azide Aza-BODIPY
 Formula

#	Peak Name	CH	TR [min]	Area [μV·sec]	Height [μV]	Area%	Height%	Quantity	NTP	Resolution	Symmetry Factor	Warning
1	Unknown	5	6.520	24667	2403	45.412	44.814	N/A	9926	5.738	1.365	
2	Unknown	5	7.987	29652	2959	54.588	55.186	N/A	16215	N/A	1.401	

Conjugate 90

Chromatogram



Chromatogram Information

User Name Administrator
 Date Modified 28/04/2016 16:54:09
 Description
 HPLC System Name hplc1
 Injection Date 28/04/2016 16:39:05
 Volume 10.00 [µL]
 Sample Number 1
 Project Name 2012-11-08
 Acquisition Time 15.0 [min]
 Acquisition Sequence Anionic Aza BODIPY MC168 0.05%TEA MeOH HPG3 purified
 Control Method Anionic Aza-BODIPY MC168 0.05%TEA MeOH HPG3
 Peak ID Table
 Calibration Method
 Additional Information

Channel & Peak Information Table

Chromatogram Name MC168-CH5
 Sample Name
 Channel Name 660.0nm
 Sampling Interval 800 [msec]
 Peak Method Anionic Azide Aza-BODIPY
 Formula
 Decision

#	Peak Name	CH	IR [min]	Area [µV·sec]	Height [µV]	Area%	Height%	Quantity	NTP	Resolution	Symmetry Factor
1	Unknown	5	6.680	122523	11781	100.000	100.000	N/A	10241	N/A	1.356
#	Warning										
1											

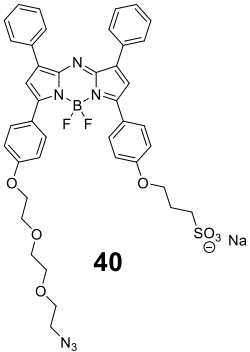
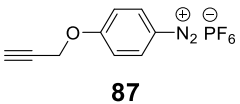
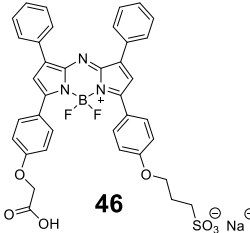
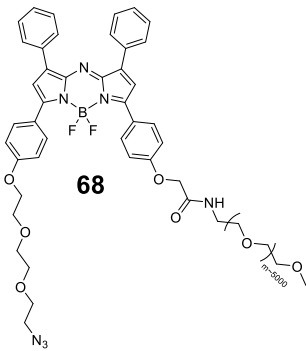
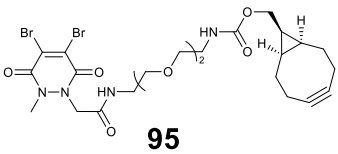
Structure	Linker	Conjugating types	Site of biomolecules	Comment
 <p>40</p>	 <p>87</p>	<ol style="list-style-type: none"> 1. Azo-coupling 2. CuAAC 	Tyrosine of protein (BSA)	<ul style="list-style-type: none"> ● Loading ratio 1.5/1 ● Controlled and regioselective bioconjugation ● Traceable reaction ● Higher loading ratio than cysteine ● More reliable loading than lysine
 <p>46</p>	N/A	Peptide bond	Lysine on Peptide (Pentixafor)	<ul style="list-style-type: none"> ● Loading ratio 1/1 ● Better than CuAAC for peptide ● Significant increase in Φ_f ● High bind affinity toward CXCR4 receptor <i>in vitro</i>
 <p>68</p>	 <p>95</p>	<ol style="list-style-type: none"> 1. Disulfide rebridging 2. SPAAC 	Cysteine on antibody (Trastuzumab)	<ul style="list-style-type: none"> ● Loading ratio 4/1 ● Regioselective and stoichiometrically-controlled bioconjugation ● Homogeneous product ● Clear reactions and mild conditions ● Significant binding toward HER2+ cells through <i>in vitro</i> imaging

Table 12. Summary of NIR fluorescence imaging conjugates.